University of Calgary

PRISM Repository **https://prism.ucalgary.ca**

The Vault Open Theses and Dissertations

2014-01-20

Ground-Based Deformation Monitoring

Ebeling, Axel

Ebeling, A. (2014). Ground-Based Deformation Monitoring (Doctoral thesis, University of Calgary, Calgary, Canada). Retrieved from https://prism.ucalgary.ca. doi:10.11575/PRISM/26325 http://hdl.handle.net/11023/1273

Downloaded from PRISM Repository, University of Calgary

UNIVERSITY OF CALGARY

Ground-Based Deformation Monitoring

by

Axel Ebeling

A DISSERTATION

SUBMITTED TO THE FACULTY OF GRADUATE STUDIES

IN PARTIAL FULFILLMENT OF THE REQUIREMENTS FOR THE

DEGREE OF DOCTOR OF PHILOSOPHY

DEPARTMENT OF GEOMATICS ENGINEERING

CALGARY, ALBERTA

January, 2014

© Axel Ebeling 2014

Abstract

The observation and analysis of movements of large structures, man-made as well as natural ones, such as high-rise buildings, dams or rock slides and earthquake zones, is a highly responsible task in engineering. Deformation monitoring is essential to public safety by reducing the risk of structural failure. It is also an important aid in the understanding of the behaviour of certain natural phenomena like glacial drift.

The procedure for a deformation analysis can be divided into three steps: a global congruency test to determine in which epochs deformations occur, the localization of the deformed points and the determination of deformations. The single-point analysis typically used in the localization step, requires the two epochs under comparison to refer to the same datum. If this is not the case an S-transformation to a common datum has to be carried out. This is only possible however, if both epochs share the same reference frame, and particularly, the same network scale.

In this dissertation a generalized model for a congruence analysis is proposed which allows the coordinates to refer to different reference frames. This model utilizes a combinatorial search for the largest similar point group based on the angular differences between epochs. This is combined with a 3D Helmert transformation that allows to derive deformations directly from the adjusted coordinates of each epoch and their, typically singular, cofactor matrices, independent of the coordinate system they are given in.

A set of computer-based simulations are carried out to evaluate the performance of the proposed algorithm. The computer simulations reveal that the proposed algorithm can reliably locate the largest similar point group between epochs. The transformation parameters as well as the deformations are accurately recovered. Finally, a real-world application, the Frank Slide / Turtle Mountain, is presented where the proposed methodology was applied.

Acknowledgements

First and foremost, I would like to express my sincere gratitude to my supervisor Dr. W. F. Teskey for his help and advice without which this thesis would not have been possible. He has given me the support and freedom which made my graduate studies experience not only a valuable but also a memorable journey.

I want to thank Dr. Robert Radovanovic from SarPoint Engineering for dragging me outside of the walls of academia and giving me the opportunity to gain a lot of valuable real-world experience. I would also like to thank Chris Tucker from SarPoint Engineering for providing a hiding place where I could forget about the rest of the world and focus on this work. Large chunks of this dissertation have been written at his condo in Kimberley, BC.

I am deeply indebted to my parents for their unconditional support, love and understanding throughout all these years. There is no way I can ever thank you enough.

Most especially I am grateful to Charlotte for being there for me and keeping me sane and motivated over the last few and most difficult months. You are truly amazing!

I want to thank all of my friends, inside and outside of university, for time well-wasted out in the mountains and at Moose McGuire's.

Finally, the Werner-Graupe Foundation as well as the Natural Sciences and Engineering Research Council of Canada are greatly acknowledged for their financial support.

Table of Contents

Abstract . . . ii
Acknowledgements . . . iii
Table of Contents . . . iv
List of Tables . . . vii
List of Figures . . . xiii
List of Symbols . . . xiv
1 INTRODUCTION . . . 1
1.1 Motivation and Objectives . . . 2
1.2 Thesis Outline . . . 3
2 BACKGROUND . . . 5
2.1 Observation techniques . . . 5
2.1.1 Geodetic observation techniques . . . 6
2.1.2 Example . . . 7
2.2 Network analysis . . . 8
2.2.1 Datum definition . . . 10
2.2.1.1 Inner-constraint approaches . . . 12
2.2.1.2 Constraint approaches . . . 16
2.2.1.3 S-transformation . . . 17
2.2.2 Solution and analysis of results . . . 18
2.2.3 Numerical examples . . . 21
2.2.4 Discussion . . . 26
2.3 Deformation analysis . . . 28
2.3.1 Classification of deformation analysis models . . . 28
2.3.2 Classical congruence analysis . . . 30
2.3.2.1 Global congruency testing . . . 31
2.3.2.2 Localization of movements . . . 33
2.3.2.3 Determination of movements . . . 34
2.3.2.4 Numerical examples . . . 35
2.3.3 Congruence analysis using a Multi-Parameter Transformation . . . 42
2.3.4 Localization of deformed points . . . 44
2.3.4.1 Least-squares and single point analysis . . . 44
2.3.4.2 Robust estimation techniques . . . 45
2.3.4.3 Combinatorial Search . . . 49
2.3.4.3.1 MSS using distance differences . . . 51
2.3.4.3.2 MSS using distance ratios . . . 56
2.3.5 Discussion . . . 60
2.4 Solutions for the over-determined 3D Helmert transformation with singular cofactor matrix . . . 64
2.4.1 3D Helmert transformation . . . 65
2.4.2 Solutions based on fictitious observations . . . 67
2.4.2.1 Explicit formulation of transformation . . . 68
2.4.2.2 Implicit formulation of transformation . . . 71

2.4.3 GAUSS-HELMERT model with singular cofactor matrix . . . 73
2.4.3.1 Iterative solution of the GAUSS-HELMERT model . . . 76
2.4.4 Total Least-Squares . . . 79
2.4.5 Discussion . . . 82
2.5 Summary . . . 85
3 METHODOLOGY . . . 88
3.1 Localization of largest similar point group based on angles . . . 88
3.1.1 The Algorithm . . . 90
3.1.2 Numerical example . . . 91
3.2 Determination of movements . . . 95
3.2.1 The approach . . . 95
3.2.2 Rotation using quaternions . . . 96
3.2.3 Derivation of functional model . . . 100
3.2.4 Solution with the non-linear GAUSS-HELMERT model . . . 102
3.2.5 Derivation of deformations . . . 103
3.2.6 Numerical Example . . . 104
3.3 Multiple-epoch comparison . . . 108
3.3.1 Localization of largest similar point group common to all epochs . . . 108
3.3.2 Determination of movements . . . 110
3.3.2.1 Derivation of functional model . . . 110
3.3.2.2 Solution of the adjustment problem . . . 111
3.3.2.3 Derivation of deformations . . . 113
3.3.2.4 Numerical example . . . 114
3.4 Discussion . . . 118
4 COMPUTER SIMULATIONS . . . 120
4.1 Scenario A . . . 122
4.1.1 Results of network analyses . . . 123
4.1.2 Global congruency testing . . . 124
4.1.3 Localization . . . 125
4.1.3.1 Classical congruence analysis . . . 126
4.1.3.2 MSS using distance differences . . . 130
4.1.3.3 MSS using distance ratios . . . 133
4.1.3.4 MSS using angles . . . 137
4.1.4 Determination . . . 139
4.1.4.1 Combined re-adjustment of observations . . . 139
4.1.4.2 Transformation-based approach . . . 145
4.1.5 Discussion . . . 151
4.2 Scenario B . . . 154
4.2.1 Results of network analysis . . . 156
4.2.2 Global congruency testing . . . 157
4.2.3 Localization . . . 158
4.2.3.1 MSS using distance ratios . . . 158
4.2.3.2 MSS using angles . . . 161
4.2.4 Determination using transformation-based approach . . . 163
4.2.5 Discussion . . . 168

4.3 Summary . . . 171
5 CASE STUDY: The Frank Slide / Turtle Mountain, Alberta . . . 173
5.1 Results of network analyses . . . 180
5.2 Global congruency testing . . . 181
5.3 Localization . . . 182
5.3.1 MSS using distance ratios . . . 183
5.3.2 MSS using angles . . . 185
5.3.3 Summary of results . . . 187
5.4 Determination . . . 188
5.5 Discussion . . . 197
6 CONCLUSIONS . . . 200
6.1 Findings from this Thesis . . . 200
6.2 Research Contributions . . . 204
BIBLIOGRAPHY . . . 206
APPENDIX . . . 212
A . . . 213
A.1 Error propagation for computation of angles from coordinates . . . 213
A.2 Design and condition matrices for two-epoch comparison . . . 216
A.3 Error propagation for derivation of deformations from coordinates and transformation parameters . . . 218
A.4 Design and condition matrices for multiple-epoch comparison . . . 221
B . . . 224
B.1 Scenario A: adjusted coordinates and standard deviations after network analysis for epochs 1 to 5 . . . 224
B.2 Scenario A: Candidates for largest congruent point group from MSS-method using distance ratios and statistical evaluation . . . 227
B.3 Scenario A: Candidates for largest congruent point group from MSS-method using angles and statistical evaluation . . . 232
B.4 Scenario A: Adjusted coordinates and standard deviations from combined readjustment of observations . . . 233
B.5 Scenario B: Adjusted coordinates and standard deviations after network analysis for epochs 1 to 5 . . . 236
B.6 Scenario B: Candidates for largest congruent point group from MSS-method using distance ratios and statistical evaluation . . . 239
B.7 Scenario B: Candidates for largest congruent point group from MSS-method using angles and statistical evaluation . . . 245
C . . . 246
C.1 Turtle Mountain: adjusted coordinates and standard deviations of HPTN points after network analysis for epochs 1 to 4 . . . 246
C.2 Turtle Mountain: candidates for similar point groups from MSS-method based on distance ratios . . . 248
C.3 Turtle Mountain: candidates for similar point groups from MSS-method based on angles . . . 252

List of Tables

2.1 Relative observations between network points 7
2.2 Datum contributions of geodetic measurements, (Kuang, 1996) 11
2.3 Initial coordinates of network points in [m] 22
2.4 Adjusted coordinates and their standard deviations for total trace minimization 22
2.5 Adjusted coordinates and their standard deviations for partial trace minimization 23
2.6 Adjusted coordinates and their standard deviations for ordinary minimal constraints 24
2.7 Adjusted coordinates and their standard deviations for over-constrained adjustment 25
2.8 Adjusted coordinates and their standard deviations for network with weak datum 26
2.9 Adjusted coordinates and their standard deviations for epoch 2 36
2.10 Test statistics for local congruency test of all five network points 37
2.11 Test statistics for local congruency test of the four remaining points 38
2.12 Adjusted coordinates and their standard deviations for epochs 1 and 2 . . . 38
2.13 Deformations and their standard deviations of point 3 between epochs 1 and 2 in [mm] 39
2.14 Adjusted coordinates and their standard deviations after scaling distances . . 39
2.15 Test statistics for local congruency test after scaling 40
2.16 Local test statistics for the four remaining points after scaling 41
2.17 Local test statistics for the three remaining points after scaling 41
2.18 Local test statistics for points 4 and 5 after scaling 41
2.19 Edge-node matrix for five point network 52
2.20 Node-node matrix for five point network with all distances 53
2.21 Distance differences and their rejection threshold for example network in [m] 54
2.22 Edge-node matrix without rejected distances 55
2.23 Resulting node-node matrix for example network 55
2.24 Sorted list of distance ratios with search windows 58
2.25 Edge-node matrix for third search window 59
2.26 Resulting node-node matrix for third search window 59
2.27 Edge-node matrix for last search window 60
2.28 Resulting node-node matrix for last search window 60

3.1 Remaining angles after elimination 92
3.2 Histogram of remaining angles 93
3.3 Angles at pt 1 93
3.4 Angles at pt 2 93
3.5 Angles at pt 3 93
3.6 Angles at pt 4 94
3.7 Angles at pt 5 94
3.8 Angles required for tetragon 1,2,4,5 94

3.9 Adjusted coordinates of 3D network in epoch 1 . . . 104
3.10 True deformations of point 3 in epoch 2 . . . 105
3.11 Adjusted coordinates of 3D network in epoch 2 . . . 105
3.12 Adjusted transformation parameters and standard deviations for epoch 2 . . 106
3.13 True transformation parameters for epoch 2 . . . 107
3.14 Estimated deformations and standard deviations in epoch 2 in [mm] . . . 107
3.15 Adjusted coordinates of 3D network in epoch 3 . . . 114
3.16 True deformations of point 3 in epochs 2 and 3 with respect to epoch 1 in [mm] 114
3.17 Adjusted transformation parameters and standard deviations for multi-epoch comparison . . . 116
3.18 True transformation parameters for epochs 2 and 3 . . . 116
3.19 Estimated deformations and standard deviations in epoch 2 with respect to epoch 1 in [mm] . . . 117
3.20 Estimated deformations and standard deviations in epoch 3 with respect to epoch 1 in [mm] . . . 117
3.21 Estimated deformations and standard deviations between epochs 2 and 3 in the system of epoch 1 in [mm] . . . 118

4.1 Simulated coordinates of network points in [m] . . . 120
4.2 True deformations of network points for epochs 3 to 5 in [mm] . . . 122
4.3 Scenario A: a posteriori standard deviations and test statistics for global test of adjustment model for all epochs . . . 124
4.4 Scenario A: test statistics and combined standard deviations . . . 124
4.5 Scenario A: quadratic forms $\hat{\Omega}^2$ and test statistics T_G for all global congruency tests . . . 125
4.6 Scenario A: local test statistics T_L for all points in epoch 2 . . . 126
4.7 Scenario A: local test statistics T_L for all points in epoch 3 . . . 127
4.8 Scenario A: local test statistics T_L for remaining points in epoch 3 after elimination of point 108 . . . 127
4.9 Scenario A: local test statistics T_L for remaining points in epoch 3 after elimination of point 102 . . . 127
4.10 Scenario A: local test statistics T_L for remaining points in epoch 3 after elimination of point 105 . . . 128
4.11 Scenario A: local test statistics T_L for remaining points in epoch 3 after elimination of point 111 . . . 128
4.12 Scenario A: results for global congruency tests for epoch 4 . . . 128
4.13 Scenario A: local test statistics T_L for all points in epoch 4 . . . 129
4.14 Scenario A: results for global congruency tests for epoch 5 . . . 129
4.15 Scenario A: local test statistics T_L for all points in epoch 5 . . . 130
4.16 Scenario A: results for global congruency tests for all candidates for congruent point groups of epoch 5 . . . 132
4.17 Scenario A: largest congruent point group and statistical test for epoch 2 . . 134
4.18 Scenario A: largest congruent point group and statistical test for epoch 3 . . 134
4.19 Scenario A: candidates of eight points and statistical test for epoch 4 135
4.20 Scenario A: candidates of seven points and statistical test for epoch 4 135

4.21 Scenario A: largest congruent point group and statistical test for epoch 4 . . 136
4.22 Scenario A: candidates of five points and statistical test for epoch 5 136
4.23 Scenario A: largest congruent point group and statistical test for epoch 5 . . 137
4.24 Scenario A: largest congruent point group and test statistic for epoch 2 . . . 138
4.25 Scenario A: largest congruent point group and test statistic for epoch 3 . . . 138
4.26 Scenario A: candidates and test statistics for epoch 4 138
4.27 Scenario A: largest congruent point group and test statistic for epoch 5 . . . 139
4.28 Scenario A: summary of statistics for combined re-adjustment of epochs 1 and 2140
4.29 Scenario A: summary of statistics for combined re-adjustment of epochs 1 and 3141
4.30 Scenario A: estimated deformations and standard deviations in epoch 3 in [mm]141
4.31 Scenario A: summary of statistics for combined re-adjustment of epochs 1 and 4142
4.32 Scenario A: estimated deformations and standard deviations in epoch 4 in [mm]142
4.33 Scenario A: summary of statistics for combined re-adjustment of epochs 1 and 5143
4.34 Scenario A: estimated deformations and standard deviations in epoch 5 in [mm]143
4.35 Scenario A: differences between estimated and true deformations at given epoch in [mm] 144
4.36 Scenario A: summary of statistics for transformation adjustment of all epochs 146
4.37 Scenario A: estimated transformation parameters and standard deviations of epochs 2 and 3 with respect to epoch 1 146
4.38 Scenario A: estimated transformation parameters and standard deviations of epochs 4 and 5 with respect to epoch 1 147
4.39 Scenario A: estimated deformations and standard deviations in epoch 2 in [mm]148
4.40 Scenario A: estimated deformations and standard deviations in epoch 3 in [mm]149
4.41 Scenario A: estimated deformations and standard deviations in epoch 4 in [mm]150
4.42 Scenario A: estimated deformations and standard deviations in epoch 5 in [mm]150
4.43 Scenario A: differences between estimated and true deformations at given epoch in [mm] 151
4.44 Overall RMS errors of estimated deformations for all epochs 153
4.45 Overall RMS errors of estimated deformations for all epochs 154
4.46 Simulated coordinates of network points in global system in [m] 155
4.47 Transformation parameters relating local and global systems 155
4.48 Scenario B: a posteriori standard deviations and test statistics for global test of adjustment model for all epochs 157
4.49 Scenario B: test statistics and combined standard deviations 157
4.50 Scenario B: quadratic forms $\hat{\Omega}^2$ and test statistics T_G for all global congruency tests 158
4.51 Scenario B: largest similar point group and statistical test for epoch 2 159
4.52 Scenario B: largest similar point group and statistical test for epoch 3 159
4.53 Scenario B: candidate of eight points and statistical test for epoch 4 159
4.54 Scenario B: candidates of seven points and statistical test for epoch 4 160
4.55 Scenario B: largest similar point group and statistical test for epoch 4 160
4.56 Scenario B: candidates of five points and statistical test for epoch 5 161
4.57 Scenario B: largest similar point group and statistical test for epoch 5 161
4.58 Scenario B: largest similar point group and test statistic for epoch 2 162
4.59 Scenario B: largest similar point group and test statistic for epoch 3 162

4.60 Scenario B: candidates and test statistic for epoch 4 163
4.61 Scenario B: largest similar point group and test statistic for epoch 5 163
4.62 Scenario B: summary of statistics for transformation adjustment of all epochs 164
4.63 Scenario B: estimated transformation parameters and standard deviations of epochs 2 and 3 with respect to epoch 1 165
4.64 Scenario B: estimated transformation parameters and standard deviations of epochs 4 and 5 with respect to epoch 1 165
4.65 Scenario B: estimated deformations and standard deviations in epoch 2 in [mm] 166
4.66 Scenario B: estimated deformations and standard deviations in epoch 3 in [mm] 167
4.67 Scenario B: estimated deformations and standard deviations in epoch 4 in [mm] 167
4.68 Scenario B: estimated deformations and standard deviations in epoch 5 in [mm] 168
4.69 Scenario B: differences between estimated and true deformations at given epoch in [mm] 169
4.70 Overall RMS errors of estimated deformations for all epochs 170

5.1 Initial approximate coordinates of HPTN points in [m] 180
5.2 Statistical results of network analyses 180
5.3 Comparison of variances and combined standard deviations 182
5.4 Global congruency tests for all epochs 182
5.5 Statistical evaluation of largest similar point group between epochs 1 and 2 . 183
5.6 Statistical evaluation of candidates for largest similar point group between epochs 1 and 3 183
5.7 Statistical evaluation of candidates for largest similar point group between epochs 1 and 4 184
5.8 Statistical evaluation of largest similar point group between epochs 2 and 3 . 184
5.9 Statistical evaluation of largest similar point group between epochs 2 and 4 . 184
5.10 Statistical evaluation of largest similar point group between epochs 3 and 4 . 185
5.11 Statistical evaluation of largest similar point group between epochs 1 and 2 . 185
5.12 Statistical evaluation of candidates for largest similar point group between epochs 1 and 3 185
5.13 Statistical evaluation of candidates for largest similar point group between epochs 1 and 4 186
5.14 Statistical evaluation of largest similar point group between epochs 2 and 3 . 186
5.15 Statistical evaluation of largest similar point group between epochs 2 and 4 . 186
5.16 Statistical evaluation of largest similar point group between epochs 3 and 4 . 187
5.17 Summary of largest similar point groups between all epochs 187
5.18 Summary of statistics for transformation adjustment of all epochs 189
5.19 Estimated transformation parameters and standard deviations of epochs 2 and 3 with respect to epoch 1 190
5.20 Estimated transformation parameters and standard deviations of epochs 4 with respect to epoch 1 191
5.21 Estimated deformations and standard deviations between epochs 1 and 2 in [mm] 191
5.22 Estimated deformations and standard deviations between epochs 1 and 3 in [mm] 192

5.23 Estimated deformations and standard deviations between epochs 1 and 4 in [mm] . . . 192
5.24 Estimated deformations and standard deviations between epochs 2 and 3 in [mm] . . . 193
5.25 Estimated deformations and standard deviations between epochs 2 and 4 in [mm] . . . 193
5.26 Summary of statistics for transformation adjustment of all epochs . . . 194
5.27 Estimated transformation parameters and standard deviations of epochs 4 with respect to epoch 3 . . . 194
5.28 Estimated deformations and standard deviations between epochs 3 and 4 in [mm] . . . 195

A.1 Order of angles α_k . . . 213

B.1 Scenario A: adjusted coordinates and standard deviations of epoch 1 . . . 224
B.2 Scenario A: adjusted coordinates and standard deviations of epoch 2 . . . 224
B.3 Scenario A: adjusted coordinates and standard deviations of epoch 3 . . . 225
B.4 Scenario A: adjusted coordinates and standard deviations of epoch 4 . . . 225
B.5 Scenario A: adjusted coordinates and standard deviations of epoch 5 . . . 226
B.6 Scenario A: candidates of six points and statistical test for epoch 4 . . . 227
B.7 Scenario A: candidates of four points and statistical test for epoch 5 . . . 228
B.8 Scenario A: candidates of three points and statistical test for epoch 5 . . . 229
B.9 Scenario A: candidates and test statistics for epoch 5 . . . 232
B.10 Scenario A: adjusted coordinates and standard deviations for epoch 2 . . . 233
B.11 Scenario A: adjusted coordinates and standard deviations for epoch 3 . . . 234
B.12 Scenario A: adjusted coordinates and standard deviations for epoch 4 . . . 234
B.13 Scenario A: adjusted coordinates and standard deviations for epoch 5 . . . 235
B.14 Scenario B: adjusted coordinates and standard deviations of epoch 1 . . . 236
B.15 Scenario B: adjusted coordinates and standard deviations of epoch 2 . . . 236
B.16 Scenario B: adjusted coordinates and standard deviations of epoch 3 . . . 237
B.17 Scenario B: adjusted coordinates and standard deviations of epoch 4 . . . 237
B.18 Scenario B: adjusted coordinates and standard deviations of epoch 5 . . . 238
B.19 Scenario B: candidates of six points and statistical test for epoch 4 . . . 239
B.20 Scenario B: candidates of four points and statistical test for epoch 5 . . . 240
B.21 Scenario B: candidates of three points and statistical test for epoch 5 . . . 242
B.22 Scenario B: candidates and test statistics for epoch 5 . . . 245

C.1 Adjusted HPTN coordinates and standard deviations in Summer 2008 (epoch 1) . . . 246
C.2 Adjusted HPTN coordinates and standard deviations in Fall 2009 (epoch 2) 246
C.3 Adjusted HPTN coordinates and standard deviations in Fall 2010 (epoch 3) 247
C.4 Adjusted HPTN coordinates and standard deviations in Fall 2011 (epoch 4) 247
C.5 Statistical evaluation of candidates for largest similar point group between epochs 2 and 3 . . . 248
C.6 Statistical evaluation of candidates for largest similar point group between epochs 2 and 4 . . . 249

C.7 Statistical evaluation of candidates for largest similar point group between epochs 3 and 4 251
C.8 Statistical evaluation of candidates for largest similar point group between epochs 2 and 3 252
C.9 Statistical evaluation of candidates for largest similar point group between epochs 2 and 4 252
C.10 Statistical evaluation of candidates for largest similar point group between epochs 3 and 4 253

List of Figures and Illustrations

2.1 2D network with observations indicated by arrows 7
2.2 Classification of Network Datum Definitions 12
2.3 Plot of network with total trace minimization 22
2.4 Plot of network with partial trace minimization 23
2.5 Plot of network with ordinary minimal constraints 24
2.6 Plot of over-constrained network 25
2.7 Plot of network with weak datum 26
2.8 Analysis Models for Structural Monitoring, (Welsch et al., 2000b) 28
2.9 Five point network 52

3.1 Example network with all angles shown 92
3.2 Rotation in 3D space using quaternions 97

4.1 Simulated monitoring network with observations indicated by arrows 121

5.1 Frank Slide / Turtle Mountain, Alberta 173
5.2 The Saddle area of Turtle Mountain where the Frank Slide broke free with North and South Peak 174
5.3 Top view of the Frank slide with locations of HPTN points, *(Google Earth, 2012)* 175
5.4 Prism on monitoring pillar (left) and Leica TCA 2003 pointing at South Peak (right) 176
5.5 Top view (left) and side view (right) of a pillar cap showing the reference point (red dot) for all measurements 177
5.6 Network in Summer 2008 with observations indicated by arrows 178
5.7 Network in Fall 2009 with observations indicated by arrows 178
5.8 HPTN points 15 and 17 with their corresponding gravity vectors 179
5.9 Horizontal deformations of HPTN points between Summer 2008 (epoch 1) and Fall 2011 (epoch 4) 196
5.10 Vertical deformations of HPTN points between Summer 2008 (epoch 1) and Fall 2011 (epoch 4) 196

List of Symbols, Abbreviations and Nomenclature

Symbol	Definition
AGS	Alberta Geological Survey
GH	Gauss-Helmert
GM	Gauss-Markov
GNSS	Global Navigation Satellite System
GPS	Global Positioning System
HPTN	High-Precision Terrestrial Network
LMS	Least Median Squares
LS	Least-Squares
MEC	Multiple-Epoch Comparison
MPT	Multi-Parameter Transformation
MSS	Maximum SubSample
PEDS	Precise Engineering and Deformation Surveys
RTK-GPS	Real Time Kinematic GPS
TEC	Two-Epoch Comparison
TLS	Terrestrial Laser Scanning
TLS	Total Least-Squares
UTM	Universal Transversal Mercator
WGS84	World Geodetic System 1984

Chapter 1

INTRODUCTION

Deformation Monitoring is a sensitive and responsible task in Geomatics Engineering. Geodetic monitoring surveys aim to recover geometric changes – *deformations* – of a structure over time. Typical monitoring objects include bridges, large dams, towers, industrial installations (e. g. turbines) as well as natural structures such as slide-endangered slopes, glaciers and tectonic plates.

The benefits of deformation monitoring are the improvement of safety by reduction of the risk of structural failure and the refinement of the structural design process for future applications. Past experience has shown that these benefits have been realized when a monitoring scheme was carefully designed and its data properly analyzed. Past experience also includes catastrophic failures of structures which were not monitored or improperly monitored. (Teskey, 1987).

Deformation monitoring is crucial to public safety in early-warning systems for rock slides, e. g. the Frank Slide / Turtle Mountain in Southern Alberta, (Fraser and Gründig, 1985; Ebeling et al., 2011), or active earthquake zones, (Denli, 2004). It is also essential to guarantee the stability and structural integrity of large buildings, such as the Calgary Tower, (Lovse et al., 1995). The underlying problem is delicate as often the deformations to be recovered are of the same order of magnitude as the accuracies of the observations from which they are derived, (Gründig and Bahndorf, 1984).

The technology applied to collect geodetic observations for monitoring purposes vastly progressed in the last few decades from mechanical theodolites and levels, (Wolf and Ghilani, 2006), to automated monitoring systems utilizing self-targeting, fully-robotic, high-precision

total stations, (Whitaker et al., 2000; Mateus, 2008), as well as GNSS receivers, (Kim et al., 2003; Bond et al., 2008), and terrestrial laser scanners, (Monserrat and Crosetto, 2008; Lo et al., 2013).

In a very general, sense the typical procedure of determining geometric movements of a deforming structure can be described as follows. Discrete monitoring points are chosen on the monitored structure which represent the object's deformations. A set of stable control points is established which defines the reference frame for the movements. At discrete time intervals, or *epochs*, geodetic observations are collected that describe the relative geometry between the monitoring and control points.

From these observations a set of coordinates and their accuracies are estimated that describe the state of the monitoring network at each epoch. If data from multiple epochs is available, deformations that occurred between these epochs can be derived from a *congruence analysis*.

1.1 Motivation and Objectives

The classical congruence analysis consists of three major steps. First, a global congruency test is carried out to learn in which epochs deformations have occurred. Then, the localization step follows in which the deformed points are identified. Typically, a single-point analysis is applied consisting of an individual local F-test for each point based on its coordinate differences between epochs. Finally, a re-adjustment of the combined observations of all epochs is performed to obtain deformations for the unstable points.

The single-point analysis typically used in the localization step, requires the two epochs under comparison to refer to the same network datum. If this is not the case, an S-transformation to a common datum can be applied. This, however, is only possible if both epochs share the same reference frame and particularly the same network scale.

While in a typical monitoring scenario the analysis of all epochs is performed in the same reference frame, the scale can often vary. The reason for the change in scale are different atmospheric conditions in each observation campaign that cannot be accurately captured. Often atmospheric conditions are only observed at the instrument station and the target points, or maybe only at the instrument stations if the target points are not accessible, but typically not along the line of observation in between them. This leads to an approximation of the true conditions which can differ throughout the network and the time of observation, particularly if observation lines with large height differences or across water exist. Furthermore, the use of different instruments in different epochs, which may or may not be properly and regularly calibrated, add to the problem. If not taken into account, scale differences between epochs can cause apparent point movements in a deformation analysis. Especially in large networks even a slight change in the scale factor can affect the outcome of a deformation analysis significantly.

Thus, the need arises for a methodology that allows to locate and determine deformations independent of and unaffected by a change in scale between epochs. A further independence of the coordinate system yields a greater flexibility in the design of a monitoring network and the choice of instrumentation.

1.2 Thesis Outline

This dissertation proposes a generalized mathematical model for a congruence analysis. It begins with a review of the well-established methodology for a deformation analysis and investigates alternative techniques. The proposed mathematical model is derived and explained in detail. The results from a series of simulations are presented and finally the proposed algorithm is demonstrated on a real-world application.

In detail this thesis is divided into the following chapters:

Chapter 2 provides an overview of the different observation types which are used to derive deformations. The geodetic network analysis is reviewed with special emphasis on the topic of datum definition which plays an important role in the derivation of deformations. The classical congruence analysis is examined closely. Recent developments in the area of deformation monitoring are investigated. Special attention is paid to the localization of unstable points in the data. 3D similarity transformations as an alternative approach to determine deformations are investigated.

Chapter 3 presents the derivation of a generalized mathematical model for a congruence analysis consisting of an algorithm for the localization of the largest similar point group between two epochs based on their angular differences which is independent of the scale or coordinate system of the given coordinates. Deformations are determined using a 3D HELMERT transformation in which the adjusted coordinates from each epoch are introduced as observations. Their fully-populated and singular cofactor matrices can be directly used in the adjustment without any preprocessing. Then, this model is extended to allow the comparison of multiple epochs simultaneously.

Chapter 4 shows results from two sets of computer simulations carried out to evaluate the performance of the proposed algorithm. The first case depicts a typical scenario where all epochs are given in the same reference frame and datum. In the second scenario the epochs are given in two completely different coordinate systems.

Chapter 5 then presents a real-world application where the proposed methodology was utilized to recover deformations. At the Frank Slide on Turtle Mountain, Alberta a small, high-precision terrestrial monitoring network has been observed in four epochs to recover long-term movements of very small magnitude.

Chapter 6 summarizes the findings from this thesis, offers conclusions drawn from the results achieved as well as recommendations for future work.

Chapter 2

BACKGROUND

2.1 Observation techniques

Deformations are derived from observations. Different observation techniques can be applied to determine deformations of an object. According to Erol et al. (2004), they can be divided into two classes, *geodetic* and *non-geodetic* techniques.

The group of non-geodetic techniques refers to geotechnical or structural measurements where the engineering properties of soil and rock are the factors of interest. A large assortment of versatile instrumentation for the monitoring of geotechnically related parameters exists including stressmeters, inclinometers, piezometers, strain gauges and extensometers. (Dunnicliff, 1988). Measurements from geotechnical instrumentation can only provide relative deformations, (Teskey, 1987). Generally, deformations of an object are measured directly. Thus non-geodetic measurements are not discussed any further in this thesis.

Geodetic methods include conventional terrestrial techniques such as the use of theodolites / total stations and levels (Guler et al., 2006), photogrammetric techniques (terrestrial, (Fraser and Riedel, 2000; Detchev et al., 2012), as well as aerial, (Fraser and Gründig, 1985)) and laser scanning (Gielsdorf et al., 2008; Gordon and Lichti, 2007), as well as space-based techniques, (DeLoach, 1989; Radovanovic, 2002). They allow the determination of deformations in 3D space and in an absolute sense, i. e. with respect to a given reference frame, (Teskey, 1987). Since geodetic observations techniques provide the data which form the foundation for the mathematical models discussed in this thesis, their main characteristics are briefly reviewed below.

2.1.1 Geodetic observation techniques

Conventional terrestrial techniques, commonly employing total stations and levels, are carried out with respect to the Earth's gravity field (i. e. the geoid) by means of leveling the instrument. They provide relative measurements between survey points (angles, distances and height differences). If proper procedures are followed and all significant systematic errors are taken into account, they can deliver high-precision results. (Uren and Price, 2006).

A line of sight is required between instrument and target and distances between survey points are limited to a few kilometres, (Rüeger, 1990), or even a few hundred metres for high-precision surveys. Observations as well as their accuracies are weather dependent. Conventional terrestrial techniques can be applied in outdoor and indoor environments.

Space-based radio ranging systems like GPS can provide absolute positions with respect to the Earth's centre of mass. These positions are defined by ellipsoidal latitude, longitude and elevation with respect to the World Geodetic System 1984 (WGS84). (Misra and Enge, 2006).

Space-based ranging systems are all-weather systems which makes them more economical. They do not require a direct line of sight between surveyed stations. This allows for greater flexibility in the selection of object point locations and for measurements over distances of hundreds of kilometres. (Erol et al., 2004).

However, a clear, unobstructed view of the sky is needed. Thus, for purposes of surveying they are limited to outdoor applications. Although three-dimensional positioning is provided, the height component is the least accurate coordinate, mainly due to inherent geometric weakness and atmospheric errors, (Featherstone et al., 1998).

Aerial photogrammetry can provide 3D information of large areas with high redundancy. The data collection is weather-dependent and rather costly. Similar to GPS, the horizontal accuracy is better than the vertical accuracy due to a weak geometry. (McGlone, 2004).

Photogrammetric and laser scanning techniques can reconstruct entire surfaces and not just specific, signalized target points, (Lichti et al., 2000). Furthermore, there is no need to access the object being monitored, (Detchev et al., 2011a). Current photogrammetric systems can be built from inexpensive, replaceable sensors, (Detchev et al., 2011a), which is desired for monitoring systems. Close-range photogrammetry can deliver sub-millimetre accuracy for 3D objects, (Detchev et al., 2011b), and can be applied in indoor as well as outdoor environments.

2.1.2 Example

To illustrate the use of geodetic observations following is an example of a small two-dimensional monitoring network consisting of five points. Figure 2.1 shows the network with arrows in-

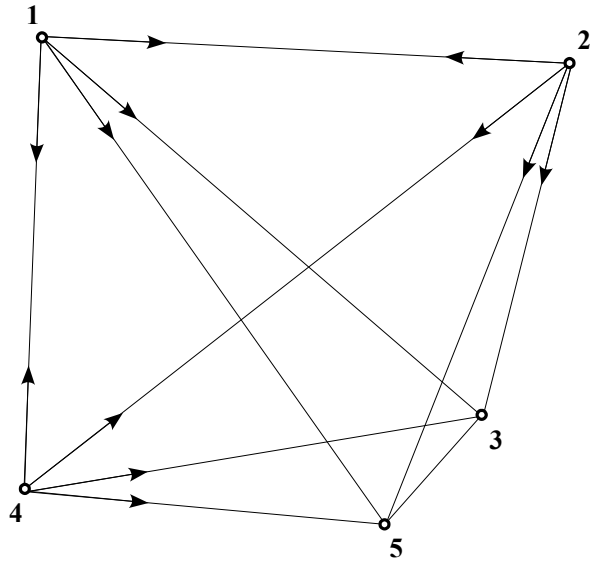

Figure 2.1: 2D network with observations indicated by arrows

From Point	To Point	Horizontal Direction [deg]	Horizontal Distance [m]
1	2	92.7921	81.950
1	3	130.6414	89.920
1	4	182.1764	70.123
1	5	145.3360	91.871
2	1	272.7905	81.962
2	3	194.0300	56.261
2	4	231.9890	107.285
2	5	202.4811	77.470
4	1	2.1768	70.116
4	2	51.9859	107.281
4	3	80.7930	71.799
4	5	95.7183	55.173

Table 2.1: Relative observations between network points

dicating the observations made between points. In this example conventional terrestrial observations were taken, consisting of horizontal directions and horizontal distances from points 1, 2 and 4 to all points in the network. Typically, several sets of measurements are observed in order to identify potential outliers in the data and increase precision. Averages

of the measurements are listed in Table 2.1.

2.2 Network analysis

To prepare the collected observations for deformation detection, a network analysis is required first. Most observations are relative measurements between points and movements derived directly from those relative measurements would be very difficult to interpret and inconclusive. Also, heterogeneous and redundant information from a number of different sources with varying accuracies may be available. Thus the necessity arises to derive a homogeneous set of coordinates that describes the network geometry at time of observation. For this to be possible a coordinate reference frame and geodetic datum are defined during the network analysis in which then deformations are expressed.

Furthermore, a network analysis allows to account for systematic errors inherent in the data and, with redundant information available, outliers can be detected in the observations. The remaining random errors can then be minimized. The variance-covariance matrix for the estimated coordinate vector is also obtained as a result of the network analysis. It is essential for the statistical evaluation of possible movements during the deformation analysis to follow.

Typically, a network analysis is performed using a parametric least-squares adjustment, also referred to as a Gauss-Markov model, which can be expressed in the form, (Niemeier, 2002)

$$\vec{l} + \vec{v} = f\left(\vec{x}\right) \tag{2.1}$$

where $\vec{l}$ denotes the observation vector, $\vec{v}$ its residuals and $\vec{x}$ the parameter vector consisting of the unknown coordinates and additional nuisance parameters, such as scale or orientation offsets, as required.

Often the functional relationship f between the observations $\vec{l}$ and the parameters $\vec{x}$ is non-linear. Thus, linearization of (2.1) and initial estimates $\vec{x}_0$ for the unknown parameters $\vec{x}$ are required. Given the relations $\vec{x} = \vec{x}_0 + \Delta\vec{x}$ and $\vec{l} = f(\vec{x}_0) + \Delta\vec{l}$, equation (2.1) can be linearized using a first-order Taylor series approximation:

$$\vec{l} + \vec{v} = f\left(\vec{x}\right) = \left.\frac{\partial f}{\partial \vec{x}}\right|_{\vec{x}=\vec{x}_0} \cdot \left(\vec{x} - \vec{x}_0\right) + f\left(\vec{x}_0\right) \tag{2.2a}$$

$$\underbrace{\vec{l} - f\left(\vec{x}_0\right)}_{=\Delta\vec{l}} + \vec{v} = \underbrace{\left.\frac{\partial f}{\partial \vec{x}}\right|_{\vec{x}=\vec{x}_0}}_{=\mathbf{A}} \cdot \underbrace{\left(\vec{x} - \vec{x}_0\right)}_{=\Delta\vec{x}} \tag{2.2b}$$

$$\Delta\vec{l} + \vec{v} = \mathbf{A} \cdot \Delta\vec{x} \tag{2.2c}$$

where the design matrix $\mathbf{A}$ contains the partial derivatives of the observation equations f with respect to to the unknown parameters $\vec{x}$. The vector of corrections $\Delta\vec{x}$ for the parameters represents the actual unknowns to be solved for. Similarly, the misclosure vector $\Delta\vec{l}$ represents the actual observations introduced in the adjustment. [1]

With the covariance matrix $\mathbf{C}_{ll}$ for the observations $\vec{l}$ and the a priori variance factor σ_0^2, the weight matrix $\mathbf{P}$ for the observations can be derived from

$$\mathbf{P} = \sigma_0^2 \cdot \mathbf{C}_{ll}^{-1} \, . \tag{2.3}$$

This requires the covariance matrix $\mathbf{C}_{ll}$ to be invertible. In a network analysis this is generally the case, although correlations may exist, e. g. for horizontal angles referring to the same back-sight or for horizontal distances and height differences derived from zenith angles and slope distances. Typically, the observation variances are either derived as variance of the mean, if multiple sets of observations are available, or can be based on instrument specifications provided by the manufacturer.

For a network with n observations and u unknowns, with $n > u$, a unique solution does not exist. To obtain a unique solution an additional condition needs to be introduced. In the

[1] It should be noted that $\vec{x}_0$ and $f(\vec{x}_0)$ represent the deterministic parts while $\Delta\vec{x}$ and $\Delta\vec{l}$ represent the stochastic parts of the parameters $\vec{x}$ and the observations $\vec{l}$, respectively.

case of a least-squares estimation, this condition minimizes the weighted squared sum of the residuals:

$$\Phi = \vec{v}^T \mathbf{P} \vec{v} \rightarrow \min \tag{2.4}$$

The least-squares normal equations for the parametric case can then be obtained by substituting $\vec{v}$ in the variation function Φ above with the linearized observation equation (2.2c) and setting its first derivative to zero. This yields

$$\underset{(u\times n)}{\mathbf{A}^T} \underset{(n\times n)}{\mathbf{P}} \underset{(n\times u)}{\mathbf{A}} \cdot \underset{(u\times 1)}{\Delta\vec{x}} = \underset{(u\times n)}{\mathbf{A}^T} \underset{(n\times n)}{\mathbf{P}} \cdot \underset{(n\times 1)}{\Delta\vec{l}} \tag{2.5}$$

And substituting $\mathbf{A}^T\mathbf{P}\mathbf{A}$ with the normal equation matrix $\mathbf{N}$, the normal equations read

$$\underset{(u\times u)}{\mathbf{N}} \cdot \underset{(u\times 1)}{\Delta\vec{x}} = \underset{(u\times n)}{\mathbf{A}^T} \underset{(n\times n)}{\mathbf{P}} \cdot \underset{(n\times 1)}{\Delta\vec{l}} \tag{2.6}$$

A unique solution for the above normal equations only exists if the normal equation matrix $\mathbf{N}$ is regular and thus invertible. In a network analysis, where the parameter vector consists of the coordinates of the network points (plus required nuisance parameters), this is often not the case, as most observations are relative measurements and do not relate to a coordinate frame. Hence, a *datum definition* is required to link the observations to the coordinates of the network points.

2.2.1 Datum definition

In a 3D network there are seven datum parameters required to define the geodetic datum of the network completely: three rotations defining the orientation of the coordinate axes, three translations defining the origin and a scale factor defining distances in the coordinate system. Those datum parameters can be described by the observations themselves. Table 2.2 gives an overview of the most common geodetic observation types and the datum parameters in a 3D network which they define. Linear observation types, such as distances, coordinate differences or absolute coordinates can be used to define the scale of a network. Angles or

Observation Types	Datum Parameters						
	Rotation			Translation			Scale
	r_x	r_y	r_z	T_x	T_y	T_z	λ
Distances	x	x	x	x	x	x	✓
Horizontal directions/angles	x	x	x	x	x	x	x
Azimuth	x	x	✓	x	x	x	x
Zenith angles	✓	✓	x	x	x	x	x
GPS positions	✓	✓	✓	✓	✓	✓	✓
3D position differences	✓	✓	✓	x	x	x	✓
2D position differences	x	x	✓	x	x	x	✓
Height differences	✓	✓	x	x	x	x	✓

Table 2.2: Datum contributions of geodetic measurements, (Kuang, 1996)

directions in a horizontal plane do not carry any datum information. Azimuth observations define the orientation in the horizontal plane while zenith angles describe the rotations about the x- and y-axes. At least two zenith angles at different orientations are required to define both x- and y-rotation, (Niemeier, 2002). 3D positions, as derived from GPS measurements, are the only observation type that can fully define all seven datum parameters. Position differences in 3D describe all three rotations but not the translations while 2D position differences only describe the orientation in the horizontal plane. Height differences instead define the two rotations about the x- and y-axes.

Unless at least one absolute point position has been observed to define the three translations, not all seven datum parameters are described by the observations. In this case it is not possible to estimate coordinates from the observation vector $\vec{l}$ alone. The resulting normal equation matrix $\mathbf{N} = \mathbf{A}^T\mathbf{PA}$ is *rank-deficient* by the number of undefined – or free – datum parameters d, and is thus singular. There are several ways to define the missing, or free, parameters. The way in which they are defined is important because the results of a deformation analysis heavily depend on the chosen network datum. Hence, the different options to define a network datum are discussed in detail below.

The approaches to define the geodetic datum of a network can be divided into two categories,

namely *free* and *constraint*. Free, or inner-constraint, approaches refer to those that do not affect the geometry of the network, whereas constraint approaches can distort the network geometry. Figure 2.2 categorizes the different approaches.

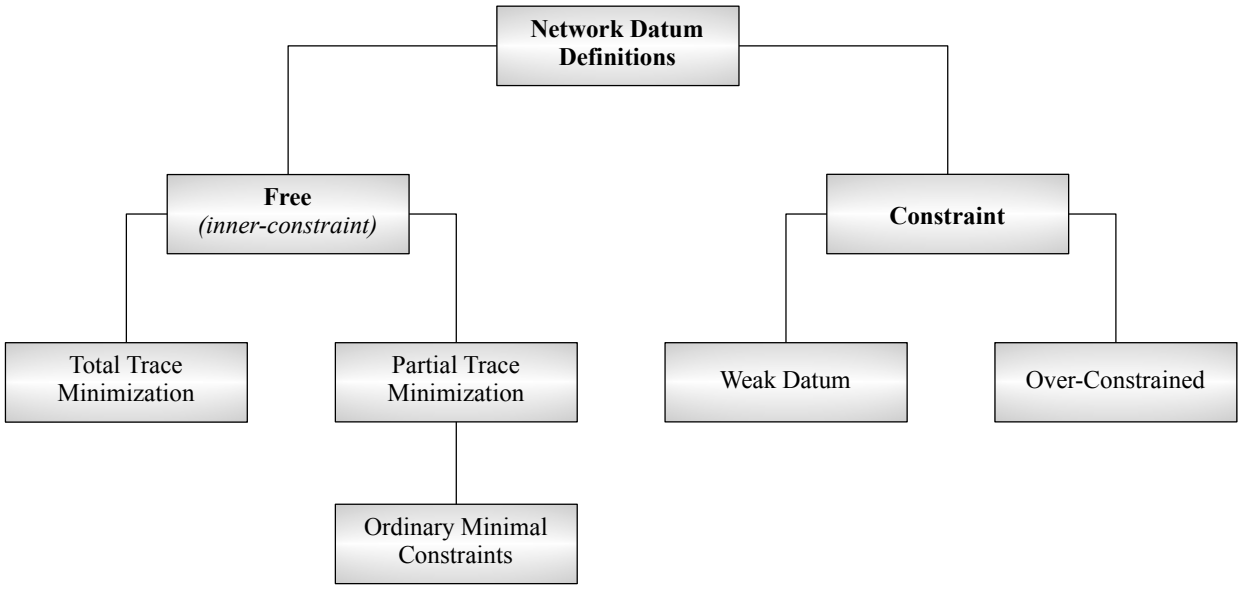

Figure 2.2: Classification of Network Datum Definitions

2.2.1.1 Inner-constraint approaches

Inner-constraint approaches are implemented by adding certain conditions for the vector of coordinate corrections $\Delta\vec{x}$ which define the d remaining free datum parameters. The following condition equations can be used to define the seven datum parameters for a 3D network, the translations along the x-, y- and z-axes, rotations about the x-, y- and z-axes and scale factor, (Teskey, 1989):

$$\begin{aligned} &\sum \Delta x_i = 0 && \sum (z_i^0 \Delta y_i - y_i^0 \Delta z_i) = 0 \\ &\sum \Delta y_i = 0 && \sum (x_i^0 \Delta z_i - z_i^0 \Delta x_i) = 0 \\ &\sum \Delta z_i = 0 && \sum (y_i^0 \Delta x_i - x_i^0 \Delta y_i) = 0 \\ &\sum (x_i^0 \Delta x_i + y_i^0 \Delta y_i + z_i^0 \Delta z_i) = 0 \ . \end{aligned} \tag{2.7}$$

In which Δx_i, Δy_i and Δz_i are the corrections to the initial coordinates as determined in the adjustment and x_i^0, y_i^0 and z_i^0 represent the initial coordinates of point i. This corresponds

to a 3D HELMERT transformation of the adjusted coordinates $\vec{x}$ to the initial estimates $\vec{x}_0$, (Niemeier, 2002).

The first three equations on the left in (2.7) define the translations in a way so that the centroid of the datum points derived from the adjusted coordinates $\vec{x}$ coincides with the centroid of the initial coordinates $\vec{x}_0$ of the chosen datum points. Similarly, the three equations on the right in (2.7) determine the rotations so that the net rotation about the centroid is zero, i. e. the axes of the system of the adjusted coordinates are parallel to those of the system of the initial coordinates. Finally, the last equation in (2.7) fixes the scale factor such that the average distance from the centroid to each of the datum points computed from the initial coordinates is equal to that computed from the adjusted coordinates, (Kuang, 1996).

In an inner-constraint approach the free datum parameters are essentially defined by the initial coordinates $\vec{x}_0$ which thus play a very important role in the datum definition.

A special characteristic of the inner-constraint approach is that the trace of the cofactor matrix $\mathbf{Q}_{xx} = \mathbf{N}^{+}$ of the adjusted coordinates is minimized for all datum points. Mathematically this is accomplished by introducing the additional requirement

$$\Delta\vec{x}_D^{\,T} \cdot \Delta\vec{x}_D \rightarrow \min \tag{2.8}$$

in the derivation of the condition equations (2.7), where $\Delta\vec{x}_D$ denotes the corrections for the datum-contributing points, (Kuang, 1996).

This allows to influence the variances of the network points by choosing which of the points contribute to the network datum. Two cases can be distinguished, often referred to as *total trace minimization* and *partial trace minimization*.

In the case of a total trace minimization, the conditions (2.7) are introduced for the whole parameter vector $\vec{x}$. This results in a minimized trace for all elements of the cofactor matrix $\mathbf{Q}_{xx}$, (Gründig and Bahndorf, 1984). It should be noted that this is only possible if no additional nuisance parameters, such as scale or zero error, exist and the parameter vector only

consists of the unknown coordinates. The conditions (2.7) obviously cannot be introduced for additional parameters and similar conditions for non-coordinate parameters cannot be geometrically interpreted, (Niemeier, 2002).

A partial trace minimization is achieved if the datum-defining condition equations (2.7) are only introduced for a subset of coordinates in the parameter vector $\vec{x}$. In this case only the trace of the submatrix of $\mathbf{Q}_{xx}$ corresponding to the participating coordinates are minimized, (Niemeier, 2002). If the parameter vector consists of coordinates as well as nuisance parameters, such as scale, zero error, orientation offsets, etc., typically a partial trace minimization is applied.

A special case of a partial trace minimization exists when only the minimum number of coordinates required to describe the d free datum parameters are used in the datum definition. This is referred to as *ordinary minimal constraints*, (Wolf and Ghilani, 1997). It is equivalent to fixing d coordinates and removing them from the parameter vector. For example, in a 2D network with measurements consisting of horizontal distances and horizontal directions, there are three free datum parameters – the translations along the x- and y-axes and the rotation about the z-axis. Assigning fixed values to the x- and y-coordinates of one point and the x-coordinate of a second point, and thus removing those three coordinates from the parameter vector, is sufficient to define the datum. The resulting normal equation matrix will be invertible. At the same time this results in the variances of the three fixed coordinates being zero, as they no longer participate in the adjustment. This is also referred to as a *zero-variance computational base*.

This property of an inner-constraint approach becomes obvious in the case depicted above. It does however exist for all inner-constraint scenarios. Neitzel (2004) shows that in case of a total trace minimization, the network centroid and the net-rotation angle between the initial and adjusted coordinates form a zero-variance computational base. The difference is that with a total trace minimization all points contribute equally to the definition of the

zero-variance elements. In any case a number of elements equivalent to the number of free datum parameters are assigned a zero variance.

For this reason the resulting cofactor matrix $\mathbf{Q}_{xx}$ from an inner-constraint approach is rank-deficient by the number of free datum parameters d. This becomes important when cofactor matrices from a free network adjustment need to be processed, for example, in a deformation analysis.

All inner-constraint approaches define the network datum through the use of additional condition equations for the coordinate corrections $\Delta\vec{x}$ (inner-constraints). The inner geometry of the network always remains undisturbed.

In practice, the implementation of an inner-constraint approach is achieved by linearizing the datum conditions (2.7) at $\vec{x}_0$. This yields the datum matrix $\mathbf{D}$ which contains the partial derivatives of the datum conditions (2.7) with respect to the elements of the parameter vector $\vec{x}$. Given a 3D network with all $d = 7$ datum parameters to be defined by inner-constraints, the datum matrix $\mathbf{D}_i$ for a single point i has the following form

$$\underset{(3\times d)}{\mathbf{D}_i^T} = \begin{bmatrix} 1 & 0 & 0 & 0 & -z_i^0 & y_i^0 & x_i^0 \\ 0 & 1 & 0 & z_i^0 & 0 & -x_i^0 & y_i^0 \\ 0 & 0 & 1 & -y_i^0 & x_i^0 & 0 & z_i^0 \end{bmatrix} \tag{2.9}$$

The first three columns define the translations in x, y and z, respectively. The following three columns define the rotations about the x, y and z-axes and the last column defines the network scale. For points not contributing to the network datum, the elements of the corresponding submatrix are all equal to zero. The datum matrix $\mathbf{D}$ is obtained by concatenating the submatrices $\mathbf{D}_i$ for all points. For a total trace minimization of a network with p points and $u = 3 \cdot p$ unknown parameters the following datum matrix $\mathbf{D}$ is obtained

$$\underset{(d\times u)}{\mathbf{D}} = \begin{bmatrix} \mathbf{D}_1 & \dots & \mathbf{D}_i & \dots & \mathbf{D}_p \end{bmatrix} \tag{2.10}$$

The extended linearized Gauss-Markov model can then be written as

$$\begin{aligned} \Delta\vec{l} + \vec{v} &= \mathbf{A} \cdot \Delta\vec{x} \\ \vec{0} &= \mathbf{D}^T \cdot \Delta\vec{x} \end{aligned} \tag{2.11}$$

The singular normal equation matrix $\mathbf{N} = \mathbf{A}^T\mathbf{P}\mathbf{A}$ is augmented with the datum matrix $\mathbf{D}$ to obtain the expanded, regular normal equation system

$$\underset{(u+d)\times(u+d)}{\begin{bmatrix} \mathbf{A}^T\mathbf{P}\mathbf{A} & \mathbf{D}^T \\ \mathbf{D} & 0 \end{bmatrix}} \cdot \underset{(u+d)\times 1}{\begin{pmatrix} \Delta\vec{x} \\ \vec{k} \end{pmatrix}} = \underset{(u+d)\times 1}{\begin{pmatrix} \mathbf{A}^T\mathbf{P} \cdot \Delta\vec{l} \\ 0 \end{pmatrix}} \tag{2.12}$$

where $\vec{k}$ denotes a vector of correlates or Lagrange multipliers.

2.2.1.2 Constraint approaches

Unlike free approaches, constraint approaches can in principle distort the network geometry. This is achieved in one of two ways.

An *over-constrained* approach is obtained when more coordinates than the number of free datum parameters d are held fixed in the adjustment. This is done by removing the datum-defining coordinates from the parameter vector $\vec{x}$. In the observation equations and their derivatives, these coordinates are treated as constants.

This approach is typically applied when an existing network is densified and the coordinates of the existing tie points are not to be changed. As a result, the inner geometry of the new network – as defined by the observations – is adapted to fit the geometry of the existing tie points. Depending on the quality of these tie points, the network geometry is distorted. Variances for the tie points cannot be estimated. Thus an identity check for these points is not possible. (Niemeier, 2002).

A so-called *weak datum* or *adjustment with stochastic a priori information* is obtained when the coordinates of the tie points are introduced as additional observations in the adjustment

rather than being eliminated completely. So instead of reducing the parameter vector, the observation vector is extended. Often the tie points are only known with a certain accuracy, so that it is not justified to use them with zero variances (over-constrained approach). (Niemeier, 2002).

The advantage of treating the tie points as observations is that a priori stochastic information about their quality can be taken into account in the adjustment in the covariance matrix of the observations. This a priori information can either be the result from a previous analysis or merely estimates. The effect on the network geometry depends on the variances associated with the coordinate observations. If their variances are large compared to the observation variances, the geometry remains largely intact. If the variances of the observed coordinates are small in comparison to the other observations, the distortion of the network geometry increases. (Niemeier, 2002).

2.2.1.3 S-transformation

The adjusted coordinates $\vec{x}$ and their cofactor matrix $\mathbf{Q}_{xx}$ are datum-dependent, i. e. the actual results of a network adjustment for the elements of the parameter vector and their standard deviations will vary depending on which points have been chosen to define the datum. In certain situations it is necessary to change the datum of a network. This can be the case in a deformation analysis in order to maintain a stable computational base if one (or more) of the datum points have been found to be unstable. If an inner-constraint approach was used to define the geodetic datum during the network analysis, it is not necessary to repeat the network adjustment with a different datum definition, instead an S-transformation can be used to obtain the coordinate vector and its cofactor matrix with respect to the new datum, (Gründig et al., 1985).

The following equations describe the transformation of the datum-dependent coordinate vector $\vec{x}_i$ and its associated cofactor matrix $\mathbf{Q}_{xx_i}$ from any arbitrary datum i to a certain

datum j as given in Gründig et al. (1985)

$$\vec{x}_j = \mathbf{S}_j \vec{x}_i \qquad \mathbf{Q}_{xx_j} = \mathbf{S}_j \mathbf{Q}_{xx_i} \mathbf{S}_j^T \tag{2.13}$$

The transformation matrix $\mathbf{S}_j$ is given by

$$\mathbf{S}_j = \mathbf{I} - \mathbf{D}^T (\mathbf{D}\mathbf{I}_R \mathbf{D}^T)^{-1} \mathbf{D}\mathbf{I}_R \tag{2.14}$$

where $\mathbf{D}$ is the datum matrix from (2.10), fully populated for all network points. The selective identity matrix $\mathbf{I}_R$ is only filled at the R^{th} positions of those coordinates which will contribute to the new datum. This allows to formulate the computational base so that it consists of all coordinates, any subset of coordinates or only the minimum number of coordinates necessary.

It is important to point out that an S-transformation can only be applied if both, the old datum i and the new datum j refer to the same set of initial coordinates, i. e. that the datum matrix $\mathbf{D}$ in (2.14) has to be populated from the same initial coordinate vector $\vec{x}_0$ that has been used in the original datum definition.

2.2.2 Solution and analysis of results

For the inner-constraint case the solution of the normal equation system can be obtained by inverting the expanded normal equation matrix and multiplying equation (2.12) with the inverse from the left. This yields

$$\underset{(u+d)\times 1}{\begin{pmatrix} \Delta\vec{x} \\ \vec{k} \end{pmatrix}} = \underset{(u+d)\times(u+d)}{\begin{bmatrix} \mathbf{A}^T\mathbf{P}\mathbf{A} & \mathbf{D}^T \\ \mathbf{D} & 0 \end{bmatrix}^{-1}} \cdot \underset{(u+d)\times 1}{\begin{pmatrix} \mathbf{A}^T\mathbf{P} \cdot \Delta\vec{l} \\ 0 \end{pmatrix}} \tag{2.15}$$

For a constraint case the rank defect is eliminated by either the reduction of the parameter vector in case of an over-constrained approach or through the additional information provided by the coordinate observations in a weak-datum approach. In either case the resulting normal

equation system in the form of (2.6) will be regular and the solution can directly be obtained through inversion of the normal equation matrix $\mathbf{N}$ and multiplication with its inverse from the left.

$$\underset{(u\times 1)}{\Delta\vec{x}} = \underset{(u\times u)}{\mathbf{N}^{-1}} \cdot \underset{(u\times n)}{\mathbf{A}^T} \underset{(n\times n)}{\mathbf{P}} \cdot \underset{(n\times 1)}{\Delta\vec{l}} \tag{2.16}$$

After the corrections $\Delta\vec{x}$ are obtained, the parameter vector is updated:

$$\vec{x}_i = \vec{x}_{i-1} + \Delta\vec{x} \tag{2.17}$$

where $\vec{x}_i$ is the estimate of the i^{th} iteration for the parameter vector $\vec{x}$.[2]

As the original adjustment problem is a non-linear one, substituted by a linearized problem, iteration is required until convergence to the non-linear solution is reached. Hence, the misclosure vector $\Delta\vec{l}$ of the observations and the design matrix $\mathbf{A}$ need to be updated with the updated parameter vector:

$$\underset{(n\times 1)}{\Delta\vec{l}} = \underset{(n\times 1)}{\vec{l}} - \underset{(n\times 1)}{f\left(\vec{x}_i\right)} \qquad \underset{(n\times u)}{\mathbf{A}} = \left.\frac{\partial f}{\partial \vec{x}}\right|_{\vec{x}=\vec{x}_i} \tag{2.18}$$

It is important to stress that the datum matrix $\mathbf{D}$, in case of an inner-constraint approach, must *not* be updated as this would correspond to a datum change in every iteration.

Now the next iteration's solution for the parameter corrections $\Delta\vec{x}$ can be determined from (2.15) or (2.16), respectively. This iterative process is repeated until the values for the parameter corrections $\Delta\vec{x}$ become sufficiently small.

Once convergence is reached, the observation residuals $\vec{v}$ are computed from

$$\underset{(n\times 1)}{\vec{v}} = \underset{(n\times 1)}{f\left(\vec{x}\right)} - \underset{(n\times 1)}{\vec{l}} \tag{2.19}$$

where $\vec{x}$ denotes the final estimate of the parameter vector and $\vec{l}$ the original observation vector. In some cases of slow convergence it is possible for the adjustment to converge but

[2]Note that $i = 0$ is represents the initial parameters $\vec{x}_0$.

not to the correct non-linear solution. Thus, a final check of the linearization should be performed according to:

$$\mathbf{A}^T\mathbf{P}\vec{v} < \delta \qquad \text{with } |\delta| > 0\,, \tag{2.20}$$

where $\vec{v}$ denote the non-linear residuals from (2.19) above and δ a chosen threshold for which the linearization error can be considered negligible.

The a posteriori variance factor $\hat{\sigma}_0^2$ then follows from

$$\hat{\sigma}_0^2 = \frac{\vec{v}^T\mathbf{P}\vec{v}}{n-u+d} \tag{2.21}$$

where $\mathbf{P}$ is the weight matrix of the observations from (2.3) and $n-u+d=r$ is the redundancy of the adjustment problem, where n is the number of observations, u the total number of unknown parameters and d denotes the number of free datum parameters.

To examine the validity of the obtained results, a *global test of the adjustment model* should be performed. This statistical test compares the the a posteriori (empirical) variance factor $\hat{\sigma}_0^2$ against the a priori (theoretical) variance factor σ_0^2 and allows to check the functional and the stochastical model as well as the conformity of the data with the applied models. The test can be carried out as follows:

- Test hypothesis H_0 : $E\left\{\sigma_0^2\right\} = E\left\{\hat{\sigma}_0^2\right\}$ (2.22a)
- Alternative hypothesis H_A : $E\left\{\sigma_0^2\right\} \neq E\left\{\hat{\sigma}_0^2\right\}$ (2.22b)
- Test statistic : $T_\chi = \dfrac{\hat{\sigma}_0^2}{\sigma_0^2}\cdot r$ (2.22c)

If the test statistic T_χ above falls in the interval of the χ^2-distribution with the boundaries defined by $\chi^2_{S=\alpha/2,f=r}$ and $\chi^2_{S=1-\alpha/2,f=r}$[3], the test hypothesis H_0 cannot be rejected and the test passes. Otherwise, the alternative hypothesis must be accepted and the test fails. Failure of this test indicates one (or more) of three things, (Niemeier, 2002):

- There are unmodelled systematic errors inherent in the data.

[3]Here, α denotes the chosen confidence level for the test and r the redundancy of the adjustment problem.

- There are outliers inherent in the data.
- The assumed a priori variances for the observations are unrealistic.

When the global test of the adjustment model passes, the covariance matrix $\mathbf{C}_{xx}$ of the estimated parameters $\vec{x}$ can be derived from

$$\mathbf{C}_{xx} = \hat{\sigma}_0^2 \cdot \mathbf{Q}_{xx} \tag{2.23}$$

where $\mathbf{Q}_{xx}$ denotes the cofactor matrix of the parameters which follows from the upper left $(u \times u)$ submatrix of the inverse of the normal equation matrix in (2.15) or (2.16), respectively. The empirical standard deviations $\hat{\sigma}_x$ of the estimated parameters $\vec{x}$ then follow from the square root of the main diagonal elements of the covariance matrix $\mathbf{C}_{xx}$.

2.2.3 Numerical examples

To illustrate the effect of different datum definitions on the adjusted network coordinates and their variances, the example from Section 2.1.2 is examined again. The network shown in Figure 2.1 shall be analyzed given the observations summarized in Table 2.1 and using different datum definitions. As scale-defining distance measurements are available in this 2D network, three free datum parameters remain, namely the rotation about the z-axis (orientation) and the two translations along the x- and y-axes.

A total of $n = 24$ observations are available, 12 horizontal directions and 12 horizontal distances, observed from the stations 1, 2 and 4 to all points in the network. The parameter vector consists of the coordinate pairs of the five network points and an additional orientation offset for each of the three instrument stations. This yields a total of $u = 13$ unknown parameters to be solved for. With $d = 3$ free datum parameters, the resulting redundancy is $r = n - u + d = 14$.

A coordinate reference frame is provided by the initial coordinates listed in Table 2.3 below.

Point	x^0	y^0
1	97.78	47.85
2	93.79	129.72
3	39.21	116.08
4	27.72	45.19
5	22.22	100.10

Table 2.3: Initial coordinates of network points in [m]

Total trace minimization

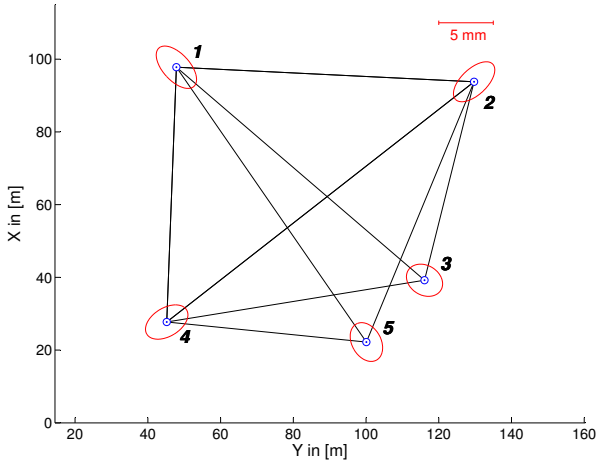

Figure 2.3: Plot of network with total trace minimization

Point	x [m]	y [m]	$\hat{\sigma}_x$ [mm]	$\hat{\sigma}_y$ [mm]
1	97.780	47.852	±1.9	±1.9
2	93.789	129.717	±1.8	±1.9
3	39.211	116.080	±1.5	±1.7
4	27.720	45.189	±1.6	±1.9
5	22.220	100.101	±1.8	±1.5

Table 2.4: Adjusted coordinates and their standard deviations for total trace minimization

First, the given network is adjusted by applying a total trace minimization[4] for the datum definition, so that all five points contribute equally to the network datum. The adjusted coordinates and their empirical standard deviations are listed in Table 2.4. Figure 2.3 shows a horizontal plot of the network points with their error ellipses at the 1σ-level in red. The red scale bar near the top represents the scale of the error ellipses.

The estimated standard deviations for all points are at about the same level, varying between ±1.5 mm and ±1.9 mm. For a total trace minimization the variance of a point increases with

[4]Technically it is a partial trace minimization since additional orientation offsets are estimated as well. However, the results are identical with a total trace minimization where the orientation offsets are eliminated by introducing horizontal angles rather than horizontal directions as observations.

its distance from the centre of the network (the zero-variance computational base). Since in this example, due to the shape of the network, all points are roughly the same distance away from the centre, their variances are at about the same level.

Partial trace minimization

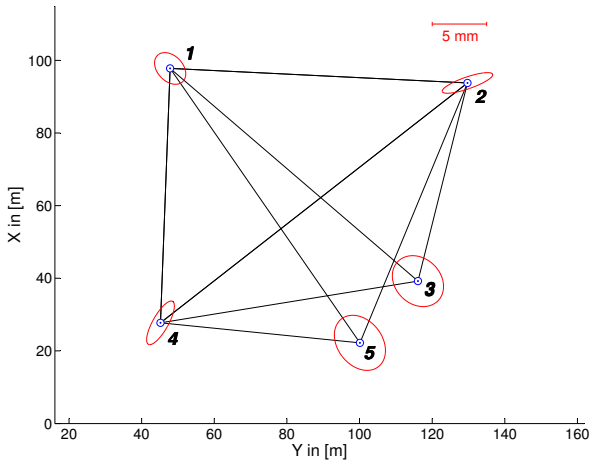

Figure 2.4: Plot of network with partial trace minimization

Point	x [m]	y [m]	$\hat{\sigma}_x$ [mm]	$\hat{\sigma}_y$ [mm]
1	97.780	47.852	±1.5	±1.4
2	93.790	129.717	±1.0	±2.3
3	39.212	116.081	±2.3	±2.4
4	27.720	45.190	±2.0	±1.3
5	22.221	100.101	±2.5	±2.3

Table 2.5: Adjusted coordinates and their standard deviations for partial trace minimization

Now the same network is adjusted again using a partial trace minimization where only points 1, 2 and 4 contribute to the datum definition. The results of the adjustment are shown in Figure 2.4 and Table 2.5, respectively. It can be noted that the estimated standard deviations of the three datum points are lower than those of the remaining two points. Furthermore, on average the standard deviations of the three datum points have decreased, compared to the previous case, whereas the standard deviations of points 3 and 5 have increased.

Ordinary Minimal Constraints

The ordinary minimal constraints are a special case of partial trace minimization where only the minimum number of coordinates required to define all datum defects are used to define the datum. The identical results are obtained when the datum-defining coordinates are eliminated from the parameter vector. In this example point 1 and the x-coordinate of

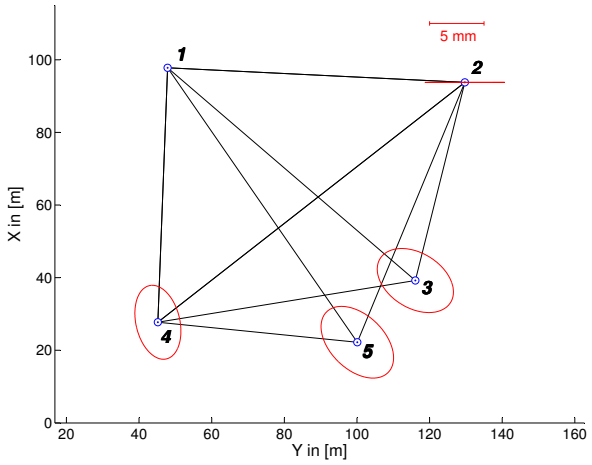

Figure 2.5: Plot of network with ordinary minimal constraints

Point	x [m]	y [m]	$\hat{\sigma}_x$ [mm]	$\hat{\sigma}_y$ [mm]
1	97.780	47.850	±0.0	±0.0
2	93.790	129.715	±0.0	±3.6
3	39.212	116.078	±2.9	±3.5
4	27.720	45.188	±3.4	±2.1
5	22.221	100.099	±3.3	±3.3

Table 2.6: Adjusted coordinates and their standard deviations for ordinary minimal constraints

point 2 were chosen to define the three free datum parameters of the network.

Figure 2.5 and Table 2.6 summarize the results from the adjustment. As expected, the variances of the three datum-defining coordinates are zero. Thus point 2 has an error bar parallel to the y-axis rather than a 2D error ellipse. The standard deviations of the points 3, 4 and 5, that are not contributing to the datum has, again, increased compared to the previous case. They now range from ±2.1 mm to ±3.5 mm. This is almost twice as large as their standard deviations for the total trace minimization.

Over-constrained network

For the over-constrained case the coordinates of the points 1, 2 and 4 have been fixed by removing them from the parameter vector. This decreases the number of unknowns by three, but at the same time the three datum defects are eliminated so that the redundancy of the adjustment problem remains unchanged. The results for the over-constrained case are shown in Figure 2.6 and Table 2.7, respectively.

Note that the coordinates of the three fixed points have been altered slightly (compare with Table 2.3). This has been done intentionally to better demonstrate the effects of

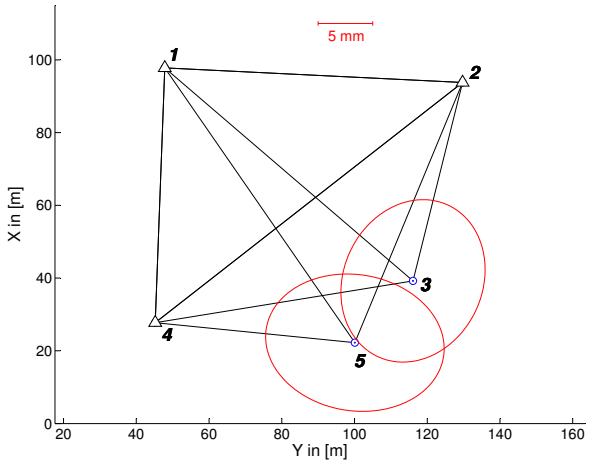

Figure 2.6: Plot of over-constrained network

Point	x [m]	y [m]	$\hat{\sigma}_x$ [mm]	$\hat{\sigma}_y$ [mm]
1	97.795	47.835	±0.0	±0.0
2	93.795	129.725	±0.0	±0.0
3	39.226	116.085	±7.4	±6.6
4	27.725	45.195	±0.0	±0.0
5	22.233	100.104	±6.3	±8.2

Table 2.7: Adjusted coordinates and their standard deviations for over-constrained adjustment

an over-constrained datum on the estimated variances of the network points. Since this is a simulation, the initial coordinates in Table 2.3 are the values that the (randomized) observations were derived from. Naturally, these values form the expectation for the adjusted values $\left(E\left\{\vec{x}\right\} = \vec{x}_0\right)$. Thus, fixing the initial coordinates would essentially represent the ideal case of fixing the unknowns to their true values. In practice however, these true values are not known and the available coordinates are often not of good quality. Hence, slightly altered values have been used for the coordinates of the fixed points.

The standard deviations for the fixed points are assumed to be zero. This results in much larger estimated standard deviations for the two remaining points, compared to the previous cases. This is an indication that the network geometry is being distorted because the coordinates of the fixed points do not agree with the observations. Further indication for this is the fact that the global test of the adjustment model fails.

Weak datum

For the weak datum approach the initial coordinates of all points from Table 2.3 were introduced as additional observations with a standard deviation of ±5 mm. This increases the number of observations by 10 while the number of unknowns remains unchanged. At the

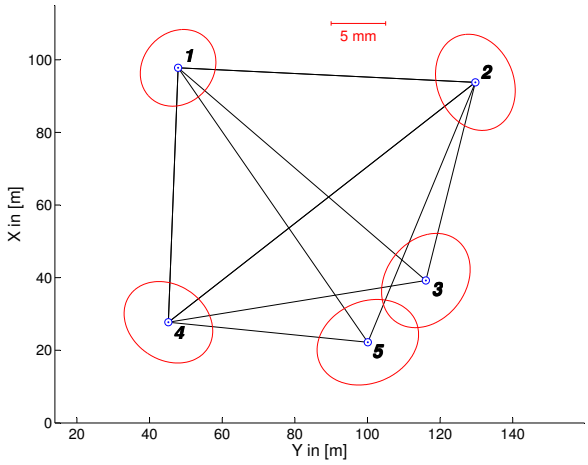

Figure 2.7: Plot of network with weak datum

Point	x [m]	y [m]	$\hat{\sigma}_x$ [mm]	$\hat{\sigma}_y$ [mm]
1	97.780	47.852	±3.5	±3.5
2	93.790	129.718	±4.4	±3.7
3	39.212	116.081	±4.3	±4.1
4	27.720	45.190	±3.7	±4.1
5	22.221	100.102	±3.9	±4.7

Table 2.8: Adjusted coordinates and their standard deviations for network with weak datum

same time the $d = 3$ datum defects are eliminated, so that an overall increase of the redundancy by 7 occurs. The results are shown in Figure 2.7 and Table 2.8. Now all points have a larger estimated standard deviations between ±3.5 mm and ±4.7 mm. In this example, distortion of the network geometry would not occur, due to the large a priori variances assigned to the datum-defining coordinate observations. An indication is that the global test of the adjustment model passes. On the other hand, the datum is not very accurately defined, since all points are free to "float" around much more than the network geometry requires (as is evident when compared to the results from the total trace minimization). Hence, the name weak datum.

2.2.4 Discussion

A network analysis is an important step in pre-processing a set of, often heterogeneous, redundant observations for a deformation analysis. In the network analysis a homogeneous set of coordinates is derived which uniquely describe the network geometry. This requires the definition of the geodetic datum which is critical as it directly affects the results of a deformation analysis. The different approaches to define the datum have been shown and their effects on the adjusted coordinates and their estimated standard deviations have been

illustrated with numerical examples in the previous section. The following conclusions can be drawn.

Constraint approaches are generally unsuited for purposes of a deformation analysis as they can, potentially severely, alter the network geometry. Those changes in the network geometry can then easily be misinterpreted as deformations. In case of an over-constrained datum definition, points are fixed at their initial positions, assuming them to have a zero variance. This makes deformation detection at these points impossible, but can lead to apparent deformations at other network points. In a weak datum approach coordinate observations are used to define the datum. If the chosen variances for these observed coordinates are overly optimistic, the same scenario exists as in the case of an over-constrained approach. If the variances are chosen too pessimistic on the other hand, the level of detectable movements is increased, which results in smaller deformations remaining undetectable.

Inner-constraint, or free approaches do not distort the network geometry. This makes them better suited for monitoring applications. Ordinary minimal constraints should be avoided though. While they do not alter the network geometry, the datum-defining coordinates form a zero-variance computational base which it makes it impossible to detect deformations in these coordinates. A partial or total trace minimization are most suited for monitoring networks. A partial trace minimization minimizes the sum of variances for a chosen part of the network. This can be useful to limit the datum definition to the control points of a monitoring network with the disadvantage of larger variances for the monitoring points, thus increasing the level of detectable movements. A total trace minimization will minimize the sum of variances of all network points. This results in the lowest level of detectable movements for all network points.

A further advantage of the inner-constraint approaches is that the computational base can be easily changed using an S-transformation, eliminating the need for a re-adjustment of the observations. This requires that both the old and new datum refer to the same reference

frame, i. e. to the same set of initial coordinates $\vec{x}_0$.

2.3 Deformation analysis

2.3.1 Classification of deformation analysis models

Monitored objects can be interpreted as dynamic systems. Dynamic systems are, in the general sense of system theory, systems (objects) which can save energy and then emit it time-delayed. Thus, the classification of models for deformation analysis is closely related to system theory. The main task of system theory is to provide models for real-world systems that allow to idealize, represent and analyze the characteristics of the system to gain information about its behaviour. A distinction has to be made between models that solely describe resulting deformations and models that consider the chain of cause, transfer behaviour and effect. Including time, explicitly or implicitly, this results in four model classes which are illustrated in Figure 2.8 and described below in more detail. (Welsch et al., 2000b).

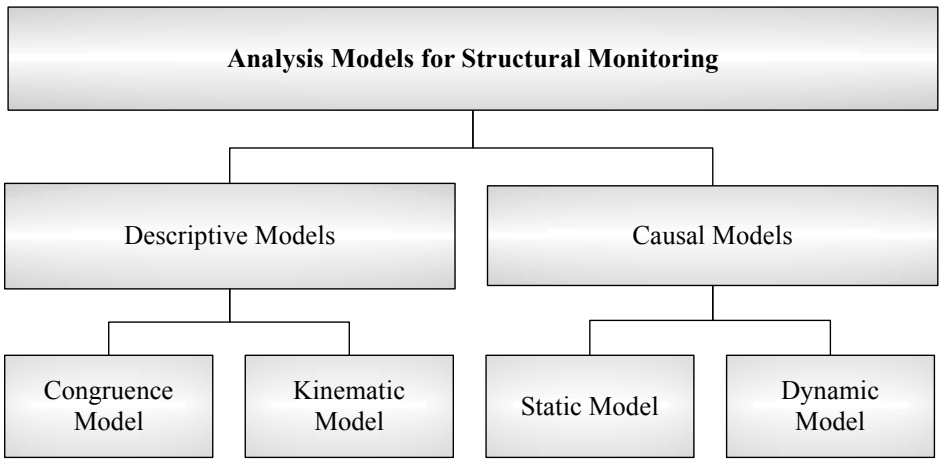

Figure 2.8: Analysis Models for Structural Monitoring, (Welsch et al., 2000b)

Congruence model

The focus of the analysis is the purely geometric comparison of one state (coordinate) of an object with another state (another coordinate) of the same object. Only the identity of the geometry of both states – *congruence* – is considered. Deformations are derived from measurements at discrete locations (object points) at discrete points in time. These results can then be generalized to describe movements of the structure as a whole.

Kinematic model

The kinematic model delivers a purely time dependent description of the behaviour of object points, especially through use of polynomials or trigonometric functions, in which their application already assumes knowledge of certain theoretical aspects. The goal is to determine object movements and their parameters from measurements made at discrete points in time. There is no connection made with any causal forces acting on the object. It is a descriptive analysis of the motion behaviour. Again, the issue of generalization occurs as movements of single object points represent the whole structure.

Static model

The static model describes the functional relationship between the force acting on an object and its physical reaction determined by means of metrology. It is required that the object is sufficiently still while measurements are taken as time is not explicitly taken into account in the model.

Dynamic model

The dynamic model analyzes metrologically determined object reactions as a function of time and load.

2.3.2 Classical congruence analysis

Geodetic monitoring networks are commonly used to determine movements and distortions of structures. They can be adapted to the requirements of a certain application in a very flexible manner, (Welsch et al., 2000b). Specific target points, installed at critical locations on the monitored object, represent the deformations of the structure. Together with a set of (presumably) stable control points, which define the geodetic datum of the network, those target or object points are observed at certain time intervals or epochs. Depending on the available geodetic observations, one-, two-, or three-dimensional coordinates $\vec{x}$ can then be derived for each epoch from a least-squares network analysis as described in the previous section. If observations from at least two epochs are available, deformations that occurred between them can be determined using the congruence model. But before a deformation analysis can be carried out, it has to be determined whether the results from the separate network analyses of the two epochs are indeed comparable. This is done by examining the a posteriori variance factors $\hat{\sigma}^2_{0_i}$ and $\hat{\sigma}^2_{0_j}$ of the epochs i and j using the following statistical test.

- Test hypothesis H_0 : $$E\left\{\hat{\sigma}^2_{0_i}\right\} = E\left\{\hat{\sigma}^2_{0_j}\right\} \tag{2.24a}$$
- Alternative hypothesis H_A : $$E\left\{\hat{\sigma}^2_{0_i}\right\} \neq E\left\{\hat{\sigma}^2_{0_j}\right\} \tag{2.24b}$$
- Test statistic : $$T_F = \frac{\hat{\sigma}^2_{0_i}}{\hat{\sigma}^2_{0_j}} \tag{2.24c}$$

If the test statistic T_F fits the FISHER-distribution, i. e. if

$$T_F \leq F_{S=1-\alpha/2, f_1=r_i, f_2=r_j}{}^{5} \tag{2.25}$$

the null hypothesis H_0 cannot be rejected. A deformation analysis of the two epochs can then be performed.

[5] where α denotes the chosen confidence level for the test, r_i and r_j are the network redundancies for epochs i and j, respectively.

For the mathematical formulation of the congruence analysis, a variety of solutions can be found in the literature. These, however, do not differ much in their theoretical approach, (Welsch et al., 2000b). Summarized below is the basic model as described in Gründig et al. (1985).

Available are the adjusted coordinate vectors $\vec{x}$, their corresponding cofactor matrices $\mathbf{Q}_{xx}$, the a posteriori variance factor $\hat{\sigma}_0^2$ and the network redundancy r for two epochs i and j from a network analysis of each epoch as discussed in the previous section. It is assumed that for both epochs the same inner-constraint datum definition has been used.

2.3.2.1 Global congruency testing

The main task of the analysis is to test if the hypothesis, that coordinates of two different epochs i and j are related to each other, or congruent, is valid. This hypothesis can be expressed as conditions between the coordinates of each epoch as

$$\mathbf{B} \cdot \begin{pmatrix} \vec{x}_i \\ \vec{x}_j \end{pmatrix} = \vec{w} \tag{2.26}$$

where $\mathbf{B}$ describes the functional relationship between the coordinates of epoch i and epoch j and $\vec{w}$ is a vector of constants. For the simplest case, where the null hypothesis states that there are no deformations between the two epochs, these conditions can be formulated as

$$\vec{x}_i - \vec{x}_j = \vec{0} \ . \tag{2.27}$$

If the test in (2.25) passes, the combined variance factor $\hat{\sigma}_0^2$ for both epochs can be derived from

$$\hat{\sigma}_0^2 = \frac{\vec{v}_i^T \mathbf{P}_i \vec{v}_i + \vec{v}_j^T \mathbf{P}_j \vec{v}_j}{r_i + r_j} = \frac{r_i \cdot \hat{\sigma}_{0_i}^2 + r_j \cdot \hat{\sigma}_{0_j}^2}{r_i + r_j} \ . \tag{2.28}$$

This corresponds to a common adjustment of the observations of both epochs where points in epochs i and j are considered as *not* identical.

To test if the conditions in (2.27) hold true, the vector of coordinate differences $\vec{d}$ between epochs i and j is derived from

$$\vec{d} = \vec{x}_i - \vec{x}_j \ . \tag{2.29}$$

Its corresponding weight matrix $\mathbf{P}_{dd}$ follows by applying the covariance law to the cofactor matrices of epochs i and j

$$\mathbf{P}_{dd} = (\mathbf{Q}_{xx_i} + \mathbf{Q}_{xx_j})^- \tag{2.30}$$

assuming no correlation between epochs. It should be pointed out again, that a generalized inverse is used here, since typically the cofactor matrices are obtained in a free network adjustment and are thus singular.

Consequently, the quadratic form $\hat{\Omega}^2$ can directly be derived from the results of the individual adjustments of each epoch

$$\hat{\Omega}^2 = \frac{\vec{d}^T \mathbf{P}_{dd} \vec{d}}{h} \tag{2.31}$$

with $h = b - d$, where b is the number of condition equations and d reflects the rank defect of the weight matrix $\mathbf{P}_{dd}$. While the inverse in (2.30) may not be unique, the resulting quadratic form (2.31) will be (Rao, 1962), so that any g-inverse can be chosen.

Another way to derive the quadratic form $\hat{\Omega}^2$ is by the use of datum-invariant functions of the adjusted coordinates, such as distances, angles or height differences. These can be computed from:

$$d\vec{l} = \vec{l}_i - \vec{l}_j = \mathbf{F}_i^T \vec{x}_i - \mathbf{F}_j^T \vec{x}_j \ . \tag{2.32}$$

Their corresponding cofactor matrix follows from:

$$\mathbf{Q}_{dl} = \mathbf{F}_i^T \mathbf{Q}_{xx_i} \mathbf{F}_i + \mathbf{F}_j^T \mathbf{Q}_{xx_j} \mathbf{F}_j, \qquad \text{with } \mathrm{rk}\,(\mathbf{Q}_{dl}) = \mathrm{rk}\,(\mathbf{P}_{dd}) = h \ . \tag{2.33}$$

The quadratic form $\hat{\Omega}^2$ can then be computed from:

$$\hat{\Omega}^2 = \frac{d\vec{l}^T \mathbf{Q}_{dl}^- d\vec{l}}{h} \tag{2.34}$$

The two quantities $\hat{\sigma}_0^2$ and $\hat{\Omega}^2$ are stochastically independent and can thus be compared to each other using the following global congruency test.

- Test hypothesis H_0 : $E\left\{\hat{\sigma}_0^2\right\} = E\left\{\hat{\Omega}^2\right\}$ (2.35a)
- Alternative hypothesis H_A : $E\left\{\hat{\sigma}_0^2\right\} < E\left\{\hat{\Omega}^2\right\}$ (2.35b)
- Test statistic : $T_G = \dfrac{\hat{\Omega}^2}{\hat{\sigma}_0^2}$ (2.35c)

If T_G fits the FISHER-distribution, i. e. if

$$T_G \leq F_{S=1-\alpha, f_1=h, f_2=r_i+r_j} \tag{2.36}$$

for a given confidence level α and the degrees of freedom $f_1 = h$ and $f_2 = r_i + r_j$ (the sum of the network redundancies), $\hat{\sigma}_0^2$ and $\hat{\Omega}^2$ must be considered statistically identical. This means that $\hat{\Omega}^2$ only exceeds $\hat{\sigma}_0^2$ by the amount of random errors inherent in the observations and the null hypothesis (2.35a) cannot be rejected. Should this global congruency test fail on the other hand, the existence of deformations between the two epochs must be accepted.

2.3.2.2 Localization of movements

To identify points that have deformed, a partitioning of the coordinate differences and their corresponding weight matrix into two subsystems has to be performed. The isolated parameters are denoted I and the remaining parameters are denoted R.

$$\vec{d} = \begin{pmatrix} d_R \\ d_I \end{pmatrix} \qquad \mathbf{P}_{dd} = \begin{bmatrix} P_{RR} & P_{IR} \\ P_{IR} & P_{II} \end{bmatrix} . \tag{2.37}$$

A local quantity to determine the validity of the conditions (2.27) for the parameters under consideration can then be derived from

$$\hat{\Omega}_I^2 = \frac{\bar{d}_I^T P_{II} \bar{d}_I}{b_I} \tag{2.38}$$

where $\bar{d}_I = d_I + P_{II}^{-1} P_{IR} d_R$ contains only the effect of the isolated parameters I and b_I is the number of conditions between them. The fully-populated weight matrix P_{II} of the isolated

parameters is of full rank b_I and thus the regular inverse can be used here, see Gründig et al. (1985); Welsch et al. (2000b).

Now, the following local test for the parameters I can be performed.

- Test hypothesis H_0 : $E\left\{\hat{\sigma}_0^2\right\} = E\left\{\hat{\Omega}_I^2\right\}$ (2.39a)
- Alternative hypothesis H_A : $E\left\{\hat{\sigma}_0^2\right\} < E\left\{\hat{\Omega}_I^2\right\}$ (2.39b)
- Test statistic : $T_L = \dfrac{\hat{\Omega}_I^2}{\hat{\sigma}_0^2}$ (2.39c)

T_L can be tested against the FISHER-distribution $F_{1-\alpha,f_1,f_2}$ with confidence level α and degrees of freedom $f_1 = b_I$ and $f_2 = r_i + r_j$. This local test analyzes the conditions stated in (2.27) with respect to a single parameter or a subset of parameters. The advantage of the local test lies in its sensitivity. In a global test, small local deviations from the considered distribution may be overshadowed by the effect of other parameters included in the test. For this reason it is possible that the global test is accepted for a whole network whereas the local test is rejected for single points.

If the local test is rejected for one of the datum points, it needs to be eliminated from the computational base. This can be done by applying an S-transformation, as described in Section 2.2.1.3, to the coordinate vectors of epochs i and j and their cofactor matrices.

2.3.2.3 Determination of movements

After all deformed points have been isolated and both global and local test pass for the remaining points, actual deformations can be derived through a network analysis, as described in Section 2.2, using the original observations of both, epoch i and epoch j. In this analysis the parameter vector consists of the coordinates of the remaining (stable) points $\vec{x}_R$ and the coordinates of the isolated points in both epochs $\vec{x}_{I_i}$ and $\vec{x}_{I_j}$. The linearized observation

equations according to (2.2) can be written as

$$\begin{pmatrix} \Delta\vec{l}_i \\ \Delta\vec{l}_j \end{pmatrix} + \begin{pmatrix} \vec{v}_i \\ \vec{v}_j \end{pmatrix} = \begin{bmatrix} \mathbf{A}_{R_i} & \mathbf{A}_{I_i} & 0 \\ \mathbf{A}_{R_j} & 0 & \mathbf{A}_{I_i} \end{bmatrix} \begin{pmatrix} \Delta\vec{x}_R \\ \Delta\vec{x}_{I_i} \\ \Delta\vec{x}_{I_j} \end{pmatrix} . \tag{2.40}$$

Resulting are, besides coordinates of the stable points and the estimated a posteriori variance factor $\hat{\sigma}_0^2$, the adjusted coordinates of all isolated (i. e. unstable) points and their corresponding cofactor matrices

$$\vec{x}_I = \begin{pmatrix} \vec{x}_{I_i} \\ \vec{x}_{I_j} \end{pmatrix} \qquad \mathbf{Q}_{II} = \begin{bmatrix} \mathbf{Q}_{I_{ii}} & \mathbf{Q}_{I_{ij}} \\ \mathbf{Q}_{I_{ji}} & \mathbf{Q}_{I_{jj}} \end{bmatrix} . \tag{2.41}$$

Deformations $\vec{d}_I$ for the isolated points can then be derived as their coordinate differences between epochs i and j. Their associated covariance matrix $\mathbf{C}_{dd_I}$ follows from the covariance law.

$$\vec{d}_I = \mathbf{F}^T\vec{x}_I \qquad \mathbf{C}_{dd_I} = \hat{\sigma}_0^2 \cdot \left(\mathbf{F}^T\mathbf{Q}_{II}\mathbf{F}\right) \tag{2.42}$$

where $\mathbf{F}^T = [-\mathbf{I} \quad \mathbf{I}]$ and $\mathbf{I}$ denotes the identity matrix.

Alternatively, the deformations can be derived by applying an S-transformation to both epoch i and j to change the datum to the (stable) remaining points $\vec{x}_R$. Then, deformations can be derived as the S-transformed coordinate differences.

It should be pointed out that the congruence analysis as described in this section assumes the network datum to be defined by inner-constraints and to be based on the same set of initial coordinates $\vec{x}_0$ for both epochs, i. e. it must refer to the same reference frame. Otherwise, the application of an S-transformation to accommodate changes from one set of datum points to another is not possible.

2.3.2.4 Numerical examples

To illustrate the method described above, the example from Section 2.2.3 is revisited. The same network is observed in a second epoch. For the second epoch deformations of $dx =$

$-30.0\,\text{mm}$ and $dy = +40.0\,\text{mm}$ are introduced to point 3. All other points remain stable. The datum is defined by applying inner-constraints to all five network points. The a posteriori variance factor for epoch 2 is $\hat{\sigma}_{0_2}^2 = (0.011831)^2$ with a network redundancy of 14. The adjusted coordinates for epoch 2 and their standard deviations are listed in Table 2.9.

Point	x [m]	y [m]	$\hat{\sigma}_x$ [mm]	$\hat{\sigma}_y$ [mm]
1	97.785	47.841	±2.1	±2.0
2	93.798	129.711	±2.0	±2.0
3	39.184	116.113	±1.6	±1.8
4	27.727	45.182	±1.7	±2.1
5	22.226	100.093	±1.9	±1.6

Table 2.9: Adjusted coordinates and their standard deviations for epoch 2

For epoch 1 the results from the total trace minimization, as listed in Table 2.4, are used as input coordinates for the congruence analysis. The a posteriori variance factor for epoch 1 is $\hat{\sigma}_{0_1}^2 = (0.011027)^2$ with a network redundancy of 14.

Before a deformation analysis of the two epochs can be performed, it has to be checked that the estimated variance factors are indeed statistically equal. This can be achieved by the F-test described in (2.24). The test statistic

$$T_F = \frac{\hat{\sigma}_{0_2}^2}{\hat{\sigma}_{0_1}^2} = \left(\frac{0.011831}{0.011027}\right)^2 = 1.15$$

is compared against the FISHER-distribution. With a chosen confidence level of $\alpha = 5\,\%$ and degrees of freedom $f_1 = f_2 = 14$, it follows that $F_{S=1-\alpha/2,f_1,f_2} = 2.98$. Since $1.15 < 2.98$, the null hypothesis (2.24a) cannot be rejected and the test passes. Thus the combined variance factor for both epochs follows as

$$\hat{\sigma}_0^2 = \frac{r_1 \cdot \hat{\sigma}_{0_1}^2 + r_2 \cdot \hat{\sigma}_{0_2}^2}{r_1 + r_2} = \frac{14 \cdot (0.011027)^2 + 14 \cdot (0.011831)^2}{28} = 1.3078 \cdot 10^{-4}.$$

Now a deformation analysis can be performed, starting with a global congruency test described in (2.35). For this, the quadratic form $\hat{\Omega}^2$ is required which can be computed from

(2.31). The test statistic for the global congruency test is then derived as follows:

$$T_G = \frac{\hat{\Omega}^2}{\hat{\sigma}_0^2} = \frac{96.3670 \cdot 10^{-4}}{1.3078 \cdot 10^{-4}} = 73.67.$$

The reference value for a chosen confidence level of $\alpha = 5\,\%$ and degrees of freedom $f_1 = h = 7^6$ and $f_2 = r_1 + r_2 = 28$ is given by $F_{S=1-\alpha,f_1,f_2} = 2.36$. With $73.67 \not\leq 2.36$ the null hypothesis (2.35a) has to be rejected. This indicates the presence of deformations in the data of epoch 2.

In the next step the deformed point(s) are identified by performing a local test for each of the network points separately according to (2.39). With the local quantities (2.38) the following test statistics $T_L = \hat{\Omega}_I^2/\hat{\sigma}_0^2$ are obtained for the five network points.

Point	1	2	3	4	5
T_L	15.29	83.69	255.41	32.81	22.57

Table 2.10: Test statistics for local congruency test of all five network points

With a reference value of $F_{S=1-\alpha,f_1,f_2} = 3.34$, for a chosen confidence level of $\alpha = 5\,\%$ and degrees of freedom $f_1 = 2$ and $f_2 = 28$, this local test fails for all of the five points. Consequently, the point with the largest test statistic T_L has to be eliminated. In this example point 3, the one point that deformations have been introduced to, has been correctly identified as unstable. Since point 3 is part of the computational base in both epochs, the datum of both, epoch 1 and 2, now has to be changed to exclude point 3. Since the datum of both epochs is identically defined using inner-constraints and based on the same coordinate frame, an S-transformation, as discussed in Section 2.2.1.3, can be applied to achieve the desired datum change.

After the datum change, the global congruency test (2.35) is carried out again to check whether any further points have experienced deformations. This time the global test statistic

[6]The rank of the weight matrix $\mathbf{P}_{dd}$ in (2.30)

results in

$$T_G = \frac{\hat{\Omega}^2}{\hat{\sigma}_0^2} = \frac{1.2755 \cdot 10^{-4}}{1.3078 \cdot 10^{-4}} = 0.98.$$

With $\alpha = 5\,\%$, $f_1 = 5$ and $f_2 = 28$, the corresponding reference value is $F_{S=1-\alpha,f_1,f_2} = 2.56$. Since $0.98 < 2.56$ the global congruency test passes now indicating no further deformations.

Nevertheless, the local test in (2.39) is repeated to confirm the identity of each point individually. Re-computing (2.39c) yields the following local test statistics for the four remaining network points.

Point	1	2	4	5
T_L	2.01	0.54	1.73	1.01

Table 2.11: Test statistics for local congruency test of the four remaining points

Comparing the local test statistics from Table 2.11 with the reference value $F_{S=0.95,f_1=2,f_2=28} = 3.34$ shows that the null hypothesis (2.39a) indeed has to be accepted for all remaining network points.

In the last step the actual deformations for the unstable point are derived as described in Section 2.3.2.3. Re-adjustment of the observations of both epochs according to (2.40) yields the following results.

Point	x [m]	y [m]	$\hat{\sigma}_x$ [mm]	$\hat{\sigma}_y$ [mm]
1	97.780	47.851	±1.3	±1.2
2	93.790	129.718	±1.2	±1.5
4	27.721	45.190	±1.2	±1.2
5	22.220	100.101	±1.4	±1.1
31	39.211	116.081	±1.8	±1.8
32	39.178	116.121	±1.9	±1.8

Table 2.12: Adjusted coordinates and their standard deviations for epochs 1 and 2

For the deformed point 3 two sets of coordinates were estimated, point 31 represents the coordinates of point 3 in epoch 1 while point 32 is its position in epoch 2. Application of

(2.42) then yields the following deformations for point 3.

Point	dx	dy	$\hat{\sigma}_{dx}$	$\hat{\sigma}_{dy}$
3	-33.1	$+39.4$	± 2.3	± 2.1

Table 2.13: Deformations and their standard deviations of point 3 between epochs 1 and 2 in [mm]

The estimated values for the deformations are within a few millimetres of their true values. Given their estimated accuracies in Table 2.13, it can be concluded that the deformations of the unstable point could be correctly recovered.

In a second example the previous analysis shall be repeated with the modification that now a scale factor of $\lambda = 300\,\text{ppm}$ is introduced to all distances of the second epoch before the network adjustment. Again, only the coordinates of point 3 are altered by the same amount as in the previous example. The re-adjustment with the scaled distances results in an a posteriori variance factor of $\hat{\sigma}_{0_2}^2 = (0.011833)^2$ and the network redundancy remains unchanged at 14. The adjusted coordinates and their standard deviations are listed in Table 2.14 below.

Point	x [m]	y [m]	$\hat{\sigma}_x$ [mm]	$\hat{\sigma}_y$ [mm]
1	97.797	47.829	± 2.1	± 2.0
2	93.809	129.723	± 2.0	± 2.0
3	39.179	116.122	± 1.6	± 1.8
4	27.719	45.170	± 1.7	± 2.1
5	22.216	100.097	± 1.9	± 1.6

Table 2.14: Adjusted coordinates and their standard deviations after scaling distances

Comparing the new variance factor to that of epoch 1, using the F-test in (2.24), yields the following test statistic:

$$T_F = \frac{\hat{\sigma}_{0_2}^2}{\hat{\sigma}_{0_1}^2} = \left(\frac{0.011833}{0.011027}\right)^2 = 1.15.$$

Comparing T_F against the FISHER-distribution for $\alpha = 5\,\%$ and $f_1 = f_2 = 14$, it follows that $T_F = 1.15 < 2.98 = F_{S=1-\alpha/2,f_1,f_2}$ and hence the test passes. Thus the combined variance

factor for both epochs now follows as

$$\hat{\sigma}_0^2 = \frac{r_1 \cdot \hat{\sigma}_{0_1}^2 + r_2 \cdot \hat{\sigma}_{0_2}^2}{r_1 + r_2} = \frac{14 \cdot (0.011027)^2 + 14 \cdot (0.011833)^2}{28} = 1.3081 \cdot 10^{-4}.$$

The congruency test from (2.35) yields the global test statistic

$$T_G = \frac{\hat{\Omega}^2}{\hat{\sigma}_0^2} = \frac{105.5797 \cdot 10^{-4}}{1.3081 \cdot 10^{-4}} = 80.71.$$

The reference value for a chosen confidence level of $\alpha = 5\,\%$ and degrees of freedom $f_1 = h = 7$ and $f_2 = r_1 + r_2 = 28$ is given by $F_{S=1-\alpha,f_1,f_2} = 2.36$. With $80.71 \not\leq 2.36$ the null hypothesis (2.35a) has to be rejected. Thus, as expected, the global congruency test fails again and the presence of deformations has to be assumed.

To identify the deformed point(s), a local test for each of the network points separately is performed according to (2.39). The local test statistics $T_L = \hat{\Omega}_I^2/\hat{\sigma}_0^2$ for the five network points are shown in Table 2.15.

Point	1	2	3	4	5
T_L	21.13	70.84	265.22	27.66	19.48

Table 2.15: Test statistics for local congruency test after scaling

With a reference value of $F_{S=0.95,f_1=2,f_2=28} = 3.34$ the local tests fail for all five network points. Point 3 is again the point with the highest test statistic and is thus eliminated from the further analysis. After performing an S-transformation to the new datum defined by the four remaining points, the global congruency test is repeated resulting in a new global test statistic of

$$T_G = \frac{\hat{\Omega}^2}{\hat{\sigma}_0^2} = \frac{9.0406 \cdot 10^{-4}}{1.3081 \cdot 10^{-4}} = 6.91.$$

With a reference value of $F_{S=1-\alpha,f_1=h,f_2=r_1+r_2} = 2.56$ for $\alpha = 5\,\%$, $f_1 = 5$ and $f_2 = 28$, the global congruency test fails again indicating further deformations. Thus another local test of the four remaining points is carried out. The results are listed in Table 2.16.

Point	1	2	4	5
T_L	2.84	4.19	0.32	1.64

Table 2.16: Local test statistics for the four remaining points after scaling

With a reference value of $F_{S=0.95,f_1=2,f_2=28} = 3.34$, the local tests pass for all points except for point 2, leading to its elimination. After another S-transformation to the datum defined by the three remaining points, the global congruency test is repeated once more. With a global test statistic of

$$T_G = \frac{\hat{\Omega}^2}{\hat{\sigma}_0^2} = \frac{11.4137 \cdot 10^{-4}}{1.3081 \cdot 10^{-4}} = 8.72 \not\leq 2.95 = F_{S=0.95,f_1=3,f_2=28}$$

the test fails again. The following local test for the three remaining points yields the local test statistics shown in Table 2.17 below.

Point	1	4	5
T_L	6.71	0.55	6.65

Table 2.17: Local test statistics for the three remaining points after scaling

Given $F_{S=0.95,f_1=2,f_2=28} = 3.34$, the local test passes only for point 2. Point 1, having the largest test value, is eliminated and an S-transformation is performed again followed by another global congruency test resulting in

$$T_G = \frac{\hat{\Omega}^2}{\hat{\sigma}_0^2} = \frac{16.8488 \cdot 10^{-4}}{1.3081 \cdot 10^{-4}} = 12.76 \not\leq 4.20 = F_{S=0.95,f_1=1,f_2=28}.$$

The final local test of the two remaining points yields the following local test statistics. Now,

Point	4	5
T_L	6.38	6.38

Table 2.18: Local test statistics for points 4 and 5 after scaling

the test fails for both remaining points. And, since both points have the same test statistic, a decision cannot be made which point should be eliminated next. This, of course, is expected because of the underlying systematic error, so that the congruence analysis for this example ultimately fails.

2.3.3 Congruence analysis using a Multi-Parameter Transformation

A different approach to a congruence analysis has been introduced in Teskey et al. (2005). A *Multi-Parameter Transformation* is utilized to relate the original and repeated measurements from a single instrument station to any number of target points. The instrument station can be realized by a total station or terrestrial laser scanner, (Teskey et al., 2006).

The mathematical model is based on a seven parameter similarity transformation using three translations in x-, y- and z-directions (T_x, T_y, T_z) and three rotations about the x-, y- and z-axes (ω, φ, κ). In addition, a scale factor (λ) relating the slope distances from the original epoch to those of the repeated epoch as well as a refraction correction (ΔR) between original and repeated zenith angles are introduced. The mathematical model can be expressed as follows, (Teskey et al., 2006):

$$\begin{aligned} x_O &= \lambda \cdot (x_R + \kappa \cdot y_R - \varphi \cdot z_R) + T_x \\ y_O &= \lambda \cdot (-\kappa \cdot x_R + y_R + \omega \cdot z_R) + T_y \\ z_O &= \lambda \cdot (\varphi \cdot x_R - \omega \cdot y_R + z_R) + T_z \end{aligned} \tag{2.43}$$

with

$$\begin{aligned} x_R &= s_R \cdot \sin(h_R) \cdot \sin(v_R + (\Delta R) \cdot s_R) \\ y_R &= s_R \cdot \cos(h_R) \cdot \sin(v_R + (\Delta R) \cdot s_R) \\ z_R &= s_R \cdot \cos(v_R + (\Delta R) \cdot s_R) \\ x_O &= s_O \cdot \sin(h_O) \cdot \sin(v_O) \\ y_O &= s_O \cdot \cos(h_O) \cdot \sin(v_O) \\ z_O &= s_O \cdot \cos(v_O) \ . \end{aligned} \tag{2.44}$$

Where h_O, v_O and s_O are the horizontal circle, vertical circle and slope distance observations of the original epoch, respectively and h_R, v_R and s_R represent the horizontal circle, vertical circle and slope distance observations of the repeated epoch, respectively. x_O, y_O and z_O are the x-, y- and z-coordinates computed from the observations of the original epoch and x_R, y_R and z_R are the x-, y- and z-coordinates computed from the observations of the repeated

epoch. It should be noted that in (2.43) small-angle approximations were used to simplify the mathematical model by eliminating trigonometric functions. This is justified for the rotations about the x- and y-axes if the instrument is levelled. But it also requires that the orientation in the horizontal plane is approximately the same in each epoch which can be easily achieved by aligning the zero mark on the horizontal circle of the instrument with a reference mark.

The mathematical model represented by equations (2.43) and (2.44) can be solved in an implicit, non-linear least-squares adjustment (GAUSS-HELMERT model) to obtain the transformation parameters ω, φ, κ, T_x, T_y, T_z, λ and the additional parameter ΔR. The movements of each target point follow from $(x_T - x_O)$, $(y_T - y_O)$ and $(z_T - z_O)$, respectively, in which x_T, y_T and z_T are transformed x-, y- and z-coordinates given by the right-hand sides of equations (2.43), (Teskey et al., 2006). The translation parameters T_x, T_y and T_z can be interpreted as the movements of the instrument setup point itself.

This mathematical model introduced in Teskey et al. (2005) has been significantly generalized and extended in Ebeling et al. (2009) for the application to networks rather than a single instrument station as will be shown in Section 3.2.

The advantage of this method is that it directly utilizes the observations, which allows to introduce the additional parameter ΔR to account for refraction effects between epochs. Furthermore, this also avoids the necessity of a network analysis and the issue of the datum definition. The datum in this case is defined by the centre of the instrument, the orientation of its vertical axis and the position of the zero mark on the horizontal circle. The scale is defined by the observed slope distances. An additional economic benefit exists as well since it is more time consuming to observe a multi-station network than it is to collect data from only a single station.

The disadvantage is that there is no redundancy in the determination of the target points.

Each point is described by a unique 3D position in form of one horizontal circle reading, one vertical circle reading and one slope distance. This can result in a poor detectability for deformations depending on the station - target geometry. It also makes it extremely important to observe all targets in multiple sets, so that outliers (e. g. point misidentification) can be found in the data and realistic values for the precision of the observations can be derived.

2.3.4 Localization of deformed points

The most critical task in a deformation analysis is to correctly identify the unstable points and isolate them from the stable points. Different approaches are suggested in the geodetic literature. These include the classical approach, already described above, robust estimation techniques and alternative techniques employing combinatorial searches. They are discussed below.

2.3.4.1 Least-squares and single point analysis

In the classical congruence analysis described in Section 2.3.2 the localization of unstable points between two epochs is implemented by successively performing a local significance test for each point. The point with the largest contribution to the squared sum of residuals is then eliminated and the process is repeated until all remaining points pass this test. This procedure is closely related to Baarda's method of data snooping (Welsch et al., 2000b).

That this method does not always lead to success has already been shown in the second example in 2.3.2.4. While the reason for the failure of this method in this case is an unmodelled systematic error (a scale change between the two epochs), the presence of multiple deformed points can have the same effect, especially when a large number of points are experiencing deformations of small magnitude. The problem is that each point is examined separately, implicitly assuming that all remaining points are stable. If this assumption does not apply,

then the test results cannot be expected to be correct.

Furthermore, the relevant test statistics are based on a least-squares estimation. Even though the actual adjustments do not have to be carried out to compute the test statistics, the assumptions on which a least-squares estimation is based must still apply. These assumptions state that the data are free of gross and systematic errors and only contain random, normally-distributed noise.

Already Baarda (1968) emphasized that data snooping "does not give certainty, only a supposition" and that it "will therefore always be a risky activity".

2.3.4.2 Robust estimation techniques

The model assumptions underlying the least-squares method do not always agree with reality. Besides the choice of parameters and the functional model, this mainly concerns the probability distribution of the observations. For normally-distributed data a least-squares adjustment will yield the most likely results for the estimated parameters. If the assumptions about the model are not true, because of unmodelled systematic errors or outliers, even of small magnitude, or correlations between the observations that cannot be described, the chosen distribution needs to be modified. Because of missing information about the nature of the deviations, it is unclear how this is to be done. Thus, so-called robust estimation techniques are introduced which try to estimate the parameters without the influence of the model deviations. (Welsch et al., 2000b).

Several estimation techniques exist which, according to Caspary (1996), can be categorized into *resistant* and *robust* techniques.

Resistant techniques are insensitive to deviations from certain model assumptions. They are mainly used for data analysis and diagnostics. Probability theory, assumptions about the probability distribution and statistical criteria are of lesser or no concern. A typical example

for a resistant technique is the L_1-norm estimation.

Robust estimation techniques are resistant and additionally meet theoretically founded estimation criteria such as efficiency, consistency, asymptotic normal distribution. Furthermore, robust estimators should meet the following important objectives:

- The impact of a single observation on the estimates should be bounded, (Welsch et al., 2000b).
- Data robustness: Estimates should be close to their "true values", even when the data are contaminated. The results should be affected very little by the contaminated data. (Niemeier, 2002).
- Model robustness: Results should mainly be based on the data conforming to the underlying model, (Niemeier, 2002).
- Given a correct model and error-free data, a robust estimator should yield nearly optimal results, i. e. the results should be close to those of a least-squares estimation, (Niemeier, 2002).
- Robust estimators should be able to withstand a large number of outliers (have a high breakdown point), (Welsch et al., 2000b; Niemeier, 2002).

Examples for robust techniques include the class of M-estimators.

Following is a brief overview of the most common estimation techniques. The class of L_p-norm estimators minimize the L_p-norm as the objective function:

$$L_p = \sum_{i=1}^{n} |v_i|^p \rightarrow \min \tag{2.45}$$

where the v_i denote the residuals resulting from a linear estimation. The most important L_p-norm estimators include the L_1- and L_2-norm. The L_2-norm estimation, or method of

least-squares, yields the well known objective function:

$$L_2 = \sum_{i=1}^{n} {v_i}^2 \rightarrow \min . \tag{2.46}$$

The L_2 estimator exhibits a certain robustness to outliers only through data-snooping and other methods, but this is of an experimental nature. Difficulties arise because of the well-known smoothing effects of outliers on the residuals of neighbouring observations. The L_2-norm is not considered a robust estimator. (Welsch et al., 2000b). Its breakdown point[7] is approximately at 3 % to 5 % of the data. (Niemeier, 2002).

The L_1-norm estimator minimizes the sum of absolute residuals instead:

$$L_1 = \sum_{i=1}^{n} |v_i| \rightarrow \min . \tag{2.47}$$

The L_1-norm is a resistant estimator whose results hardly vary due to large deviations of a small fraction of the data or due to small deviations in a large number of observations, (Welsch et al., 2000b). It has a breakdown point of about 50 %. This makes it well-suited for the detection of outliers. On the other hand, it does not provide optimal results for uncontaminated data and should thus not be used for parameter estimation, (Niemeier, 2002).

The class of M-estimators are generalized maximum-likelihood estimators based on a mixed distribution, e. g. a normal distribution in the centre and an exponential distribution along the tails. They minimize different functions ρ of the residuals v_i so that, (Welsch et al., 2000b):

$$\sum_{i=1}^{n} \rho\left(v_i\right) \rightarrow \min . \tag{2.48}$$

The desired properties of an estimator can be obtained by choosing the appropriate function $\rho\left(v_i\right)$. The M-estimators are a class of robust estimators with a breakdown point of approximately 5 % to 10 %, (Niemeier, 2002).

[7] The largest possible fraction of contaminated data an estimator can withstand before it produces wrong results or breaks down, (Niemeier, 2002).

Another technique with a high breakdown point is the LMS[8]-estimator that can handle up to 50 % of the data being contaminated. In an LMS-estimation the u parameters are uniquely determined from a subset of u out of n observations. From the result residuals are computed for all observations. This is repeated for all possible combinations of u observations. The solution is the one that meets the requirement:

$$\text{median}\left(\vec{v}^2\right) \rightarrow \min . \tag{2.49}$$

The advantage of this estimator is that the solution is not affected by the geometry of the observations. But it does require a high computational effort to compute all combinations of possible solutions with u out of n observations. (Neitzel, 2004).

To obtain a numerical solution a non-linear equation system needs to be solved for all resistant and robust estimation techniques. A closed-form solution does usually not exist. Hence, iterative algorithms are required to compute a solution. (Neitzel, 2004). An often-used algorithm repeatedly computes a least-squares solution with iteratively altered observation weights according to some function of the residuals, which is defined by the estimator used, (Welsch et al., 2000b). In a series of examples simulating an L_1-norm estimation Neitzel (2004) shows that the computation by iteratively altered observation weights can converge to a wrong solution. Furthermore, the convergence rate is very slow and the obtained solution strongly depends on the chosen termination criterion for the iteration.

The simple integration into existing software is often given as a reason for the use of the re-weighted least-squares algorithm. For the numerical solution of the L_1-estimation the so-called *Simplex*-algorithm exists but for other estimators alternative solution methods typically do not exist. (Neitzel, 2004).

Neitzel (2004) also summarizes the results from examinations of robust estimation techniques by different authors with the conclusion that the success rate of robust estimation techniques

[8]Least Median Squares

even with larger redundancies is low. In some cases outliers may be indicated where none exist in the data. Although some estimators have a high breakdown point it is not always guaranteed that all outliers are correctly identified. Their reliability depends on the number of unknowns, the number, magnitude and type of outliers in the data and the geometry of the observations. The reliability decreases rapidly with an increasing number of unknowns.

While it appears obvious to apply robust estimation techniques, especially those with a high breakdown point, to the analysis of monitoring networks to identify unstable points, above-mentioned conclusions of the analyses by several authors show that these techniques can lead to unreasonable results, (Neitzel, 2004).

Finally something should be pointed out that has already been cautioned against in Caspary (1996) and Neitzel (2004). Robust estimation techniques should not be used for parameter estimation, but should only serve as analysis tools to identify outliers in the observations. These observations should then be closely examined, eliminated and, if required, re-observed. Once all outliers have been dealt with in this way, the final parameter estimation should be performed by a least-squares estimation using the remaining, good data only.

2.3.4.3 Combinatorial Search

As has become evident from the above discussion, neither the classical least-squares-based single point analysis nor robust estimation techniques can reliably separate stable from unstable points in all scenarios. While the former is simply over-powered with more than 3 % to 5 % of outliers in the data, the latter can handle up to 50 % contaminated data but that depends largely on the given geometry.

One of the robust estimation techniques that is outstanding from the rest is the LMS-method. It employs a combinatorial search and thus eliminates all issues regarding the geometry of the points. But since only a minimal configuration is computed, this method can lead to unreasonable results, (Neitzel, 2004). The idea of a combinatorial search however,

shall be further investigated.

In Neitzel (2004) the author suggests a new method with the idea to find the largest congruent point group in a direct way. The *"MSS - maximum subsample method"* is defined in Neitzel (2004) as the method which employs a combinatorial search to find the maximum subsample of all data which yield an agreeable result in a least-squares adjustment. It is noted that it depends on the application at hand when results are agreeable. Possible criteria include the standardized residuals of the observations or a statistical test (such as the global congruency test in a deformation analysis).

Applied to a deformation analysis, the basic idea is to perform the global congruency test in (2.35) for *all* possible combinations of points. The group with the smallest quadratic form $\hat{\Omega}^2$ from (2.31), for a given number of points, for which the null hypothesis cannot be rejected is considered the largest congruent point group. To illustrate this, consider the following example. A monitoring network, observed in two epochs, consists of ten points. In the first step the global congruency test from (2.35) is carried out for all ten points, as usual. If this test fails, the presence of deformations somewhere in the network must be assumed. In the next step all possible combinations of nine out of ten points are analyzed with the global congruency test. If none of these ten combinations leads to acceptance of the null hypothesis, the test is repeated for all possible combinations of 8 out of 10 points. This continues until a combination has been found that passes the test.

It is obvious that this quite easily can lead to a large number of combinations depending on how many points remain stable. Assuming that only three points did not move, even in this small example there would have been

$$\begin{pmatrix} 10 \\ 9 \end{pmatrix} + \begin{pmatrix} 10 \\ 8 \end{pmatrix} + \begin{pmatrix} 10 \\ 7 \end{pmatrix} + \ldots + \begin{pmatrix} 10 \\ 3 \end{pmatrix} = 967$$

combinations to be computed. While this still sounds manageable given modern computing power, for a monitoring network with 30 stable points out of a total of 50 points, the total

number of combinations that would have to be computed until the largest congruent point group is found is $1.1408 \cdot 10^{14}$.

Conclusively, a method is required that allows to reduce the number of possible combinations to a reasonable level. In Neitzel (2004) the following two strategies are proposed.

2.3.4.3.1 MSS using distance differences

For this type of pre-analysis all possible distances are computed from the adjusted coordinates in both, epoch i and j. Their corresponding cofactor matrix can be derived by the application of the covariance law.

$$\vec{l}_i = \mathbf{F}_i^T \vec{x}_i, \quad \mathbf{Q}_{ll_i} = \mathbf{F}_i^T \mathbf{Q}_{xx_i} \mathbf{F}_i \qquad \text{and} \qquad \vec{l}_j = \mathbf{F}_j^T \vec{x}_j, \quad \mathbf{Q}_{ll_j} = \mathbf{F}_j^T \mathbf{Q}_{xx_j} \mathbf{F}_j \tag{2.50}$$

Then the distance difference vector $d\vec{l}$ and its cofactor matrix $\mathbf{Q}_{dl}$ follow from

$$d\vec{l} = \vec{l}_j - \vec{l}_i, \quad \mathbf{Q}_{dl} = \mathbf{Q}_{ll_i} + \mathbf{Q}_{ll_j}. \tag{2.51}$$

With the combined variance factor of both epochs $\hat{\sigma}_0^2$, standard deviations $\hat{\sigma}_{dl}$ for the distance differences are available. These data can now be analyzed to identify which of the distances have significantly changed in between epochs.

The simplest way to do this is to compare the elements dl_k of the difference vector $d\vec{l}$ against a pre-defined value such that

$$|dl_k| > T \cdot \hat{\sigma}_{dl_k} \tag{2.52}$$

where T is a value based on experience. For $T = 3$ for example the well-know $3\,\sigma$-criterion is established. If the inequality in (2.52) is satisfied, the assumption $E\{dl_k\} = 0$ is dismissed. The significantly changed distance differences are eliminated and do not partake in the further analysis.

Using the remaining distances possible congruent point groups are then identified by their topological relations. Topological relations in a network can be described by an edge-node

matrix. The network points are considered nodes that are connected by edges. The observations are assigned to the edges so that the topological relationships can be described in an edge-node matrix $\mathbf{C}$. For the five point network from previous examples, shown again in Figure 2.9, the corresponding edge-node matrix is given in Table 2.19. It is of no concern which distances were actually observed and which were not, as all distances are computed from the adjusted coordinates of each epoch. Hence, in the example below all distances are shown. In $\mathbf{C}$ the i^{th} observation is assigned to the j^{th} point according to the following definition:[9]

$c_{ij} = \quad 1$, if the i^{th} observations originates in point j,

$c_{ij} = -1$, if the i^{th} observations ends in point j,

$c_{ij} = \quad 0$, in all other cases.

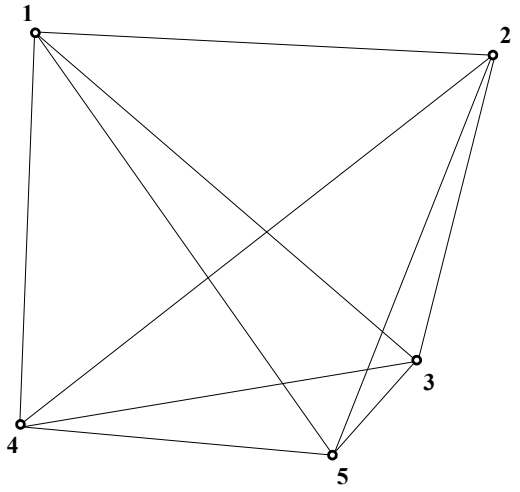

Figure 2.9: Five point network

	Pt 1	Pt 2	Pt 3	Pt 4	Pt 5
$l_{1,2}$	1	−1	0	0	0
$l_{1,3}$	1	0	−1	0	0
$l_{1,4}$	1	0	0	−1	0
$l_{1,5}$	1	0	0	0	−1
$l_{2,3}$	0	1	−1	0	0
$l_{2,4}$	0	1	0	−1	0
$l_{2,5}$	0	1	0	0	−1
$l_{3,4}$	0	0	1	−1	0
$l_{3,5}$	0	0	1	0	−1
$l_{4,5}$	0	0	0	1	−1

Table 2.19: Edge-node matrix for five point network

From the edge-node matrix $\mathbf{C}$, the symmetric node-node matrix $\bar{\mathbf{C}} = \mathbf{C}^T\mathbf{C}$ can be derived. For the example of the five point network with all distances existing, the node-node matrix is shown in Table 2.20.

[9]Note that the indices i and j refer to the rows and columns of the matrix $\mathbf{C}$ and *not* to the two epochs under consideration.

	Pt 1	Pt 2	Pt 3	Pt 4	Pt 5
Pt 1	4	−1	−1	−1	−1
Pt 2	−1	4	−1	−1	−1
Pt 3	−1	−1	4	−1	−1
Pt 4	−1	−1	−1	4	−1
Pt 5	−1	−1	−1	−1	4

Table 2.20: Node-node matrix for five point network with all distances

The elements of the node-node matrix $\bar{\mathbf{C}}$ can be interpreted as follows:[10]

$\bar{c}_{ii}$ = number of edges meeting at point i,

$\bar{c}_{ij} = -1$, if an edge connection exists between point i and point j,

$\bar{c}_{ij} = \quad 0$, if no edge connection exists between point i and point j.

For the identification of the largest congruent point group all possible distances are computed in both epochs. After eliminating those distances that indicate deformations, the edge-node matrix $\mathbf{C}$ is populated with the remaining distances. The corresponding node-node matrix $\bar{\mathbf{C}}$ can then be derived. Using $\bar{\mathbf{C}}$ the localization of the largest congruent point group can be carried out in the following steps:

1. Search all $\bar{c}_{ii}$ for the largest element $\bar{c}_{ii} = max$.

2. Determine how many elements n with $\bar{c}_{ii} \geq max$ exist. If $n \geq max + 1$, congruent point groups of $max + 1$ points can potentially exist.

3. If the number of points $n = max + 1$, it can be checked whether all distances (edges) exist between those points. If this is the case, then this group is a candidate for a possible congruent point group.

4. If $n > max + 1$, all possible combinations of $(max + 1)$ out of n points have to be checked for the existence of all edges. Those point groups that contain

[10]Note that the indices i and j refer to the rows and columns of the matrix $\bar{\mathbf{C}}$ and *not* to the two epochs under consideration.

all edges are candidates for congruent point groups.

5. The candidates are examined with the global congruency test in (2.35). The candidate passing the test is the largest congruent point group. Further congruent point groups can be found by eliminating all points of the largest group from $\bar{\mathbf{C}}$ under the assumption that different congruent point groups do not have points in common. The search for further congruent groups can then be continued with step 1.

6. If no congruent point group could be found, the localization is continued with step 2 with $max = max - 1$.

To illustrate the search for the largest congruent point group, the first example from Section 2.3.2.4 is revisited. From the adjusted coordinates for epoch 1 (see Table 2.4) all possible distances in the network are computed. Likewise, all distances are computed for epoch 2 from the adjusted coordinates in Table 2.9. The distance differences and their standard deviations are then derived. To evaluate the distance differences with respect to possible changes, the $3\,\sigma$-criterion is chosen as a rejection threshold. The distance differences and their rejection thresholds are given in Table 2.21 below. A look at the table shows that

From	To	dl	$3\,\hat{\sigma}_{dl}$
1	2	0.0047	0.0160
1	3	0.0546	0.0166
1	4	-0.0033	0.0148
1	5	0.0012	0.0172
2	3	0.0247	0.0133
2	4	0.0006	0.0188
2	5	0.0028	0.0153
3	4	0.0341	0.0146
3	5	0.0042	0.0104
4	5	-0.0005	0.0135

Table 2.21: Distance differences and their rejection threshold for example network in [m]

three distances exceed their rejection threshold and are thus to be eliminated. These are

the distances from point 1 to point 3, from point 2 to point 3 and from point 3 to point 4. Populating the edge-node matrix $\mathbf{C}$ with the remaining distances and deriving the node-node matrix $\bar{\mathbf{C}}$ yields the following results.

	Pt 1	Pt 2	Pt 3	Pt 4	Pt 5
$l_{1,2}$	1	-1	0	0	0
$l_{1,4}$	1	0	0	-1	0
$l_{1,5}$	1	0	0	0	-1
$l_{2,4}$	0	1	0	-1	0
$l_{2,5}$	0	1	0	0	-1
$l_{3,5}$	0	0	1	0	-1
$l_{4,5}$	0	0	0	1	-1

Table 2.22: Edge-node matrix without rejected distances

	Pt 1	Pt 2	Pt 3	Pt 4	Pt 5
Pt 1	3	-1	0	-1	-1
Pt 2	-1	3	0	-1	-1
Pt 3	0	0	1	0	-1
Pt 4	-1	-1	0	3	-1
Pt 5	-1	-1	-1	-1	4

Table 2.23: Resulting node-node matrix for example network

Using the node-node matrix in Table 2.23 the largest congruent point group can now be located as follows:

- The largest diagonal element is $\bar{c}_{55} = max = 4$ indicating the existence of a pentagon, since four edges meet in the vertex of a pentagon.
- There is only one element $n = 1$ with $\bar{c}_{ii} \geq max$, thus a pentagon cannot exist.
- Set $max = max - 1 = 3$.
- There are $n = 4$ elements with $\bar{c}_{ii} \geq max$, which means that only one tetragon can exist, consisting of the points 1, 2, 4 and 5.

Thus the largest congruent point group is correctly identified. The global congruency test for this group shows that the null hypothesis indeed has to be accepted. Removing the four points of this group from the node-node matrix leaves only point 3, so that no further congruent point groups can exist in this example.

This small example only served the purpose of illustrating how the MSS-algorithm works. However, it also indicates the reduced computational effort. Only one global congruency

test had to be performed to verify the largest congruent point group, whereas a total of five combinations of four out of five points would have had to be computed without this pre-analysis.

2.3.4.3.2 MSS using distance ratios

Since the above approach is based on the distance differences for the elimination of impossible combinations, it can obviously not lead to success if larger scale differences between the two epochs are to be expected. For this reason a different approach to the pre-analysis is proposed in Neitzel (2004).

Instead of the distance differences between epochs, the *distance ratios* are analyzed. Again, all distances in both epochs are derived according to (2.50). For the k^{th} distance l_{k_i} from epoch i and the corresponding distance l_{k_j} in epoch j, the distance ratio s_k follows as:

$$s_k = \frac{l_{k_i}}{l_{k_j}} \tag{2.53}$$

and, given the standard deviations $\hat{\sigma}_{k_i}$ and $\hat{\sigma}_{k_j}$, the standard deviations for the distance ratio s_k can be derived as:

$$\hat{\sigma}^2_{s_k} = \left(\frac{1}{l_{k_j}} \cdot \hat{\sigma}_{k_i}\right)^2 + \left(\frac{l_{k_i}}{l^2_{k_j}} \cdot \hat{\sigma}^2_{k_j}\right)^2 . \tag{2.54}$$

This expression can be simplified by assuming that $l_{k_i} = l_{k_j} = l_k$:

$$\hat{\sigma}_{s_k} = \frac{1}{l_k}\sqrt{\hat{\sigma}^2_{k_i} + \hat{\sigma}^2_{k_j}} . \tag{2.55}$$

As the true scale factor between epochs i and j is unknown, the distance ratios in (2.53) cannot be compared against a fixed value. Nonetheless, a preselection can be made to narrow down the number of combinations. This is achieved by using an estimate for the empirical standard deviation of the scale factor obtained from inserting the shortest distance of the network into equation (2.55). And, choosing a tolerance factor T (e. g. $T = 3$), one obtains a tolerance for the scale factor of

$$T_s = T \cdot \hat{\sigma}_s . \tag{2.56}$$

T_s defines a search window for the scale factor. If a congruence analysis with all p points fails, the largest similar point group can be found by sorting all distance ratios s_k from (2.53) by size in ascending order and proceeding in the following manner:

1. Compute T_s; the size of the search window in which similar point groups have to be included.
2. Start the search window in row $k = 1$ in the list of sorted distance ratios.
3. Check if a similar point group of $p-1$ points exists within the search window. This can be done using topology matrices. If one (or more) point group(s) exist, then these are candidates for a similar point group.
4. Start the search window in row $k = k + 1$ and perform step 3.
5. Once the end of the list of scale ratios is reached and candidates for similar point groups were found, the search is terminated. If no group of $p-1$ points exists, the search is continued with $p-2$ points with step 2.
6. Verify the candidates through a least-squares adjustment.

Unlike in the case of distance differences, a global congruency test cannot be derived directly from the observations because the scale factor is still unknown. Hence, a least-squares analysis that solves for the unknown scale factor is required. As mathematical model for the adjustment one of the transformation approaches discussed in the Section 2.4 can be used. The final solution is the one that yields the smallest standardized residuals[11] $|w_k| \leq c$, where c is a chosen rejection threshold[12]

This strategy shall be illustrated by revisiting the second example from Section 2.3.2.4. From the coordinates in Table 2.4 for epoch 1 and the scaled coordinates in Table 2.14 all distances

[11] The standardized residuals are obtained by dividing the residuals by their theoretical standard deviations: $w_k = v_k/\sigma_{v_k}$.

[12] Typically, a value of $2.5 \leq c \leq 4$ is chosen, (Niemeier, 2002).

in the network and their corresponding distance ratios have been computed. The standard deviation for the scale factor was computed through variance propagation of the covariance matrices of the adjusted coordinates of each epoch. The shortest distance in the network is 23 m. The size of the search window thus follows as:

$$T_s = 3 \cdot \frac{1}{23}\sqrt{0.0024^2 + 0.0025^2} = 452\,\text{ppm}\ . \tag{2.57}$$

Table 2.24 lists the computed scale ratios in ascending order and shows the search windows

k	From	To	Distance ratios in [ppm]
1	1	3	−906.4
2	3	4	−774.7
3	2	3	−738.9
4	3	5	−478.2
5	1	2	−357.2
6	2	5	−335.7
7	1	5	−313.1
8	2	4	−306.0
9	4	5	−290.4
10	1	4	−253.1

Table 2.24: Sorted list of distance ratios with search windows

with a size of 452 ppm. On this basis the search for the largest similar point group can now be conducted in the following manner:

- An adjustment with $p = 5$ points did not result in an acceptable solution. Hence, a similar tetragon ($p = 4$) is now wanted.
- Starting with the first row in Table 2.24, a search window of 452 ppm is created. As this window contains only four distances; a tetragon cannot exist.
- A new search window is created beginning in the second row. This window

contains only five distances; a tetragon cannot exist.

- The search window starting in row three yields seven distances so that a tetragon can possibly exist. To check this combination, the edge-node matrix (Table 2.25) is populated and with it the node-node matrix (Table 2.26) is calculated.

	Pt 1	Pt 2	Pt 3	Pt 4	Pt 5
$l_{2,3}$	0	1	-1	0	0
$l_{3,5}$	0	0	1	0	-1
$l_{1,2}$	1	-1	0	0	0
$l_{2,5}$	0	1	0	0	-1
$l_{1,5}$	1	0	0	0	-1
$l_{2,4}$	0	1	0	-1	0
$l_{4,5}$	0	0	0	1	-1

Table 2.25: Edge-node matrix for third search window

	Pt 1	Pt 2	Pt 3	Pt 4	Pt 5
Pt 1	2	-1	0	0	-1
Pt 2	-1	4	-1	-1	-1
Pt 3	0	-1	2	0	-1
Pt 4	0	-1	0	2	-1
Pt 5	-1	-1	-1	-1	4

Table 2.26: Resulting node-node matrix for third search window

- A look at the nod-nod matrix in Table 2.26 reveals, that this combination is not a possible candidate for a similar group, as only in points 2 and 5 three or more edges meet. Thus, the distances in this group cannot form a tetragon.
- Similarly, the next search window, starting in row four, does not yield a valid candidate either. (Edge-node matrix and node-node matrix not shown.)
- The last search window, starting in row five, contains six distances, so that a tetragon can possibly exist. The corresponding edge-node and node-node matrices are shown in Table 2.27 and Table 2.28, respectively.
- The node-node matrix in Table 2.28 for the last search window shows that this combination consists of four points with three edges meeting at each of them. Thus, this combination forms the only candidate for the largest similar point group.
- For the one candidate found, a least squares adjustment has to be computed

	Pt 1	Pt 2	Pt 3	Pt 4	Pt 5
$l_{1,2}$	1	-1	0	0	0
$l_{2,5}$	0	1	0	0	-1
$l_{1,5}$	1	0	0	0	-1
$l_{2,4}$	0	1	0	-1	0
$l_{4,5}$	0	0	0	1	-1
$l_{1,4}$	1	0	0	-1	0

Table 2.27: Edge-node matrix for last search window

	Pt 1	Pt 2	Pt 4	Pt 5
Pt 1	3	-1	-1	-1
Pt 2	-1	3	-1	-1
Pt 4	-1	-1	3	-1
Pt 5	-1	-1	-1	3

Table 2.28: Resulting node-node matrix for last search window

to estimate the scale factor and verify that the candidate is indeed the correct solution.

This example illustrates how similar point groups can be found if a change in scale has occurred between epochs. Compared to Section 2.3.2.4, where the classical congruence analysis fails, the MSS method using distance ratios succeeds in finding the correct point group, even though a rather large scale difference of 300 ppm exists between epochs. Furthermore, in the presented example, with help of the MSS method, the possible combinations could be narrowed down to one candidate – the final solution – so that only one least-squares adjustment is required.

2.3.5 Discussion

In Section 2.3.2 the basic mathematical model for a congruence analysis has been introduced. It can be divided into three steps: global congruency testing, localization of deformed points and determination of movements. The global congruency test establishes whether changes in the overall size and shape of the network have occurred between the two epochs under consideration. Interesting here is the possibility to derive this test either from the coordinates of each epoch or datum-invariant quantities such as distances. The localization step is comprised of a series of localized tests examining the null hypothesis, that no deformations have occurred, for each point individually. The point with the largest test statistic is eliminated

first and the local tests are repeated for the remaining points. This procedure is continued until all remaining points pass the local test. If an unstable point is part of the datum definition it has to be removed from the computational base with an S-transformation. In the final step deformations for the unstable points are determined. This can either be achieved through a common adjustment of the observations from both epochs or, again, through the application of an S-transformation.

Two numerical examples were presented to illustrate this method. Two epochs of a monitoring network consisting of five points are analyzed. Only one of the points is subject to deformations. The coordinates for each epoch are derived from a network analysis. Both epochs have the same datum defined by all five network points. In the first example the deformed point is correctly identified and realistic values are obtained for its deformations. No other points were mistakenly identified as unstable. In the second example a scale factor of 300 ppm is introduced to the distances of the second epoch and the analysis is repeated. In this case the congruence analysis fails because both global and local tests are affected by the change in scale.

An alternative method for a congruence analysis proposed by Teskey et al. (2005) is then introduced. It is based on a 3D similarity transformation and allows for a change in scale between epochs. It can also accommodate further parameters such as a refraction coefficient, if required. This method utilizes the observations directly thus avoiding the issues of datum definition and S-transformation entirely. It is more economical than observation of a multi-station network as it only requires data from a single instrument setup. However, this results in the target points in each epoch only being uniquely determined without any redundancy. The major disadvantage of this method is the integration of the deformation detection with the estimation of the transformation parameters. This means that the parameter estimation is performed before deformed points are eliminated from the data, possibly causing absorption of deformations in the transformation parameters. And, as well as the

classical approach, it relies on a single point analysis to localize deformed points.

The problem with the single point analysis is the implied assumption that only the point under consideration is presumably unstable while the remaining points are fixed. This, of course, is often not the case. And smoothing effects of deformed points on the test statistics of stable points can lead to wrong identification of stable points as deformed. Furthermore, the single point analysis is based on least-squares principles which require the data to be free of systematic influences and only to possess Gaussian noise. Then, and only then, a small number of outliers (deformed points), typically 3 % to 5 %, can be detected in the data. If these requirements are not met, the single point analysis cannot be expected to be successful.

Robust estimation techniques were investigated as they have higher breakdown points. For the class of M-estimators the breakdown point is at approximately 5 % to 10 %. For the purpose of a deformation analysis this still is not sufficient as easily more than 10 % of the points in a monitoring network can be subject to deformations. Some robust techniques have breakdown down points as high as 50 %, such as the L_1-norm estimator or the LMS-estimator. However, these techniques can lead to wrong results as well and do not always correctly identify all contaminated data, especially if outliers/deformations of small magnitude are inherent in the data. Furthermore, they require iterative solution algorithms which are typically implemented as an iterative re-weighted least-squares solution. In Neitzel (2004) it has been shown that these do not always converge to the correct solution, that the convergence is slow and that the results heavily depend on the chosen termination criterion for the iteration.

After investigating the classical approach and its single point analysis as well as robust estimation techniques it becomes evident that there is a need for an alternative methodology that is capable of distinguishing between stable and deformed points even when a large percentage of points is subject to deformations and even when systematic influences such as

scale changes between epochs occur.

The method proposed in Neitzel (2004) is based on a combinatorial search and aims to find the largest congruent point group between two epochs rather than to eliminate single deformed points. The great advantage of a combinatorial search is that it will always lead to the correct solution if all possible combinations are examined. The number of possible combinations, on the other hand, can quickly become very high, especially for large networks with only a few stable points. Thus a pre-analysis is required to eliminate impossible combinations right off the bat. Neitzel (2004) suggests two methods to achieve this. The first approach analyzes differences in the distances between epochs eliminating those distances that show significant changes. Topological relations between the remaining distances are then used to easily and quickly establish those point combinations that potentially could form the largest congruent point group. The candidates that were found can be verified with a global congruency test whose test quantity can be derived directly from the distance differences, so that there is no need to perform a full least-squares analysis.

The second approach compares the ratios of the same distances in each epoch rather than their differences. Unlike, the distance difference approach, this method is not affected by changes in the scale between epochs. Since the true scale factor is unknown, however, a direct comparison cannot be made so that this approach requires a more elaborate search for the largest similar point group. An error estimate for the scale factor is derived which is used to define the size of a search window. This search window is used to methodically work through the list of sorted distance ratios to find point combinations that lie within the window. Again, topological relations of the point combinations found lead to a quick assessment whether they are a possible candidate for the largest similar point group or not. To verify the candidates found a transformation-based least-squares adjustment is required in which the unknown scale factor is estimated and the candidates can be judged by the resulting standardized residuals.

The major advantage of the distance ratios approach is that it is insusceptible to scale changes between epochs, which in real-world applications often occur. But compared to the distance differences approach it is not as computationally efficient. Because the error estimate for the scale factor is only approximate it can lead to a rather large search window which in turn results in more candidates for similar point groups than actually exist. Furthermore, since the scale factor is unknown, a global congruency test cannot simply be applied as is possible with the distance difference approach. Instead, the computation of a least-squares solution to determine the unknown scale factor is required for each candidate found.

2.4 Solutions for the over-determined 3D Helmert transformation with singular cofactor matrix

As has been shown in the previous section, alternative approaches for the classical congruence analysis are required, specifically those that do not utilize a single point analysis to distinguish between stable and unstable points. Two such methods, employing a combinatorial search, have been discussed in Section 2.3.4.3. To finalize the deformation analysis and derive movement vectors for the group of unstable points, after localization according to Section 2.3.4.3, a transformation-based approach can be applied. Such an approach is particularly of interest if further systematic effects, such as a change in scale between epochs, need to be taken into account. In the event that the two epochs under comparison are given in different coordinate systems, a full 3D similarity transformation may even be applicable. For this reason, similarity or Helmert transformations in 3D space and different solution algorithms for over-determined transformation problems are discussed below. Particular attention is paid to the cofactor matrices of the coordinates as they originate from a free network adjustment and are thus singular.

2.4.1 3D HELMERT transformation

A HELMERT or similarity transformation relates the coordinates of a point $\vec{x}$ in a system j to its coordinates in a system i through three rotations ω, φ, κ about the coordinate axes, three translations T_x, T_y, T_z along the coordinate axes and a scale factor λ. In general form this can be written as:

$$\vec{x}_i = \lambda \cdot \mathbf{R} \cdot \vec{x}_j + \vec{T} \,, \tag{2.58}$$

where $\mathbf{R}$ denotes the rotation matrix and $\vec{T}$ the vector of translations. In more explicit form equation (2.58) can be written as, (Niemeier, 2002):

$$\begin{pmatrix} x \\ y \\ z \end{pmatrix}_i = \lambda \cdot \mathbf{R}_z(\kappa) \cdot \mathbf{R}_y(\varphi) \cdot \mathbf{R}_x(\omega) \cdot \begin{pmatrix} x \\ y \\ z \end{pmatrix}_j + \begin{pmatrix} T_x \\ T_y \\ T_z \end{pmatrix} \,, \tag{2.59}$$

where $\mathbf{R}_x(\omega)$, $\mathbf{R}_y(\varphi)$ and $\mathbf{R}_z(\kappa)$ represent the three elementary rotations about the x-, y- and z-axis, respectively. From the three elementary rotations the combined rotation matrix $\mathbf{R}$ follows as:

$$\begin{aligned} \mathbf{R} &= \begin{bmatrix} \cos(\kappa) & -\sin(\kappa) & 0 \\ \sin(\kappa) & \cos(\kappa) & 0 \\ 0 & 0 & 1 \end{bmatrix} \cdot \begin{bmatrix} \cos(\varphi) & 0 & \sin(\varphi) \\ 0 & 1 & 0 \\ -\sin(\varphi) & 0 & \cos(\varphi) \end{bmatrix} \cdot \begin{bmatrix} 1 & 0 & 0 \\ 0 & \cos(\omega) & -\sin(\omega) \\ 0 & \sin(\omega) & \cos(\omega) \end{bmatrix} \\ &= \begin{bmatrix} \cos(\varphi)\cos(\kappa) & \sin(\omega)\sin(\varphi)\cos(\kappa) - \cos(\omega)\sin(\kappa) & \cos(\omega)\sin(\varphi)\cos(\kappa) + \sin(\omega)\sin(\kappa) \\ \cos(\varphi)\sin(\kappa) & \cos(\omega)\cos(\kappa) + \sin(\omega)\sin(\varphi)\sin(\kappa) & \cos(\omega)\sin(\varphi)\sin(\kappa) - \sin(\omega)\cos(\kappa) \\ -\sin(\varphi) & \sin(\omega)\cos(\varphi) & \cos(\omega)\cos(\varphi) \end{bmatrix} \end{aligned} \tag{2.60}$$

or in short form:

$$\mathbf{R} = \begin{bmatrix} r_{11} & r_{12} & r_{13} \\ r_{21} & r_{22} & r_{23} \\ r_{31} & r_{32} & r_{33} \end{bmatrix} \,. \tag{2.61}$$

Thus, the transformation in (2.59) can be re-written as:

$$\begin{aligned} x_i &= \lambda \cdot (r_{11} \cdot x_j + r_{12} \cdot y_j + r_{13} \cdot z_j) + T_x \\ y_i &= \lambda \cdot (r_{21} \cdot x_j + r_{22} \cdot y_j + r_{23} \cdot z_j) + T_y \\ z_i &= \lambda \cdot (r_{31} \cdot x_j + r_{32} \cdot y_j + r_{33} \cdot z_j) + T_z \end{aligned} \quad . \tag{2.62}$$

If the seven transformation parameters ω, φ, κ, T_x, T_y, T_z and λ are known, equation (2.59) allows one to determine the coordinates of point $\vec{x}$ in system i, given the coordinates of $\vec{x}$ in system j. If, on the other hand, the coordinates of a set of points in system i as well as the coordinates of the same set of points in system j are known, the transformation parameters between the two systems can be estimated. Given the coordinates of three or more points in both systems, an overdetermined adjustment problem exists, in which the unknown transformation parameters can be estimated.

If the coordinates $\vec{x}_i$ and $\vec{x}_j$ were obtained in a free network adjustment, their corresponding cofactor matrices $\mathbf{Q}_{xx_i}$ and $\mathbf{Q}_{xx_j}$ are singular. This is of importance, as the singular cofactor matrices contain stochastic as well as deterministic information. A solution to the adjustment problem can only be obtained if the deterministic information is included in the functional model, (Neitzel, 2004). In the following sections different approaches to solve this adjustment problem are discussed. It should be noted here, that only the problem is considered where the coordinates of both, system i and system j, are introduced as observations. Each has their own, fully populated and singular cofactor matrix. The problems where only the coordinates in one system are considered as observations while the other set of coordinates is considered constant along with the case where both sets of coordinates are observations but with only a diagonal cofactor matrix, are neglected here, as these do not apply to deformation monitoring.

2.4.2 Solutions based on fictitious observations

In Neitzel (2004) the following two approaches are proposed in which the deterministic and stochastic information of the singular cofactor matrices are separated by introducing a minimal configuration of estimable quantities as fictitious observations. The deterministic part is then incorporated into the functional model by the explicit introduction of condition equations for the datum definition.

The estimable quantities are computed from the adjusted coordinates in both systems such that the network geometry is uniquely determined. Whether the computed quantities describe actual measurements or not is of no concern. The simplest way to describe the network geometry is through the use of spatial distances between the network points. Given a network with known scale and a rank defect of $d = 6$ of the cofactor matrix, $n = u - d$ distances (u being the number of coordinates) are required to uniquely describe the geometry. Formally, these distances can be derived from

$$\underset{(n\times 1)}{\vec{l}} = \underset{(n\times u)}{\mathbf{F}^T}\,\underset{(u\times 1)}{\vec{x}}\,, \qquad \underset{(n\times n)}{\mathbf{Q}_{ll}} = \underset{(n\times u)}{\mathbf{F}^T}\,\underset{(u\times u)}{\mathbf{Q}_{xx}}\,\underset{(u\times n)}{\mathbf{F}} \tag{2.63}$$

with

$$l_{pq} = \sqrt{(x_p - x_q)^2 + (y_p - y_q)^2 + (z_p - z_q)^2}\,. \tag{2.64}$$

In (2.63) $\mathbf{F}$ denotes the functional matrix that links the adjusted coordinates $\vec{x}$ to the computed distances $\vec{l}$ and contains the partial derivatives of (2.64) with respect to $\vec{x}$:

$$\mathbf{F} = \frac{\partial \vec{l}}{\partial \vec{x}}\,. \tag{2.65}$$

The resulting cofactor matrix $\mathbf{Q}_{ll}$ of the distances is regular and thus invertible since it describes a minimal configuration. Hence, the corresponding weight matrix $\mathbf{P}$ follows from

$$\mathbf{P} = \mathbf{Q}_{ll}^{-1}\,. \tag{2.66}$$

The distances $\vec{l}$ and their corresponding cofactor matrices $\mathbf{Q}_{ll}$ and weight matrices $\mathbf{P}$ are computed for both coordinate systems i and j.

2.4.2.1 Explicit formulation of transformation

With the fictitious distance observations $\vec{l}_i$ in the target system i and $\vec{l}_j$ in the source system j and their weight matrices $\mathbf{P}_i$ and $\mathbf{P}_j$, respectively, the following approach for a transformation can be derived.

The following unknown parameters are to be estimated in the adjustment:

$\vec{x}_i$	... coordinates in the target system
$\vec{x}_j$	... coordinates in the source system
ω, φ, κ	... rotation angles about the x-, y-, z-axes
T_x, T_y, T_z	... translations along the x-, y-, z-axes
λ	... scale factor

The following n_i observation equations can be written for the target system i:

$$f_{k_i}: \qquad l_{pq_i} + v_{pq_i} = \sqrt{\left(x_{p_i} - x_{q_i}\right)^2 + \left(y_{p_i} - y_{q_i}\right)^2 + \left(z_{p_i} - z_{q_i}\right)^2} \tag{2.67}$$

and likewise for the source system j the following n_j observation equations exist:

$$f_{k_j}: \qquad l_{pq_j} + v_{pq_j} = \sqrt{\left(x_{p_j} - x_{q_j}\right)^2 + \left(y_{p_j} - y_{q_j}\right)^2 + \left(z_{p_j} - z_{q_j}\right)^2}\,. \tag{2.68}$$

In addition to the observation above a datum definition is required in both target- and source system. Only points that are given in both systems and are known to be stable in both systems are allowed to contribute to the datum definition. As differences in the configuration of the two networks are possible as well as point movements, a separation in h datum points $\mathrm{P_D}$ and g non-datum points $\mathrm{P_N}$ is required. According to (2.7) the conditions for the datum definition in the target system i can be written as

$$\begin{aligned}
c_{1_i}: &\quad \sum_{k=1}^{h} \Delta x_{\mathrm{Dk}_i} = 0 \quad c_{4_i}: \quad \sum_{k=1}^{h} \left(z^0_{\mathrm{D}k_i} \Delta y_{\mathrm{D}k_i} - y^0_{\mathrm{D}k_i} \Delta z_{\mathrm{D}k_i}\right) = 0 \\
c_{2_i}: &\quad \sum_{k=1}^{h} \Delta y_{\mathrm{Dk}_i} = 0 \quad c_{5_i}: \quad \sum_{k=1}^{h} \left(x^0_{\mathrm{D}k_i} \Delta z_{\mathrm{D}k_i} - z^0_{\mathrm{D}k_i} \Delta x_{\mathrm{D}k_i}\right) = 0 \\
c_{3_i}: &\quad \sum_{k=1}^{h} \Delta z_{\mathrm{Dk}_i} = 0 \quad c_{6_i}: \quad \sum_{k=1}^{h} \left(y^0_{\mathrm{D}k_i} \Delta x_{\mathrm{D}k_i} - x^0_{\mathrm{D}k_i} \Delta y_{\mathrm{D}k_i}\right) = 0
\end{aligned} \tag{2.69}$$

Accordingly, the condition equations for the datum definition in the source system j can be written as

$$\begin{aligned}
c_{1_j}: &\quad \sum_{k=1}^{h} \Delta x_{\mathrm{Dk}_j} = 0 \quad c_{4_j}: \quad \sum_{k=1}^{h} \left(z^0_{\mathrm{D}k_j} \Delta y_{\mathrm{D}k_j} - y^0_{\mathrm{D}k_j} \Delta z_{\mathrm{D}k_j} \right) = 0 \\
c_{2_j}: &\quad \sum_{k=1}^{h} \Delta y_{\mathrm{Dk}_j} = 0 \quad c_{5_j}: \quad \sum_{k=1}^{h} \left(x^0_{\mathrm{D}k_j} \Delta z_{\mathrm{D}k_j} - z^0_{\mathrm{D}k_j} \Delta x_{\mathrm{D}k_j} \right) = 0 \\
c_{3_j}: &\quad \sum_{k=1}^{h} \Delta z_{\mathrm{Dk}_j} = 0 \quad c_{6_j}: \quad \sum_{k=1}^{h} \left(y^0_{\mathrm{D}k_j} \Delta x_{\mathrm{D}k_j} - x^0_{\mathrm{D}k_j} \Delta y_{\mathrm{D}k_j} \right) = 0
\end{aligned} \tag{2.70}$$

In the above equations the conditions $c_{1\text{-}3_{i/j}}$ describe the three translations whereas $c_{4\text{-}6_{i/j}}$ describe the three rotations.

The transformation from the source system to the target system for the datum points $\mathrm{P_D}$ can be achieved through the following condition equations based on (2.62):

$$\begin{aligned}
t_x: &\quad \lambda \cdot \left(r_{11} \cdot x_{\mathrm{D}_j} + r_{12} \cdot y_{\mathrm{D}_j} + r_{13} \cdot z_{\mathrm{D}_j} \right) + T_x - x_{\mathrm{D}_i} = 0 \\
t_y: &\quad \lambda \cdot \left(r_{21} \cdot x_{\mathrm{D}_j} + r_{22} \cdot y_{\mathrm{D}_j} + r_{23} \cdot z_{\mathrm{D}_j} \right) + T_y - y_{\mathrm{D}_i} = 0 \\
t_z: &\quad \lambda \cdot \left(r_{31} \cdot x_{\mathrm{D}_j} + r_{32} \cdot y_{\mathrm{D}_j} + r_{33} \cdot z_{\mathrm{D}_j} \right) + T_z - z_{\mathrm{D}_i} = 0
\end{aligned} \tag{2.71}$$

This describes a Gauss-Markov model, for which the solution can be derived by linearization at suitable initial estimates $\vec{x}_0$ and iteration. The vector of unknowns can be expressed as follows:

$$\begin{aligned}
\Delta\vec{x} \;=\; (\; & \Delta x_{\mathrm{D}1_i} \quad \Delta y_{\mathrm{D}1_i} \quad \Delta z_{\mathrm{D}1_i} \quad \ldots \quad \Delta x_{\mathrm{D}h_i} \quad \Delta y_{\mathrm{D}h_i} \quad \Delta z_{\mathrm{D}h_i} \\
& \Delta x_{\mathrm{N}1_i} \quad \Delta y_{\mathrm{N}1_i} \quad \Delta z_{\mathrm{N}1_i} \quad \ldots \quad \Delta x_{\mathrm{N}g_i} \quad \Delta y_{\mathrm{N}g_i} \quad \Delta z_{\mathrm{N}g_i} \\
& \Delta x_{\mathrm{D}1_j} \quad \Delta y_{\mathrm{D}1_j} \quad \Delta z_{\mathrm{D}1_j} \quad \ldots \quad \Delta x_{\mathrm{D}h_j} \quad \Delta y_{\mathrm{D}h_j} \quad \Delta z_{\mathrm{D}h_j} \\
& \Delta x_{\mathrm{N}1_j} \quad \Delta y_{\mathrm{N}1_j} \quad \Delta z_{\mathrm{N}1_j} \quad \ldots \quad \Delta x_{\mathrm{N}g_j} \quad \Delta y_{\mathrm{N}g_j} \quad \Delta z_{\mathrm{N}g_j} \\
& \Delta T_x \quad \Delta T_y \quad \Delta T_z \quad \Delta\omega \quad \Delta\varphi \quad \Delta\kappa \quad \Delta\lambda \;)^T \, .
\end{aligned} \tag{2.72}$$

The design matrix $\mathbf{A}_1$ is derived by taking the partial derivatives of the observation equations (2.67) in the target system i. Likewise, the design matrix $\mathbf{A_2}$ is obtained by taking the partial derivatives of the observation equations (2.68) in the source system j. Linearization of the condition equations (2.69) for the datum definition and (2.70) yield the condition matrices

$\mathbf{B}_1$ and $\mathbf{B}_2$ for the target and source system, respectively. And finally, linearization of the transformation equation (2.71) results in the condition matrix $\mathbf{B}_\mathrm{T}$.

The difference vector of the observations is given by

$$\Delta\vec{l} = \left(\begin{array}{c} \vdots \\ l_{pq_i} - \sqrt{\left(x^0_{p_i} - x^0_{q_i}\right)^2 + \left(y^0_{p_i} - y^0_{q_i}\right)^2 + \left(z^0_{p_i} - z^0_{q_i}\right)^2} \\ \vdots \\ \hline \vdots \\ l_{pq_j} - \sqrt{\left(x^0_{p_j} - x^0_{q_j}\right)^2 + \left(y^0_{p_j} - y^0_{q_j}\right)^2 + \left(z^0_{p_j} - z^0_{q_j}\right)^2} \\ \vdots \end{array}\right) \tag{2.73}$$

and the misclosure vector for the conditions follows from

$$\vec{w} = \left(\begin{array}{c} 0 \\ \vdots \\ 0 \\ \hline 0 \\ \vdots \\ 0 \\ \hline \vdots \\ 0 - \left(\lambda \cdot \left(r_{11} \cdot x_{\mathrm{D}_j} + r_{12} \cdot y_{\mathrm{D}_j} + r_{13} \cdot z_{\mathrm{D}_j}\right) + T_x - x_{\mathrm{D}_i}\right) \\ 0 - \left(\lambda \cdot \left(r_{11} \cdot x_{\mathrm{D}_j} + r_{12} \cdot y_{\mathrm{D}_j} + r_{13} \cdot z_{\mathrm{D}_j}\right) + T_x - x_{\mathrm{D}_i}\right) \\ 0 - \left(\lambda \cdot \left(r_{31} \cdot x_{\mathrm{D}_j} + r_{32} \cdot y_{\mathrm{D}_j} + r_{33} \cdot z_{\mathrm{D}_j}\right) + T_z - z_{\mathrm{D}_i}\right) \\ \vdots \end{array}\right) \tag{2.74}$$

Given

$$\mathbf{A} = \begin{bmatrix} \mathbf{A}_1 \\ \mathbf{A}_2 \end{bmatrix}, \quad \mathbf{B} = \begin{bmatrix} \mathbf{B}_1 \\ \mathbf{B}_2 \\ \mathbf{B}_\mathrm{T} \end{bmatrix}, \quad \mathbf{P} = \begin{bmatrix} \mathbf{P}_i & 0 \\ 0 & \mathbf{P}_j \end{bmatrix} \tag{2.75}$$

the normal equation system for the Gauss-Markov model can be written as

$$\begin{bmatrix} \mathbf{A}^T\mathbf{P}\mathbf{A} & \mathbf{B}^T \\ \mathbf{B} & 0 \end{bmatrix} \begin{pmatrix} \Delta\vec{x} \\ \vec{k} \end{pmatrix} = \begin{pmatrix} \mathbf{A}^T\mathbf{P}\Delta\vec{l} \\ \vec{w} \end{pmatrix} . \tag{2.76}$$

This corresponds to a common network adjustment of both epochs simultaneously combined with a transformation in a one-step solution. The fictitious observations of a minimal configuration in each system serve as input together with their regular cofactor matrices. The results include the adjusted coordinates of both epochs as well as the adjusted transformation parameters.

2.4.2.2 Implicit formulation of transformation

Another approach proposed in Neitzel (2004) abandons the condition equations (2.71) for the transformation and simplifies the functional model by implicitly formulating the transformation instead. Now only the coordinates of the target system i are introduced as unknowns reducing the parameters to be estimated in the adjustment to

$$\begin{aligned} \vec{x}_i &\quad \ldots \text{coordinates in the target system} \\ \lambda &\quad \ldots \text{scale factor} \end{aligned}$$

The input is again given by the fictitious observations of a minimal configuration from (2.63) in both systems, so that $\vec{l}_i$ and $\vec{l}_j$ as well as their weight matrices $\mathbf{P}_i$ and $\mathbf{P}_j$ are available.

Using the reduced set of parameters the n_i observation equations for the target system i can be written as

$$f_{k_i}: \qquad l_{pq_i} + v_{pq_i} = \sqrt{(x_{p_i} - x_{q_i})^2 + (y_{p_i} - y_{q_i})^2 + (z_{p_i} - z_{q_i})^2} \tag{2.77}$$

while the n_j observation equations for the source system j are now expressed as a function of the coordinates in the target system i such that

$$f_{k_j}: \qquad l_{pq_j} + v_{pq_j} = \frac{1}{\lambda}\sqrt{(x_{p_i} - x_{q_i})^2 + (y_{p_i} - y_{q_i})^2 + (z_{p_i} - z_{q_i})^2} . \tag{2.78}$$

The datum definition is realized using the condition equations (2.69), again separating the coordinate vector in datum points $\mathrm{P_D}$ and non-datum points $\mathrm{P_N}$. Since only one coordinate vector is estimated, the non-datum points have to be excluded from the datum definition as well as from the implicit formulation of the transformation. This is achieved by introducing two different sets of coordinates with different point IDs (a and b) in the target system.

The solution for this adjustment problem can be derived by linearization at suitable initial estimates $\vec{x}_0$ and iteration. The vector of unknowns can be expressed as follows:

$$\begin{aligned} \Delta\vec{x} \;=\; (\; & \Delta x_{\mathrm{D}1_i} \quad \Delta y_{\mathrm{D}1_i} \quad \Delta z_{\mathrm{D}1_i} \quad \dots \quad \Delta x_{\mathrm{D}h_i} \quad \Delta y_{\mathrm{D}h_i} \quad \Delta z_{\mathrm{D}h_i} \\ & \Delta x_{\mathrm{N}1a_i} \quad \Delta y_{\mathrm{N}1a_i} \quad \Delta z_{\mathrm{N}1a_i} \quad \dots \quad \Delta x_{\mathrm{N}ga_i} \quad \Delta y_{\mathrm{N}ga_i} \quad \Delta z_{\mathrm{N}ga_i} \\ & \Delta x_{\mathrm{N}1b_i} \quad \Delta y_{\mathrm{N}1b_i} \quad \Delta z_{\mathrm{N}1b_i} \quad \dots \quad \Delta x_{\mathrm{N}gb_i} \quad \Delta y_{\mathrm{N}gb_i} \quad \Delta z_{\mathrm{N}gb_i} \\ & \Delta\lambda \;)^T \; , \end{aligned} \tag{2.79}$$

where the non-datum points ending in a refer to points in the target system i while non-datum points ending in b correspond to points transformed from the source system j into the target system i.

The design matrix $\mathbf{A}_1$ is derived by taking the partial derivatives of the observation equations (2.77) in the target system i. Likewise, the design matrix $\mathbf{A}_2$ is obtained by taking the partial derivatives of the observation equations (2.78) in the target system i. Linearization of the condition equations (2.69) for the datum definition yield the condition matrix $\mathbf{B}$ for the target system.

The difference vector of the observations and the misclosure vector for the conditions are

given by

$$\Delta\vec{l} = \begin{pmatrix} \vdots \\ l_{pq_i} - \sqrt{\left(x^0_{p_i} - x^0_{q_i}\right)^2 + \left(y^0_{p_i} - y^0_{q_i}\right)^2 + \left(z^0_{p_i} - z^0_{q_i}\right)^2} \\ \vdots \\ \hline \vdots \\ l_{pq_j} - \sqrt{\left(x^0_{p_i} - x^0_{q_i}\right)^2 + \left(y^0_{p_i} - y^0_{q_i}\right)^2 + \left(z^0_{p_i} - z^0_{q_i}\right)^2} \\ \vdots \end{pmatrix}, \quad \vec{w} = \begin{pmatrix} 0 \\ 0 \\ 0 \\ 0 \\ 0 \\ 0 \end{pmatrix} \tag{2.80}$$

Given

$$\mathbf{A} = \begin{bmatrix} \mathbf{A}_1 \\ \mathbf{A}_2 \end{bmatrix}, \quad \mathbf{P} = \begin{bmatrix} \mathbf{P}_i & 0 \\ 0 & \mathbf{P}_j \end{bmatrix} \tag{2.81}$$

the normal equation system from (2.76) for the Gauss-Markov model can be solved to obtain the unknown parameters.

As a result of the estimation coordinates in the target system are obtained. For points not participating in the datum definition and the implicit formulation of the transformation two sets of coordinates are obtained. One set represents the adjusted coordinates in the target system while the other set represents the transformed coordinates from the source into the target system. Because of the implicit formulation of the transformation, only the scale factor has to be estimated. The translation and rotation parameters are not part of the parameter vector but can be back-calculated exactly, if desired.

2.4.3 Gauss-Helmert model with singular cofactor matrix

The approaches considered so far are based on the Gauss-Markov model and utilize a minimal configuration of estimable quantities as fictitious observations, thus extracting the stochastic information from the singular cofactor matrices of the original coordinates. Following, another approach is discussed that utilizes the singular cofactor matrices from the free network adjustments directly.

Considering the adjusted coordinates $\vec{x}_i$ in the target system i as well as the adjusted coordinates $\vec{x}_j$ in the source system j directly as observations, equation (2.59) yields three condition equations for each point observed in both systems. These three condition equations for the transformation from the source system j to the target system i can be explicitly written as:

$$\begin{aligned} f_x: \quad & \lambda \cdot (r_{11} \cdot x_j + r_{12} \cdot y_j + r_{13} \cdot z_j) + T_x - x_i &= 0 \\ f_y: \quad & \lambda \cdot (r_{21} \cdot x_j + r_{22} \cdot y_j + r_{23} \cdot z_j) + T_y - y_i &= 0 \\ f_y: \quad & \lambda \cdot (r_{31} \cdot x_j + r_{32} \cdot y_j + r_{33} \cdot z_j) + T_z - z_i &= 0 \end{aligned} \tag{2.82}$$

where r_{pq} are the elements of the rotation matrix $\mathbf{R}$ given by (2.60). The unknowns to be solved for in this case are the seven transformation parameters:

ω, φ, κ	... rotation angles about the x-, y-, z-axes
T_x, T_y, T_z	... translations along the x-, y-, z-axes
λ	... scale factor.

If three or more identical points are available in both systems, equation (2.82) describes a non-linear adjustment problem in the form of a Gauss-Helmert model:

$$f\left(\vec{l}, \vec{x}\right) = \vec{0}. \tag{2.83}$$

With the observation vector and its cofactor matrix given by

$$\vec{l}_0 = \begin{pmatrix} \vec{x}_i \\ \vec{x}_j \end{pmatrix}, \quad \mathbf{Q}_{ll} = \begin{bmatrix} \mathbf{Q}_{xx_i} & 0 \\ 0 & \mathbf{Q}_{xx_j} \end{bmatrix} \tag{2.84}$$

and the parameter vector described by

$$\vec{x} = \begin{pmatrix} \omega & \varphi & \kappa & T_x & T_y & T_z & \lambda \end{pmatrix}^T. \tag{2.85}$$

The non-linear functional relationship in (2.83) needs to be linearized first. This can be

accomplished by a first-order Taylor series with suitable approximations $\vec{l}_0$ and $\vec{x}_0$:

$$\begin{aligned} f\left(\vec{l},\vec{x}\right) &= \underbrace{\left.\frac{\partial f}{\partial \vec{x}}\right|_{\vec{l}_0,\vec{x}_0}}_{=\mathbf{A}} \cdot \underbrace{\left(\vec{x}-\vec{x}_0\right)}_{=\Delta\vec{x}} + \underbrace{\left.\frac{\partial f}{\partial \vec{l}}\right|_{\vec{l}_0,\vec{x}_0}}_{=\mathbf{B}} \cdot \underbrace{\left(\vec{l}-\vec{l}_0\right)}_{=\vec{v}} + \underbrace{f\left(\vec{l}_0,\vec{x}_0\right)}_{=-\vec{w}} = \vec{0} \\ &= \mathbf{A}\Delta\vec{x} + \mathbf{B}\vec{v} - \vec{w} = \vec{0} \end{aligned} \tag{2.86}$$

Where $\mathbf{A}$ is the design matrix containing the partial derivatives of the condition equations (2.82) with respect to the unknown parameters $\vec{x}$ and $\mathbf{B}$ is the condition matrix consisting of the partial derivatives of (2.82) with respect to the observations $\vec{l}$. The corrections for the approximations of the unknowns are denoted as $\Delta\vec{x}$; $\vec{v}$ are the residuals of the observation vector and $\vec{w}$ represents the misclosure vector.

Introducing the vector of Lagrange multipliers $\vec{k}$, the variation function Φ can be formed:

$$\Phi = \vec{v}^T\mathbf{P}\vec{v} - 2\vec{k}^T\left(\mathbf{A}\Delta\vec{x} + \mathbf{B}\vec{v} - \vec{w}\right) \rightarrow \min. \tag{2.87}$$

Taking the partial derivatives of the variation function Φ with respect to the unknown quantities $\vec{v}$, $\vec{k}$ and $\Delta\vec{x}$ and simplifying the expressions yields the linearized normal equations

$$\begin{aligned} \mathbf{B}\mathbf{Q}_{ll}\mathbf{B}^T\vec{k} \;+\; \mathbf{A}\Delta\vec{x} &= \vec{w} \\ \mathbf{A}^T\vec{k} &= \vec{0}. \end{aligned} \tag{2.88}$$

Given p identical points in both systems i and j, with $p \geq 3$, the dimensions of this adjustment problem can be described as follows:

$$\begin{aligned} n &= 6p && \ldots \text{number of observations} \\ b &= 3p && \ldots \text{number of conditions} \\ u &= 7 && \ldots \text{number of unknowns} \\ r &= b - u = 3p - 7 && \ldots \text{redundancy.} \end{aligned}$$

The $(b \times n)$ condition matrix $\mathbf{B}$ always has full row rank b since each set of condition equations (f_x, f_y, f_z) in (2.82) describes the relationship between the coordinates in system i and system j for a different point. Hence, all condition equations must be linearly independent.

Similarly, the seven transformation parameters in (2.85) are linearly independent such that the $(b \times u)$ design matrix $\mathbf{A}$ is always of full column rank $q = u$. The cofactor matrix of the observations $\mathbf{Q}_{ll}$ has a rank defect of d as it results from a free network adjustment. Consequently, the rank of the matrix product of $\mathbf{B}$ and $\mathbf{Q}_{ll}$ is less than the rank of $\mathbf{B}$:

$$\mathrm{rk}\,(\mathbf{B}\mathbf{Q}_{ll}) < \mathrm{rk}\,(\mathbf{B})\,. \tag{2.89}$$

In Neitzel and Schaffrin (2013b) it is shown that the normal equations in (2.88), in the case of (2.89), have a unique solution for $\Delta\vec{x}$ and $\vec{k}$ under the conditions that

$$\mathrm{rk}\,([\mathbf{A} \;\; \mathbf{B}\mathbf{Q}_{ll}]) = r + q = \mathrm{rk}\,(\mathbf{B}) \quad \text{and} \tag{2.90a}$$

$$\mathrm{rk}\,(\mathbf{A}) = q = u. \tag{2.90b}$$

While the ranks of $\mathbf{A}$ and $\mathbf{B}$ have already been discussed above and condition (2.90b) is fulfilled for the parameters in (2.85), condition (2.90a) can only be checked numerically and thus has to be evaluated for each case individually.

2.4.3.1 Iterative solution of the Gauss-Helmert model

The rigorous analysis of the Gauss-Helmert model is important in order to reach convergence to the correct solution. Unfortunately, some pitfalls exist in the iterative linearization procedure that have already been pointed out by Pope (1972). Nevertheless, some of these pitfalls can be found in numerous least-squares textbooks, such as Wolf and Ghilani (1997) and Niemeier (2002), for example. In Lenzmann and Lenzmann (2004) a detailed comparison of algorithms with inapplicable approximations is provided that may converge to a solution, but it may not be the non-linear least-squares solution. Neitzel (2010) as well as Neitzel and Schaffrin (2013b) also point out the importance of the rigorous evaluation of the iterative linearization.

With the approximations $\vec{l}_0$ and $\vec{x}_0$, the design matrix $\mathbf{A}_0$ and condition matrix $\mathbf{B}_0$ of the initial iteration step can be determined according to (2.86). Similarly, the initial misclosure

vector $\vec{w}_0$ follows by inserting the approximate values into the condition equations (2.82). As suitable approximations for the adjusted observations the original coordinates from the free network adjustment can be used for the first iteration step, assuming the initial residual vector to be $\vec{v}_0 = \vec{0}$.

For the transformation parameters approximations can be derived by computing inverses between two points and comparing these between systems. The scale factor follows from the ratio of a distance in system i and a distance in system j. The rotation about the z-axis can be derived by comparing a bearing between two points in system i to the bearing of the same two points in system j, etc. Once approximate values for the rotations and scale are computed, the translations follow from re-arranging (2.82) and using the coordinates of a set of identical points in both systems together with the approximations for the rotation angles and scale factor to solve for the translation parameters.

Now, the solution for $\vec{k}$ and $\Delta\vec{x}$ for the first iteration step can be computed from the normal equations (2.88) by inversion of the normal equation matrix:

$$\begin{pmatrix} \vec{k}_1 \\ \Delta\vec{x}_1 \end{pmatrix} = \begin{bmatrix} \mathbf{B}_0\mathbf{Q}_{ll}\mathbf{B}_0^T & \mathbf{A}_0 \\ \mathbf{A}_0^T & 0 \end{bmatrix}^{-1} \begin{pmatrix} \vec{w}_0 \\ \vec{0} \end{pmatrix} . \tag{2.91}$$

Again, the normal equation matrix is uniquely invertible if the conditions in (2.90) are satisfied. The updates for the next iteration step then follow from:

$$\begin{aligned} \vec{x}_1 &= \vec{x}_0 + \Delta\vec{x}_1 \\ \vec{v}_1 &= \vec{v}_0 + \mathbf{Q}_{ll}\mathbf{B}_0^T\vec{k}_1 = \mathbf{Q}_{ll}\mathbf{B}_0^T\vec{k}_1 \\ \vec{l}_1 &= \vec{l}_0 + \vec{v}_1 \end{aligned} \tag{2.92}$$

With the updated observation vector $\vec{l}_1$ and parameter vector $\vec{x}_1$, the design and condition matrices can be re-evaluated such that

$$\mathbf{A}_1 = \left.\frac{\partial f}{\partial \vec{x}}\right|_{\vec{l}_1, \vec{x}_1} \qquad \mathbf{B}_1 = \left.\frac{\partial f}{\partial \vec{l}}\right|_{\vec{l}_1, \vec{x}_1} . \tag{2.93}$$

Furthermore, the misclosure vector needs to be re-computed as

$$\vec{w}_1 = \mathbf{B}_1 \vec{v}_1 - f\left(\vec{l}_1, \vec{x}_1\right) \tag{2.94}$$

where the $-f\left(\vec{l}_1, \vec{x}_1\right)$ represents the linearization error and $\mathbf{B}_1\vec{v}_1$ expresses the misfit between the coordinates of identical points in system i and system j due to the errors inherent in the coordinate vectors.

Introducing the iteration counter $k = 1$, the solution for the next iteration step $k+1$ can now be obtained by inverting the normal equations (2.88):

$$\begin{pmatrix} \vec{k}_{k+1} \\ \Delta\vec{x}_{k+1} \end{pmatrix} = \begin{bmatrix} \mathbf{B}_k\mathbf{Q}_{ll}\mathbf{B}_k^T & \mathbf{A}_k \\ \mathbf{A}_k^T & 0 \end{bmatrix}^{-1} \begin{pmatrix} \vec{w}_k \\ \vec{0} \end{pmatrix} . \tag{2.95}$$

The updates for the next iteration step then follow from:

$$\begin{aligned} \vec{x}_{k+1} &= \vec{x}_k + \Delta\vec{x}_{k+1} \\ \vec{v}_{k+1} &= \vec{v}_k + \mathbf{Q}_{ll}\mathbf{B}_k^T\vec{k}_{k+1} \\ \vec{l}_{\,k+1} &= \vec{l}_{\,0} + \vec{v}_{k+1} \end{aligned} \tag{2.96}$$

Then, the design matrix, condition matrix and misclosure vector are re-evaluated as well as the misclosure vector to obtain the input for the following iteration step:

$$\mathbf{A}_{k+1} = \left.\frac{\partial f}{\partial \vec{x}}\right|_{\vec{l}_{\,k+1}, \vec{x}_{k+1}} \qquad \mathbf{B}_{k+1} = \left.\frac{\partial f}{\partial \vec{l}}\right|_{\vec{l}_{\,k+1}, \vec{x}_{k+1}} \qquad \vec{w}_{k+1} = \mathbf{B}_{k+1}\vec{v}_{k+1} - f\left(\vec{x}_{k+1}, \vec{l}_{\,k+1}\right) . \tag{2.97}$$

This iteration continues until a chosen termination criterion $\left|\Delta\vec{x}_k\right| < \delta$ with $\delta > 0$ is reached.

The final parameter vector $\vec{x}$ and residual vector $\vec{v}$ are given by

$$\vec{x} = \vec{x}_{k-1} + \Delta\vec{x}_k \qquad\qquad \vec{v} = \vec{v}_{k-1} + \mathbf{Q}_{ll}\mathbf{B}_{k-1}^T\vec{k}_k . \tag{2.98}$$

The sum $\hat{\Omega}^2$ of weighted squared residuals can be derived from, (Neitzel and Schaffrin, 2013a):

$$\hat{\Omega}^2 = \vec{w}_{k-1}\left(\vec{k}_k + \left(\mathbf{B}_{k-1}\mathbf{Q}_{ll}\mathbf{B}_{k-1}^T\right)^{-}\mathbf{B}_{k-1}\vec{v}_{k-1}\right) \tag{2.99}$$

and the a posteriori variance factor then follows as

$$\hat{\sigma}_0^2 = \frac{\hat{\Omega}^2}{r} \,. \tag{2.100}$$

Finally, the covariance matrix of the adjusted parameters $\mathbf{C}_{xx}$ can be taken directly from the inverse of the normal equation matrix for the final iteration step k, (Neitzel and Schaffrin, 2013a):

$$\begin{bmatrix} \mathbf{C}_{\lambda\lambda} & \times \\ \times & -\mathbf{C}_{xx} \end{bmatrix} = \hat{\sigma}_0^2 \cdot \begin{bmatrix} \mathbf{B}_{k-1}\mathbf{Q}_{ll}\mathbf{B}_{k-1}^T & \mathbf{A}_{k-1} \\ \mathbf{A}_{k-1}^T & 0 \end{bmatrix}^{-1} \tag{2.101}$$

with

$$\mathbf{C}_{vv} = \mathbf{Q}_{ll}\mathbf{B}_{k-1}^T\mathbf{C}_{\lambda\lambda}\mathbf{B}_{k-1}\mathbf{Q}_{ll} \tag{2.102}$$

resulting as the covariance matrix of the residuals $\vec{v}$. Note that the "$\times$" for the off-diagonal elements of (2.101) indicates that there is no correlation between the parameters and the residuals.

2.4.4 Total Least-Squares

An alternative to the Gauss-Helmert model described above is the so-called *total least-squares* (or TLS) model introduced by Golub and Van Loan (1980). The mathematical model is derived by extending the parametric least-squares model for problems where the elements in the design matrix $\mathbf{A}$ contain random errors as well, (Acar et al., 2006):

$$\vec{l} - \vec{e}_l = (\mathbf{A} - \mathbf{E}_A) \cdot \vec{x} \tag{2.103}$$

where $\vec{l}$ denotes an $(n \times 1)$ observation vector, $\vec{e}_l$ its $(n \times 1)$ error vector; $\mathbf{A}$ is the $(n \times u)$ design matrix, $\mathbf{E}_A$ its corresponding $(n \times u)$ error matrix and $\vec{x}$ is the $(u \times 1)$ vector of unknowns. This model is referred to as *errors-in-variables* (or EIV) model, (Acar et al., 2006).

In the basic TLS method the errors in $\vec{e}_l$ and $\mathbf{E}_A$ are assumed to have independent and identically distributed rows with a zero mean and the same variance. An optimization

is performed by minimizing the elements of the error vector $\vec{e}_l$ and the error matrix $\mathbf{E}_A$ according to, (Golub and Van Loan, 1980; Acar et al., 2006):

$$\left\| \left[\mathbf{E}_A \;\; \vec{e}_l \right] \right\|_F \rightarrow \min . \tag{2.104}$$

Here, $\|\mathbf{H}\|_F$ represents the Frobenius norm of an $(m \times n)$ matrix $\mathbf{H}$ as given by, (Acar et al., 2006):

$$\|\mathbf{H}\|_F = \sqrt{\sum_{i=1}^{m} \sum_{j=1}^{n} h_{ij}^2} = \sqrt{\mathrm{tr}\left(\mathbf{H}^T \mathbf{H}\right)} \tag{2.105}$$

where tr() denotes the trace of a matrix. The solution algorithm based on singular value decomposition (SVD) can be found e. g. in Golub and Van Loan (1980).

So far, no weighting of the observations has been considered. In most practical applications however, the variances of the elements of the observation vector and the design matrix are not identical. Furthermore, not all columns of the design matrix contain errors. (Acar et al., 2006). The following extension of the basic TLS model described above addresses these issues, (Van Huffel, 1991).

$$\vec{l} - \vec{e} = \left[\begin{array}{cc} \mathbf{A}_1 & \mathbf{A}_2 - \mathbf{E}_{A_2} \end{array} \right] \cdot \left(\begin{array}{c} \vec{x}_1 \\ \\ \vec{x}_2 \end{array} \right) \tag{2.106}$$

Here, $\mathbf{A}_1$ contains the error-free columns, associated with the subset of parameters $\vec{x}_1$ and $\mathbf{A}_2$ contains the erroneous columns associated with the subset of parameters $\vec{x}_2$. $\mathbf{E}_{A_2}$ denotes the error matrix of $\mathbf{A}_2$. Additionally, the $(n \times n)$ weight matrix $\mathbf{D}$ of the observations and the $(u_2 + 1 \times u_2 + 1)$ weight matrix $\mathbf{C}$ that reflects the relative accuracies of the observations with respect to the elements of the design matrix elements of $\mathbf{A}_2$ are introduced, (Van Huffel, 1991). This leads to the extended objective function

$$\left\| \mathbf{D} \cdot \left[\mathbf{E}_{A_2} \;\; \vec{e}_l \right] \cdot \mathbf{C} \right\|_F \rightarrow \min . \tag{2.107}$$

This extended model is referred to as *generalized* total least-squares model (or GTLS), (Van Huffel, 1991).

While a complete formulation for the solution of the GTLS model with fully-populated, non-singular weight matrices $\mathbf{C}$ and $\mathbf{D}$ is given in Van Huffel, 1991 and Mühlich and Mester, 2004, it is often dismissed in the literature as too complicated (Acar et al., 2006; Akyilmaz, 2007), thus reducing the weight matrices $\mathbf{C}$ and $\mathbf{D}$ to diagonal matrices with the justification that "in geodetic applications, covariance matrices are generally block-diagonal dominant matrices", (Acar et al., 2006).

Many more modifications of the basic TLS method exist, such as restricted TLS (Van Huffel and Zha, 1991), constrained TLS (Abatzoglou and Mendel, 1991), weighted TLS (Schaffrin, 2006), weighted multivariate TLS (Schaffrin and Wieser, 2009), improved weighted TLS and improved constrained weighted TLS (Tong et al., 2011).

It has been shown in Neitzel (2010) that TLS does not represent a new adjustment method, but rather another adjustment model (EIV model) in the frame of the method of least-squares. Also Acar et al., 2006 states that the mathematical model of the basic TLS approach is identical to that of the generalized LS method and that (2.103) represents a non-linear GH-model. Furthermore, Neitzel (2010) shows on the example of a 2D similarity transformation that the EIV model can be regarded as a special case of the non-linear GH-model and that the TLS solution can be achieved by a rigorous analysis of the non-linear GH-model *if* the *identical* objective function is minimized subject to an *identical* functional relationship, i. e. if in both cases the exact same problem is addressed. Hence, it follows that TLS can generally be applied to solve an over-determined similarity transformation.

The advantage of TLS is that, at least for the basic model and some other variations, a closed-form solution exists which eliminates the need for iteration, thus offering higher numerical stability and efficiency. This is especially useful for applications with large data sets as it can significantly reduce the computational effort.

The disadvantage of TLS is that, while there are variations such as GTLS that allow weights

for the observations and the elements of the error matrix and even allow fully-populated weight matrices, they all require non-singular matrices. A TLS approach that can handle the singular covariance matrices from a free network adjustment does not exist. In case of a deformation analysis, the input covariance matrices of the observations will typically be derived from a free network adjustment and thus will be singular. In this scenario it is also not acceptable to ignore the covariances and only use diagonal matrices instead. Hence, the TLS model and its derivatives are not considered any further in this thesis.

2.4.5 Discussion

The general model for a 3D Helmert transformation has been introduced. The required 3D rotation matrix combining the three elementary rotations about the coordinate axes has been given without any approximations. Different solution algorithms for over-determined transformation problems have been discussed. Two methods, proposed in Neitzel (2004), are based on fictitious observations which require the calculation of a minimal configuration of estimable quantities such as distances to separate the deterministic and stochastic information in the singular cofactor matrices of the adjusted coordinates in each system.

In the explicit formulation of transformation all seven transformation parameters are estimated together with the coordinates in both, the target and the source system. Additional condition equations define the datum in both systems as well as the transformation between identical points. A set of observation equations for the fictitious observations, uniquely describing the geometry in each system, is introduced to solve for the unknown coordinates. Thus, the problem can be solved as a Gauss-Markov model with a regular covariance matrix for the fictitious observations. This results in a rather large normal equation system. Considering a network of ten points where all ten points are observed in both systems and all ten points contribute to the datum, this would result in $10 \cdot 3 \cdot 2 = 60$ coordinate unknowns plus 7 unknown transformation parameters plus $6 \cdot 2 = 12$ condition equations for

the datum definition plus $10 \cdot 3 = 30$ condition equations describing the transformation, so that a (109×109) normal equation matrix would need to be inverted. Furthermore, with the rotations given by (2.60), the normal equation system is highly non-linear. This means that good initial approximations for the unknowns are required to assure convergence to the correct non-linear least-squares solution. Also, it can cause a rather slow convergence rate. Hence, this approach does not offer a numerically very efficient and stable solution.

The second method proposed in Neitzel (2004) presents a very elegant solution. Through the implicit formulation of the transformation the parameter vector can be reduced so that only coordinates in the target system and the scale factor need to be solved for. The translation and rotation parameters do not need to be estimated. Additional condition equations are only required for the datum definition of the target system. Thus, the resulting normal equation matrix of the GAUSS-MARKOV model for the same ten-point network has the size of $10 \cdot 3 = 30$ coordinate unknowns plus 6 condition equations for the datum definition plus 1 unknown transformation parameter (the scale factor), in total (37×37). Furthermore, by avoiding an explicit formulation of the rotation, the adjustment problem is numerically more stable and now only an approximation for the scale factor is needed. In most application $\lambda_0 = 1$ will be sufficient but if necessary, a more accurate estimate can easily be obtained by comparing (already available) distances in both systems. Hence, this approach presents a numerically more efficient and more stable solution. And while the rotation and translation parameters do not become available as a result of the adjustment, they can be back-calculated exactly, if desired. Still, the computation of a minimal configuration of estimable quantities is required in order to separate the deterministic and stochastic information contained in the singular cofactor matrix of the coordinates.

The third method presented utilizes the GAUSS-HELMERT model by introducing the adjusted coordinates of each system directly as observations. Then, condition equations for the transformation of each identical point from the source into the target system can be

explicitly given. The parameter vector consists only of the seven transformation parameters. Further condition equations for the datum definition in each system are not required since the original, singular cofactor matrices of the adjusted coordinates in each system can directly be processed in the adjustment, provided that the rank conditions in (2.90) are satisfied. Hence, a separation of the deterministic and stochastic information of the cofactor matrices through computation of a minimal configuration of estimable quantities and introduction of fictitious observations is omitted completely. The resulting normal equation matrix for the Gauss-Helmert model for the ten-point network has the size of $10 \cdot 3 = 30$ condition equations for the transformation plus 7 unknown transformation parameters, in total (37×37), which is identical to the size of the normal equation matrix of the implicit transformation. The transformation parameters are readily available as a result of the adjustment. On the other hand, this approach again results in a highly non-linear normal equation system due to the explicit formulation of the rotations, for which, again, good approximate values have to be derived. Conclusively, this method leads to a more numerically efficient but equally unstable solution compared to the explicit formulation of the transformation.

Finally, the total least-squares method has been discussed as an alternative solution to the Gauss-Helmert model. In the TLS approach only the coordinates in the target system are considered observations while the coordinates in the source system are considered as constants. This leads to errors in the design matrix for which then an error matrix is introduced, resulting in the errors-in-variables or EIV model. As has been shown in Neitzel (2010), the TLS method is equivalent to the Gauss-Helmert model, if the same objective function is minimized subject to an identical functional relationship, so that in principle total least-squares can be applied to solve transformation problems. Its advantage is an elegant closed-form solution algorithm based on a singular value decomposition, which yields high numerical efficiency and stability. However, this solution algorithm only exists for the basic, unweighted approach. Algorithms that can handle fully-populated, singular cofactor

matrices for the target and source system do not exist. Hence, the TLS approach is not appropriate for deformation monitoring applications where correct estimates of the standard deviations of the coordinates in each epoch and their correlations are of great importance, as they essentially define the level of detectability of the deformations.

2.5 Summary

In Section 2.1 different observation techniques applied in deformation monitoring are given. The focus is on geodetic techniques used in monitoring networks. Their special characteristics are discussed.

The network analysis of geodetic observations as an important pre-analysis step is discussed in Section 2.2. From the network analysis a homogeneous set of coordinates is obtained that uniquely and completely describes the network geometry at time of observation. To be able to estimate coordinates from the, mostly relative, observations, a reference frame and datum definition are required. Both are defined during the network analysis. The different options to define the geodetic datum of a network are discussed and its effects on the coordinates and their accuracies are illustrated on an example network. It was concluded that constrained approaches are generally not suitable for deformation monitoring as they can cause distortion of the geometry which can be misinterpreted as movements. Inner-constraints pose a better choice for deformation monitoring purposes, as they do not alter the network geometry. Ordinary minimal constraints should be avoided however, because then the chosen datum-defining coordinates form a zero-variance computational base, which makes it impossible to detect deformations in. A total trace minimization minimizes the sum of variances of all network points resulting in the lowest possible level of detectability for the movements of all points and is thus the recommended choice. An S-transformation allows to change the datum easily from one set of points to another without the need of

re-adjusting the observations with a new datum definition, provided that the given datum is defined by inner-constraints.

In Section 2.3 an overview of different deformation monitoring models is given. Then, focussing on the congruence model, the basic mathematical model for the classical congruence analysis is discussed in detail and illustrated on two examples. It shows that, ones a change in scale between the epochs is introduced, the analysis fails. Furthermore, different techniques for the localization of unstable points are examined. A single point analysis, as applied in the classical congruence model, cannot lead to correct results if a large percentage of points is deformed or additional systematic effects occur between epochs. Robust estimation techniques are investigated as they have a high breakdown point of up to 50 %. But these too can lead to wrong results and are not always able to identify all deformed points. The outcome strongly depends on the geometry, the number of points in the network, the redundancy and other factors. Results from the iterative solution algorithms, often based on a re-weighted least-squares solution, heavily depend on the chosen termination criteria for the iteration.

Thus the need for better for better localization methods arises. Two methods, based on a combinatorial search are introduced. They aim to find the largest congruent point group between two epochs of a network rather than to find and eliminate single deformed points, one at a time. A combinatorial search has the advantage that, if all combinations are tried, eventually the correct solution will be found. However, the total number of combinations can easily exceed a manageable level. The two methods presented are able to systematically eliminate impossible combinations by using topological relations so that the computational load of trying out combinations is greatly reduced. The MSS approach based on distance ratios is even insusceptible to scale changes but requires a least-squares adjustment for every possible candidate to solve or the unknown scale factor and verify the correct solution. It can also easily lead to an increased number of candidate solutions as only an approximate

error estimate for the unknown scale factor is available.

Finally, 3D HELMERT or similarity transformations are discussed in Section 2.4 as they pose a viable option for the determination of deformations once the largest congruent point group has been correctly identified with one of the methods discussed above. After introducing the general mathematical model, four different methods to solve the over-determined transformation problem are examined. Two approaches, based on a GAUSS-MARKOV model , utilize a minimal configuration of fictitious observations to separate deterministic and stochastic information of the singular cofactor matrices of the given coordinates. The implicit transformation approach presents a very elegant solution in which the scale factor is the only transformation parameter that is estimated.

A further possible solution introduces the coordinates in both systems directly as observations in a non-linear GAUSS-HELMERT model based on condition equations for the transformation as functional model. This approach allows to process the singular cofactor matrices of the coordinate vectors directly and without any pre-processing. But due to the explicit form of the rotation it is a highly non-linear problem that requires good initial approximations for the unknown rotation parameters.

Total least-squares is discussed as an alternative to the GAUSS-HELMERT model but since this approach cannot handle the fully-populated, singular cofactor matrices resulting from a free network adjustment, it should not be applied for the estimation of deformations.

Chapter 3

METHODOLOGY

3.1 Localization of largest similar point group based on angles

In Section 2.3.4.3.1 a combinatorial search based on distance differences was applied to identify the largest congruent point group between two epochs of a monitoring network. This is a powerful and reliable method that will yield the correct solution even if a large percentage of points are subject to deformations. But it is not applicable if a change in scale occurs between epochs.

In that event the MSS-method based on distance ratios rather than distance differences is proposed in Neitzel (2004) and discussed in Section 2.3.4.3.2. This approach works as reliably as the distance-difference approach with regard to the correct results. But since the scale factor is unknown and only an approximate error estimate is available, no firm significance threshold for the distance ratios can be determined. Instead a search window has to be used. This can easily lead to a large number of candidates for similar point groups. Then, for each candidate a least-squares adjustment has to be computed to estimate the unknown scale factor and identify the correct solution. This makes the distance-ratios approach potentially a lot more computationally intense than the distance-difference approach.

Hence, a different approach is proposed to find the largest similar point group between two epochs with different scales. It is based on a combinatorial search as well and thus shares the advantages of above-mentioned methods in regards to its reliability. But it utilizes angles rather than distances which allows a direct evaluation of angular differences between epochs while still being independent of scale changes. This approach is explained below.

Given three points A $(x_A \;\; y_A \;\; z_A)^T$, B $(x_B \;\; y_B \;\; z_B)^T$ and C $(x_C \;\; y_C \;\; z_C)^T$ the angle α at A from B to C can be derived from the two difference vectors

$$\begin{aligned} \vec{b} &= \begin{pmatrix} x_b & y_b & z_b \end{pmatrix}^T = \begin{pmatrix} x_B - x_A & y_B - y_A & z_B - z_A \end{pmatrix}^T \quad \text{and} \\ \vec{c} &= \begin{pmatrix} x_c & y_c & z_c \end{pmatrix}^T = \begin{pmatrix} x_C - x_A & y_C - y_A & z_C - z_A \end{pmatrix}^T \end{aligned} \tag{3.1}$$

through the scalar (or dot) product

$$\begin{aligned} \vec{b} \cdot \vec{c} &= x_b \cdot x_c + y_b \cdot y_c + z_b \cdot z_c = \left|\vec{b}\right| \left|\vec{c}\right| \cdot \cos\alpha \\ &= \sqrt{x_b^2 + y_b^2 + z_b^2} \cdot \sqrt{x_c^2 + y_c^2 + z_c^2} \cdot \cos\alpha \; . \end{aligned} \tag{3.2}$$

The angle α then follows as

$$\begin{aligned} \alpha &= \arccos\left(\frac{\vec{b} \cdot \vec{c}}{\left|\vec{b}\right| \left|\vec{c}\right|}\right) \\ &= \arccos\left(\frac{x_b \cdot x_c + y_b \cdot y_c + z_b \cdot z_c}{\sqrt{x_b^2 + y_b^2 + z_b^2} \cdot \sqrt{x_c^2 + y_c^2 + z_c^2}}\right) . \end{aligned} \tag{3.3}$$

Given the adjusted coordinate vectors $\vec{x}_i$ and $\vec{x}_j$ from two epochs i and j together with their singular cofactor matrices $\mathbf{Q}_{xx_i}$ and $\mathbf{Q}_{xx_j}$, the angles $\vec{\alpha}$ and their cofactor matrix $\mathbf{Q}_{\alpha\alpha}$ in *each* epoch can be derived from:

$$\vec{\alpha}_i = \mathbf{F}_i^T \vec{x}_i, \quad \mathbf{Q}_{\alpha\alpha_i} = \mathbf{F}_i^T \mathbf{Q}_{xx_i} \mathbf{F}_i \qquad \text{and} \qquad \vec{\alpha}_j = \mathbf{F}_j^T \vec{x}_j, \quad \mathbf{Q}_{\alpha\alpha_j} = \mathbf{F}_j^T \mathbf{Q}_{xx_j} \mathbf{F}_j \tag{3.4}$$

The derivation of the functional matrix $\mathbf{F}$ and the error propagation for the angles is in detail given in Appendix A.1.

Now, the vector of angular differences between epochs $d\vec{\alpha}$ and its cofactor matrix can be computed from:

$$d\vec{\alpha} = \vec{\alpha}_j - \vec{\alpha}_i, \qquad \mathbf{Q}_{d\alpha} = \mathbf{Q}_{\alpha\alpha_i} + \mathbf{Q}_{\alpha\alpha_j} \; . \tag{3.5}$$

Together with the combined variance factor $\hat{\sigma}_0^2$ of both epochs from (2.28) and a chosen tolerance value T, a significance threshold can be established such that the assumption $E\{d\alpha_k\} = 0$ is dismissed if

$$|d\alpha_k| > T \cdot \hat{\sigma}_0 \cdot \sqrt{q_{d\alpha_{kk}}} \; . \tag{3.6}$$

It should be pointed out that the value T should be chosen with care. If T is chosen too small, some angles may be rejected for which the assumption $E\{d\alpha_k\} = 0$ is true. This can lead to false results. If, on the other hand, T is chosen too large, fewer angles can be eliminated resulting in a higher number of possible candidates that have to be examined. It is thus preferred to choose T rather too large than too small. From experience, values of $3 \leq T \leq 5$ work well.

3.1.1 The Algorithm

In a network consisting of p points, at each of the network points $\sum_{i=1}^{p-2} i$ angles exist. After eliminating those angles that exhibit significant changes between epochs, which are an indication of point deformations, candidates for the largest similar point group can be found through a histogram-based search in the following manner:

1. Compute the histogram listing the number of angles existing at each network point after elimination of the significantly changed angles.
2. Start with search for group of $p_{max} = p - 1$ points.
3. Compute the number of angles max_α at each point for a group of p_{max} points from $max_\alpha = \sum_{i=1}^{p_{max}-2} i$.
4. Search histogram for all points p_{found} with number of angles $n_\alpha \geq max_\alpha$. If $p_{found} = p_{max}$, one preliminary candidate exists. If $p_{found} > p_{max}$, multiple preliminary candidates exist.
5. If $p_{found} < p_{max}$, no candidates exist. Set $p_{max} = p_{max} - 1$ and continue search with step 3.

For the preliminary candidate(s) it has to be established if all angles still exist. This can be accomplished by populating a three-dimensional array $\mathbf{C}$ from the list of remaining angles.

The array has a size of $(p \times p \times p)$ where p is the total number of points in the network. The three dimensions of the array correspond to the three points that form an angle, the origin (at), starting point (from) and end point (to). If, for example, the angle at point 1 from point 2 to point 3 still exists, the corresponding entry in $\mathbf{C}$ is $\mathbf{C}\,(\text{at, from, to}) = \mathbf{C}\,(1,\,2,\,3) = 1$. If, on the other hand, this angle was eliminated because it showed significant change between epochs, the corresponding entry would be $\mathbf{C}\,(\text{at, from, to}) = \mathbf{C}\,(1,\,2,\,3) = 0$.

To identify if all angles for a preliminary candidate group of m points exist, first a list of all theoretically possible $m \cdot \sum_{i=1}^{m-2} i$ angles is created. Then, the values in $\mathbf{C}$ for all the theoretically possible angels are summed up. If this sum is equal to the number of theoretically possible angles $m \cdot \sum_{i=1}^{m-2} i$, it means that all theoretically possible angles indeed exist for this preliminary candidate. Hence, this preliminary candidate becomes a final candidate.

Once this procedure has been carried out for all preliminary candidates, the remaining final candidates for similar point groups can be examined with a global congruency test as described in Section 2.3.2.1. It is advisable to compute the quadratic form $\hat{\Omega}^2$ directly from the angular differences in (3.5) according to (2.34). Together with the combined variance factor $\hat{\sigma}_0^2$ from (2.28), the global congruency test for each final candidate can be carried out as described in (2.35) without the necessity of performing a least-squares estimation.

3.1.2 Numerical example

Naturally, can this method be applied analogously to the 2D case. Hence, to illustrate the search for the largest congruent point group using angles, the second example from Section 2.3.2.4 is revisited once more. The network consisting of $p = 5$ points is shown again in Figure 3.1 with all $n = p \cdot \sum_{i=1}^{p-2} i = 30$ angles highlighted in bold. The coordinates for epoch 1 are given in Table 2.4 and the coordinates for epoch 2 can be found in Table 2.14. It should be mentioned here again, that the distances in epoch 2 were scaled by 300 ppm and

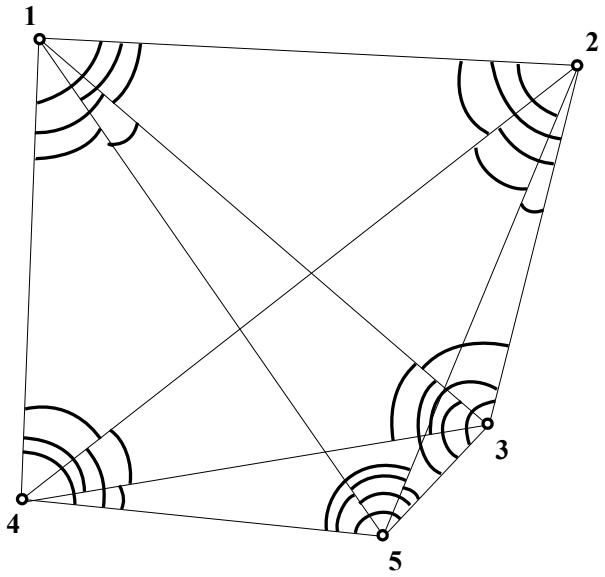

Figure 3.1: Example network with all angles shown

deformations of $dx = -30.0\,\text{mm}$ and $dy = +40\,\text{mm}$ were introduced in point 3.

After the comparison of the variance factors of both epochs and the initial global congruency test, which have already been performed in Section 2.3.2.4, all existing angles $\vec{\alpha}_i$ and $\vec{\alpha}_j$ are computed from the adjusted coordinates in each epoch along with their cofactor matrices. Then, the angular differences between epochs are calculated from (3.5) and evaluated according to (3.6). A tolerance factor of $T = 3$ was chosen, so that the 3σ-criterion is applied as a significance threshold. After eliminating the significantly changed angles, 15 out of 30 angles remain. They are listed in Table 3.1 below.

Angle	1	2	3	4	5	6	7	8	9	10	11	12	13	14	15
at	1	1	1	1	1	1	2	2	2	4	4	4	5	5	5
from	2	2	2	3	3	4	1	1	4	1	1	2	1	1	2
to	3	4	5	4	5	5	4	5	5	2	5	5	2	4	4

Table 3.1: Remaining angles after elimination

With the remaining 15 angles a histogram can be populated, listing the number of angles at each network point. This histogram is given in tabular form in Table 3.2 below.

The search for preliminary candidates for the largest similar point group can now be con-

Point	1	2	3	4	5
Number of angles	6	3	0	3	3

Table 3.2: Histogram of remaining angles

ducted as follows:

- Start with search for a group of $p_{max} = p - 1 = 4$ points (tetragon).
- In a tetragon $max_\alpha = \sum_{i=1}^{p_{max}-2} i = 3$ angles exist at each point.
- Search histogram for all points with $\geq max_\alpha = 3$ angles. $p_{found} = 4$ points exist with ≥ 3 angles.
- Since $p_{found} = 4 = p_{max}$, only one preliminary candidate for a similar group of four points exists, (points 1,2,4,5).

To check whether all angles for the preliminary candidates exist, a $(5 \times 5 \times 5)$ array $\mathbf{C}$ is created in which each angle in the 5 point network is assigned a value at the position of its "at", "from" and "to" points such that $\mathbf{C}$ (at, from, to) = 1 for all remaining points in Table 3.1 and $\mathbf{C}$ (at, from, to) = 0 for angles that were eliminated. Below the array is represented by 5 (5×5) tables, each table showing the angles at one of the five network points.

From \To	1	2	3	4	5
1	0	0	0	0	0
2	0	0	1	1	1
3	0	0	0	1	1
4	0	0	0	0	1
5	0	0	0	0	0

Table 3.3: Angles at pt 1

From \To	1	2	3	4	5
1	0	0	0	1	1
2	0	0	0	0	0
3	0	0	0	0	0
4	0	0	0	0	1
5	0	0	0	0	0

Table 3.4: Angles at pt 2

From \To	1	2	3	4	5
1	0	0	0	0	0
2	0	0	0	0	0
3	0	0	0	0	0
4	0	0	0	0	0
5	0	0	0	0	0

Table 3.5: Angles at pt 3

In a tetragon a total of twelfe angles exist, three at each point. For the preliminary candidate, the tetragon 1,2,4,5, these twelfe angles are listed in Table 3.8.

Summing up all values of the elements in $\mathbf{C}$ for the angles in Table 3.8 yields a value of twelve. That means that all twelve angles for the candidate were found in the array. Thus,

From \To	1	2	3	4	5
1	0	1	0	0	1
2	0	0	0	0	1
3	0	0	0	0	0
4	0	0	0	0	0
5	0	0	0	0	0

Table 3.6: Angles at pt 4

From \To	1	2	3	4	5
1	0	1	0	1	0
2	0	0	0	1	0
3	0	0	0	0	0
4	0	0	0	0	0
5	0	0	0	0	0

Table 3.7: Angles at pt 5

Angle	1	2	3	4	5	6	7	8	9	10	11	12
at	1	1	1	2	2	2	4	4	4	5	5	5
from	2	2	4	1	1	4	1	1	2	1	1	2
to	4	5	5	4	5	5	2	5	5	2	4	4

Table 3.8: Angles required for tetragon 1,2,4,5

the preliminary candidate becomes the only final candidate.

Finally, a global congruency test is performed to verify the candidate. The quadratic form $\hat{\Omega}^2$ can directly be derived from the angular differences of the angles listed in Table 3.8. The combined variance factor $\hat{\sigma}_0^2$ is already given in Section 2.3.2.4. The test statistic follows as:

$$T_G = \frac{\hat{\Omega}^2}{\hat{\sigma}_0^2} = \frac{1.2632 \cdot 10^{-4}}{1.3078 \cdot 10^{-4}} = 0.96.$$

The reference value for the FISHER-distribution for a confidence level of $\alpha = 5\,\%$ and degrees of freedom $f_1 = h = 5$ and $f_2 = r_1 + r_2 = 28$ is given by $F_{S=1-\alpha,f_1,f_2} = 2.56$. With $0.96 \leq 2.56$ the null hypothesis cannot be rejected and the global congruency test for the candidate solution passes.

In this example it has been shown that the MSS-method with angles presents a viable alternative to the distance approaches. The advantage of utilizing angular differences are that they are not affected by any scale changes between epochs and that the final candidates can be verified with a global congruency test that can be derived directly from the angular differences, so that no least-squares adjustment is necessary. In that sense, the angle approach combines the advantages of both distance approaches.

3.2 Determination of movements

After the largest similar point group between the two epochs has been identified, using the method proposed above, movements have to be derived for the unstable points. This can be accomplished by utilizing the transformation-based approach, shown in this section.

3.2.1 The approach

As starting point for the derivation, the transformation approach in Section 2.4.3, the Gauss-Helmert model with singular cofactor matrix, is chosen. It can handle the singular cofactor matrices from the free network adjustments of each epoch directly without requiring any preprocessing. Furthermore, the coordinate vectors from both epochs are treated as observations, leaving only the transformation parameters to be estimated.

Given are the coordinate vectors $\vec{x}_i$ and $\vec{x}_j$, which shall now refer to two states (or epochs) i and j of the *same* network, and their singular, fully-populated cofactor matrices $\mathbf{Q}_{xx_i}$ and $\mathbf{Q}_{xx_j}$:

$$\vec{x}_{i/j} = \begin{pmatrix} x_1 \\ y_1 \\ z_1 \\ \vdots \\ x_p \\ y_p \\ z_p \end{pmatrix}_{i/j} \qquad \mathbf{Q}_{xx_{i/j}} = \begin{bmatrix} q_{x_1,x_1} & q_{x_1,y_1} & q_{x_1,z_1} & \cdots & q_{x_1,x_p} & q_{x_1,y_p} & q_{x_1,z_p} \\ q_{x_1,y_1} & q_{y_1,y_1} & q_{y_1,z_1} & \cdots & q_{y_1,x_p} & q_{y_1,y_p} & q_{y_1,z_p} \\ q_{x_1,z_1} & q_{y_1,z_1} & q_{z_1,z_1} & \cdots & q_{z_1,x_p} & q_{z_1,y_p} & q_{z_1,z_p} \\ \vdots & \vdots & \vdots & \ddots & \vdots & \vdots & \vdots \\ q_{x_1,x_p} & q_{y_1,x_p} & q_{z_1,x_p} & \cdots & q_{x_p,x_p} & q_{x_p,y_p} & q_{x_p,z_p} \\ q_{x_1,y_p} & q_{y_1,y_p} & q_{z_1,y_p} & \cdots & q_{x_p,y_p} & q_{y_p,y_p} & q_{y_1,z_p} \\ q_{x_1,z_p} & q_{y_1,z_p} & q_{z_1,z_p} & \cdots & q_{x_p,z_p} & q_{y_p,z_p} & q_{z_p,z_p} \end{bmatrix}_{i/j} \tag{3.7}$$

In general form the 3D Helmert transformation relating the coordinates of epoch i to those of epoch j can be written as:

$$\vec{x}_i = \lambda \cdot \mathbf{R} \cdot \vec{x}_j + \vec{T} \,, \tag{3.8}$$

where $\mathbf{R}$ denotes the 3D rotation matrix, $\vec{T}$ the vector of translations and λ the scale factor. The problem is that the rotation matrix $\mathbf{R}$, shown in (2.60), consists of highly non-linear terms, thus requiring good initial approximations for the rotation angles. Furthermore, this can cause slow convergence and generally a numerically unstable normal equation system.

This problem could be solved by introducing the small-angle approximations $\sin(\theta) = \theta$ and $\cos(\theta) = 1$ and furthermore assuming that the product of two or more small angles $\theta \cdot \theta = 0$. This will reduce the rotation matrix to

$$\mathbf{R} = \begin{bmatrix} 1 & -\kappa & \varphi \\ \kappa & 1 & -\omega \\ -\varphi & \omega & 1 \end{bmatrix} . \tag{3.9}$$

If both epochs are given in the same datum, these assumptions are most likely justified, although this should be proven for each individual case before using them. If, however, the coordinates of both epochs are given in different coordinate systems, the above approximations may not hold true anymore. Since the goal is to develop a general model that should also be capable of handling 3D rotations of any magnitude, the small-angle approximations above are not applied here.

Instead, the three EULER rotations are replaced by a quaternion rotation.

3.2.2 Rotation using quaternions

Quaternions are an alternative way to describe rotations in 3D space. They were first applied in photogrammetry by Schut (1959) and Thompson (1959). Horn (1987) derived a closed-form solution for the absolute orientation using quaternions.

Instead of using the three elementary rotations about the coordinate axes, a single three-dimensional rotation about the vector $\vec{r} = (r_x \; r_y \; r_z)^T$ is performed with the rotation angle

θ as illustrated in Figure 3.2. This can easily be expressed using quaternions. Quaternions

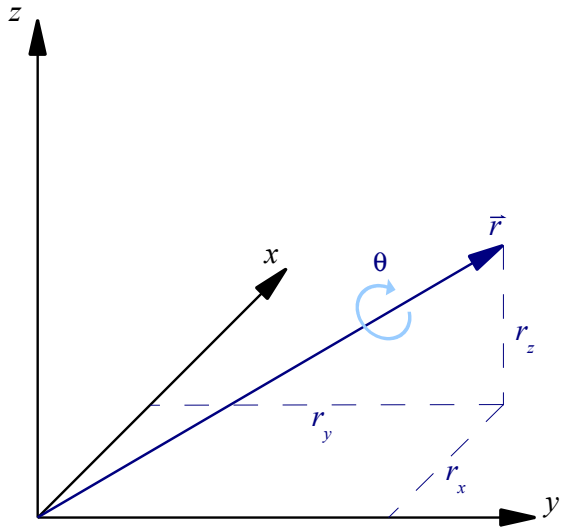

Figure 3.2: Rotation in 3D space using quaternions

are essentially four-dimensional complex numbers with one real part and three imaginary parts. They can be written as follows, (Kuipers, 1996),

$$\tilde{q} = q_0 + iq_x + jq_y + kq_z \qquad \text{or} \qquad \tilde{q} = \begin{bmatrix} q_0, & \begin{pmatrix} q_x \\ q_y \\ q_z \end{pmatrix} \end{bmatrix} \tag{3.10}$$

The element q_0 describes the rotation angle while the three imaginary elements $(q_x,\ q_y,\ q_z)^T$ describe the rotation vector. For quaternions certain rules such as addition, multiplication and inversion are defined similar to those for two-dimensional complex numbers. Below are some basic rules which are important to describe a rotation using quaternions.

Addition

The addition of two quaternions $\tilde{p}$ and $\tilde{q}$ is defined by

$$\tilde{p} + \tilde{q} = \begin{bmatrix} p_0 + q_0, & \begin{pmatrix} p_x + q_x \\ p_y + q_y \\ p_z + q_z \end{pmatrix} \end{bmatrix} \tag{3.11}$$

Multiplication

The multiplication of two quaternions $\tilde{p}$ and $\tilde{q}$ is defined by

$$\tilde{p} \cdot \tilde{q} = \begin{bmatrix} p_0 \cdot q_0 - \begin{pmatrix} p_x \\ p_y \\ p_z \end{pmatrix} \cdot \begin{pmatrix} q_x \\ q_y \\ q_z \end{pmatrix}, & \begin{pmatrix} p_x \\ p_y \\ p_z \end{pmatrix} \times \begin{pmatrix} q_x \\ q_y \\ q_z \end{pmatrix} + p_0 \cdot \begin{pmatrix} q_x \\ q_y \\ q_z \end{pmatrix} + q_0 \cdot \begin{pmatrix} p_x \\ p_y \\ p_z \end{pmatrix} \end{bmatrix} \tag{3.12}$$

Magnitude (Length)

The magnitude (length) of a quaternion $\tilde{q}$ is defined by

$$\|\tilde{q}\| = \sqrt{q_0^2 + q_x^2 + q_y^2 + q_z^2} \tag{3.13}$$

Inversion

The inverse of a quaternion $\tilde{q}$ is defined by

$$\tilde{q}^{-1} = \frac{\left[q_0, \ (-q_x \ -q_y \ -q_z)^T\right]}{\|\tilde{q}\|^2} \tag{3.14}$$

Rotation

Unlike a rotation using three EULER angles, quaternions need four components to describe a rotation in 3D space. Hence, the following equation, which constrains the magnitude of the quaternion to 1, must be met in order to obtain three degrees of freedom again.

$$\|\tilde{q}\| = \sqrt{q_0^2 + q_x^2 + q_y^2 + q_z^2} = 1 \tag{3.15}$$

Using the unit vector $\vec{r} = (r_x \; r_y \; r_z)^T$ and the rotation angle θ (see Figure 3.2) the components of the unit quaternion can be determined from

$$\begin{aligned} q_0 &= \cos\left(\tfrac{\theta}{2}\right) \\ q_x &= r_x \cdot \sin\left(\tfrac{\theta}{2}\right) \\ q_y &= r_y \cdot \sin\left(\tfrac{\theta}{2}\right) \\ q_z &= r_z \cdot \sin\left(\tfrac{\theta}{2}\right) \end{aligned} \tag{3.16}$$

The rotation of a vector $\vec{v} = (v_x \; v_y \; v_z)^T$ using a quaternion $\tilde{q}$ and its inverse $\tilde{q}^{-1}$ can be described by the following simple expression

$$\tilde{v}_{rot} = \tilde{q} \cdot \tilde{v} \cdot \tilde{q}^{-1} \tag{3.17}$$

where $\tilde{v} = \left[0, \, \vec{v}\right]$ is a quaternion representing the vector to be rotated and $\tilde{v}_{rot} = \left[0, \, \vec{v}_{rot}\right]$ is a quaternion representing the rotated vector $\vec{v}_{rot}$. For a unit quaternion $\tilde{q} = \left[q_0, \, (q_x \; q_y \; q_z)^T\right]$, its inverse can simply be determined by negating the three imaginary components such that $\tilde{q}^{-1} = \left[q_0, \, (-q_x \; -q_y \; -q_z)^T\right]$.

It is also possible to derive a rotation matrix $\mathbf{R}(\tilde{q})$ directly from the quaternion $\tilde{q}$:

$$\mathbf{R}(\tilde{q}) = \begin{bmatrix} 1 - 2\left(q_y^2 + q_z^2\right) & 2\left(q_x q_y - q_0 q_z\right) & 2\left(q_x q_z + q_0 q_y\right) \\ 2\left(q_x q_y + q_0 q_z\right) & 1 - 2\left(q_x^2 + q_z^2\right) & 2\left(q_y q_z - q_0 q_x\right) \\ 2\left(q_x q_z - q_0 q_y\right) & 2\left(q_y q_z + q_0 q_x\right) & 1 - 2\left(q_x^2 + q_y^2\right) \end{bmatrix}. \tag{3.18}$$

Should the EULER angles be required, they can be back-calculated from the rotation matrix above. However, this conversion is not unique. A rotation sequence for the EULER angles needs to be defined first. Given the rotation sequence $\mathbf{R}_x(\omega) \rightarrow \mathbf{R}_y(\varphi) \rightarrow \mathbf{R}_z(\kappa)$, as defined in (2.60), the three rotation angles ω, φ, κ can be determined through comparison of the elements of the rotation matrices (2.60) and (3.18) as follows:

$$\omega = \arctan\left(\frac{2\left(q_y q_z + q_0 q_x\right)}{1 - 2\left(q_x^2 + q_y^2\right)}\right) \quad \varphi = \arcsin\left(2 q_0 q_y - 2 q_x q_z\right) \quad \kappa = \arctan\left(\frac{2\left(q_x q_y + q_0 q_z\right)}{1 - 2\left(q_y^2 + q_z^2\right)}\right) \tag{3.19}$$

For more information on quaternions and their application see Kuipers (1996).

The following are some advantages of quaternions over EULER angles:

- The rotation is described directly by one vector and one angle. There is no need to split up the rotation in three elementary components about the coordinate axes. Hence, the issue of the order of rotations, as inherent with EULER angles, does not exist.
- A quaternion needs only four elements to describe a rotation instead of 9 elements in a rotation matrix.
- There is no need for trigonometric functions. A rotation can be described by a simple quaternion multiplication, see equation (3.17). This makes their use numerically very efficient.
- The problem of the Gimbal Lock does not exist, (Kuipers, 1996).
- If required, a rotation matrix can directly be computed from the quaternion.

3.2.3 Derivation of functional model

Replacing the EULER rotation matrix in (3.8) with a quaternion rotation yields the following quaternion equation:

$$\tilde{x}_i = \lambda \cdot \left(\tilde{q} \cdot \tilde{x}_j \cdot \tilde{q}^{-1}\right) + \tilde{T} \tag{3.20}$$

where $\tilde{q} = \left[q_0, \left(q_x \; q_y \; q_z\right)^T\right]$ is the quaternion defining the rotation between systems, $\tilde{x}_i = \left[0, \vec{x}_i\right]$ is the quaternion representing the coordinate vector in epoch i, $\tilde{x}_j = \left[0, \vec{x}_j\right]$ is the quaternion representing the coordinate vector in epoch j and $\tilde{T} = \left[0, \vec{T}\right]$ is the quaternion representing the translation vector. Multiplication of equation (3.20) with $\tilde{q}$ from the right hand-side will get rid of the quadratic components of the quaternion. Then, moving all terms

to one side of the equation yields:

$$\lambda \cdot \tilde{q} \cdot \tilde{x}_j + \tilde{T} \cdot \tilde{q} - \tilde{x}_i \cdot \tilde{q} = 0 \tag{3.21}$$

These are four condition equations that can be written for each point that has been observed in both epochs. The first equation exists only because of the four dimensions of the rotation quaternion. It reduces to $0 = 0$ and can thus be neglected. The remaining three equations, describing the transformation between system i and system j, written in explicit form, are:

$$\begin{aligned}
f_x: &\quad q_0 (T_x - x_i + \lambda \cdot x_j) + q_z (T_y - y_i - \lambda \cdot y_j) + q_y (-T_z + z_i + \lambda \cdot z_j) = 0 \\
f_y: &\quad q_z (-T_x + x_i + \lambda \cdot x_j) + q_0 (T_y - y_i + \lambda \cdot y_j) + q_x (T_z - z_i - \lambda \cdot z_j) = 0 \\
f_z: &\quad q_y (T_x - x_i - \lambda \cdot x_j) + q_x (-T_y + y_i + \lambda \cdot y_j) + q_0 (T_z - z_i + \lambda \cdot z_j) = 0
\end{aligned} \tag{3.22}$$

An additional condition equation g, following from equation (3.15), is required to obtain three degrees of freedom for the rotation again.

$$g: \qquad q_0^2 + q_x^2 + q_y^2 + q_z^2 - l_{\|\tilde{q}\|} = q_0^2 + q_x^2 + q_y^2 + q_z^2 - 1 = 0 \tag{3.23}$$

In the condition equation g above, the magnitude of the quaternion is introduced as a pseudo-observation with $l_{\|\tilde{q}\|} = 1$. Via its corresponding element in the cofactor matrix $\mathbf{Q}_{ll}$ it can be controlled how strictly this condition is satisfied.

The equations (3.22) clearly illustrate the advantages of quaternions over Euler angles. There are no trigonometric functions required to describe the rotation. Instead, they are replaced by simple multiplications and summations. As a result, observations and unknowns are only connected multiplicatively which yields a bi-linear, numerically more stable normal equation system. Furthermore, there is no need for the computation of approximate values for the rotation parameters and no small-angle approximations are required. The determination of initial estimates is critical to converge to the correct solution when Euler angles are used. This is not the case for quaternions. Any quaternion that satisfies equation (3.23) can be used as an initial estimate and will yield the correct solution.

3.2.4 Solution with the non-linear Gauss-Helmert model

Given three or more identical points p in both systems, an over-determined adjustment problem exists in which the coordinates in each system can be treated as observations and the transformation parameters as unknowns. The dimensions of this adjustment problem can be described as follows:

- Number of observations: $n = 6p + 1$
- Number of conditions: $b = 3p + 1$
- Number of unknowns: $u = 8$
- Redundancy: $r = b - u = 3p - 7$

Each point observed in both epochs contributes six coordinate observations, three in each system, and a set of three condition equations (3.22). One additional pseudo-observation and condition equation is given by (3.23) for the magnitude of the quaternion. The unknowns consist of the four components of the rotation quaternion, the three translations and the scale factor.

This constitutes an overdetermined least-squares problem in the form of a non-linear Gauss-Helmert model as given by (2.83) where the observation vector and its cofactor matrix are given by

$$\underset{(n\times 1)}{\vec{l}_0} = \begin{pmatrix} \vec{x}_i \\ \vec{x}_i \\ l_{\|\tilde{q}\|} \end{pmatrix}, \qquad \underset{(n\times n)}{\mathbf{Q}_{ll}} = \begin{bmatrix} \mathbf{Q}_{xx_i} & 0 & 0 \\ 0 & \mathbf{Q}_{xx_j} & 0 \\ 0 & 0 & q_{l_{\|\tilde{q}\|}} \end{bmatrix} \tag{3.24}$$

and the unknown parameter vector is described by

$$\underset{(u\times 1)}{\vec{x}_{TP}} = \begin{pmatrix} q_0 & q_x & q_y & q_z & T_x & T_y & T_z & \lambda \end{pmatrix}^T . \tag{3.25}$$

Note that the last diagonal element of the cofactor matrix $q_{l_{\|\tilde{q}\|}}$ corresponds to the pseudo-observation for the quaternion magnitude.

Initial approximations for the elements in the parameter vector are required in order to solve this non-linear problem. This, however, does not necessitate any computations. As

mentioned before, for the quaternion any values satisfying (3.23) are acceptable. The translations are linear so that again any values can be chosen and for the scalar factor a value of 1 is typically a good approximation.

For the linearization, the design matrix $\mathbf{A}$ and condition matrix $\mathbf{B}$ are required as well as the initial misclosure vector $\vec{w}_0$. These are obtained by differentiating the condition equations in (3.22) and (3.23) with respect to to the parameters $\vec{x}_{TP}$ and observations $\vec{l}$ and computing the values for these equations from the initial approximations, respectively:

$$\underset{(b\times u)}{\mathbf{A}} = \begin{bmatrix} \partial \vec{f} \big/ \partial \vec{x}_{TP} \\ \partial g / \partial \vec{x}_{TP} \end{bmatrix} \quad \underset{(b\times n)}{\mathbf{B}} = \begin{bmatrix} \partial \vec{f} \big/ \partial \vec{l} \\ \partial g \big/ \partial \vec{l} \end{bmatrix} \quad \underset{(b\times 1)}{\vec{w}_0} = \begin{pmatrix} 0 - \vec{f}\left(\vec{l}_0, \vec{x}_{TP_0}\right) \\ 0 - g\left(\vec{l}_0, \vec{x}_{TP_0}\right) \end{pmatrix} . \quad (3.26)$$

A detailed description of the structures of $\mathbf{A}$ and $\mathbf{B}$ together with the partial derivatives they contain is given in Appendix A.2.

Now the linearized equation system in (2.88) can be iteratively solved as shown in detail in Section 2.4.3.1. The validity of the condition (2.90a) has to be verified. The condition (2.90b) is satisfies thanks to the additional requirement in (3.23), yielding three degrees of freedom for the rotation again. The cofactor element for the pseudo-observation of the quaternion magnitude can be set to $q_{l_{\|\tilde{q}\|}} = 0$ in order to enforce the exact adherence of the condition equation (3.23). This is permissible as long as the condition in (2.90a) is still satisfied.

3.2.5 Derivation of deformations

After the parameters $\vec{x}_{TP}$, the a posteriori variance factor $\hat{\sigma}_0^2$ and the cofactor matrix of the parameters $\mathbf{Q}_{xx_{TP}}$ have been determined as results of the adjustment, the final task is to derive deformations for the group of unstable points. This is accomplished by applying the adjusted transformation parameters to the original coordinates of all points in epoch j according to:

$$\tilde{x}_j^{tr} = \lambda \cdot \left(\tilde{q} \cdot \tilde{x}_j \cdot \tilde{q}^{-1}\right) + \tilde{T} \quad (3.27)$$

where, again, $\tilde{x}_j$ and $\tilde{T}$ are quaternion representations for the coordinate vector $\vec{x}_j$ and the translation vector $\vec{T}$; $\tilde{q}$ is the rotation quaternion and $\tilde{x}_j^{tr} = \left[0, \vec{x}_j^{tr}\right]$ is the quaternion representation of the transformed coordinate vector $\vec{x}_j^{tr}$ in the system of epoch i. Once all coordinates are given in the same system, the deformations can simply be derived as the coordinate differences:

$$\vec{d}_{ij} = \vec{x}_j^{tr} - \vec{x}_i \; . \tag{3.28}$$

The derivation of the corresponding cofactor matrix of the deformations $\mathbf{Q}_{dd_{ij}}$ is shown in detail in Appendix A.3.

3.2.6 Numerical Example

The following is an example to demonstrate the proposed transformation-based algorithm for the determination of deformations between two epochs of a monitoring network. Again, the five-point network from previous examples, shown in Figure 3.1, is used. This time however, it is extended to all three dimensions. The coordinates and their standard deviations for epoch 1, which were derived from a free network adjustment, are given in Table 3.9 below. The a posteriori variance factor of the network adjustment is $(\pm 0.009858)^2$ with a network redundancy of 22.

Point	x [m]	y [m]	z [m]	$\hat{\sigma}_x$ [mm]	$\hat{\sigma}_y$ [mm]	$\hat{\sigma}_z$ [mm]
1	97.779	47.851	10.071	±1.1	±1.1	±0.6
2	93.790	129.719	11.210	±1.1	±1.1	±0.6
3	39.209	116.078	9.479	±1.2	±1.2	±0.8
4	27.721	45.191	10.750	±1.0	±1.1	±0.6
5	22.221	100.101	9.991	±1.2	±1.2	±0.8

Table 3.9: Adjusted coordinates of 3D network in epoch 1

Deformations were introduced at point 3 again. Its true deformations are listed in Table 3.10.

Point	dx [mm]	dy [mm]	dz [mm]
3	−30.0	40.0	−20.0

Table 3.10: True deformations of point 3 in epoch 2

Then, the coordinates of the second epoch are derived in a different coordinate system. The adjusted coordinates for epoch 2 are shown in Table 3.11. The a posteriori variance factor for epoch 2 is $(\pm 0.009988)^2$ and the network redundancy is again 22.

Point	x [m]	y [m]	z [m]	$\hat{\sigma}_x$ [mm]	$\hat{\sigma}_y$ [mm]	$\hat{\sigma}_z$ [mm]
1	97.364	−27.901	1.041	±1.2	±1.0	±0.7
2	148.581	32.927	−18.804	±1.0	±1.2	±0.7
3	99.360	60.189	−17.072	±1.2	±1.1	±0.8
4	44.467	18.078	2.308	±1.0	±1.1	±0.6
5	76.487	60.513	−12.478	±1.3	±1.1	±0.9

Table 3.11: Adjusted coordinates of 3D network in epoch 2

In both epochs all five points contribute to the datum definition. The free datum parameters consist of the rotation about the z-axis and the translations along all three coordinate axes, so that the resulting cofactor matrices have a rank defect of four.

The largest similar point group between the two epochs has been correctly identified as the group consisting of points 1, 2, 4 and 5 using the method proposed in the previous section. Hence, only these $p = 4$ identical points are used to determine the transformation parameters. The dimensions of the adjustment problem then follow as:

- Number of observations: $n = 6p + 1 = 25$
- Number of conditions: $b = 3p + 1 = 13$
- Number of unknowns: $u = 8$
- Redundancy: $r = b - u = 3p - 7 = 5$.

Initial approximations for the parameter vector are given by

$$\vec{x}_{TP} = \begin{pmatrix} q_0 & q_x & q_y & q_z & T_x & T_y & T_z & \lambda \end{pmatrix}^T = \begin{pmatrix} 1 & 0 & 0 & 0 & 0 & 0 & 0 & 1 \end{pmatrix}^T$$

so that no computations of initial approximate values are necessary.

After populating the design and condition matrices as well as the initial misclosure vector according to (3.26), a numerical check is performed to verify that the condition in (2.90a) is indeed satisfied. After this is confirmed the unknown parameters can be obtained by iteratively solving the linearized equation system given in (2.88) as is described in Section 2.4.3.1.

After six iterations the termination criterion for the corrections $\Delta\vec{x}$ for the parameter vector of

$$\left|\Delta\vec{x}\right| < 10^{-12}$$

is reached and the results listed in Table 3.12 are obtained for the estimated transformation parameters. The a posteriori standard deviation, given by (2.100), is $\hat{\sigma}_0^2 = (\pm 0.004230)^2$. From the covariance matrix of the parameters in (2.101) the standard deviations of the transformation parameters, also listed in Table 3.12, are derived as the square root of the main diagonal elements. Since the components of the quaternion are difficult to interpret, they have been converted to EULER angles according to (3.19), assuming a rotation sequence of $\mathbf{R}_x(\omega) \rightarrow \mathbf{R}_y(\varphi) \rightarrow \mathbf{R}_z(\kappa)$.

Parameter	Value	$\hat{\sigma}$	Parameter	Value	$\hat{\sigma}$
q_0	0.9227540829	$\pm 6.07 \cdot 10^{-7}$			
q_x	0.1202321977	$\pm 3.35 \cdot 10^{-6}$	ω	11.000488 °	$\pm 1.4''$
q_y	−0.0467719864	$\pm 3.03 \cdot 10^{-6}$	φ	−9.999752 °	$\pm 1.4''$
q_z	0.3631549290	$\pm 1.30 \cdot 10^{-6}$	κ	41.999442 °	$\pm 0.6''$
T_x	7.4900 m	±0.54 mm			
T_y	3.6845 m	±0.92 mm			
T_z	−2.6021 m	±0.56 mm			
λ	+196.7 ppm	±10.6 ppm			

Table 3.12: Adjusted transformation parameters and standard deviations for epoch 2

For comparison the true transformation parameters are given in Table 3.13 below. The standard deviations for the estimated rotation parameters are at about the 1″-level for all

Parameter	ω	φ	κ	T_x	T_y	T_z	λ
Value	11.0 °	−10.0 °	42.0 °	7.5 m	3.7 m	−2.6 m	200.0 ppm

Table 3.13: True transformation parameters for epoch 2

three rotations. Their deviations from the true rotations are between 1″ and 2″. Thus the rotation parameters can be considered as accurately determined. The derived standard deviations for the translation parameters are at the sub-millimetre level. Their deviations from the true translations on the other hand range from 2.1 mm for the z-component to 1.55 cm for the y-component. These significant differences are attributed to a datum change, since point 3 was omitted from the determination of the transformation parameters. The scale factor with an estimated standard deviation of ±10.6 ppm and a deviation of only 3.3 ppm from its true value was successfully recovered. The overall high accuracies for the estimated parameters are of course due to the high accuracies of the input coordinates which are at the millimetre-level.

The estimated deformations of the five points together with their standard deviations are shown in Table 3.14 below. The deformations estimated for the four stable points are at the

Point	dx	dy	dz	$\hat{\sigma}_{dx}$	$\hat{\sigma}_{dy}$	$\hat{\sigma}_{dz}$
1	−0.2	−0.1	−0.2	±1.6	±1.6	±1.0
2	−0.1	0.3	0.4	±1.6	±1.6	±1.0
3	−28.2	43.2	−18.4	±1.6	±1.7	±1.2
4	−0.2	0.1	0.3	±1.9	±1.6	±0.9
5	0.5	−0.4	−0.7	±1.7	±1.7	±1.2

Table 3.14: Estimated deformations and standard deviations in epoch 2 in [mm]

sub-millimetre level while their standard deviations vary between ±1.0 mm and ±2.0 mm. Hence, they can be considered insignificant. The estimated deformations of the unstable point 3 deviate between 1.6 mm and 3.2 mm from their true values given in Table 3.10. Thus, it can be said that they have been recovered successfully.

3.3 Multiple-epoch comparison

So far only two epochs have been compared with each other. If more than two epochs are available, multiple two-epoch comparisons, as described above, can be carried out. Given m epochs of a monitoring network, a total of $\sum_{i=1}^{m-1} i$ independent two-epoch transformation adjustments can be performed. Moreover, if the deformations between different epochs are to be compared (e. g. to analyze movement patterns and velocities), further transformations into a common system have to be carried out. For example, given $m = 3$ epochs, three independent two-epoch transformation adjustments can be computed: from epoch 2 to epoch 1, from epoch 3 to epoch 1 and from epoch 3 to epoch 2. If now the deformations between epochs 1 and 2 shall be compared to those between epochs 2 and 3, an additional transformation (e. g. of the deformations between epochs 2 and 3 into the system of epoch 1) has to be carried out[1].

Alternatively, each epoch can only be compared to a chosen base (or reference) epoch. The deformations with respect to epochs other than the base epoch can then be calculated directly as straight differences of the coordinates transformed into the system of the base epoch. This reduces the number of necessary transformation adjustments to $m - 1$. Furthermore, the comparison of multiple epochs with respect to one base epoch can be conveniently performed in one single multiple-epoch adjustment rather than a series of multiple two epoch adjustments. How this is accomplished is explained in this section.

3.3.1 Localization of largest similar point group common to all epochs

To identify the largest similar point group between multiple epochs, the algorithm proposed in Section 3.1 should be executed for all for all two-epoch comparisons with respect to the

[1]Note that no further adjustment for the determination of the transformation parameters is required, as the transformation parameters from epoch 2 to epoch 1 have already been computed and can directly be applied to the deformations.

chosen reference epoch. Thus, the stable computational base for each epoch with respect to the base epoch is obtained which is then used to determine the transformation parameters between the base epoch and each subsequent epoch. But typically this stable computational base is going to change over epochs due to points starting, and possibly ceasing, to move over time. This means that, although after transformation the coordinates of all epochs are known in the system of the base epoch, they do not necessarily refer all to the same datum. As a result the coordinates of the different epochs cannot be compared amongst each other but only to those of the base epoch.

To illustrate this, let's consider the following example. A monitoring network consisting of five points has been observed in three epochs. In epoch 2 only point 3 was found to be unstable, so that the remaining points 1, 2, 4 and 5 can form the stable computational base for the transformation from epoch 2 to epoch 1. In epoch 3 it has been found that in addition to point 3 also point 5 has moved significantly. Consequently, the stable computational base for the transformation from epoch 3 to epoch 1 can only consist of the points 1,2 and 4. As a result the transformed coordinates of epoch 2 in the system of epoch 1 cannot directly be compared to the transformed coordinates of epoch 3 in the system of epoch 1 since they both relate to different datum definitions. If epochs 2 and 3 are to be compared as well, only points 1, 2 and 4 have to be chosen as computational base for both, the transformation from epoch 2 to epoch 1 as well as the transformation from epoch 3 to epoch 1.

This means that if multiple epochs are to be compared amongst each other and not only to the base epoch, the stable computational base common to *all* epochs needs to be established. This can only be accomplished by performing the search for the largest similar point group for all possible $\sum_{i=1}^{m-1} i$ two-epoch comparisons. Then, only the coordinates of the group of similar points common to all epochs will form the input observations for the transformation adjustment.

3.3.2 Determination of movements

The mathematical model presented in Section 3.2 can easily be extended to solve for the transformations of more than two epochs at a time.

3.3.2.1 Derivation of functional model

Given a monitoring network observed in m epochs and considering epoch 1 as the reference epoch, one can write the transformation from epoch 2 to epoch 1 according to equation (3.20) as follows:

$$\tilde{x}_1 = \lambda_2^1 \cdot \left(\tilde{q}_2^1 \cdot \tilde{x}_2 \cdot \left(\tilde{q}_2^1 \right)^{-1} \right) + \tilde{T}_2^1 \ . \tag{3.29}$$

Similarly, the transformation from epoch i to epoch 1 can be expressed as:

$$\tilde{x}_1 = \lambda_i^1 \cdot \left(\tilde{q}_i^1 \cdot \tilde{x}_i \cdot \left(\tilde{q}_i^1 \right)^{-1} \right) + \tilde{T}_i^1 \ . \tag{3.30}$$

And finally, the transformation of the last epoch m to the base epoch 1 can be written as:

$$\tilde{x}_1 = \lambda_m^1 \cdot \left(\tilde{q}_m^1 \cdot \tilde{x}_m \cdot \left(\tilde{q}_m^1 \right)^{-1} \right) + \tilde{T}_m^1 \ . \tag{3.31}$$

Each of the three equations above represents a two-epoch comparison between the base epoch 1 and one of the following epochs. Combining all of the above equations and modifying them according to equation (3.21) yields the following system of equations f. Note that for reasons of readability the superscript index "1" of the base epoch has been omitted from the transformation parameters as epoch 1 is the base epoch for all transformations.

$$\begin{aligned} & & \lambda_2 \cdot \tilde{q}_2 \cdot \tilde{x}_2 + \tilde{T}_2 \cdot \tilde{q}_2 - \tilde{x}_1 \cdot \tilde{q}_2 &= 0 \\ & & & \vdots \\ f: & & \lambda_i \cdot \tilde{q}_i \cdot \tilde{x}_i + \tilde{T}_i \cdot \tilde{q}_i - \tilde{x}_1 \cdot \tilde{q}_i &= 0 \\ & & & \vdots \\ & & \lambda_m \cdot \tilde{q}_m \cdot \tilde{x}_m + \tilde{T}_m \cdot \tilde{q}_m - \tilde{x}_1 \cdot \tilde{q}_m &= 0 \end{aligned} \tag{3.32}$$

In addition, for each of the above transformations an additional condition equation for each quaternion of the form (3.23) is required, to maintain the three degrees of freedom for the rotation. This yields the following system of equations g:

$$
\begin{aligned}
& & (q_0^2)_2 + (q_x^2)_2 + \left(q_y^2\right)_2 + (q_z^2)_2 - \left(l_{\|\tilde{q}\|}\right)_2 &= 0 \\
& & &\vdots \\
g: & & (q_0^2)_i + (q_x^2)_i + \left(q_y^2\right)_i + (q_z^2)_i - \left(l_{\|\tilde{q}\|}\right)_i &= 0 \\
& & &\vdots \\
& & (q_0^2)_m + (q_x^2)_m + \left(q_y^2\right)_m + (q_z^2)_m - \left(l_{\|\tilde{q}\|}\right)_m &= 0
\end{aligned}
\tag{3.33}
$$

In this *interconnected transformation* the two-epoch transformations from all subsequent epochs to the reference epoch are solved *in one step* using all available information about the monitoring network together.

3.3.2.2 Solution of the adjustment problem

To get an idea of the size of the equation system, let's assume a monitoring network has been observed in m epochs and that a stable computational base of p points is common to all epochs. The dimensions of the adjustment problem are as follows:

- Number of transformations: $t = m - 1$
- Number of observations: $n = 3 \cdot p \cdot m + t$
- Number of conditions: $b = 3 \cdot p \cdot t + t$
- Number of unknowns: $u = 8 \cdot t$
- Redundancy: $r = b - u = (m - 1) \cdot (3 \cdot p - 7)$.

Each point contributes three coordinate observations for each epoch it has been observed in. Furthermore, there is one additional pseudo-observation of the quaternion magnitude for each transformation. Each point also establishes three condition equations (3.22) for each transformation. Additionally there is one condition equation (3.23) for the magnitude of each quaternion. For m epochs, $(m - 1)$ transformations are performed as every subsequent

epoch is transformed back to the base epoch. The unknowns now consist of the $(m-1)$ sets of transformation parameters $(\tilde{q},\, \vec{T},\, \lambda)$. Looking at the redundancy, it becomes obvious that at least two epochs need to be available and that a minimum of three points need to be observed in each epoch in order to obtain an over-determined system.

If this is the case, an adjustment problem in the form of a non-linear Gauss-Helmert model as given by (2.83) exists, where the observation vector and its cofactor matrix are given by

$$\underset{(n\times 1)}{\vec{l}_0} = \begin{pmatrix} \vec{x}_1 \\ \vdots \\ \vec{x}_m \\ l_{\|\tilde{q}\|_2} \\ \vdots \\ l_{\|\tilde{q}\|_m} \end{pmatrix}, \qquad \underset{(n\times n)}{\mathbf{Q}_{ll}} = \begin{bmatrix} \mathbf{Q}_{xx_1} & 0 & 0 & 0 & 0 & 0 \\ 0 & \ddots & 0 & 0 & 0 & 0 \\ 0 & 0 & \mathbf{Q}_{xx_m} & 0 & 0 & 0 \\ 0 & 0 & 0 & q_{\|\tilde{q}\|_2} & 0 & 0 \\ 0 & 0 & 0 & 0 & \ddots & 0 \\ 0 & 0 & 0 & 0 & 0 & q_{\|\tilde{q}\|_m} \end{bmatrix} \tag{3.34}$$

and the unknown parameter vector is described by

$$\underset{(u\times 1)}{\vec{x}_{TP}} = \begin{pmatrix} \begin{pmatrix} q_0 & q_x & q_y & q_z & T_x & T_y & T_z & \lambda \end{pmatrix}_2^T \\ \vdots \\ \begin{pmatrix} q_0 & q_x & q_y & q_z & T_x & T_y & T_z & \lambda \end{pmatrix}_m^T \end{pmatrix}. \tag{3.35}$$

Like for the two-epoch comparison, the pseudo-observations are given with $l_{\|\tilde{q}\|_i} = 1$ and their corresponding elements in the cofactor matrix can be set to $q_{\|\tilde{q}\|_i} = 0$ to enforce the exact adherence of the condition equations (3.23).

Initial approximations for the transformation parameters, as before, do not have to be computed but can be defined as $\tilde{q}_0 = \left[1,\, (0\,0\,0)^T\right]$ for all quaternions, $\vec{T}_0 = (0\,0\,0)^T$ for all translations and $\lambda_0 = 1$ for all scale factors.

With that in mind the design and condition matrices $\mathbf{A}$ and $\mathbf{B}$ as well as the initial misclosure vector $\vec{w}_0$ can be populated according to (3.26) where f and g now represent the functions

in (3.32) and (3.33), respectively. The structure of the two matrices is shown in more detail in Appendix A.4.

Now the linearized equation system in (2.88) can be iteratively solved as shown in detail in Section 2.4.3.1. It is important to stress that the validity of the condition (2.90a) has to be verified. The condition (2.90b) is always satisfies because of the additional requirement in (3.23).

3.3.2.3 Derivation of deformations

After the transformation parameters are determined, the coordinates of all subsequent epochs can be transformed into the system of the reference epoch by

$$\begin{aligned} \tilde{x}_2^{tr} &= \lambda_2 \cdot \left(\tilde{q}_2 \cdot \tilde{x}_2 \cdot (\tilde{q}_2)^{-1}\right) + \tilde{T}_2 \\ &\vdots \\ \tilde{x}_i^{tr} &= \lambda_i \cdot \left(\tilde{q}_i \cdot \tilde{x}_i \cdot (\tilde{q}_i)^{-1}\right) + \tilde{T}_i \\ &\vdots \\ \tilde{x}_m^{tr} &= \lambda_m \cdot \left(\tilde{q}_m \cdot \tilde{x}_m \cdot (\tilde{q}_m)^{-1}\right) + \tilde{T}_m \end{aligned} \tag{3.36}$$

where $\tilde{x}_i^{tr} = \left[0, \vec{x}_i^{tr}\right]$ is the quaternion representation of the transformed coordinate vector $\vec{x}_i^{tr}$ in the system of the base epoch. The deformations $\vec{d}_{1i}$ between the base epoch 1 and an arbitrary epoch i then follow from:

$$\vec{d}_{1i} = \vec{x}_i^{tr} - \vec{x}_1 \ . \tag{3.37}$$

Similarly, the transformations between any two arbitrary epochs i and j can be derived from:

$$\vec{d}_{ij} = \vec{x}_j^{tr} - \vec{x}_i^{tr} \ . \tag{3.38}$$

The derivation of the cofactor matrices $\mathbf{Q}_{xx_i^{tr}}$ is given in Appendix A.3. The cofactor matrices $\mathbf{Q}_{dd_{ij}}$ for the deformations $\vec{d}_{ij}$ follow from:

$$\mathbf{Q}_{dd_{ij}} = \mathbf{Q}_{xx_i^{tr}} + \mathbf{Q}_{xx_j^{tr}} \ . \tag{3.39}$$

3.3.2.4 Numerical example

To demonstrate the multi-epoch transformation adjustment a third epoch is added to the example shown in 3.2.6 and all three epochs are analyzed together. The adjusted coordinates and their standard deviations for epoch 3 are listed in Table 3.15. The a posteriori variance factor of the third epoch is $(\pm 0.010064)^2$ and the network redundancy remains 22. The

Point	x [m]	y [m]	z [m]	$\hat{\sigma}_x$ [mm]	$\hat{\sigma}_y$ [mm]	$\hat{\sigma}_z$ [mm]
1	−13.467	96.326	52.450	±1.1	±1.0	±0.8
2	−93.086	115.581	49.876	±1.0	±1.1	±0.7
3	−93.400	64.687	25.761	±1.1	±1.1	±0.9
4	−28.379	34.090	23.852	±1.1	±1.0	±0.7
5	−82.268	45.139	19.561	±1.2	±1.1	±0.9

Table 3.15: Adjusted coordinates of 3D network in epoch 3

coordinates for epoch 1 and 2 are taken from Table 3.9 and Table 3.11, respectively. Again, in all three epochs the datum is defined by all five points.

Applying the algorithm proposed in Section 3.1 to compare each two of the three epochs yields the largest similar point group common to all three epochs. In this case point 3 is the only unstable point in both, epochs 2 and 3, so that the common stable computational base consists of points 1, 2, 4 and 5. The true deformations of point 3 for epochs 2 and 3 in the system of epoch 1 are given in Table 3.16.

Epoch	dx	dy	dz
2	−30.0	40.0	−20.0
3	−70.0	90.0	−30.0

Table 3.16: True deformations of point 3 in epochs 2 and 3 with respect to epoch 1 in [mm]

With $p = 4$ identical points and $m = 3$ epochs the dimensions of the adjustment problem are:

- Number of transformations: $t = m - 1 = 2$
- Number of observations: $n = 3 \cdot p \cdot m + t = 38$
- Number of conditions: $b = 3 \cdot p \cdot t + t = 26$
- Number of unknowns: $u = 8 \cdot t = 16$
- Redundancy: $r = b - u = (m - 1) \cdot (3 \cdot p - 7) = 10$.

Initial approximations for the parameter vector are given by

$$\underset{(u\times 1)}{\vec{x}_{TP}} = \begin{pmatrix} \begin{pmatrix} q_0 & q_x & q_y & q_z & T_x & T_y & T_z & \lambda \end{pmatrix}_{2_T}^{T} \\ \begin{pmatrix} q_0 & q_x & q_y & q_z & T_x & T_y & T_z & \lambda \end{pmatrix}_{3}^{T} \end{pmatrix} = \begin{pmatrix} \begin{pmatrix} 1 & 0 & 0 & 0 & 0 & 0 & 0 & 1 \end{pmatrix}_{2_T}^{T} \\ \begin{pmatrix} 1 & 0 & 0 & 0 & 0 & 0 & 0 & 1 \end{pmatrix}_{3}^{T} \end{pmatrix} .$$

After populating the design and condition matrices as well as the initial misclosure vector, a numerical check is performed to verify that the condition in (2.90a) is indeed satisfied. After this is confirmed the unknown parameters can be obtained by iteratively solving the linearized equation system given in (2.88) as is described in Section 2.4.3.1.

The iteration reaches the convergence threshold of $\left|\Delta\vec{x}\right| < 10^{-12}$ after six steps. The a posteriori variance factor for the adjustment is $\hat{\sigma}_0^2 = (\pm 0.004820)^2$. The adjusted transformation parameters for the transformation from epoch 2 to epoch 1 and epoch 3 to epoch 1 together with their standard deviations are listed in Table 3.17. Note that for lack of space only the geometrically interpretable EULER angles are given for the rotation parameters. For comparison, the true transformation parameters for epochs 2 and 3 are given in Table 3.18 below.

The estimated transformation parameters for epoch 2 are almost identical to those from the two-epoch comparison shown in Table 3.12. The differences are at the sub-arcsecond and sub-millimetre level, respectively and can thus be considered insignificant. Again, the translation parameters show a significant difference from the true values, which can be interpreted as a datum change due to point 3 being eliminated from the stable computational base.

Transformation from Ep. 2 to Ep. 1			Transformation from Ep. 3 to Ep. 1		
Parameter	Value	$\hat{\sigma}$	Parameter	Value	$\hat{\sigma}$
ω	$11.000455\,^\circ$	$\pm 1.7''$	ω	$-23.500005\,^\circ$	$\pm 1.2''$
φ	$-9.999728\,^\circ$	$\pm 1.6''$	φ	$7.999975\,^\circ$	$\pm 1.4''$
κ	$41.999449\,^\circ$	$\pm 0.7''$	κ	$-75.500246\,^\circ$	$\pm 0.7''$
T_x	7.4900 m	± 0.62 mm	T_x	-5.0144 m	± 0.77 mm
T_y	3.6845 m	± 1.05 mm	T_y	8.8819 m	± 1.01 mm
T_z	-2.6020 m	± 0.64 mm	T_z	-1.4024 m	± 0.66 mm
λ	+196.7 ppm	± 12.1 ppm	λ	+234.4 ppm	± 12.1 ppm

Table 3.17: Adjusted transformation parameters and standard deviations for multi-epoch comparison

Parameter	ω	φ	κ	T_x	T_y	T_z	λ
Epoch 2	$11.0\,^\circ$	$-10.0\,^\circ$	$42.0\,^\circ$	7.5 m	3.7 m	-2.6 m	+200.0 ppm
Epoch 3	$-23.5\,^\circ$	$8.0\,^\circ$	$-75.5\,^\circ$	-5.0 m	8.9 m	-1.4 m	+250.0 ppm

Table 3.18: True transformation parameters for epochs 2 and 3

For epoch 3 the estimated rotation parameters are very close to their true values with differences at the sub-arcsecond level. Their standard deviations are at about the $1''$-level which is comparable to those for epoch 2. The magnitude of the differences of the translations vary between 2.4 mm in z-direction up to 1.8 cm in y-direction compared to the true values. This again is similar to the translations for epoch 2 and can be explained with a datum shift to the new computational base. The standard deviations of the translations are at the 1 mm-level; very similar to epoch 2 as well. The deviation of the scale factor from its true value is about 15.6 ppm, which is much larger than the deviation of 3.3 ppm for the second epoch, and exceeds its standard deviation of 12.1 ppm slightly.

The estimated deformations of the five monitoring points between epochs 1 and 2 together with their standard deviations are shown in Table 3.19 below. Like the transformation parameters, the deformations are identical to those from the two-epoch comparison, shown in Table 3.14.

The estimated deformations between epochs 1 and 3 together with their standard deviations are listed in Table 3.20. Similarly, to the previous comparison, the apparent movements

Point	dx	dy	dz	$\hat{\sigma}_{dx}$	$\hat{\sigma}_{dy}$	$\hat{\sigma}_{dz}$
1	−0.2	−0.1	−0.2	±1.7	±1.6	±1.0
2	−0.1	0.3	0.3	±1.7	±1.6	±1.0
3	−28.2	43.2	−18.4	±1.7	±1.7	±1.2
4	−0.2	0.1	0.4	±1.5	±1.7	±0.9
5	0.5	−0.4	−0.7	±1.7	±1.7	±1.2

Table 3.19: Estimated deformations and standard deviations in epoch 2 with respect to epoch 1 in [mm]

of the stable points are at the sub-millimetre level, while the standard deviations for all deformations are between 1 mm and 2 mm. Comparing the estimated deformations of point 3 with its true movements in Table 3.18 shows that, with deviations of less than 2 mm, they have been accurately recovered.

Point	dx	dy	dz	$\hat{\sigma}_{dx}$	$\hat{\sigma}_{dy}$	$\hat{\sigma}_{dz}$
1	0.7	−0.3	−0.1	±1.7	±1.6	±1.0
2	−0.5	−0.2	0.4	±1.7	±1.6	±1.0
3	−68.4	90.4	−28.1	±1.7	±1.7	±1.2
4	−0.3	0.5	0.4	±1.5	±1.7	±0.9
5	−0.1	0.2	−0.9	±1.7	±1.7	±1.2

Table 3.20: Estimated deformations and standard deviations in epoch 3 with respect to epoch 1 in [mm]

Finally, the estimated deformations between epochs 2 and 3, in the system of epoch 1, together with their standard deviations are shown in Table 3.21 below. Again, the apparent movements of the stable points are at the sub-millimetre level while the standard deviations for all deformations range vary between 1 mm and 2 mm. The true deformations of point 3 follow as the difference of its deformations in epoch 3 and 2 with respect to epoch 1, given in Table 3.18. The estimated movements of point 3, with deviations of less than 3 mm from their true values, have been accurately determined.

It should be pointed out again, that these deformations are derived directly as the differences of the transformed coordinates of epoch 3 and the transformed coordinates of epoch 2 in the system of epoch 1. Consequently, the total sum of deformations over all epochs

Point	dx	dy	dz	$\hat{\sigma}_{dx}$	$\hat{\sigma}_{dy}$	$\hat{\sigma}_{dz}$
1	0.9	−0.2	0.1	±1.7	±1.6	±1.1
2	−0.4	−0.5	0.1	±1.8	±1.7	±1.1
3	−40.2	47.2	−9.7	±1.7	±1.7	±1.2
4	−0.1	0.4	0.0	±1.5	±1.8	±1.0
5	−0.6	0.6	−0.2	±1.8	±1.7	±1.3

Table 3.21: Estimated deformations and standard deviations between epochs 2 and 3 in the system of epoch 1 in [mm]

$\left(\vec{d}_{12} + \vec{d}_{23} - \vec{d}_{13}\right)$ equates exactly to zero, ensuring that the estimated deformations are always consistent.

3.4 Discussion

A modified MSS-method is proposed utilizing angles rather than distances in a combinatorial search for the largest similar point group between two epochs of a monitoring network. The comparison of angles between epochs helps to reduce the number of combinations that have to be examined by eliminating those angles that exhibit significant changes. The use of a histogram of the distribution of the remaining angles in the network in combination with a three-dimensional array to verify the existence of all required angles for a temporary candidate, make the search very efficient.

The angle-based approach requires a higher initial computational effort to calculate the angles in all epochs, since the number of angles in a network with p points is with $p \cdot \sum_{i=1}^{p-2} i > \sum_{i=1}^{p-1} i$, the number of distances in a network. This however, pays off later, as the statistical test for each candidate solution can directly be derived from the angular differences between epochs without the computation of a least-squares estimation, which is required for the distance-ratios approach. While the distance-difference approach does not require a least-squares adjustment either, it is not applicable if scale changes between epochs are expected. In this regard, the angle-based MSS-approach combines the advantages of both distance-

based MSS-methods. An example to illustrate the proposed method has been presented. With the angle-based MSS-method the number of combinations to be analyzed could be reduced to only one: the correct solution. A further advantage of the MSS-method in general is that the localization of the largest similar (or congruent) point group can be carried out independently of the coordinate system and datum definition of each individual epoch, since only datum-invariant elements (distances or angles) are used.

A transformation-based approach is chosen to determine deformations from the adjusted coordinates of a monitoring network in each epoch. The advantage of a transformation-based approach is that, not only different scales between epochs can be accommodated. Moreover, each epoch can have its own coordinate system. The approach chosen here, on the basis of a non-linear Gauss-Markov model furthermore allows the use of the singular cofactor matrices directly without requiring any preprocessing. Merely the compliance with a rank condition needs to be verified.

The highly non-linear elementary rotations with Euler-angles are replaced with a quaternion rotation, yielding a numerically more stable normal equation system. This allows to omit the computation of initial approximations for the unknown transformation parameters. Furthermore, no assumptions are made that restrict the validity of the model.

If more than two epochs are available for analysis, the approach can be extended so that all epochs can be processed simultaneously in one multiple-epoch comparison, rather than in multiple two-epoch comparisons. In two numerical examples it is demonstrated that in a two-epoch comparison or multiple-epoch comparison, the arbitrarily chosen 3D transformations as well as the introduced deformations are accurately recovered.

Chapter 4

COMPUTER SIMULATIONS

In this chapter the performance of the proposed methodologies for the search of the largest similar point group and the transformation-based determination of deformations shall be evaluated in comparison to other methods. For this purpose a simulated monitoring network observed in five epochs is analyzed in two scenarios. In the first case, Scenario A, a typical monitoring scenario is depicted where all epochs are given in the same coordinate system and refer to the same computational base. Furthermore, no scale changes are inherent between epochs. The second scenario describes a case where the coordinate system changes between the base epoch and the subsequent epochs, so that a full 3D transformation, including a scale change, is required to compare coordinates and derive deformations.

The monitoring network consists of twelve points. The 3D coordinates of the monitoring points are simulated in a local coordinate system. The simulated (true) coordinates of the

Point	x	y	z
101	10922.23	5081.20	97.13
102	10836.93	5332.83	98.23
103	10947.37	5568.03	101.06
104	10873.50	5786.00	103.96
105	10748.03	5481.27	96.70
106	10687.77	5474.07	99.65
107	10714.33	5544.37	105.58
108	10739.43	5710.70	98.08
109	10526.47	5804.63	101.35
110	10575.93	5539.33	104.21
111	10712.20	5171.50	100.82
112	10526.47	5028.83	99.56

Table 4.1: Simulated coordinates of network points in [m]

twelve points for the base epoch can be found in Table 4.1. A horizontal plot of the network

points is shown in Figure 4.1. The true coordinates for the subsequent epochs are obtained

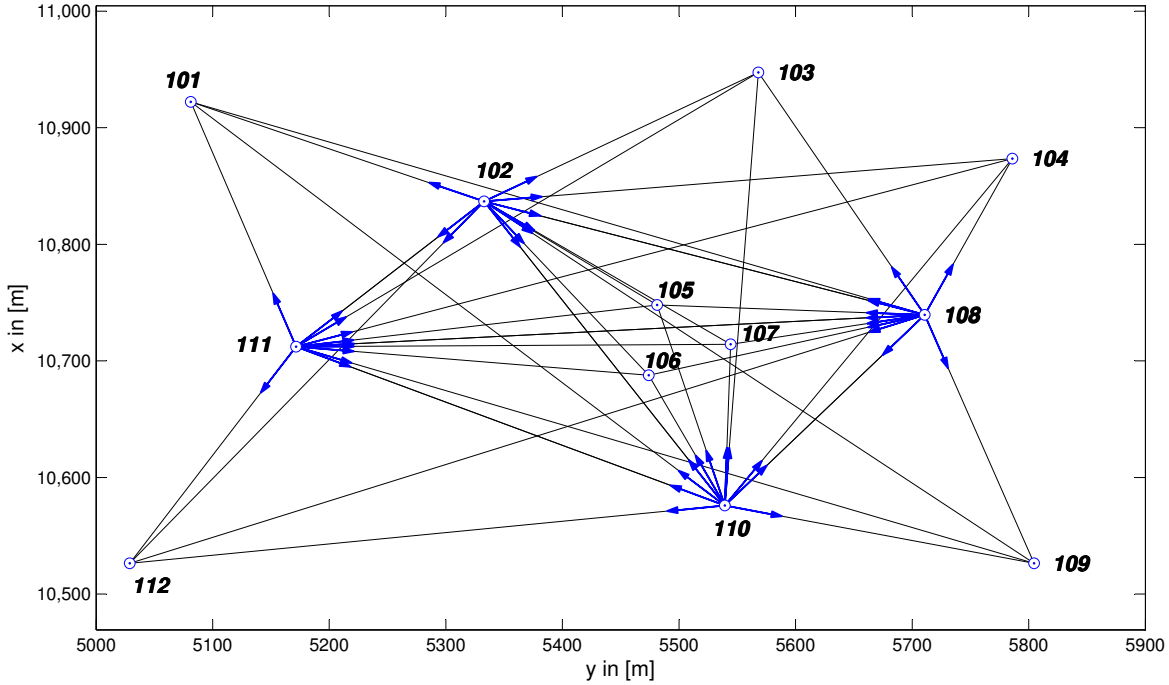

Figure 4.1: Simulated monitoring network with observations indicated by arrows

by adding simulated deformations for each epoch to the coordinates of the base epoch. No deformations were introduced in epoch 2, so that the true coordinates for that epoch are identical to those of the base epoch. In epoch 3 deformations were introduced to three of the twelve points. This number was increased to six deformed points in epoch 4 and nine unstable points in epoch 5. The simulated deformations for the epochs 3 to 5 are listed in Table 4.2 below.

The network points 102, 108, 110 and 111 were chosen as instrument stations from which observations are back-calculated to all other points in the network. The observations consist of horizontal directions, zenith angles and slope distances. Random noise was then added to simulate observations with standard deviations of $\pm 5''$ for horizontal directions and zenith angles and $\pm\,(5\,\text{mm} + 3\,\text{ppm})$ for the slope distances.

A network analysis is performed to determine a set of coordinates from the generated obser-

	Epoch 3			Epoch 4			Epoch 5		
Point	dx	dy	dz	dx	dy	dz	dx	dy	dz
101	0.0	0.0	0.0	0.0	0.0	0.0	0.0	0.0	0.0
102	−16.0	21.0	−11.0	−32.0	32.0	−20.0	47.0	37.0	−26.0
103	0.0	0.0	0.0	0.0	0.0	0.0	23.0	18.0	−14.0
104	0.0	0.0	0.0	0.0	0.0	0.0	0.0	0.0	0.0
105	19.0	−17.0	−10.0	39.0	−23.0	−20.0	47.0	−39.0	−28.0
106	0.0	0.0	0.0	19.0	−23.0	−8.0	42.0	−33.0	−27.0
107	0.0	0.0	0.0	0.0	0.0	0.0	−17.0	−23.0	−11.0
108	12.0	−24.0	−14.0	33.0	−47.0	−26.0	55.0	−58.0	−38.0
109	0.0	0.0	0.0	10.0	−17.0	−12.0	19.0	−40.0	−19.0
110	0.0	0.0	0.0	0.0	0.0	0.0	−13.0	−20.0	−11.0
111	0.0	0.0	0.0	0.0	0.0	0.0	0.0	0.0	0.0
112	0.0	0.0	0.0	−20.0	24.0	−17.0	−32.0	40.0	−51.0

Table 4.2: True deformations of network points for epochs 3 to 5 in [mm]

vations that describes the geometry of the network in each epoch. The measurements already determine some of the datum parameters. The rotations about the x- and y-axes are defined by zenith angle observations at different orientations and the scale factor is determined by the observed slope distances. An inner-constraints approach is used to define the remaining four datum parameters, the rotation about the z-axis and the three translations along the coordinate axes. All points contribute to the network datum in every epoch. Since additional nuisance parameters in the form of orientation offsets are required, this is achieved by performing a partial trace minimization for all coordinate unknowns.

4.1 Scenario A

The first scenario depicts a standard case in the sense that all epochs are given in the same local reference frame and with identical datum definitions. This allows to apply the classical congruence analysis as described in Section 2.3.2 to the data set as well. After the global congruency testing, the localization step is carried out using four different methods: a single-point analysis as is used in the classical approach, the MSS-method based on distance

differences and distance ratios, proposed in Neitzel (2004), and the MSS-method based on angles, as shown in Section 3.1. The following determination of the deformations is performed in two ways: by a re-adjustment of the original observations, as shown in Section 2.3.2.3 and used in the classical congruence analysis, and by the transformation-based approach proposed in Section 3.3.

4.1.1 Results of network analyses

Before a deformation analysis can be performed, a network analysis has to be carried out to obtain coordinates and their standard deviations for each epoch. As input for the network adjustment serve the simulated observations and their standard deviations described above. The observations are considered uncorrelated so that their cofactor matrix is a diagonal and thus regular matrix. The coordinates in Table 4.1 serve as initial approximations for the coordinate unknowns in the network adjustment for all epochs and hence define the reference frame for the monitoring network in this scenario.

In each epoch 132 observations were collected. The parameter vector consists of 40 unknowns; $3 \cdot 12$ coordinates of the monitoring points and one orientation offset for each of the four instrument stations. With the four additional constraint equations defining the free datum parameters, the network redundancy for each epoch is 96. The a priori standard deviation was chosen as $\sigma_0 = \pm 1$ for all epochs.

The a posteriori standard deviations $\hat{\sigma}_{0_k}$ (for $k = 1 \ldots 5$) together with the test statistics $T_{\chi^2_k}$ of the global test of the adjustment model from (2.22) are summarized in Table 4.3 below. The upper and lower boundaries for the global test of the adjustment model are given by $\chi^2_{S=0.975,\,r=96} = 125.00$ and $\chi^2_{S=0.025,\,r=96} = 70.78$ respectively, for a chosen confidence level of $\alpha = 5\,\%$. A look at Table 4.3 shows that all epochs pass the global test of the adjustment model indicating appropriately chosen functional and stochastical models as well as the

Epoch	$\hat{\sigma}_{0_k}$	$T_{\chi^2_k}$
1	±1.001125	96.22
2	±1.092602	114.60
3	±0.951760	86.96
4	±0.978961	92.00
5	±0.990137	94.12

Table 4.3: Scenario A: a posteriori standard deviations and test statistics for global test of adjustment model for all epochs

absence of outliers in the observations.

The adjusted coordinates and their estimated standard deviations can be found in Appendix B.1. The estimated standard deviations vary roughly between ±1 mm and ±5 mm throughout all epochs, where points closer to the centroid of the network have better accuracies while for points further away the accuracy decreases, due to the inner-constraints datum definition. Finally, it should be noted that the resulting cofactor matrix of the adjusted coordinates is rank-deficient by four.

4.1.2 Global congruency testing

Before a global congruency test can be performed to determine whether deformations have occurred, it has to be verified that the coordinates of the five epochs are indeed comparable. This can be done by examining the a posteriori variances with the statistical test described in (2.24). In this simulation all subsequent epochs are compared to the base epoch 1 only, so that a comparison of the variance factor of the base epoch with those of the following epochs is required. The test statistics T_F for these tests are given in Table 4.4 below. With

Epochs	T_F	$\hat{\sigma}_0$
1 and 2	1.19	±1.047862
1 and 3	1.11	±0.976754
1 and 4	1.04	±0.990105
1 and 5	1.02	±0.995646

Table 4.4: Scenario A: test statistics and combined standard deviations

the same network redundancy for all epochs and a chosen confidence level of $\alpha = 5\,\%$, the boundary value is constant for all epochs and is given by $F_{S=0.975,\, f_1=f_2=96} = 1.50$. Hence, this test passes for all epochs and the combined variance factors $\hat{\sigma}_0^2$ can be derived from (2.28). The resulting standard deviations $\hat{\sigma}_0$ are shown in Table 4.4 as well.

The global congruency test can now be carried out for epochs 2 to 5 with respect to epoch 1 according to (2.35). The quadratic forms $\hat{\Omega}^2$ following from (2.31) and the test statistics T_G according to (2.35c) for the four congruency tests are shown in Table 4.5. The reference value

Epochs	$\hat{\Omega}^2$	T_G
2	1.024820	0.93
3	18.543589	19.44
4	62.056041	63.30
5	91.588294	92.39

Table 4.5: Scenario A: quadratic forms $\hat{\Omega}^2$ and test statistics T_G for all global congruency tests

for the test follows from the FISHER-distribution with a chosen confidence level of $\alpha = 5\,\%$, $f_1 = h = 32$ and $f_2 = r_i + r_j = 192$ as $F_{S=0.95,\, f_1=32,\, f_2=192} = 1.50$ for all epochs. A look at Table 4.5 reveals that the global congruency test only passes for epoch 2 while it fails for epochs 3 to 5, so that the presence of deformations in these epochs must be assumed. This, of course, is in accordance with the simulated data.

4.1.3 Localization

With the outcome of the congruency tests in mind, the next step is now to identify stable and unstable points in each epoch. This is done with four different methods: the traditional single-point analysis as described in Section 2.3.2.2, the MSS-method based on distance differences and distance ratios as shown in Section 2.3.4.3.1 and Section 2.3.4.3.2, respectively as well as the MSS-method based on angles, introduced in Section 3.1.

4.1.3.1 Classical congruence analysis

The single-point analysis consists of a series of localized F-tests according to (2.39) for each epoch. Of all points that fail the test, the one with the largest local test statistic T_L is eliminated. After an S-transformation of the remaining points and their cofactor matrix to the new computational base, reduced by the eliminated point, the global congruency test is repeated. If it still fails, this procedure is repeated until the global congruency test passes for all remaining points.

Epoch 2

For the epoch 1 – epoch 2 comparison the global congruency test did pass. But according to (Gründig et al., 1985), the local test is more sensitive and may uncover small, local deviations that may be overshadowed by the effects of other parameters included in a global test. For this reason the local tests shall be carried out to ensure that all points pass these as well. Table 4.6 below lists the local test statistics T_L from (2.39c) for all twelve network points in epoch 2. The boundary value for the local test is the same for all epochs and is given by

Point	101	102	103	104	105	106	107	108	109	110	111	112
T_L	1.78	1.45	0.59	0.51	1.49	0.79	0.28	0.87	1.23	0.67	1.75	0.56

Table 4.6: Scenario A: local test statistics T_L for all points in epoch 2

$F_{S=0.95,\, f_1=3,\, f_2=192} = 2.65$. In this case all twelve monitoring points pass the local test.

Epoch 3

For the comparison of epoch 3 with epoch 1 it is expected that at least one point fails the local test, due to the outcome of the global congruency test. The local test statistics for all points in epoch 3 are listed in Table 4.7. In epoch 3 eight points fail the local test. Point 108 is the one with the largest test statistic $T_L = 107.33$ and is thus eliminated. After an S-transformation to the reduced computational base, the global congruency test is repeated

Point	101	102	103	104	105	106	107	108	109	110	111	112
T_L	2.85	86.36	1.58	7.83	25.37	3.11	1.88	**107.33**	2.30	1.41	4.94	3.31

Table 4.7: Scenario A: local test statistics T_L for all points in epoch 3

with the result:

$$T_G = 10.34 > F_{S=0.95,\, f_1=29,\, f_2=192} = 1.53\,,$$

so that the local tests are re-computed for the eleven remaining points yielding the local test statistics shown in Table 4.8 below. Now seven points fail the test and point 102 is

Point	101	102	103	104	105	106	107	109	110	111	112
T_L	3.22	**64.47**	3.17	0.65	39.63	1.96	2.84	1.29	1.02	3.64	3.27

Table 4.8: Scenario A: local test statistics T_L for remaining points in epoch 3 after elimination of point 108

eliminated next. After an S-transformation, the global congruency test for the remaining points fails again with:

$$T_G = 4.10 > F_{S=0.95,\, f_1=26,\, f_2=192} = 1.55\,.$$

The local test statistics for the next iteration are listed in Table 4.9. Point 105 has the

Point	101	103	104	105	106	107	109	110	111	112
T_L	1.90	0.34	1.01	**25.35**	0.88	0.21	2.12	0.55	7.90	2.59

Table 4.9: Scenario A: local test statistics T_L for remaining points in epoch 3 after elimination of point 102

largest local test statistic and is thus eliminated. Now, all three points that deformations have been introduced to in epoch 3 have been correctly identified and the repeated global congruency test passes with:

$$T_G = 1.33 \leq F_{S=0.95,\, f_1=23,\, f_2=192} = 1.58\,.$$

But when checking each point with a local test again, the results in Table 4.10 indicate that deformations are still inherent in point 111. After the (incorrect) elimination of point 111,

Point	101	103	104	106	107	109	110	111	112
T_L	1.78	0.54	0.82	0.59	0.54	1.43	0.36	**5.69**	2.40

Table 4.10: Scenario A: local test statistics T_L for remaining points in epoch 3 after elimination of point 105

the global congruency test passes again with:

$$T_G = 0.67 \leq F_{S=0.95,\, f_1=20,\, f_2=192} = 1.62\,.$$

And finally, all local tests pass as well:

Point	101	103	104	106	107	109	110	112
T_L	0.32	1.29	0.59	0.68	0.48	1.36	0.26	0.30

Table 4.11: Scenario A: local test statistics T_L for remaining points in epoch 3 after elimination of point 111

Epoch 4

For the comparison of epoch 4 with epoch 1, the results of the repeated global congruency tests and local tests are summarized in tabular form, as the analysis becomes quite lengthy. In Table 4.12 the quantities related to the global congruency tests are listed, including the rank h of the weight matrix of the coordinate differences $\mathbf{P}_{dd}$ in (2.30) and the global test statistic T_G from (2.35c) for each iteration of the test, starting with the initial congruency test already shown in Table 4.5.

Iteration	h	T_G	$F_{S=0.95,\, f_1=h,\, f_2=192}$
1	32	63.30	1.50
2	29	34.90	1.53
3	26	12.47	1.55
4	23	7.42	1.58
5	20	4.74	1.62
6	17	2.89	1.68
7	14	0.61	1.74

Table 4.12: Scenario A: results for global congruency tests for epoch 4

A look at Table 4.12 shows that the global congruency test for epoch 3 does not pass until the seventh iteration, which means that six points are eliminated before the remaining points are found to be stable. The corresponding local test quantities T_L for each iteration are listed in Table 4.13, with the point being eliminated highlighted in bold. The points found to be

Point \ Iteration	101	102	103	104	105	106	107	108	109	110	111	112
1	3.2	303.3	10.4	33.8	53.4	28.3	7.1	**337.0**	13.1	9.8	9.3	18.3
2	5.3	**229.2**	2.2	2.4	89.4	50.6	1.9	×	28.6	3.3	6.8	10.3
3	0.7	×	3.6	1.6	**51.2**	20.9	2.4	×	9.6	10.9	4.7	14.6
4	0.5	×	2.5	0.8	×	**25.3**	0.8	×	11.9	2.8	1.5	15.5
5	0.5	×	1.9	0.4	×	×	0.2	×	14.0	1.0	1.0	**15.2**
6	0.4	×	1.9	0.3	×	×	0.2	×	**13.5**	1.3	1.6	×
7	0.6	×	1.7	0.4	×	×	0.0	×	×	0.1	1.0	×

Table 4.13: Scenario A: local test statistics T_L for all points in epoch 4

unstable, in order of elimination, are 108, 102, 105, 106, 112 and 109. These are all points that deformations were introduced to in epoch 4, so that the single-point analysis yields the correct results. Also, the outcome of the global and local tests agree, such that after passing of the global congruency test, the local test passes for all points as well.

Epoch 5

Iteration	h	T_G	$F_{S=0.95,\, f_1=h,\, f_2=192}$
1	32	92.39	1.50
2	29	51.41	1.53
3	26	36.04	1.55
4	23	30.12	1.58
5	20	24.84	1.62
6	17	19.37	1.68
7	14	14.82	1.74
8	11	9.58	1.84
9	8	7.28	1.99
10	5	4.71	2.26
11	2	1.54	3.04

Table 4.14: Scenario A: results for global congruency tests for epoch 5

The results of the global congruency test for the comparison of epoch 5 with epoch 1 are

listed in Table 4.14, again starting with the initial iteration from Table 4.5. In this case it takes eleven iterations of the single-point analysis before the global congruency test passes, which means that ten points are eliminated as unstable. The local test statistics T_L for each iteration are shown in Table 4.15, with the point being eliminated in each iteration highlighted in bold. The ten points found to be unstable in epoch 5 are, in order of elimination,

Pt. \ It.	101	102	103	104	105	106	107	108	109	110	111	112
1	15.7	251.4	15.0	52.4	36.1	24.6	52.6	**488.5**	20.2	100.0	59.9	64.2
2	6.0	**184.6**	9.8	5.9	79.7	47.8	31.9	×	38.9	69.6	46.6	57.4
3	6.1	×	22.2	2.4	**81.5**	53.8	20.3	×	29.0	63.2	32.4	52.2
4	3.9	×	25.3	2.7	×	**65.3**	16.5	×	35.3	44.6	21.8	54.2
5	2.7	×	30.1	3.4	×	×	13.0	×	40.8	31.6	15.6	**55.8**
6	2.3	×	32.2	4.9	×	×	11.2	×	**40.6**	20.5	22.4	×
7	1.2	×	**34.0**	7.6	×	×	11.8	×	×	20.8	13.1	×
8	1.1	×	×	10.2	×	×	9.7	×	×	11.6	**15.7**	×
9	4.8	×	×	**11.6**	×	×	5.5	×	×	3.3	×	×
10	**6.8**	×	×	×	×	×	5.3	×	×	2.6	×	×
11	×	×	×	×	×	×	1.0	×	×	1.0	×	×

Table 4.15: Scenario A: local test statistics T_L for all points in epoch 5

108, 102, 105, 106, 112, 109, 103, 111, 104 and 101. The last three points being eliminated are the only stable points in epoch 5. After that, both global and local tests pass, with only two points remaining. Note that the local test statistics in the final iteration are identical for both remaining points, similar to the second example in Section 2.3.2.4. This indicates that with only two points remaining a decision as to which one is more likely to have deformed cannot be made, regardless whether their deviations are significant or not.

4.1.3.2 MSS using distance differences

Next, the localization shall be performed using the MSS-method based on distance differences proposed in Neitzel (2004) and described in detail in Section 2.3.4.3.1. For this combinatorial search the distances between all network points are computed in each epoch together with their corresponding cofactor matrices. The distances can then be compared between epochs,

eliminating those whose differences exceed a certain threshold. In this example the 3σ-criterion is chosen as a threshold, meaning that those distances are eliminated whose inter-epochal differences exceed three times their standard deviations. Through the use of topology matrices those point groups are identified which still have all distances. Each of these candidates is then examined with a global congruency test. The quadratic form $\hat{\Omega}^2$ for the test can be derived directly from the distance differences, according to (2.34).

Epoch 2

For the comparison of epoch 2 with epoch 1 the MSS-method quickly confirms the outcome of the global congruency test in Table 4.5. Non of the distance differences between epochs 2 and 1 differ significantly from zero, so that the only candidate group consists of all twelve points. Repeating the global congruency test, this time derived from the distance differences, if only for reasons of completeness, yields:

$$T_G = \frac{\hat{\Omega}^2}{\sigma_0^2} = \frac{1.049723}{1.098015} = 0.96 \leq 1.52 = F_{S=0.95,\, f_1=h=30,\, f_2=r_1+r_2=192} \ ,$$

so that the outcome is equivalent to that of the test performed with coordinate differences, as is expected.

Epoch 3

For the comparison of epochs 3 and 1 only one candidate is found after the elimination of the significant distance differences. The candidate consists of nine points, namely the points 101, 103, 104, 106, 107, 109, 110, 111 and 112. The global congruency test for the this point group passes with the following result:

$$T_G = \frac{\hat{\Omega}^2}{\sigma_0^2} = \frac{1.369451}{0.954049} = 1.44 \leq 1.61 = F_{S=0.95,\, f_1=h=21,\, f_2=r_1+r_3=192} \ .$$

Thus, the maximum congruent point group could be correctly identified for epoch 3.

Epoch 4

For the comparison of epoch 4 and epoch 1 two candidate solutions were found after the elimination of the significantly changed distances. Both candidates consist of a group of six points. The first candidate consists of the points 101, 103, 104, 107, 110 and 111. The global congruency test for this candidate passes with

$$T_G = 0.62 \leq 1.80 = F_{S=0.95,\, f_1=h=12,\, f_2=r_1+r_4=192} \,.$$

The second candidate consists of the points 101, 103, 104, 107, 111 and 112. The global congruency test in this case fails:

$$T_G = 4.03 \not\leq 1.80 = F_{S=0.95,\, f_1=h=12,\, f_2=r_1+r_4=192} \,.$$

Again, the largest congruent point group was correctly identified. The only other existing candidate could be ruled out with help of the global congruency test.

Epoch 5

For the comparison of epoch 5 and epoch 1 a total of seven candidates were found, consisting of three points each. The candidates together with their respective global test statistics T_G can be found in Table 4.16 below. The correct solution is highlighted in bold in the table. The boundary value for this test is given by $F_{S=0.95,\, f_1=h=3,\, f_2=r_1+r_5=192} = 2.65$. From the

Candidate	T_G
101, 103, 104	9.64
101, 104, 111	**0.93**
103, 104, 106	0.95
103, 104, 109	2.36
103, 105, 106	7.78
103, 106, 109	3.43
104, 106, 109	1.85

Table 4.16: Scenario A: results for global congruency tests for all candidates for congruent point groups of epoch 5

test statistics in Table 4.16 it can be seen, that now four out of seven candidates pass the global congruency test. This indicates that now multiple congruent triangles exist which means that for these candidates all three points must exhibit similar deformations. Under the assumption that the group consisting of the stable points has overall smaller differences between epochs, the candidate with the smallest global test quantity T_G is accepted as the final solution. In this case, this leads to the correct identification of the largest congruent point group between epochs 1 and 5.

4.1.3.3 MSS using distance ratios

Now the monitoring network is analyzed with the MSS-method based on distance ratios proposed in Neitzel (2004) and explained in detail in Section 2.3.4.3.2. Although this method is particular meant for scenarios in which a change in scale occurs between epochs, it is applied here for comparison with the other methods. In this approach the distance ratios of the same distances between epochs are analyzed rather than their differences. An error estimate for the scale factor is derived and with it a search window can be created. Again, topology matrices are used to find those point groups for which all existing distances lie within the same search window. These point groups form possible candidates. To verify the candidates an adjustment based on the transformation approach introduced in Section 2.3.4.3.2 is performed. To assess the candidates the a posteriori standard deviation $\hat{\sigma}_0$ of the adjustment is evaluated with a global test of the adjustment model, similar to the one given in (2.22). Only in this case the alternative hypothesis is formulated as

$$H_A: \qquad E\left\{\sigma_0^2\right\} < E\left\{\hat{\sigma}_0^2\right\} \ ,$$

because the presence of deformations in the candidate group will lead to an increase in the a posteriori variance factor. This results in a one-tailed test with the boundary value given by $\chi^2_{S=1-\alpha,\, f=r}$. If the test passes, it can be assumed that the data conforms to the functional and stochastical models and no outliers exist. If this test fails on the other hand,

the existence of deformations in the data is likely, so that the candidate under consideration is rejected.

In this example the search window for the distance ratios is created at a size of $1.5\hat{\sigma}_s$, where $\hat{\sigma}_s$ denotes the error estimate for the scale factor. The reason for this is to reduce the number of candidate solution to a presentable level. For the transformation adjustment an a priori standard deviation of $\sigma_0 = 1$ has been used for all epochs.

Epoch 2

Again, the method is applied to epoch 2 as well. Only one candidate consisting of all twelve network points is found. The transformation-based adjustment yields the results listed in Table 4.17 for the candidate solution. The test statistic for the global test of the adjustment

Candidate	$\hat{\sigma}_0$	Redundancy	T_χ	Test outcome
All twelve points	± 0.989229	29	28.38	pass

Table 4.17: Scenario A: largest congruent point group and statistical test for epoch 2

model is given by (2.22c). The boundary value for the χ^2-test for a confidence level of $\alpha = 5\,\%$ follows from $\chi^2_{S=0.95,\,f=r=29} = 42.56$. Thus, the correct solution was found for epoch 2.

Epoch 3

For epoch 3 only one candidate is found consisting of nine points. The transformation adjustment for the one candidate solution is carried out again and the results listed in Table 4.18 are obtained. The boundary value for the global test of the adjustment model is given by

Candidate	$\hat{\sigma}_0$	Redundancy	T_χ	Test outcome
101, 103, 104, 106, 107, 109, 110, 111, 112	± 1.226615	20	30.09	pass

Table 4.18: Scenario A: largest congruent point group and statistical test for epoch 3

$\chi^2_{S=0.95,\,f=r=20} = 31.41$, so that the test passes and the candidate solution reflects the largest

congruent point group between epochs 1 and 3. Again, this decision is correct, as only the three points 102, 105 and 108 missing from the solution were subject to deformations in epoch 3.

Epoch 4

In epoch 4 at first one candidate consisting of eight points is found. The results of the transformation adjustment for this candidate, given in Table 4.19, indicate that this candidate does not form a congruent point group, as the global test of the adjustment model with a boundary value of $\chi^2_{S=0.95,\, f=r=17} = 27.56$, fails.

Candidate	$\hat{\sigma}_0$	Redundancy	T_χ	Test outcome
101, 103, 104, 107, 109, 110, 111, 112,	±2.267622	17	87.42	fail

Table 4.19: Scenario A: candidates of eight points and statistical test for epoch 4

The search is then continued for a congruent point group of less than eight points and eight candidates are found, each consisting of seven points. For each of these eight candidates the transformation adjustment is performed. The results are given in Table 4.20 below. With a

Candidate	$\hat{\sigma}_0$	Redundancy	T_χ	Test outcome
101, 103, 104, 107, 109, 110, 111	±1.809480	14	45.84	fail
101, 103, 104, 107, 109, 110, 112	±2.358459	14	77.87	fail
101, 103, 104, 107, 109, 111, 112	±2.373585	14	78.87	fail
101, 103, 104, 107, 110, 111, 112	±1.928669	14	52.08	fail
101, 103, 104, 109, 110, 111, 112	±2.485653	14	86.50	fail
101, 103, 107, 109, 110, 111, 112	±2.439569	14	83.32	fail
101, 104, 107, 109, 110, 111, 112	±2.338951	14	76.59	fail
103, 104, 107, 109, 110, 111, 112	±2.422185	14	82.14	fail

Table 4.20: Scenario A: candidates of seven points and statistical test for epoch 4

reference value of $\chi^2_{S=0.95,\, f=r=14} = 23.68$ the global test of the adjustment model fails again for all eight candidates. Thus, the search continues for a congruent group of less than seven points.

This leads to a list of 32 candidates consisting of six points. After the transformation adjustment has been carried out for all 32 candidates, the global test of the adjustment model, with a reference value of $\chi^2_{S=0.95,\, f=r=11} = 19.68$, passes only for one candidate. This candidate, together with the test results is listed in Table 4.21 below. The largest congruent

Candidate	$\hat{\sigma}_0$	Redundancy	T_χ	Test outcome
101, 103, 104, 107, 110, 111	±0.719884	11	5.70	pass

Table 4.21: Scenario A: largest congruent point group and statistical test for epoch 4

point group between epochs 1 and 4 has been correctly identified. A list of the rejected 31 candidates and their corresponding test results can be found in Table B.6 in Appendix B.2.

Epoch 5

The search for the largest congruent point group between epochs 1 and 5 first results in a list of nine candidate groups consisting of five points each. The candidates and the parameters of the global test of the adjustment model are listed in Table 4.22. Given the boundary

Candidate	$\hat{\sigma}_0$	Redundancy	T_χ	Test outcome
101, 103, 104, 109, 111	±4.292742	8	147.42	fail
101, 103, 104, 111, 112	±4.208039	8	141.66	fail
101, 104, 106, 109, 111	±4.833361	8	186.89	fail
101, 107, 109, 110, 111	±2.976424	8	70.87	fail
103, 104, 105, 106, 109	±2.315300	8	42.88	fail
103, 104, 106, 109, 112	±5.856611	8	274.40	fail
104, 106, 108, 111, 112	±8.293931	8	550.31	fail
104, 106, 109, 111, 112	±5.730471	8	262.71	fail
107, 109, 110, 111, 112	±3.947802	8	124.68	fail

Table 4.22: Scenario A: candidates of five points and statistical test for epoch 5

value of $\chi^2_{S=0.95,\, f=r=8} = 15.51$, all of theses candidates are rejected. The search continues for a group of less than five points and yields a list of 45 candidates of four points, all of which are rejected. The candidates and their corresponding test results can be found in Table B.7 in Appendix B.2.

The search for congruent point groups of less than four points results in a list of 83 candidates of three points. After performing a transformation adjustment for all candidates, the final solution is found and given in Table 4.23. The boundary value for the global test of the

Candidate	$\hat{\sigma}_0$	Redundancy	T_χ	Test outcome
101, 104, 111	± 1.119205	2	2.51	pass

Table 4.23: Scenario A: largest congruent point group and statistical test for epoch 5

adjustment model follows from $\chi^2_{S=0.95,\, f=r=2} = 5.99$. The remaining candidates and their test results are listed in Table B.8 in Appendix B.2. It should be noted that although the correct solution was identified as the one with the smallest test statistic T_χ, other candidates have passed this test as well, indicating that further congruent triangles exist. Reason for this, again, are points with similar deformations.

4.1.3.4 MSS using angles

Finally, the monitoring network is examined with the MSS-method based on angular differences, proposed in Section 3.1. Instead of distances all possible combinations of angles are computed in each epoch and compared between epochs. Those angles whose differences exceed the 3σ-threshold are eliminated. Utilizing a histogram of the angle distribution in the network coupled with a three-dimensional search array, point groups for which all angles still exist are identified and form candidate solutions. The candidates can be verified by a global congruency test, which can directly be derived from the angular differences.

Epoch 2

One candidate solution is found for the comparison of epoch 2 and epoch 1. The candidate consists of all twelve network points. With a boundary value of $F_{S=0.95,\, f_1=h=29,\, f_2=r_1+r_2=192} = 1.53$ the global congruency test passes, which confirms that the largest congruent point group indeed consists of all network points. The test results are summarized in Table 4.24.

Candidate	T_G	Test outcome
101, 102, 103, 104, 105, 106, 107, 108, 109, 110, 111, 112	0.98	pass

Table 4.24: Scenario A: largest congruent point group and test statistic for epoch 2

Epoch 3

Similarly for the epoch 3 – epoch 1 comparison, the search for the largest congruent point group only yields one candidate consisting of nine points. The boundary value for the global

Candidate	T_G	Test outcome
101, 103, 104, 106, 107, 109, 110, 111, 112	1.50	pass

Table 4.25: Scenario A: largest congruent point group and test statistic for epoch 3

congruency test follows from $F_{S=0.95,\, f_1=h=20,\, f_2=r_1+r_3=192} = 1.62$, so that the test passes for the candidate solution and again the correct point group has been identified.

Epoch 4

In epoch 4 six candidate solutions are found consisting of six points. The reference value for the global congruency test is given by $F_{S=0.95,\, f_1=h=11,\, f_2=r_1+r_4=192} = 1.84$. The results in Table 4.26 show that only one candidate passes the test. Again, the correct point group has been identified.

Candidate	T_G	Test outcome
101, 103, 104, 107, 109, 110	3.71	fail
101, 103, 104, 107, 110, 111	0.52	pass
101, 103, 104, 107, 110, 112	3.74	fail
101, 103, 107, 110, 111, 112	4.41	fail
101, 104, 107, 109, 110, 111	3.36	fail
101, 107, 109, 110, 111, 112	6.09	fail

Table 4.26: Scenario A: candidates and test statistics for epoch 4

Epoch 5

For the comparison of the first and the final epoch a total of 28 candidate solutions were found. The global test of the adjustment model was performed for all candidates. The boundary value for the test is $F_{S=0.95,\, f_1=h=2,\, f_2=r_1+r_5=192} = 3.04$. The candidate with the

Candidate	T_G	Test outcome
101, 104, 111	0.25	pass

Table 4.27: Scenario A: largest congruent point group and test statistic for epoch 5

smallest test statistic T_G is shown in Table 4.27 and is the correct solution. The remaining candidates and their test results are shown in Table B.9 in Appendix B.3. It should be noted that further candidates pass the gobal congruency test. As before, this is an indication for the existence of multiple congruent triangles, caused by points with similar deformations.

4.1.4 Determination

After the largest congruent point groups have been identified, the final task is now to determine values for the deformations and their standard deviations. Two different methods are used to do that. First, a combined re-adjustment of the observations is performed as is commonly used in the classical congruence analysis and is described in Section 2.3.2.3. Then, the deformations are determined again using the transformation-based approach introduced in Section 3.3.

4.1.4.1 Combined re-adjustment of observations

With this method the deformations are derived from the original observations of the two epochs under consideration. The network analysis is repeated, combining the observations of both epochs. The stable points are now solved using the observations from both epochs. For the deformed points two different point IDs are introduced; one for the coordinates in

the base epoch and one for the coordinates in the subsequent epoch. The deformations then follow as the differences of the two sets of coordinates.

The datum definition is implemented using an inner-constraints approach again where all stable points form the computational base. The four datum parameters to be defined are, as before, the orientation in the horizontal plane and the three translations along the coordinate axes. The reference frame is defined by the same approximate coordinates as were used for the initial network analyses and which are listed in Table 4.1. The input standard deviations for the observations remain the same as well, which are $\pm 5''$ for horizontal directions and zenith angles and $\pm\,(5\,\mathrm{mm} + 3\,\mathrm{ppm})$ for slope distances. The a priori standard deviation is chosen as $\sigma_0 = \pm 1$ in all cases.

Epoch 2

In epoch 2 none of the monitoring points have been found to be unstable. Hence, only one set of coordinates is estimated for each point using the observations from epoch 1 and epoch 2 together. Consequently, the deformations for all points in epoch 2 are all exactly zero. All twelve network points contribute to the datum. The statistical results from the network adjustment are given in Table 4.28 below. The adjusted coordinates and their respective standard deviations can be found in Table B.10 in Appendix B.4.

Number of points in network	12
Number of observations	264
Number of unknowns	40
Redundancy	228
A posteriori standard deviation $\hat{\sigma}_0$	± 1.035552
Global test statistic T_χ	244.50
Lower boundary value $\chi^2_{S=0.025,\,r}$	188.07
Upper boundary value $\chi^2_{S=0.975,\,r}$	271.71
Outcome of global test of adjustment model	pass

Table 4.28: Scenario A: summary of statistics for combined re-adjustment of epochs 1 and 2

Epoch 3

In epoch 3 four points were found to be unstable during the single-point analysis, namely points 102, 105, 108 and, incorrectly, point 111. For these four points two sets of coordinates are estimated, one set for epoch 1 with point IDs starting with 1 and one set for epoch 3 with point IDs starting with 3. The differences of these two sets of coordinates represent the deformations between epoch 3 and epoch 1.

The computational base is formed by the remaining eight stable points. The statistical results for the network analysis are listed in Table 4.29. The adjusted coordinates and their standard deviations can be found in Table B.11 in Appendix B.4.

Number of points in network	16
Number of observations	264
Number of unknowns	55
Redundancy	213
A posteriori standard deviation $\hat{\sigma}_0$	± 0.959819
Global test statistic T_χ	196.23
Lower boundary value $\chi^2_{S=0.025,\,r}$	174.47
Upper boundary value $\chi^2_{S=0.975,\,r}$	255.31
Outcome of global test of adjustment model	pass

Table 4.29: Scenario A: summary of statistics for combined re-adjustment of epochs 1 and 3

The estimated deformations between epoch 3 and epoch 1 for the deformed points together with their standard deviations are shown in Table 4.30. The deformations for the remaining points are zero exactly. It can be noted that the deformation in x-direction for the incorrectly

Point	dx	dy	dz	$\hat{\sigma}_{dx}$	$\hat{\sigma}_{dy}$	$\hat{\sigma}_{dz}$
102	-18.9	17.9	-6.0	± 2.5	± 2.1	± 2.6
105	19.9	-22.6	-9.4	± 3.9	± 3.5	± 3.7
108	12.7	-27.6	-17.1	± 2.6	± 1.9	± 2.4
111	-12.3	0.9	3.6	± 3.1	± 2.0	± 3.0

Table 4.30: Scenario A: estimated deformations and standard deviations in epoch 3 in [mm]

as unstable classified point 111 is very high in magnitude, considering that no deformation

was introduced in that point in epoch 3. This must be due to a large amount amount of random errors accumulating in the x-coordinate of this point in epoch 3.

Epoch 4

In epoch four six points were correctly identified to be unstable. These six points are excluded from the datum definition in the re-adjustment of this epoch. A separate set of coordinates with an ID starting with 4 is estimated for these points in epoch 4. The adjusted coordinates of all points can be found in Table B.12 in Appendix B.4. The statistical results are given in Table 4.31 below.

Number of points in network	18
Number of observations	264
Number of unknowns	60
Redundancy	208
A posteriori standard deviation $\hat{\sigma}_0$	± 0.981396
Global test statistic T_χ	200.33
Lower boundary value $\chi^2_{S=0.025,\,r}$	169.95
Upper boundary value $\chi^2_{S=0.975,\,r}$	249.83
Outcome of global test of adjustment model	pass

Table 4.31: Scenario A: summary of statistics for combined re-adjustment of epochs 1 and 4

The estimated deformations and standard deviations for the six unstable points are listed in Table 4.32. Again, for the six remaining stable points the deformations are zero.

Point	dx	dy	dz	$\hat{\sigma}_{dx}$	$\hat{\sigma}_{dy}$	$\hat{\sigma}_{dz}$
102	-27.9	32.3	-15.5	± 2.6	± 2.2	± 2.6
105	39.6	-27.5	-20.8	± 4.0	± 3.5	± 3.8
106	22.6	-25.5	-2.4	± 5.0	± 3.8	± 5.1
108	37.0	-48.0	-28.8	± 2.9	± 2.0	± 2.6
109	9.4	-20.0	-12.4	± 5.6	± 4.2	± 5.7
112	-19.5	24.6	-21.6	± 5.8	± 4.2	± 6.4

Table 4.32: Scenario A: estimated deformations and standard deviations in epoch 4 in [mm]

Epoch 5

In epoch 5 ten out of twelve points have been found to be unstable during the single-point analysis, incorrectly eliminating the only three stable points in this epoch which are points 101, 104 and 111. This only leaves points 107 and 110 to define the computational base in the re-adjustment. The statistical results for of the analysis are given in Table 4.33. The adjusted coordinates and their standard deviations can be found in Table B.13 in Appendix B.4.

Number of points in network	22
Number of observations	264
Number of unknowns	73
Redundancy	195
A posteriori standard deviation $\hat{\sigma}_0$	± 1.001951
Global test statistic T_χ	195.76
Lower boundary value $\chi^2_{S=0.025,\,r}$	158.22
Upper boundary value $\chi^2_{S=0.975,\,r}$	235.56
Outcome of global test of adjustment model	pass

Table 4.33: Scenario A: summary of statistics for combined re-adjustment of epochs 1 and 5

The deformations of the points 107 and 110 is formally zero. For the points identified as unstable the estimated deformations and standard deviations are shown in Table 4.34 below.

Point	dx	dy	dz	$\hat{\sigma}_{dx}$	$\hat{\sigma}_{dy}$	$\hat{\sigma}_{dz}$
101	16.9	25.4	6.6	± 10.7	± 7.6	± 6.2
102	60.3	52.7	-14.1	± 5.1	± 5.0	± 3.2
103	40.8	32.7	-4.0	± 4.5	± 8.0	± 5.7
104	18.0	17.9	4.4	± 7.0	± 6.5	± 5.2
105	64.5	-19.1	-17.9	± 4.4	± 4.5	± 4.0
106	59.0	-10.7	-10.2	± 4.4	± 3.7	± 3.6
108	71.0	-41.1	-28.4	± 4.6	± 3.4	± 3.0
109	28.4	-21.5	-3.8	± 7.4	± 4.5	± 5.9
111	12.4	21.1	12.8	± 8.2	± 3.1	± 3.8
112	-14.2	55.3	-31.5	± 11.8	± 4.7	± 6.9

Table 4.34: Scenario A: estimated deformations and standard deviations in epoch 5 in [mm]

It can be noted that the standard deviations of the deformations in epoch 5 show a quite significant increase compared to previous epochs. This is due to the datum being defined by only two points now, which were subject to deformations.

Comparison of true and estimated deformations

In Table 4.35 the errors ϵ of the estimated deformations are shown, calculated as the differences of the estimated deformations and the true deformations: $\vec{\epsilon} = \vec{d}_{est} - \vec{d}_{true}$.

	Epoch 3			Epoch 4			Epoch 5		
Point	ϵ_x	ϵ_y	ϵ_z	ϵ_x	ϵ_y	ϵ_z	ϵ_x	ϵ_y	ϵ_z
101	0	0	0	0	0	0	16.9	25.4	6.6
102	−2.9	−3.1	5	4.1	0.3	4.5	13.3	15.7	11.9
103	0	0	0	0	0	0	17.8	14.7	10.0
104	0	0	0	0	0	0	18.0	17.9	4.4
105	0.9	−5.6	0.6	0.6	−4.5	−0.8	17.5	19.9	10.1
106	0	0	0	3.6	−2.5	5.6	17.0	22.3	16.8
107	0	0	0	0	0	0	17.0	23.0	11.0
108	0.7	−3.6	−3.1	4.0	−1.0	−2.8	16.0	16.9	9.6
109	0	0	0	−0.6	−3.0	−0.4	9.4	18.5	15.2
110	0	0	0	0	0	0	13.0	20.0	11.0
111	−12.3	0.9	3.6	0	0	0	12.4	21.1	12.8
112	0	0	0	0.5	0.6	−4.6	17.8	15.3	19.5

Table 4.35: Scenario A: differences between estimated and true deformations at given epoch in [mm]

The errors for the deformations of epoch 2 are omitted from the table because they are all exactly zero, as only one set of coordinates is estimated for the stable points, so that no coordinate differences exist. In epoch 3 the errors are at the low millimetre level, within 2σ of their standard deviations, with the exception of the x-deformation of point 111, which was incorrectly identified as unstable. In epoch 4 the errors of the estimated deformations range between 0 and about 5 mm in magnitude and are all within 2σ of their standard deviations. In epoch 5 the errors of the estimated deformations range from about 5 mm to over 10 mm, exceeding 3σ of their standard deviations for most of the points. The reason for this is

the wrong result of the localization phase with the single-point analysis. As a result the determination of movements is based on an unstable computational base which in turn leads to incorrect deformations.

For epochs 2 to 4 the classical congruence analysis is successful, with the exception of point 11 in epoch 3. The unstable points are correctly identified, even when deformations are introduced to half of the points in epoch 4. Furthermore, reasonable estimates for the true deformations are obtained for epochs 2 to 4. In epoch 5, however, when only three out of twelve points are stable, the single-point analysis cannot identify the truely stable point group which leads to wrong results for the estimated deformations of all points, so that for epoch 5 the classical congruence analysis fails.

4.1.4.2 Transformation-based approach

With this approach transformation parameters are estimated between the base epoch and each of the subsequent epochs based on the largest congruent point groups identified in Section 4.1.3.4. With the help of the estimated transformation parameters the adjusted coordinates of each epoch can then be transformed into the system of the base epoch in a datum defined by the congruent points. Deformations for all points are then obtained as coordinate differences in the system of the base epoch.

The adjusted coordinates of each epoch listed in Appendix B.1 together with their fully-populated and singular cofactor matrices can directly be used as input for the transformation. The a priori standard deviation for the transformation adjustment was chosen as $\sigma_0 = \pm 1$.

The statistical results for the transformation adjustment are summarized in Table 4.36 below.

The estimated transformation parameters and their standard deviations are listed in Table

	Ep 1	Ep 2	Ep 3	Ep 4	Ep 5	Total
Number of points	12	12	9	6	3	42
Number of observations	36	36	27	18	9	126
Number of conditions	–	37	28	19	10	94
Number of unknowns	–	8	8	8	8	32
Redundancy	–	29	20	11	2	62
A posteriori standard deviation $\hat{\sigma}_0$						± 1.037771
Global test statistic T_χ						66.77
Lower boundary value $\chi^2_{S=0.025,\,r}$						42.13
Upper boundary value $\chi^2_{S=0.975,\,r}$						85.65
Test outcome						pass

Table 4.36: Scenario A: summary of statistics for transformation adjustment of all epochs

4.37 for epochs 2 and 3 and in Table 4.38 for epochs 4 and 5, respectively. For epoch 2 the estimated rotation parameters are at the 1″-level with standard deviations slightly larger than the magnitude of the angles themselves. The translations are at the level of 10^{-12} m with standard deviations exceeding them by almost an order of magnitude and the estimated scale factor is insignificantly small as well. Overall it can be said that the transformation parameters are negligible. This makes sense, since both epochs are given in the same coordinate system and share the same datum definition, so that no changes should occur. In epoch 3 the transformation parameters are still very accurately determined but

	Epoch 2		Epoch 3	
Parameter	Value	$\hat{\sigma}$	Value	$\hat{\sigma}$
q_0	0.999999999990085	$\pm 0.1999 \cdot 10^{-10}$	0.999999999993265	$\pm 0.1087 \cdot 10^{-10}$
q_x	0.0000028595	$\pm 3.4392 \cdot 10^{-6}$	0.0000031497	$\pm 3.4413 \cdot 10^{-6}$
q_y	−0.0000034137	$\pm 4.9066 \cdot 10^{-6}$	−0.0000000033	$\pm 4.9335 \cdot 10^{-6}$
q_z	−0.0000000148	$\pm 0.0177 \cdot 10^{-6}$	−0.0000018840	$\pm 0.3609 \cdot 10^{-6}$
ω	1.2″	±1.4″	1.3″	±1.4″
φ	−1.4″	±2.0″	−0.0″	±2.0″
κ	−0.0″	±0.0″	−0.8″	±0.1″
T_x	$0.16 \cdot 10^{-12}$ m	$\pm 0.26 \cdot 10^{-10}$ m	0.001535 m	±0.000449 m
T_y	$-0.83 \cdot 10^{-12}$ m	$\pm 0.17 \cdot 10^{-10}$ m	−0.002260 m	±0.000391 m
T_z	$-0.27 \cdot 10^{-16}$ m	$\pm 0.15 \cdot 10^{-10}$ m	−0.002727 m	±0.000468 m
λ	+1.6 ppm	±3.1 ppm	−1.2 ppm	±3.2 ppm

Table 4.37: Scenario A: estimated transformation parameters and standard deviations of epochs 2 and 3 with respect to epoch 1

now show some significance. The rotations are still at the 1″-level but with the z-rotation now eight times larger than its standard deviation. The translations vary between 1 mm and 3 mm in magnitude but have standard deviations of almost one order of magnitude smaller, so that some small but significant translations exist, too. As before, the scale factor is still small with a standard deviation of more than twice its magnitude and can thus be considered insignificant. These small but significant transformation parameters can be attributed to the change in datum between epochs 1 and 3, since now the computational base is reduced to the nine points that form the largest congruent point group between the two epochs.

In epoch 4 the estimated transformation parameters increase in magnitude compared to the two previous epochs. A significant rotation about the z-axis of almost 6″ can be observed as well as translations between 5 mm and 9 mm. The scale factor has increased slightly as well but is still at a negligible level. In epoch 5 the increase in magnitude of the transformation

	Epoch 4		Epoch 5	
Parameter	Value	$\hat{\sigma}$	Value	$\hat{\sigma}$
q_0	0.9999999999	$\pm 0.3212 \cdot 10^{-10}$	0.9999999999	$\pm 0.6022 \cdot 10^{-10}$
q_x	0.0000010528	$\pm 3.7923 \cdot 10^{-6}$	0.0000034905	$\pm 4.5660 \cdot 10^{-6}$
q_y	−0.0000034205	$\pm 5.3104 \cdot 10^{-6}$	−0.0000053732	$\pm 10.7422 \cdot 10^{-6}$
q_z	−0.0000140755	$\pm 1.8330 \cdot 10^{-6}$	−0.0000092152	$\pm 2.6658 \cdot 10^{-6}$
ω	0.4″	±1.6″	1.4″	±1.9″
φ	−1.4″	±2.2″	−2.2″	±4.4″
κ	−5.8″	±0.8″	−3.8″	±1.1″
T_x	0.004776 m	±0.000862 m	0.012625 m	±0.001891 m
T_y	−0.005001 m	±0.000709 m	−0.009805 m	±0.001444 m
T_z	−0.008626 m	±0.000869 m	−0.017176 m	±0.002449 m
λ	−6.5 ppm	±3.7 ppm	+5.7 ppm	±5.1 ppm

Table 4.38: Scenario A: estimated transformation parameters and standard deviations of epochs 4 and 5 with respect to epoch 1

parameters continues, except for the z-rotation and the scale factor. An increase in the standard deviations can also be noted. This can be explained with the reduction of the computational base to only three points in epoch 5 and the resulting loss in accuracy.

Looking at the transformation parameters of epochs 3 to 5, it becomes obvious that the

significant parameters are the four free datum parameters which were defined by inner-constraints of all twelve points in the network analyses of each epoch. These are the rotation about the z-axis and the translations along all three coordinate axes. The more points are eliminated from the original computational base, the more pronounced this datum change becomes.

After the transformation parameters are determined, they can be applied to the adjusted coordinates of epochs 2 to 4 according to (3.27) to obtain transformed coordinates in the respective datum defined by the congruent points. Then, deformations can be derived as the coordinate differences with respect to the coordinates of epoch 1 according to (3.28).

The estimated deformations for epoch 2 together with their standard deviations are shown in Table 4.39 below. Since no true deformations were introduced in epoch 2, these estimated

Point	dx	dy	dz	$\hat{\sigma}_{dx}$	$\hat{\sigma}_{dy}$	$\hat{\sigma}_{dz}$
101	2.4	4.8	−6.6	±4.4	±4.0	±6.4
102	−0.6	−2.9	3.9	±2.4	±2.1	±2.8
103	−2.5	1.3	−0.5	±4.2	±4.1	±5.7
104	2.2	3.2	−2.4	±4.4	±3.7	±5.5
105	−2.8	−4.3	−4.0	±3.9	±3.4	±3.6
106	2.7	0.8	5.2	±3.9	±3.2	±3.5
107	−0.1	−2.3	0.7	±3.9	±3.2	±3.5
108	3.2	0.7	−1.7	±2.4	±2.0	±3.0
109	−1.4	−0.2	9.0	±4.6	±3.9	±6.3
110	2.9	0.9	−0.7	±2.3	±2.1	±2.9
111	−5.3	1.8	0.2	±2.7	±2.1	±3.6
112	−0.7	−3.8	−3.2	±4.5	±4.0	±7.4

Table 4.39: Scenario A: estimated deformations and standard deviations in epoch 2 in [mm]

deformations are entirely due to random errors in the coordinates from which they were derived. This is reflected by the fact that all deformations are within 2σ of their standard deviations, which vary roughly between ±2 mm and ±7 mm.

In epoch 3 deformations were introduced to points 102, 105 and 108. This becomes evident from the estimated deformations for these points given in Table 4.40. For the remaining

points the estimated deformations are at the millimetre-level with standard deviations comparable to those from the previous epoch. Notable is the larger x-deformation of point 111 of $-10.0\,\text{mm}$ which exceeds its standard deviation by four times and would thus be considered a significant movement. This is the same effect that could already be observed during the classical congruence analysis, where because of it point 111 was incorrectly identified as deformed.

Point	dx	dy	dz	$\hat{\sigma}_{dx}$	$\hat{\sigma}_{dy}$	$\hat{\sigma}_{dz}$
101	2.0	1.5	−7.2	±4.2	±3.8	±6.1
102	−17.3	19.1	−6.5	±2.3	±2.0	±2.7
103	1.2	−5.7	3.8	±3.9	±3.9	±5.4
104	2.4	3.0	−2.5	±4.2	±3.5	±5.3
105	21.8	−21.2	−9.0	±3.7	±3.2	±3.4
106	2.1	4.0	3.6	±3.7	±3.0	±3.2
107	2.6	−2.0	2.1	±3.6	±3.0	±3.3
108	13.3	−27.1	−15.7	±2.3	±2.0	±3.0
109	−7.4	−0.4	0.0	±4.3	±3.7	±6.0
110	2.5	1.6	1.3	±2.2	±2.0	±2.7
111	−10.0	2.0	1.4	±2.5	±2.0	±3.4
112	5.3	−1.9	−4.2	±4.2	±3.8	±6.9

Table 4.40: Scenario A: estimated deformations and standard deviations in epoch 3 in [mm]

The estimated deformations of epoch 4 together with their standard deviations are given in Table 4.41 below. In this epoch the number of deformed points has increased to six, namely points 101, 105, 106, 108, 109 and 112. Again this is reflected by their estimated deformations. The apparent movements of the six stable points are at the millimetre-level. Although the computational base has been reduced from twelve to six points, there is no significant increase in the standard deviations of the deformations visible compared to epoch 2.

The estimated deformations of epoch 5 together with their standard deviations are shown in Table 4.42. In the final epoch all points except for 101, 104 and 111 experience movements. Again, this is clearly visible from their estimated deformations. The three stable points show

Point	dx	dy	dz	$\hat{\sigma}_{dx}$	$\hat{\sigma}_{dy}$	$\hat{\sigma}_{dz}$
101	−1.8	−1.0	−3.4	±4.5	±3.9	±6.3
102	−30.0	32.8	−14.7	±2.5	±2.1	±2.9
103	3.0	5.1	1.8	±4.1	±4.0	±5.5
104	−0.6	−3.0	−2.6	±4.4	±3.7	±5.5
105	38.5	−28.0	−20.0	±3.8	±3.3	±3.6
106	21.8	−25.4	−1.8	±3.8	±3.1	±3.4
107	0.6	0.3	1.1	±3.8	±3.1	±3.4
108	37.8	−49.6	−28.5	±2.6	±2.2	±3.2
109	12.1	−21.1	−12.7	±4.6	±4.0	±6.4
110	1.7	0.8	0.5	±2.4	±2.3	±3.0
111	−4.4	1.2	−0.0	±2.9	±2.2	±3.6
112	−21.3	27.9	−23.2	±4.7	±4.1	±7.2

Table 4.41: Scenario A: estimated deformations and standard deviations in epoch 4 in [mm]

only apparent movements at the millimetre-level. The standard deviation of the deformations show an increase now for only a few points, most notably in the z-components of points 109 and 110, compared to those with the full computational base in epoch 2.

Point	dx	dy	dz	$\hat{\sigma}_{dx}$	$\hat{\sigma}_{dy}$	$\hat{\sigma}_{dz}$
101	0.5	4.1	−4.2	±4.6	±4.0	±7.1
102	43.7	32.7	−24.0	±2.8	±2.2	±3.1
103	25.3	14.0	−11.2	±4.5	±4.3	±6.2
104	2.5	0.6	−1.9	±5.2	±4.3	±6.1
105	47.8	−37.8	−28.1	±4.2	±3.6	±4.2
106	42.0	−29.1	−21.4	±4.2	±3.4	±4.6
107	−19.9	−22.8	−5.8	±4.3	±3.5	±4.6
108	54.3	−58.7	−36.4	±3.6	±3.0	±4.7
109	10.8	−38.0	−14.1	±5.5	±4.8	±9.8
110	−17.1	−17.4	−12.6	±3.2	±2.9	±6.1
111	−5.2	0.3	0.4	±3.1	±2.3	±3.8
112	−33.0	34.4	−47.0	±4.9	±4.3	±8.3

Table 4.42: Scenario A: estimated deformations and standard deviations in epoch 5 in [mm]

Table 4.43 below shows the errors $\vec{\epsilon}$ in the estimated deformations computed as the difference between the estimated and true deformations: $\vec{\epsilon} = \vec{d}_{est} - \vec{d}_{true}$. With the exception of the x-deformation of point 111 in epoch 3, all errors are within 2σ of their standard deviations. Consequently, it can be concluded that the true deformations of the deformed points were

accurately estimated throughout all epochs, even when 75 % of the monitoring points are subject to deformations.

	Epoch 2			Epoch 3			Epoch 4			Epoch 5		
Point	ϵ_x	ϵ_y	ϵ_z	ϵ_x	ϵ_y	ϵ_z	ϵ_x	ϵ_y	ϵ_z	ϵ_x	ϵ_y	ϵ_z
101	2.4	4.8	−6.6	2.0	1.5	−7.2	−1.8	−1.0	−3.4	0.5	4.1	−4.2
102	−0.6	−2.9	3.9	−1.3	−1.9	4.5	2.0	0.8	5.3	−3.3	−4.3	2.0
103	−2.5	1.3	−0.5	1.2	−5.7	3.8	3.0	5.1	1.8	2.3	−4.0	2.8
104	2.2	3.2	−2.4	2.4	3.0	−2.5	−0.6	−3.0	−2.6	2.5	0.6	−1.9
105	−2.8	−4.3	−4.0	2.8	−4.2	1.0	−0.5	−5.0	−0.0	0.8	1.2	−0.1
106	2.7	0.8	5.2	2.1	4.0	3.6	2.8	−2.4	6.2	0.0	3.9	5.6
107	−0.1	−2.3	0.7	2.6	−2.0	2.1	0.6	0.3	1.1	−2.9	0.2	5.2
108	3.2	0.7	−1.7	1.3	−3.1	−1.7	4.8	−2.6	−2.5	−0.7	−0.7	1.6
109	−1.4	−0.2	9.0	−7.4	−0.4	0.0	2.1	−4.1	−0.7	−8.2	2.0	4.9
110	2.9	0.9	−0.7	2.5	1.6	1.3	1.7	0.8	0.5	−4.1	2.6	−1.6
111	−5.3	1.8	0.2	−10.0	2.0	1.4	−4.4	1.2	−0.0	−5.2	0.3	0.4
112	−0.7	−3.8	−3.2	5.3	−1.9	−4.2	−1.3	3.9	−6.2	−1.0	−5.6	4.0

Table 4.43: Scenario A: differences between estimated and true deformations at given epoch in [mm]

4.1.5 Discussion

After checking that the epochs are indeed comparable, global congruencey tests are carried out for all epochs with respect to the base epoch. The test only passes for epoch 2, which is correct since epochs 3 to 5 contain deformations.

The localization of the largest congruent point group is first carried out using the traditional single-point analysis. While successful in epochs 2 and 4, in epoch 3 point 111 is incorrectly identified as unstable after all truly deformed points are eliminated and the global congruency test passes. According to Gründig et al. (1985), the local test may still fail then, because of small localized deformations. Apparently, this also can be triggered by larger random errors when no deformations are inherent. This is concerning because all deformed points were already eliminated, so that no smoothing effects from deformed points can be blamed. Furthermore, the stable computational base is still sufficiently large, so that inaccuracies

due to a poorly defined datum cannot be a cause either. In epoch 5 with only three stable points remaining, the single-point analysis eliminates all but two unstable points for which the global congruency test as well as the local tests are then accepted. Although the single-point analysis is expected to fail in this case, as it has a breakdown point of only about 3 % to 5 %, the outcome may be misleading as it indicates success.

The localization step is next performed with the MSS-method based on distance differences and leads to the correct solution in all cases. The same results are achieved for the MSS-method based on distance ratios and the MSS-method based on angles. Comparing the three MSS-approaches, it is found that the distance difference approach is by far the most efficient in the sense that it produces the fewest number of candidates. Then follows the angle-based approach. These two have the additional advantage that candidates can be evaluated with a global congruency test which can directly be derived from the already available differences in distances and angles, respectively. The distance ratios approach tends to find more candidates, especially when the congruent point groups get smaller with respect to to the total number of points in the network. In epoch 5 for example, a total of 137 candidates are found compared to 28 with the angle-based approach and only 7 for the distance-difference approach. Furthermore, a transformation adjustment has to be solved to evaluate each candidate. This makes it the least efficient of the three approaches. Something that can be observed in all three methods is that the evaluation of the candidates, either by transformation adjustment or congruency test, sometimes passes for more than one candidate. This is frequently the case in search for congruent triangles. The reason for it is that points with the same deformations also form congruent groups and are thus identified as candidates. In this scenario, however, all solutions could correctly be identified as those candidates with the smallest test statistic.

The deformations for each epoch are determined in two ways; by the re-adjustment of the combined observations from both epochs and by the transformation-based approach pre-

sented in Section 3.3. The re-adjustment requires the availability of the original observations of each epoch. For all stable points a new set of coordinates is estimated from the combined observations of both epochs. This has the effect that the deformations for the stable points are exactly zero. The random errors inherent in the observations do not affect the deformations but are completely absorbed by the observation residuals. In turn, the coordinates of the stable points now change with each new epoch that is observed, for comparison see the lists of adjusted coordinates after re-adjustment of observations in Appendix B.4.

For epochs 2 to 4 the true deformations have been accurately recovered. In epoch 5, as a result of the wrong localization with the single-point analysis, the estimated deformations deviate from their true values by up to 25 mm. To get an idea of the overall quality of the solution and to be able to compare results easier with the transformation-based approach, the overall RMS of the errors in the estimated deformations has been determined as the square root of the sum of the squared errors from Table 4.35 for each epoch. The results are listed in Table 4.44 below. Since no deformations have occurred in epoch 2 and all stable

	Epoch 2	Epoch 3	Epoch 4	Epoch 5
RMS in [mm]	0.0	16.2	12.8	143.8

Table 4.44: Overall RMS errors of estimated deformations for all epochs

points have deformations of exactly zero, the RMS error for epoch 2 is consequently zero as well. It is extremely large in epoch 5 which, of course, is due to the wrong localization of the stable points.

For the transformation-based approach deformations can be derived from the adjusted coordinates of each epoch together with their singular cofactor matrix through a transformation of each subsequent epoch into the datum of the base epoch. The original observations are not required. The transformation parameters are accurately recovered for all four transformations. Interesting is that the datum change can be observed in epochs 3 to 5 in the three translation as well as the z-rotation and it becomes clearly more pronounced as the computa-

tional base is reduced from twelve to nine to six to three points. In the transformation-based approach deformations are estimated for all points including the stable ones, for which they are insignificant. This happens because of the propagation of random errors in the coordinates. But the original coordinates of each epoch remain unchanged.

The RMS of the errors of the estimated deformations from Table 4.43 are summarized in Table 4.45 below. The RMS error is approximately the same for all epochs, varying only by

	Epoch 2	Epoch 3	Epoch 4	Epoch 5
RMS in [mm]	19.3	21.5	17.9	19.8

Table 4.45: Overall RMS errors of estimated deformations for all epochs

about 4 mm. Since apparent movements are derived for the stable points, the RMS error is not zero in epoch 2. For the same reason, it is larger for epochs 3 and 4 compared to those from Table 4.44. In epoch 5 it has a more realistic value than the one obtained from the re-adjustment of the observations in Table 4.44. This is, of course, because the deformations have now been estimated on the basis of the correct congruent points.

4.2 Scenario B

The second scenario was chosen to show the strength of the methodology proposed in Chapter 3. While the coordinate system for the base epoch remains the same as in the previous scenario, a different coordinate system was chosen for the subsequent epochs. A possible situation where this could occur would be a monitoring application where the base epoch is defined in a local coordinate system related to the monitored object and the subsequent epochs consist of GPS-coordinates given in WGS84. With this in mind, the coordinate system for epochs 2 to 5 was chosen to simulate a global 3D cartesian coordinate system.

The approximate coordinates that define the reference frame for epochs 2 to 5 are listed in Table 4.46 below. For the local system of epoch 1 the same approximate coordinates as for

the previous scenario are used, which are shown in Table 4.1.

Point	x	y	z
101	−1713147.04	−3774007.53	4834108.56
102	−1713101.53	−3774263.21	4834164.70
103	−1712926.08	−3774441.87	4834095.25
104	−1712886.68	−3774663.36	4834143.83
105	−1713100.94	−3774425.95	4834223.47
106	−1713145.72	−3774438.37	4834262.50
107	−1713096.52	−3774493.24	4834247.51
108	−1713013.03	−3774638.01	4834227.81
109	−1713119.91	−3774789.67	4834368.38
110	−1713194.76	−3774532.30	4834336.96
111	−1713253.14	−3774154.85	4834247.55
112	−1713441.61	−3774083.71	4834367.02

Table 4.46: Simulated coordinates of network points in global system in [m]

The transformation parameters relating the global system to the local system are given in Table 4.47. The coordinates for epochs 2 to 5 where derived by first adding the simu-

	x	y	z
Rotation	37.79509270 °	−15.54410971 °	−70.93797044 °
Translation	5 520 429.355717 m	−2 723 472.247585 m	−1 657 291.941328 m
Scale	−125 ppm		

Table 4.47: Transformation parameters relating local and global systems

lated deformations from Table 4.2 to the approximate coordinates in the local system and transforming these deformed coordinates to the global system. Then, to obtain randomized coordinates with a suitable associated cofactor matrix, observations consisting of angles with respect to to the z-axis, directions in the x, y-plane[1] and slope distances are back-calculated. Random errors of $\pm 5''$ for the angular observation types and $\pm\,(5\,\text{mm} + 5\,\text{ppm})$ for the slope distances are then added to the observations and a network adjustment is performed to obtain the adjusted coordinates for each epoch and their cofactor matrix. In the network analysis the datum needs to be defined. This is done using an inner-constraint approach again with

[1]These are equivalent to zenith angles and horizontal directions with the difference that the global system does not refer to the vertical or the horizontal plane.

all network points contributing. As a result the cofactor matrices are rank deficient by four again. This, of course, is not the case for real GPS coordinates where the datum is defined by the reference stations and thus this issue does not occur. However, for the purpose of the simulation, this is of no concern, so that the fully-populated and rank-deficient cofactor matrices are used for the analysis here.

Because of the two different coordinate systems used in this scenario, the classical congruence analysis cannot be applied to this data set without considerable pre-processing to convert the data back to the standard case where all epochs are given in the same reference frame, datum and scale. For this reason, the classical congruence analysis is not applied in this scenario. After the global congruency testing, the localization step is carried out using the MSS-method based on distance ratios and angles. The distance-difference based MSS-approach cannot be applied either because a change in scale exists between epochs. After the largest similar point group has been found, deformations are determined using the transformation-based approach from Section 3.3.

4.2.1 Results of network analysis

To obtain adjusted coordinates and their associated cofactor matrices, again a network analysis is performed for every epoch. As before, 132 observations are available in each epoch and the parameter vector consists of the 36 coordinates of the twelve monitoring points plus one orientation offset for each of the four instrument stations. With the four additional constraint equations that define the free datum parameters the network redundancy is again 96 for all epochs. The a priori standard deviation was chosen as ± 1.

The statistical test results for the network analyses consisting of the a posteriori standard deviations $\hat{\sigma}_{0_k}$ and the test statistics $T_{\chi^2_k}$ are summarized in Table 4.48. With the lower boundary value for the global test of the adjustment model given by $\chi^2_{S=0.025,\, f=r=96} = 70.78$

Epoch	$\hat{\sigma}_{0_k}$	$T_{\chi^2_k}$
1	±1.014220	98.75
2	±0.995742	95.18
3	±1.008363	97.61
4	±0.967021	89.77
5	±1.002043	96.39

Table 4.48: Scenario B: a posteriori standard deviations and test statistics for global test of adjustment model for all epochs

and its upper boundary given by $\chi^2_{S=0.975,\, f=r=96} = 125.00$, the test passes for all epochs. The adjusted coordinates and their standard deviations for all epochs can be found in Appendix B.5.

4.2.2 Global congruency testing

Before the global congruency tests can be carried out, it has to be confirmed that the epochs being compared refer to the same empirical standard deviation. This can be done by applying the F-test shown in (2.24). The test statistics T_F for the comparison of the reference epoch 1 with each of the subsequent epochs are given in Table 4.49. With a boundary value of

Epochs	T_F	$\hat{\sigma}_0$
1 and 2	1.04	±1.005023
1 and 3	1.01	±1.011296
1 and 4	1.10	±0.990902
1 and 5	1.02	±1.008150

Table 4.49: Scenario B: test statistics and combined standard deviations

$F_{S=0.975, f_1=96, f_2=96} = 1.50$ the test passes for all epochs. Now the combined variance factors can be derived according to (2.28). Their square root, the combined standard deviations $\hat{\sigma}_0$ are also listed in Table 4.49.

Now the global congruency tests can be performed. Because of the two different coordinate systems the data are given in, the test statistics have to be derived from datum-invariant (and scale-invariant) functions of the adjusted coordinates according to equations (2.32) to

(2.34). For this reason angular differences between epochs have been chosen to compute the quadratic forms $\hat{\Omega}^2$ for the test, which, together with the global test statistics T_G, are shown in Table 4.50. The reference value for the test follows from the FISHER-distribution

Epochs	$\hat{\Omega}^2$	T_G
2	0.933158	0.92
3	10.313794	10.08
4	35.276105	35.93
5	69.495773	68.38

Table 4.50: Scenario B: quadratic forms $\hat{\Omega}^2$ and test statistics T_G for all global congruency tests

with a chosen confidence level of $\alpha = 5\,\%$, $f_1 = h = 29$ and $f_2 = r_i + r_j = 192$ as $F_{S=0.95,\, f_1=29,\, f_2=192} = 1.53$ for all epochs. From Table 4.50 it becomes evident that the test passes only for epoch 2. This indicates the presence of deformations in epochs 3 to 5.

4.2.3 Localization

4.2.3.1 MSS using distance ratios

At first the localization of the largest similar point group is carried out using the MSS-method based on distance ratios. Again, the size of the search window for the distance ratios is chosen as $1.5\hat{\sigma}_s$, where $\hat{\sigma}_s$ refers to the error estimate for the scale factor, in order to reduce the number of candidate solutions to a manageable level.

Epoch 2

For epoch 2 only one candidates solution consisting of all twelve points is found. After performing a transformation adjustment followed by a global test of the adjustment model, the results listed in Table 4.51 are obtained. The test statistic for the global test of the adjustment model is given by (2.22c). The boundary value for the χ^2-test for a confidence

Candidate	$\hat{\sigma}_0$	Redundancy	T_χ	Test outcome
All twelve points	± 0.965865	29	27.05	pass

Table 4.51: Scenario B: largest similar point group and statistical test for epoch 2

level of $\alpha = 5\,\%$ follows from $\chi^2_{S=0.95,\, f=r=29} = 42.56$. Thus, the correct solution was found for epoch 2.

Epoch 3

For epoch 3 only one candidate is found as well, consisting of nine points. The results from the transformation adjustment are shown in Table 4.52. The boundary value for the global

Candidate	$\hat{\sigma}_0$	Redundancy	T_χ	Test outcome
101, 103, 104, 106, 107, 109, 110, 111, 112	± 1.218877	20	29.71	pass

Table 4.52: Scenario B: largest similar point group and statistical test for epoch 3

test of the adjustment model is given by $\chi^2_{S=0.95,\, f=r=20} = 31.41$, so that the test passes and the candidate is correctly accepted as the largest similar point group between epochs 1 and 3.

Epoch 4

In epoch 4 one candidate of eight points is found, for which the global test of the adjustment model with a boundary value of $\chi^2_{S=0.95,\, f=r=17} = 27.56$ fails.

Candidate	$\hat{\sigma}_0$	Redundancy	T_χ	Test outcome
101, 103, 104, 107, 109, 110, 111, 112	± 2.246980	17	85.83	fail

Table 4.53: Scenario B: candidate of eight points and statistical test for epoch 4

Continuing the search for a similar point group of less than eight points results in eight candidates of seven points. The results of the transformation adjustment for these candidates are listed in Table 4.54 below. With a reference value of $\chi^2_{S=0.95,\, f=r=14} = 23.68$ the global

Candidate	$\hat{\sigma}_0$	Redundancy	T_χ	Test outcome
101, 103, 104, 107, 109, 110, 111	±1.563117	14	34.21	fail
101, 103, 104, 107, 109, 110, 112	±2.218565	14	68.91	fail
101, 103, 104, 107, 109, 111, 112	±2.159360	14	65.28	fail
101, 103, 104, 107, 110, 111, 112	±2.195159	14	67.46	fail
101, 103, 104, 109, 110, 111, 112	±2.384479	14	79.60	fail
101, 103, 107, 109, 110, 111, 112	±2.436107	14	83.08	fail
101, 104, 107, 109, 110, 111, 112	±2.402702	14	80.82	fail
103, 104, 107, 109, 110, 111, 112	±2.411263	14	81.40	fail

Table 4.54: Scenario B: candidates of seven points and statistical test for epoch 4

test of the adjustment model fails for all eight candidates, so that the search is continued for a similar group of less than seven points.

This results in a total of 32 candidates consisting of six points. With a boundary value of $\chi^2_{S=0.95,\, f=r=11} = 19.68$, only one of the candidates, shown in Table 4.55, passes the global test of the adjustment model. The 31 rejected candidates and their test results can be found in Table B.19 in Appendix B.6. Again, the correct point group has been identified.

Candidate	$\hat{\sigma}_0$	Redundancy	T_χ	Test outcome
101, 103, 104, 107, 110, 111	±1.255927	11	17.35	pass

Table 4.55: Scenario B: largest similar point group and statistical test for epoch 4

Epoch 5

In epoch 5, 14 candidates consisting of five points are found first. Their test results are listed in Table 4.56 below. Given the boundary value of $\chi^2_{S=0.95,\, f=r=8} = 15.51$, all of the 14 candidates are rejected and the search is continued for a similar group of less than five points.

This leads to a list of 64 candidates of four points. After performing the transformation adjustment and global test of adjustment model, they are all rejected. Their test results can be found in Table B.20 in Appendix B.6.

Candidate	$\hat{\sigma}_0$	Redundancy	T_χ	Test outcome
101, 103, 104, 106, 109	±3.538055	8	100.14	fail
101, 103, 104, 109, 111	±3.567383	8	101.81	fail
101, 104, 106, 108, 111	±7.755838	8	481.22	fail
101, 104, 106, 109, 111	±3.161746	8	79.97	fail
101, 104, 107, 110, 111	±2.407723	8	46.38	fail
101, 104, 109, 110, 111	±2.575243	8	53.06	fail
101, 107, 109, 110, 111	±2.376879	8	45.20	fail
103, 104, 105, 109, 112	±5.964601	8	284.61	fail
103, 104, 106, 109, 112	±5.217789	8	217.80	fail
104, 105, 109, 111, 112	±5.802612	8	269.36	fail
104, 106, 108, 111, 112	±8.280435	8	548.52	fail
104, 106, 109, 111, 112	±5.115469	8	209.34	fail
104, 109, 110, 111, 112	±5.036194	8	202.91	fail
107, 109, 110, 111, 112	±4.754375	8	180.83	fail

Table 4.56: Scenario B: candidates of five points and statistical test for epoch 5

Finally, a total of 95 candidates of three points are found. With a boundary value of $\chi^2_{S=0.95,\, f=r=2} = 5.99$, multiple candidates pass the test this time. The final solution is the one with the smallest test quantity T_χ, which is given in Table 4.57 below. The remaining 94 candidates are listed in Table B.21 in Appendix B.6. After a total of 173 candidates have

Candidate	$\hat{\sigma}_0$	Redundancy	T_χ	Test outcome
101, 104, 111	±0.649365	2	0.84	pass

Table 4.57: Scenario B: largest similar point group and statistical test for epoch 5

been examined with a transformation adjustment, the correct solution for the largest similar point group between epochs 1 and 5 has finally been found.

4.2.3.2 MSS using angles

Now the search for the largest similar point group is repeated using the MSS-method based on angular differences. As a threshold for the elimination of significantly changed angles, the 3σ-criterion is used here again. The global congruency test required to verify the candidate solutions is again derived directly from angular differences.

Epoch 2

One candidate solution is found for the comparison of epoch 2 and epoch 1. The candidate consists of all twelve network points. With a boundary value of $F_{S=0.95,\, f_1=h=29,\, f_2=r_1+r_2=192} = 1.53$ the global congruency test passes, which confirms that the largest congruent point group indeed consists of all network points. The test results are summarized in Table 4.58.

Candidate	T_G	Test outcome
101, 102, 103, 104, 105, 106, 107, 108, 109, 110, 111, 112	0.92	pass

Table 4.58: Scenario B: largest similar point group and test statistic for epoch 2

Epoch 3

Only one candidate is found for the comparison of epochs 1 and 3, consisting of nine points. Given the boundary value of boundary value of $F_{S=0.95,\, f_1=h=20,\, f_2=r_1+r_2=192} = 1.62$ for the global congruency test, the candidate is accepted as the largest similar point group between epochs 1 and 3. Details are given in Table 4.59 below.

Candidate	T_G	Test outcome
101, 103, 104, 106, 107, 109, 110, 111, 112	1.48	pass

Table 4.59: Scenario B: largest similar point group and test statistic for epoch 3

Epoch 4

For the epoch 1 – epoch 4 comparison the search for the largest similar point group delivers three candidates consisting of six points. The candidates together with their results of the global congruency test are shown in Table 4.60. Given the boundary value of $F_{S=0.95,\, f_1=h=11,\, f_2=r_1+r_2=192} = 1.84$, only one candidate passes the test and thus is correctly accepted as the largest similar point group between epochs 1 and 4.

Candidate	T_G	Test outcome
101, 103, 104, 107, 109, 111	2.12	fail
101, 103, 104, 107, 110, 111	1.56	pass
101, 103, 104, 109, 110, 111	2.40	fail

Table 4.60: Scenario B: candidates and test statistic for epoch 4

Epoch 5

For epoch 5 a total of 27 candidates consisting of three points are found. Multiple of these candidates pass the global congruency test with a reference value of $F_{S=0.95,\, f_1=h=2,\, f_2=r_1+r_2=192} = 3.04$. The final solution is again the one with the smallest test quantity T_G, which is given in Table 4.61. The remaining candidates can be found in Table B.22 in Appendix B.7.

Candidate	T_G	Test outcome
101, 104, 111	0.34	pass

Table 4.61: Scenario B: largest similar point group and test statistic for epoch 5

After the largest similar point groups have all been correctly identified, the deformations for Scenario B can now be determined.

4.2.4 Determination using transformation-based approach

In order to determine the deformations a transformation as described in Section 3.3 has been performed. As input serve the adjusted coordinates in each epoch listed in Appendix B.5 and their fully-populated, singular cofactor matrices. To avoid numerical stability issues caused by the large coordinate values in the global system, the coordinates in each epoch are reduced to their respective centroids before the transformation is performed. This has no effect on the outcome of the adjustment other than that the translations are reduced to zero. The full translations can be recovered from the rotated centroids after the adjustment, if desired. For the determination of deformations this is of no concern however, as they can be derived in the reduced systems as well.

Again, the a priori standard deviation for the adjustment has been chosen as $\sigma_0 = \pm 1$. The statistical results for the transformation adjustment are summarized in Table 4.62 below.

The estimated transformation parameters and their standard deviations for epochs 2 and 3 are listed in Table 4.63. For epoch 2 the deviations of the rotation parameters from their true values given in Table 4.47 are small and with $-2.4''$, $1.7''$ and $0.9''$ for ω, φ and κ, respectively, at the same level as their corresponding standard deviations. The translations and their standard deviations are at the level of 10^{-10} m and can thus be considered negligible. And the scale factor only deviates from its true value by about 4 ppm. The parameters for epoch 2 are accurately recovered.

	Ep 1	Ep 2	Ep 3	Ep 4	Ep 5	Total
Number of points	12	12	9	6	3	42
Number of observations	36	36	27	18	9	126
Number of conditions	–	37	28	19	10	94
Number of unknowns	–	8	8	8	8	32
Redundancy	–	29	20	11	2	62
A posteriori standard deviation $\hat{\sigma}_0$						± 1.088281
Global test statistic T_χ						73.43
Lower boundary value $\chi^2_{S=0.025,\,r}$						42.13
Upper boundary value $\chi^2_{S=0.975,\,r}$						85.65
Test outcome						pass

Table 4.62: Scenario B: summary of statistics for transformation adjustment of all epochs

In epoch 3 the deviations of the three rotations ω, φ and κ are $-0.1''$, $3.9''$ and $2.8''$. The translations are now at the millimetre-level with sub-millimetre standard deviations which may be due to the change in datum between the two epochs. The scale factor is again very accurately determined.

The estimated transformation parameters for epochs 4 and 5 are given in Table 4.64 below. In epoch 4 the deviations of the rotation angles ω, φ and κ are $2.8''$, $0.9''$ and $-0.1''$. The translations further increase in magnitude while the scale factor deviates less than 2 ppm

	Epoch 2		Epoch 3	
Parameter	Value	$\hat{\sigma}$	Value	$\hat{\sigma}$
q_0	0.7888697420	$\pm 1.8639 \cdot 10^{-6}$	0.7888705638	$\pm 2.0287 \cdot 10^{-6}$
q_x	0.1871099138	$\pm 4.6924 \cdot 10^{-6}$	0.1871184940	$\pm 5.0844 \cdot 10^{-6}$
q_y	−0.2904014544	$\pm 5.0627 \cdot 10^{-6}$	−0.2903994661	$\pm 5.6095 \cdot 10^{-6}$
q_z	−0.5082729636	$\pm 1.5075 \cdot 10^{-6}$	−0.5082696655	$\pm 1.6559 \cdot 10^{-6}$
ω	37.79443796 °	±1.9″	37.79505347 °	±2.1″
φ	−15.54362579 °	±1.9″	−15.54302232 °	±2.1″
κ	−70.93771165 °	±1.0″	−70.93720242 °	±1.1″
T_x	$5.72 \cdot 10^{-10}$ m	$\pm 0.22 \cdot 10^{-10}$ m	0.001670 m	±0.000662 m
T_y	$5.96 \cdot 10^{-10}$ m	$\pm 0.26 \cdot 10^{-10}$ m	−0.001833 m	±0.000562 m
T_z	$-5.31 \cdot 10^{-10}$ m	$\pm 0.32 \cdot 10^{-10}$ m	−0.002339 m	±0.000668 m
λ	−128.7 ppm	±5.3 ppm	−125.8 ppm	±5.8 ppm

Table 4.63: Scenario B: estimated transformation parameters and standard deviations of epochs 2 and 3 with respect to epoch 1

from its true value. A slight increase in the standard deviations of all parameters compared to the previous epoch can be noted. In epoch 5 the deviation for the three rotation angles

	Epoch 4		Epoch 5	
Parameter	Value	$\hat{\sigma}$	Value	$\hat{\sigma}$
q_0	0.7888663486	$\pm 2.4051 \cdot 10^{-6}$	0.7888612385	$\pm 4.6764 \cdot 10^{-6}$
q_x	0.1871179021	$\pm 5.4238 \cdot 10^{-6}$	0.1871220946	$\pm 7.5119 \cdot 10^{-6}$
q_y	−0.2904097304	$\pm 5.9277 \cdot 10^{-6}$	−0.2904233202	$\pm 13.2681 \cdot 10^{-6}$
q_z	−0.5082705610	$\pm 2.3883 \cdot 10^{-6}$	−0.5082691839	$\pm 4.2331 \cdot 10^{-6}$
ω	37.79586864 °	±2.2″	37.79739097 °	±3.9″
φ	−15.54385565 °	±2.2″	−15.54473144 °	±4.8″
κ	−70.93798710 °	±1.4″	−70.93872009 °	±2.5″
T_x	0.002692 m	±0.001246 m	0.006900 m	±0.002782 m
T_y	−0.005737 m	±0.001067 m	−0.011562 m	±0.002513 m
T_z	−0.008671 m	±0.001228 m	−0.019949 m	±0.003604 m
λ	−126.6 ppm	±6.6 ppm	−133.3 ppm	±8.8 ppm

Table 4.64: Scenario B: estimated transformation parameters and standard deviations of epochs 4 and 5 with respect to epoch 1

ω, φ and κ are now 8.3″, −2.2″ and −2.7″. The deviation in ω seems unusually high compared to the previous epochs. The translations are now at the centimetre-level and the deviation of the scale factor has increased to about 8 ppm. A further increase of all standard deviations can be observed in epoch 5 as well. The increase of both, the magnitudes of the

transformation parameters and their standard deviations, can be attributed to the change of the computational base to three points only.

While the effect of the datum change is obvious in the translation parameters when comparing results from epochs 2 to 5, it cannot be observed as clearly in the angles due to the overlapping rotations. The scale factor does not show any significant change over the epochs and seems unaffected by the datum change.

In Table 4.65 below the estimated deformations for epoch are listed together with their standard deviations. Since no deformations were introduced in epoch 2, the estimated deformations are apparent movements due to random errors in the coordinates from which they are derived. Although they are notably higher than in Scenario A, reaching as much as 11 mm in magnitude, they are all within 2σ of their estimated standard deviations.

Point	dx	dy	dz	$\hat{\sigma}_{dx}$	$\hat{\sigma}_{dy}$	$\hat{\sigma}_{dz}$
101	−2.9	−1.9	3.5	±6.1	±5.6	±7.4
102	−3.4	3.4	0.2	±2.9	±3.0	±3.3
103	10.7	−1.0	0.8	±5.7	±5.1	±6.7
104	−9.5	−4.2	3.0	±6.2	±5.1	±6.4
105	−1.0	6.8	−2.2	±4.7	±4.3	±4.3
106	−1.0	2.2	0.2	±4.9	±4.1	±4.1
107	−0.1	−4.0	−0.0	±4.6	±3.6	±4.1
108	3.4	−2.7	1.0	±3.2	±2.9	±3.5
109	4.4	3.4	−10.1	±6.2	±5.5	±7.4
110	−4.4	2.3	2.0	±3.1	±2.8	±3.4
111	−3.8	−2.7	0.3	±3.6	±3.2	±4.1
112	7.6	−1.5	1.2	±6.5	±5.9	±8.4

Table 4.65: Scenario B: estimated deformations and standard deviations in epoch 2 in [mm]

In epoch 3 deformations were introduced in points 102, 105 and 108 only which can be found in Table 4.66 below. The apparent movements for the remaining points are within 2σ of their estimated standard deviation.

The estimated deformations of epoch 4 are listed in Table 4.67 together with their standard deviations. Half of the points are subject to deformations now. Again, the estimated defor-

Point	dx	dy	dz	$\hat{\sigma}_{dx}$	$\hat{\sigma}_{dy}$	$\hat{\sigma}_{dz}$
101	0.3	−1.0	8.0	±6.2	±5.7	±7.7
102	−14.0	25.4	−11.0	±3.1	±3.1	±3.5
103	−3.8	4.4	−2.4	±5.9	±5.2	±6.9
104	−2.2	−6.1	0.4	±6.3	±5.2	±6.7
105	19.9	−16.5	−6.2	±4.8	±4.4	±4.4
106	−1.5	−2.3	−2.4	±5.0	±4.2	±4.2
107	7.6	−7.1	1.0	±4.7	±3.7	±4.2
108	14.5	−28.2	−12.9	±3.4	±3.1	±3.8
109	−5.6	8.6	−4.3	±6.3	±5.7	±7.6
110	1.2	2.2	3.1	±3.2	±2.9	±3.5
111	0.7	−3.4	−4.1	±3.7	±3.3	±4.2
112	2.9	5.7	2.6	±6.6	±6.1	±8.6

Table 4.66: Scenario B: estimated deformations and standard deviations in epoch 3 in [mm]

mations for the stable points are within 2σ of their standard deviations. So far, no significant increase in the standard deviations of the deformations compared to the previous epochs can be found.

Point	dx	dy	dz	$\hat{\sigma}_{dx}$	$\hat{\sigma}_{dy}$	$\hat{\sigma}_{dz}$
101	2.9	0.8	4.8	±6.3	±5.8	±7.7
102	−32.6	34.1	−19.7	±3.2	±3.1	±3.5
103	−2.0	5.1	5.2	±5.8	±5.2	±6.8
104	−4.5	−7.5	−4.0	±6.4	±5.3	±6.7
105	41.1	−21.8	−15.7	±4.8	±4.4	±4.4
106	18.0	−26.0	−9.0	±5.0	±4.2	±4.2
107	8.6	−6.3	−2.0	±4.7	±3.8	±4.3
108	36.7	−53.3	−26.5	±3.6	±3.3	±4.0
109	2.2	−16.8	−20.3	±6.4	±5.9	±7.8
110	−0.6	2.3	2.4	±3.4	±3.1	±3.8
111	−2.9	−3.3	−1.9	±3.9	±3.4	±4.4
112	−33.7	25.5	−17.4	±6.9	±6.1	±8.7

Table 4.67: Scenario B: estimated deformations and standard deviations in epoch 4 in [mm]

The estimated deformations of the final epoch are given in Table 4.68 below together with their standard deviations. Now nine out of twelve points experience deformations leaving only three points to form the stable computational base for this epoch. This results in a notable increase in the standard deviations of the estimated deformations for most points,

Point	dx	dy	dz	$\hat{\sigma}_{dx}$	$\hat{\sigma}_{dy}$	$\hat{\sigma}_{dz}$
101	−1.1	2.1	5.8	±6.6	±6.1	±9.0
102	46.3	42.1	−18.6	±3.8	±3.5	±4.1
103	21.6	24.2	−12.8	±6.9	±5.8	±8.0
104	−1.8	−4.3	0.1	±8.0	±6.5	±8.0
105	54.7	−41.5	−16.8	±5.5	±5.0	±5.6
106	35.7	−33.1	−24.2	±5.7	±5.0	±6.2
107	−6.2	−32.3	−21.5	±5.6	±4.7	±6.2
108	60.1	−67.6	−42.6	±5.3	±4.9	±6.6
109	19.2	−46.6	−28.3	±7.8	±7.8	±13.2
110	−10.8	−19.3	−17.5	±4.5	±4.6	±8.4
111	−1.2	−3.3	−1.0	±4.3	±3.7	±4.9
112	−40.6	40.9	−62.3	±7.5	±6.6	±10.6

Table 4.68: Scenario B: estimated deformations and standard deviations in epoch 5 in [mm]

especially in z-direction. For the three stable points 101, 104 and 111, the estimated apparent movements are well within 2σ of their standard deviations.

The errors $\vec{\epsilon}$ of the estimated deformations, computed by removing the true deformations according to $\vec{\epsilon} = \vec{d}_{est} - \vec{d}_{true}$, are shown in Table 4.69. An increase of the errors in the fifth epoch is notable. Again, this can be explained with the reduced computational base in this epoch, consisting of three points only. But with their standard deviations also increasing the errors are still within 2σ of their estimated standard deviations for all epochs.

Conclusively, it can be found that the deformations for all epochs are accurately recovered within their given accuracies, even when 75 % of the monitoring points are subject to deformations.

4.2.5 Discussion

After the comparison of the variances of the adjusted coordinates of each epoch, a series of global congruency tests is performed to identify those epochs where deformations have occurred. The test statistics cannot be derived from coordinates as the epochs refer to different coordinate systems. Thus, datum-invariant functions of the coordinates are used

	Epoch 2			Epoch 3			Epoch 4			Epoch 5		
Point	ϵ_x	ϵ_y	ϵ_z	ϵ_x	ϵ_y	ϵ_z	ϵ_x	ϵ_y	ϵ_z	ϵ_x	ϵ_y	ϵ_z
101	−2.9	−1.9	3.5	0.3	−1.0	8.0	2.9	0.8	4.8	−1.1	2.1	5.8
102	−3.4	3.4	0.2	2.0	4.4	0.0	−0.6	2.1	0.3	−0.7	5.1	7.4
103	10.7	−1.0	0.8	−3.8	4.4	−2.4	−2.0	5.1	5.2	−1.4	6.2	1.2
104	−9.5	−4.2	3.0	−2.2	−6.1	0.4	−4.5	−7.5	−4.0	−1.8	−4.3	0.1
105	−1.0	6.8	−2.2	0.9	0.5	3.8	2.1	1.2	4.3	7.7	−2.5	11.2
106	−1.0	2.2	0.2	−1.5	−2.3	−2.4	−1.0	−3.0	−1.0	−6.3	−0.1	2.8
107	−0.1	−4.0	−0.0	7.6	−7.1	1.0	8.6	−6.3	−2.0	10.8	−9.3	−10.5
108	3.4	−2.7	1.0	2.5	−4.2	1.1	3.7	−6.3	−0.5	5.1	−9.6	−4.6
109	4.4	3.4	−10.1	−5.6	8.6	−4.3	−7.8	0.2	−8.3	0.2	−6.6	−9.3
110	−4.4	2.3	2.0	1.2	2.2	3.1	−0.6	2.3	2.4	2.2	0.7	−6.5
111	−3.8	−2.7	0.3	0.7	−3.4	−4.1	−2.9	−3.3	−1.9	−1.2	−3.3	−1.0
112	7.6	−1.5	1.2	2.9	5.7	2.6	−13.7	1.5	−0.4	−8.6	0.9	−11.3

Table 4.69: Scenario B: differences between estimated and true deformations at given epoch in [mm]

instead. As there is also a change in scale present between epochs, distances cannot be used either. For this reason, angles are computed in each epoch and angular differences between epochs are used to derive the test statistics. From the outcome of the global congruency tests it becomes evident that deformations are inherent in epochs 3 to 5.

The localization of the largest similar point group is then carried out, first by the MSS-method based on distance ratios followed by the angle-based approach. With the distance ratios approach only one candidate is found for the largest similar point groups of epochs 2 and 3, so that the correct solution could be immediately determined through a single transformation adjustment for each of the two epochs. In epoch 4, 40 candidates are identified for each of which a transformation adjustment has to be run. Only the correct solution passed this evaluation. In epoch 5, a total of 173 candidates are found. 173 transformation adjustments later, the correct solution is identified as the candidate with the smallest test statistic for the global test of the adjustment model.

The angle-based MSS-approach also identifies the largest similar point groups for epochs 2 and 3 with only one candidate. In epoch 4, three candidates are found but the two wrong candidates are rejected by the global congruency test. In epoch 5 a total of 27 candidates

are found. The correct solution is identified as the candidate with the smallest test statistic for the global congruency test.

The deformations are then determined using the transformation-based approach introduced in Section 3.3. Again, the transformation parameters are accurately determined. The effects of the datum change can be observed in the three translations, but are not obvious in the angles, due to the large rotations between the coordinate systems. The errors for the estimated deformations are all within 2σ of their standard deviations, so that they can be considered as accurately determined. An increase of the standard deviations of the deformations in the last epoch is evident. This is a result of the computational base being reduced to only three points. The RMS of the errors of the estimated deformations in Table 4.69 are summarized in Table 4.70 below. For epochs 2 to 4 the RMS errors are at

	Epoch 2	Epoch 3	Epoch 4	Epoch 5
RMS in [mm]	24.9	23.4	27.3	35.6

Table 4.70: Overall RMS errors of estimated deformations for all epochs

approximately the same level at about 25 mm. A clear increase is visible in epoch 5 to about 35 mm. This may, at least partially, be due to the reduced computational base and the resulting loss of accuracy in epoch 5.

This scenario shows that the proposed methodology can successfully be applied to epochs given in different coordinate systems. Angular differences are perfectly suited to derive the test statistics for the global congruency test, as they are not only coordinate- but also scale-invariant. For the same reason they can be used for the localization of the largest similar point group. And, although both, the distance-ratios approach and the angle-based approach, are very reliable in identifying the largest similar point group, the angle-based approach is much more efficient. This is because fewer candidates are found in general and the evaluation of the candidates can be performed by a global congruency test, so that no additional adjustment is required. The transformation-based approach combines the

transformation between coordinate systems with the necessary datum transformation.

4.3 Summary

The simulations have shown that all three MSS-approaches discussed here are equally reliable in the localization of the largest congruent point group and clearly out-perform the traditional single-point analysis. While the approach based on distance differences is the most efficient one in terms of the number of candidate solutions found, it cannot be applied if the coordinates of the two epochs refer to different scales. The angle-based MSS-approach is more efficient than the approach based on distance ratios as it produces fewer candidates and does not require an adjustment to evaluate the candidates. Thus, it is the preferred approach when scale changes are suspected.

The transformation-based approach for the determination of deformations introduced in Section 3.2 has the advantage that the adjusted coordinates and their singular cofactor matrices can directly be utilized, so that the original observations of each epoch are not required. Furthermore, it can be applied in scenarios where different coordinate systems are in use. Thanks to the use of a quaternion rotation, no approximate values for the rotation parameters need to be calculated and the rotation can be arbitrarily large, as no small-angle approximations are applied.

The re-adjustment of the combined observations of the epochs requires, obviously, the availability of the original observations of each epoch. This approach however, can be generalized to the approach with implicit formulation of transformation proposed in Neitzel (2004) and explained in detail in Section 2.4.2.2. Rather than using the original observations, a minimal configuration of observable quantities, e. g. distances, is calculated from the adjusted coordinates together with their corresponding cofactor matrix, which will be regular. With the introduction of a scale factor, the re-adjustment based on the fictitious observations can

then be performed in any arbitrary system without the need to compute the transformation parameters explicitly (other than the scale factor) or initial approximates thereof.

The difference between the two methods is that with the implicit formulation a pre-processing of the coordinates and their singular cofactor matrices is required, whereas with the explicit formulation a post-adjustment transformtion of all coordinates into a common coordinate / datum system is required to derive the deformations. Furthermore, the implicit transformation provides deformations only for the unstable points while for all stable points the resulting deformations are exactly zero, as all random errors are completely absorbed by the observation residuals. As a consequence, the stable points obtain a new set of coordinates in each epoch which can lead to inconsistency issues.

With the explicit transformation deformations, or apparent movements respectively, are obtained for all points. This results in a higher RMS error of the estimated deformations. However, the original coordinates remain unchanged, so that the coordinates and their deformations are always consistent.

Chapter 5

CASE STUDY: The Frank Slide / Turtle Mountain, Alberta

Turtle Mountain is located in the Crownsnest Pass in southwestern Alberta. On April 29^{th} 1903, $30 \cdot 10^6\,\text{m}^3$ of limestone broke away from the east face of Turtle Mountain. The rock slide killed over 70 people, buried half of the town of Frank and the Canadian Pacific Railway line and dammed the Crowsnest River. This rock slide, the worst landslide disaster in Canadian history, is known as the Frank Slide. (Froese et al., 2009). Figure 5.1 pictures Turtle Mountain and the Frank Slide.

Figure 5.1: Frank Slide / Turtle Mountain, Alberta

Since the occurrence of the Frank Slide, Turtle Mountain has been subject to extensive monitoring and research by geologists, geophysicists and surveyors, (Froese et al., 2009; Fraser and Gründig, 1985). South Peak and the so-called Saddle, just below South Peak to the north (see Figure 5.2), are of particular interest. Large crevasses and fractures on Turtle Mountain, especially in the Saddle where the Frank slide broke free, suggest that a second slide might occur.

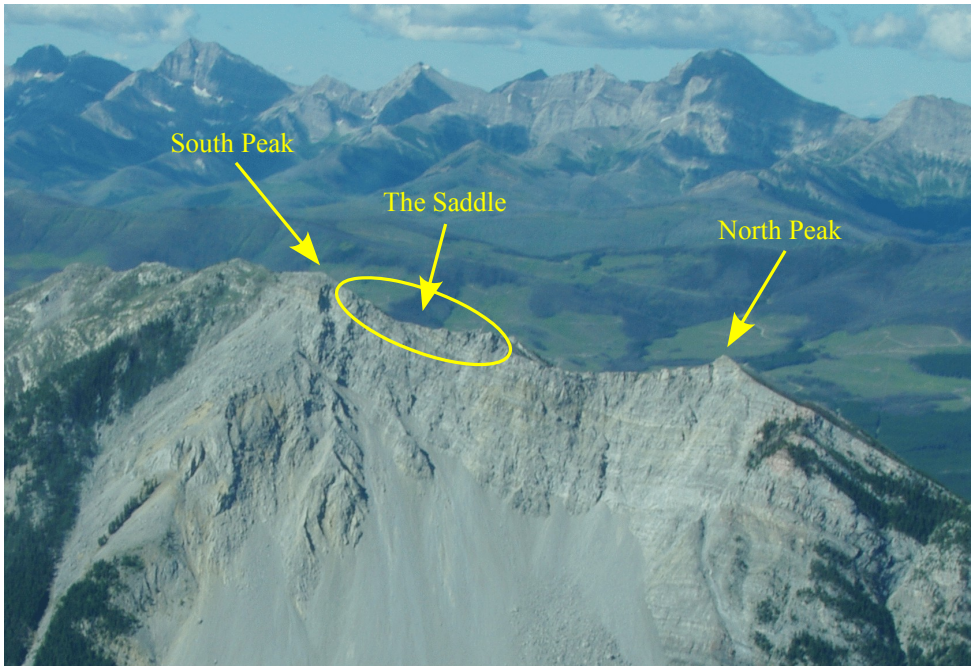

Figure 5.2: The Saddle area of Turtle Mountain where the Frank Slide broke free with North and South Peak

The towns of Frank and Hillcrest, with a combined population of about 500 people, border Turtle Mountain to the north and east, respectively. An industrial park, a public baseball field as well as several private properties are located in the vicinity of the mountain. Hence, there is a substantial concern for public safety. An array of mainly non-geodetic monitoring sensors, located around South Peak and the Saddle area, forms an early warning system which sends the collected data to the nearby Frank Slide Interpretive Centre via a radio link.

In May 2007 the **P**recise **E**ngineering and **D**eformation **S**urveys (PEDS) group in the Department of Geomatics Engineering at the University of Calgary started a new research project in collaboration with **A**lberta **G**eological **S**urvey (AGS). The goal of this research project was to determine long-term movements of Turtle Mountain in order to contribute to a better understanding of the behaviour of this natural structure and of what might have caused the Frank Slide.

As part of this research project a high-precision terrestrial network (HPTN) was established in the Saddle area just below South Peak. This network consists of seven intervisible monitoring points which are located at critical spots along the major fracture in the Saddle. The locations for these points were carefully chosen together with the responsible geologist and are shown in Figure 5.3. The resulting shape of the network is very elongated and thus the network geometry is very poor. (Ebeling et al., 2011).

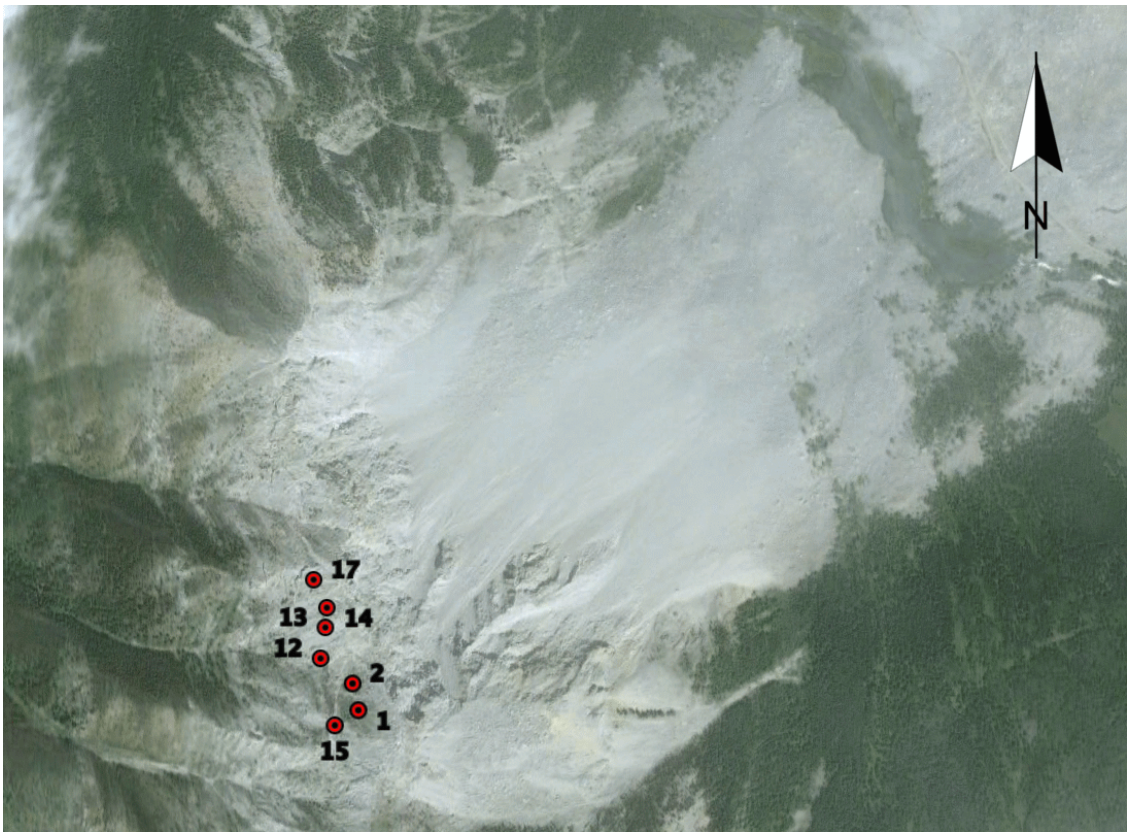

Figure 5.3: Top view of the Frank slide with locations of HPTN points, *(Google Earth, 2012)*

The monitoring points are built from a 1 ft length of structural steel and are securely bolted to a slab of intact rock. The structural steel pillars are topped with a galvanized steel cap that holds a $^5/_8$ in threaded bolt which can accommodate a tribrach. This allows for installation of a survey target as well as a total station or other survey equipment as required. A typical target setup is shown in Figure 5.4.

Figure 5.4: Prism on monitoring pillar (left) and LEICA TCA 2003 pointing at South Peak (right)

The collected observations consist of horizontal directions, zenith angles and slope distances between the monitoring points, as well as height of instrument (HI) and height of target (HT) information. All measurements were reduced to the centre of the $^5/_8$ in bolt at the top of the nut which holds the bolt in place as illustrated in Figure 5.5. This is the reference point for all derived coordinates and deformations.

Observations were collected using a LEICA TCA 2003 high-precision total station with an angular accuracy of $\pm 0.5''$ for horizontal and vertical circle readings and $\pm\,(1\,\text{mm} + 1\,\text{ppm})$ for slope distances, according to the manufacturer. For distance measurements a standard LEICA round prism was used. The instrument and reflector can be seen in Figure 5.4. The additive constant of the instrument / reflector combination was determined to be insignificant

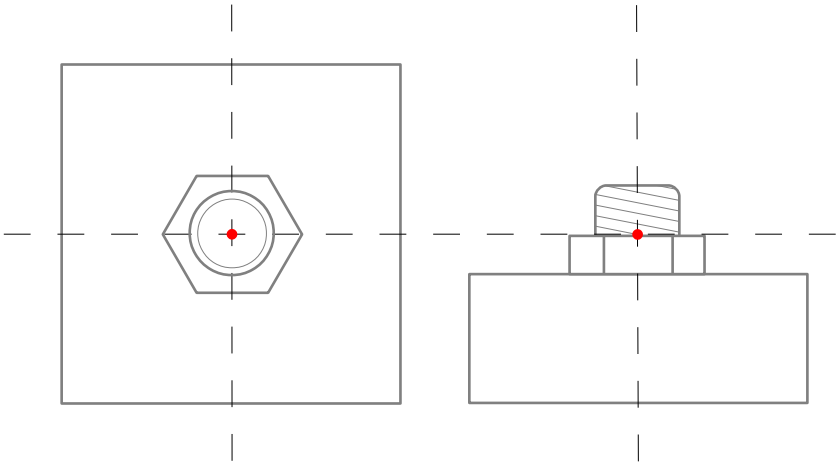

Figure 5.5: Top view (left) and side view (right) of a pillar cap showing the reference point (red dot) for all measurements

by means of calibration. Temperature, atmospheric pressure and humidity were observed at each instrument station to account for atmospheric refraction of the measured slope distances. Instrument and target heights were determined as averages of three independent tape measurements. At each instrument two to three sets of observations were collected to all visible points in the network.

The network was observed in four epochs – in Summer 2008, Fall 2009, Fall 2010 and Fall 2011. Initially, the network was observed from four of the seven points, namely 1, 14, 15 and 17. In Fall 2009 point 13 was added as an instrument station. Further shots were added as well by using an extension for the prism to observe otherwise invisible points. Figures 5.6 and 5.7 show the HPT-network with observation lines and arrows indicating instrument stations and target points in Summer 2008 and Fall 2009, respectively.

A network analysis was performed, as explained in detail in Section 2.2, to obtain adjusted coordinates and their cofactor matrices for each epoch. Before the network adjustment the observed zenith angles and slope distances were converted to horizontal distances and height differences and reduced to the reference point shown in Figure 5.5 using the HI and HT measurements. The standard deviations of the averages derived from the repeated measure-

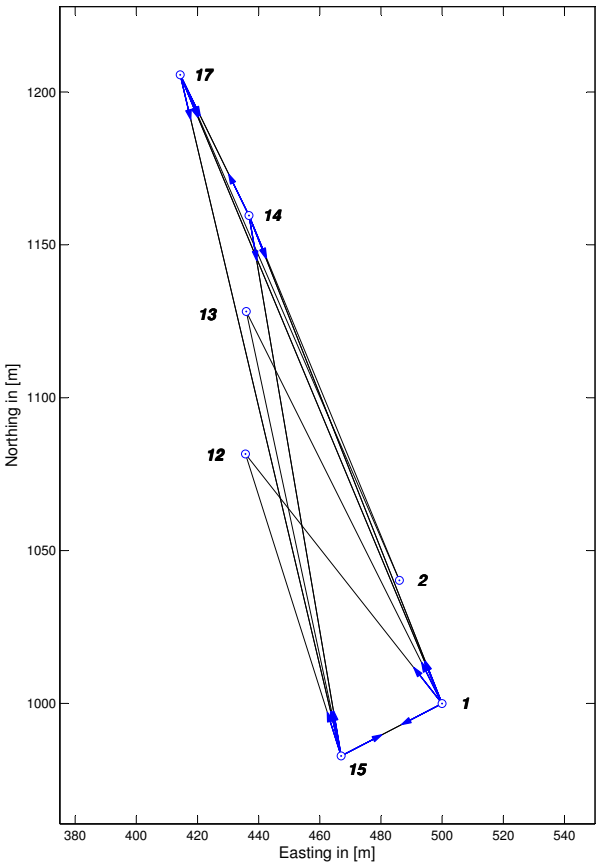

Figure 5.6: Network in Summer 2008 with observations indicated by arrows

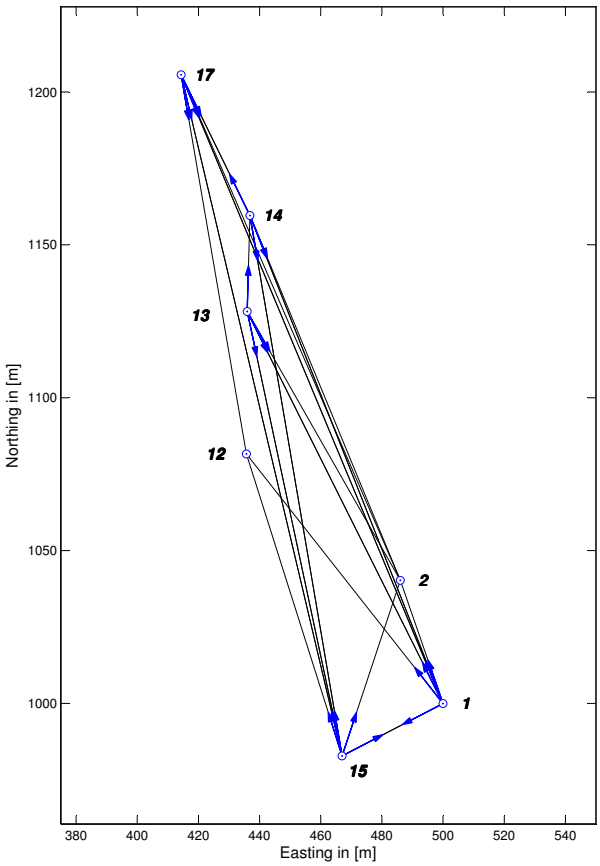

Figure 5.7: Network in Fall 2009 with observations indicated by arrows

ments were smaller than the instrument accuracies specified by the manufacturer mentioned above, so that the instrument accuracies were used as input standard deviations for the observations. The standard deviations of the HI / HT measurements were assumed as ± 1 mm. Error propagation was performed to obtain standard deviations and their correlations for the horizontal distances and height differences used in the network adjustment. The a priori standard deviation was chosen as $\sigma_0 = \pm 0.001$ for all epochs.

The trigonometric height differences were adjusted for the effect of earth curvature by adding the well-known correction, (see e. g. Wolf and Ghilani (2006)):

$$\Delta R = \frac{s_H^2}{2R},$$

where ΔR denotes the earth curvature correction, s_H the horizontal distance between points

and R the Earth's radius. Related to this effect is the convergence of the plumb lines illustrated in Figure 5.8 between the southernmost point 15 and the northernmost point 17 in the HPT network. In the figure, $\vec{g}$ denote the gravity vectors in point 15 and 17, respectively,

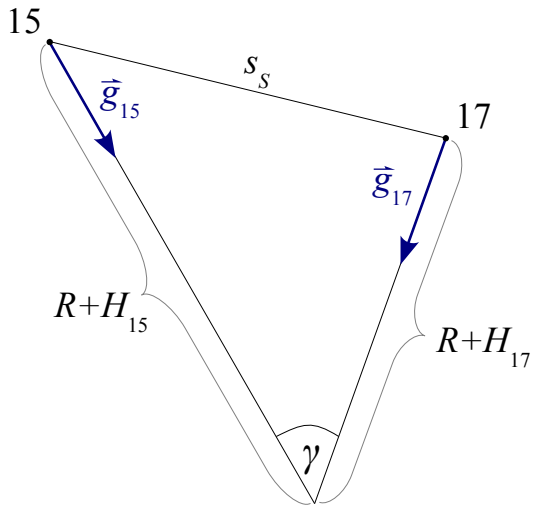

Figure 5.8: HPTN points 15 and 17 with their corresponding gravity vectors

and γ is their intersection angle at the Earth's centre of mass. With point elevations above the geoid of $H_{15} = 2200\,\text{m}$ and $H_{17} = 2150\,\text{m}$, the Earth's radius of $R = 6,378,000\,\text{m}$ and a slope distance of $s_s = 233\,\text{m}$ between points 15 and 17, the intersection angle follows from the cosine law as $\gamma = 7.3''$. This significant error affects not only the height differences but also the observations in the horizontal plane (directions and distances). However, since this is a systematic error, constant for all epochs, it will affect the coordinates in each epoch but not the resulting deformations. For this reason the effect is neglected and a planar model is assumed for all further computations.

The coordinate system was established as a local level frame by assigning coordinates of $(E\ N\ H)_1^T = (500.0000\ 1000.0000\ 100.0000)_1^T$ m to point 1 and using the azimuth from point 1 to point 17 , available from GPS observations, to align it with geodetic North. A subset of observations from the first epoch, uniquely describing the network geometry, was then used to calculate initial approximate values for the remaining points in the network. The

so-obtained initial coordinates for all epochs are listed in Table 5.1 An inner-constraints approach utilizing all seven network points was applied to define the four free parameters of the geodetic datum – the orientation in the horizontal plane and the translations along all three coordinate axis. After the network adjustment a variance component estimation was performed to obtain more realistic accuracy estimates for the coordinates.

Point	*Easting*	*Northing*	*Height*
1	500.00	1000.00	100.00
2	486.01	1040.26	76.35
12	435.71	1081.60	44.73
13	435.95	1128.17	40.03
14	436.84	1159.60	44.74
15	466.98	982.87	92.75
17	414.33	1205.58	48.63

Table 5.1: Initial approximate coordinates of HPTN points in [m]

5.1 Results of network analyses

The statistical results from the network analyses of the four epochs are summarized in Table 5.2, including the number of observations n, the number of unknowns u and the redundancy r. As can be seen from the table the number of observations increases after the first epoch due to the introduction of the additional instrument station and further lines of observations, which leads to a significant increase in redundancy. An orientation offset

Epoch	n	u	r	$\hat{\sigma}_{0_k}$	$T_{\chi^2_k}$	Test outcome
1	54	25	33	± 0.001001	33.07	pass
2	75	26	53	± 0.001013	54.39	pass
3	75	26	53	± 0.000994	52.36	pass
4	75	26	53	± 0.000946	47.43	pass

Table 5.2: Statistical results of network analyses

required for the additional instrument station increases the number of unknown parameters to 26. The a posteriori standard deviations $\hat{\sigma}_{0_k}$ (for $k = 1 \ldots 4$), after variance component

estimation, together with their test statistics $T_{\chi^2_k}$ for the global test of the adjustment model are listed in the table as well. The test passes for all epochs.

The adjusted coordinates for all epochs and their standard deviations can be found in Appendix C.1. The estimated standard deviations of the coordinates in epoch 1 vary between ± 0.4 mm and ± 1.2 mm in the horizontal plane and between ± 1.3 mm and ± 4.4 mm in the vertical. The standard deviations improve in epoch 2, now ranging between ± 0.2 mm and ± 0.4 mm horizontally and between ± 0.7 mm and ± 1.3 mm vertically. For epochs 3 and 4 the estimated standard deviations can be summarized as varying from ± 0.2 mm to ± 0.7 mm in the horizontal plane and from ± 0.4 mm to ± 0.8 mm in the vertical. These numbers clearly reflect the high precision obtained for the network coordinates. An improvement in precision between the first and the subsequent epochs is also notable. This is a consequence of the increased network redundancy after the first epoch.

Due to the chosen datum definition, the estimated cofactor matrices of the adjusted coordinates for all epochs are rank-deficient by four.

5.2 Global congruency testing

For this application it is of interest to compare not only the subsequent epochs with the base epoch but also to compare all epochs among each other to gain a better insight of the movements on a year-to-year basis. Hence, the global congruency test needs to be carried out for all six combinations of the four epochs. Before this can be done, it has to be ensured that all epochs refer to the same a posteriori variance factor by using the test described in (2.24). The results from the tests are shown in Table 5.3. After it has been confirmed that all epochs are indeed comparable, the combined variance factors for all six two-epoch comparisons can be derived. Their square root, the combined standard deviations $\hat{\sigma}_0$ are given in Table 5.3 as well.

Epochs	T_F	$F_{S,\,f_1,\,f_2}$	Test outcome	$\hat{\sigma}_0$
1 and 2	1.02	1.91	pass	±0.0010084
1 and 3	1.01	1.82	pass	±0.0009967
1 and 4	1.12	1.82	pass	±0.0009675
2 and 3	1.04	1.72	pass	±0.0010035
2 and 4	1.15	1.72	pass	±0.0009801
3 and 4	1.10	1.72	pass	±0.0009703

Table 5.3: Comparison of variances and combined standard deviations

Now the global congruency tests can be performed according to (2.32) to (2.35). The test

Epochs	$\hat{\Omega}^2$	T_G	$F_{S,\,f_1,\,f_2}$	Test outcome
1 and 2	$1.42 \cdot 10^{-6}$	1.40	1.81	pass
1 and 3	$3.12 \cdot 10^{-6}$	3.14	1.81	fail
1 and 4	$2.42 \cdot 10^{-6}$	2.59	1.81	fail
2 and 3	$1.60 \cdot 10^{-6}$	15.91	1.79	fail
2 and 4	$7.64 \cdot 10^{-6}$	7.96	1.79	fail
3 and 4	$5.12 \cdot 10^{-6}$	5.45	1.79	fail

Table 5.4: Global congruency tests for all epochs

statistics are derived from angular differences between epochs again. The results are listed in Table 5.4. The boundary values of the FISHER-distribution are given for a confidence level of $\alpha = 5\,\%$ and degrees of freedom $f_1 = h = 14$ and $f_2 = r_i + r_j$, the sum of redundancies of both epochs, being 86 or 106, respectively. It becomes evident from the results that, with the exception of epoch 2, deformations have to be expected in all other epochs.

5.3 Localization

After it has been determined that deformations are inherent, the search for the largest similar point group is conducted using the MSS-method based on distance-ratios as well as the angle-based approach. Since scale changes between epochs are suspected, the distance-difference approach is not applied.

5.3.1 MSS using distance ratios

Although, the global congruency test already stated that no measurable deformations are inherent between epochs 2 and 1, for reasons of completeness the search for the largest similar point group is performed as well. The result is shown in Table 5.5 below. The only candidate

Candidate	$\hat{\sigma}_0$	Redundancy	T_χ	Test outcome
1, 2, 12, 13, 14, 15, 17	±1.18825765	14	19.77	pass

Table 5.5: Statistical evaluation of largest similar point group between epochs 1 and 2

found includes all seven points. After performing the obligatory transformation adjustment, the outcome of the global congruency test can be confirmed. The reference value for the χ^2-test is given by $\chi^2_{S=0.95,\, f=r=14} = 23.68$.

The results of the search for the largest similar point group between epochs 1 and 3 are listed in Table 5.6. Two candidates consisting of six points are found. With a boundary value of

Candidate	$\hat{\sigma}_0$	Redundancy	T_χ	Test outcome
1, 2, 12, 13, 14, 17	±1.53263313	11	25.84	fail
2, 12, 13, 14, 15, 17	±1.19944369	11	15.83	pass

Table 5.6: Statistical evaluation of candidates for largest similar point group between epochs 1 and 3

$\chi^2_{S=0.95,\, f=r=11} = 19.68$, the global test of the adjustment model passes for only one of the two, so that the final solution is found and no further searches have to be conducted.

For the comparison of epochs 1 and 4, two candidates are found as well. With the same reference value as before of $\chi^2_{S=0.95,\, f=r=11} = 19.68$, the global test of the adjustment model passes for one candidate only which thus forms the final solution. The results for the two candidates are summarized in Table 5.7 below.

For the comparison of epoch 2 and epoch 3 the search for the largest similar point group first delivers two candidates of six points. After transformation, the global test of the adjustment

Candidate	$\hat{\sigma}_0$	Redundancy	T_χ	Test outcome
1, 2, 13, 14, 15, 17	±1.62397845	11	29.01	fail
2, 12, 13, 14, 15, 17	±1.31110192	11	18.91	pass

Table 5.7: Statistical evaluation of candidates for largest similar point group between epochs 1 and 4

model fails for both. The search is continued for a group of five points and results in 11 candidates, likewise they are all rejected. In search for a group of four points, a total of 25

Candidate	$\hat{\sigma}_0$	Redundancy	T_χ	Test outcome
12, 14, 15, 17	±0.89631285	5	4.02	pass

Table 5.8: Statistical evaluation of largest similar point group between epochs 2 and 3

candidates are discovered of which three candidates pass the global test of the adjustment model. The one with the smallest test statistic forms the final solution and is given in Table 5.8. All remaining candidates and their statistical evaluations can be found in Table C.5 in Appendix C.2.

Between epochs 2 and 4 a total of 67 candidates are found. The final solution consists of four points and is shown in Table 5.9 below. All remaining candidates are listed in Table C.6 in Appendix C.2.

Candidate	$\hat{\sigma}_0$	Redundancy	T_χ	Test outcome
12, 14, 15, 17	±0.88623094	5	3.93	pass

Table 5.9: Statistical evaluation of largest similar point group between epochs 2 and 4

For the comparison of epochs 3 and 4, the distance-ratios approach provides a total of 28 candidates. The final solution consisting of four points is listed in Table 5.10 below. The remaining solutions can be found in Table C.7 in Appendix C.2.

Candidate	$\hat{\sigma}_0$	Redundancy	T_χ	Test outcome
1, 12, 13, 15	± 0.56551964	5	1.60	pass

Table 5.10: Statistical evaluation of largest similar point group between epochs 3 and 4

5.3.2 MSS using angles

Now the search for the largest similar point group is repeated using the angle-based MSS-method. For the comparison of epochs 2 and 1 only one candidate is found consisting of all points. The global congruency test, obviously, passes again. The solution and its test results are shown in Table 5.11 below.

Candidate	T_G	Test outcome
1, 2, 12, 13, 14, 15, 17	1.40	pass

Table 5.11: Statistical evaluation of largest similar point group between epochs 1 and 2

For epochs 1 and 3 only two candidate solutions are found consisting of six points. With a boundary value of $F_{S=0.95,\, f_1=11,\, f_2=86} = 1.90$, one candidate fails the global congruency test while the other one passes, thus forming the final solution. The results for both candidates are given in Table 5.12 below.

Candidate	T_G	Test outcome
1, 2, 12, 13, 14, 17	2.37	fail
2, 12, 13, 14, 15, 17	1.45	pass

Table 5.12: Statistical evaluation of candidates for largest similar point group between epochs 1 and 3

Similarly, two candidates including six points are found for the comparison of epoch 1 and epoch 4. With the same boundary value of $F_{S=0.95,\, f_1=11,\, f_2=86} = 1.90$, again one candidate passes while the other is rejected. The test results are summarized in Table 5.13 below.

For the comparison between epochs 2 and 3 the algorithm delivers eight candidates of four points. With a reference value of $F_{S=0.95,\, f_1=5,\, f_2=106} = 2.30$, two candidates pass the global

Candidate	T_G	Test outcome
1, 2, 12, 13, 14, 17	2.00	fail
2, 12, 13, 14, 15, 17	1.80	pass

Table 5.13: Statistical evaluation of candidates for largest similar point group between epochs 1 and 4

congruency test. The candidate with the smaller test statistic forms the final solution and is shown in Table 5.14. The remaining candidates are listed in Table C.8 in Appendix C.3.

Candidate	T_G	Test outcome
12, 14, 15, 17	0.81	pass

Table 5.14: Statistical evaluation of largest similar point group between epochs 2 and 3

A total of 13 candidates are produced by the angle-based MSS-method for the comparison of epochs 2 and 4. Given the same reference value for the FISHER-distribution as before of $F_{S=0.95,\, f_1=5,\, f_2=106} = 2.30$, multiple candidates pass the test. The final solution is shown in Table 5.15 below. All remaining candidates and their test results are listed in Table C.9 in Appendix C.3.

Candidate	T_G	Test outcome
12, 14, 15, 17	0.77	pass

Table 5.15: Statistical evaluation of largest similar point group between epochs 2 and 4

For the comparison of epoch 3 and epoch 4, first three candidates of five points are found which are all rejected. Continuing the search for groups of four points leads to 16 candidates. Multiple of these candidates pass the global congruency test. The final solution is, again, identified as the candidate with the smallest test statistic T_G. The final solution and its statistical evaluation is shown in Table 5.16 below. All other candidates and their test results are given in Table C.10 in Appendix C.3.

Candidate	T_G	Test outcome
1, 12, 13, 15	0.32	pass

Table 5.16: Statistical evaluation of largest similar point group between epochs 3 and 4

5.3.3 Summary of results

After both MSS-based approaches applicable to scaled data have been applied to the Turtle Mountain data sets, it is found that both yield identical results for the localization of the largest similar point groups. While the approach based on distance-ratios still provides more candidates overall than the angle-based approach, the number of candidates found has reduced compared to the simulation from the previous chapter. Particularly, when only one point has deformed, the number of candidates is low. This is, at least partially, related to the lower number of points in the network. The high precision of the observations is also beneficial.

The largest similar point groups for each two-epoch comparisons are summarized in Table 5.17 below. Looking at the results with respect to epoch 1, it shows that only point 1

Epochs	Largest similar point groups
1 and 2	1, 2, 12, 13, 14, 15, 17
1 and 3	2, 12, 13, 14, 15, 17
1 and 4	2, 12, 13, 14, 15, 17
2 and 3	12, 14, 15, 17
2 and 4	12, 14, 15, 17
3 and 4	1, 12, 13, 15

Table 5.17: Summary of largest similar point groups between all epochs

is identified as unstable in epochs 3 and 4. No movements are found in epoch 2. From the results with respect to epoch 2 however, it becomes obvious that, in addition to point 1, points 2 and 13 experienced deformations. The deformations of these two points were not discovered with respect to epoch 1. This can be explained with the difference in precision of the two epochs. Due to the additional instrument station and observation lines in epochs 2

to 4, the standard deviations of the adjusted coordinates for these epochs have significantly improved over those in epoch 1. In other words, epoch 1 is not determined precisely enough to pick up deformations with a magnitude of those occurring on Turtle Mountain.

The results with respect to epoch 3 suggest that points 1 and 13 did not experience any further deformations after epoch 3 was observed, since they are part of the largest similar point group between epoch 3 and epoch 4. Point 2, on the other hand, appears to be moving continuously since it is identified as unstable in both, epochs 3 and 4. Furthermore, now deformations are inherent in points 14 and 17 which have not shown up in the comparison with respect to epoch 2. While the estimated standard deviations of the horizontal coordinates in epoch 2 and 3 are at the same level, their standard deviations in the vertical are slightly better in epochs 3 and 4 than they are in epoch 2. If the movements of points 14 and 17 occurred mainly in vertical direction, this could explain why they have not been picked up with respect to epoch 2.

Overall, only two points, namely 12 and 15, remain stable throughout all epochs. While no deformations were discovered in epoch 2, the only point unstable throughout the remaining epochs is point 2.

5.4 Determination

After the stable and unstable points have been identified, the deformations occurring in the Turtle Mountain HPTN points shall be derived from a multiple-epoch transformation as described in Section 3.3. For this, a stable computational base for the determination of the transformation parameters needs to be chosen. Since in this application it is of interest to compare all epochs among each other and not only with respect to the base epoch, the chosen computational base should include only points that are stable throughout all epochs. In this case, only two points were found to be stable throughout all epochs but three or more

points are required for the transformation.

Based on the results of the localization step, the point group from which the transformation parameters are derived is chosen as 12, 14, 15 and 17. These points are stable for all comparisons with respect to epochs 1 and 2, so that results on their basis are comparable between these epochs. The adjusted coordinates listed in Appendix C.1 and their singular cofactor matrices serve as input for the transformation adjustment. The a priori standard deviation for the adjustment was chosen as $\sigma_0 = \pm 1$. The statistical results of the transformation adjustment are summarized in Table 5.18 below.

	Ep 1	Ep 2	Ep 3	Ep 4	Total
Number of points	4	4	4	4	16
Number of observations	12	12	12	12	48
Number of conditions	–	13	13	13	39
Number of unknowns	–	8	8	8	24
Redundancy	–	5	5	5	15
A posteriori standard deviation $\hat{\sigma}_0$					± 1.033739
Global test statistic T_χ					16.03
Lower boundary value $\chi^2_{S=0.025,\,r}$					6.26
Upper boundary value $\chi^2_{S=0.975,\,r}$					27.49
Test outcome					pass

Table 5.18: Summary of statistics for transformation adjustment of all epochs

The estimated transformation parameters and their standard deviations for epochs 2 and 3 are given in Table 5.19 and the parameters for epoch 4 and their standard deviations follow in Table 5.20. Looking at the tables it can be noted that the estimated standard deviations of the parameters are almost the same for all epochs. While the parameters show larger variations than their standard deviations, they are still at about the same level for all epochs, with the exception of the scale factor. This makes sense, since the stable computational base is the same for all three transformations. In epoch 2 and 3 the rotation about the x-axis clearly has the largest magnitude with about $10''$ while the other two rotations are less than $5''$ in magnitude. In epoch four all three rotations have a magnitude

	Epoch 2		Epoch 3	
Parameter	Value	$\hat{\sigma}$	Value	$\hat{\sigma}$
q_0	0.999999999598734	$\pm 4.0362 \cdot 10^{-10}$	0.999999999667881	$\pm 3.6511 \cdot 10^{-10}$
q_x	0.0000269583	$\pm 14.7092 \cdot 10^{-6}$	0.0000230081	$\pm 16.1526 \cdot 10^{-6}$
q_y	0.0000048872	$\pm 5.4368 \cdot 10^{-6}$	0.0000092321	$\pm 5.2746 \cdot 10^{-6}$
q_z	-0.0000072041	$\pm 3.2954 \cdot 10^{-6}$	-0.0000070451	$\pm 3.6184 \cdot 10^{-6}$
ω	$11.1''$	$\pm 6.1''$	$9.5''$	$\pm 6.7''$
φ	$2.0''$	$\pm 2.2''$	$3.8''$	$\pm 2.2''$
κ	$-3.0''$	$\pm 1.4''$	$-2.9''$	$\pm 1.5''$
T_x	0.000136 m	± 0.000263 m	0.000047 m	± 0.000278 m
T_y	0.000116 m	± 0.000344 m	-0.000440 m	± 0.000356 m
T_z	0.000099 m	± 0.000755 m	0.000076 m	± 0.000721 m
λ	-0.8 ppm	± 3.9 ppm	$+66.8$ ppm	± 4.0 ppm

Table 5.19: Estimated transformation parameters and standard deviations of epochs 2 and 3 with respect to epoch 1

of less than $5''$. The translation parameters are at the sub-millimetre level in all three epochs with the only exception being the z-translation of epoch 4 with about -1.3 mm. An obvious change in scale of about 67 ppm can be observed in epochs 3 and 4 with respect to epoch 1. In epoch 2 the estimated scale factor is negligible.

With the exception of the z-rotation in epoch 2, all estimated rotation parameters are within 2σ of their standard deviations. All translations are well within 2σ of their standard deviations. Hence, datum changes are not obvious in the estimated transformation parameters[1]. Overall the estimated standard deviations indicate that the parameters were determined very precisely, despite the small computational base of only four points. This is a consequence of the high precision of the adjusted coordinates.

The estimated deformations can be found in the tables below. Points found to be unstable in the localization step are highlighted in bold.

In epoch 2 no measurable deformations have occurred. The apparent movement of the seven HPTN points together with their standard deviations are listed in Table 5.21. It can be noted that the estimated movements are very small, especially in *Easting*. They are largest

[1] Again, with the exception of the scale factor in epochs 3 and 4.

	Epoch 4	
Parameter	Value	$\hat{\sigma}$
q_0	0.999999999900845	$\pm 2.0306 \cdot 10^{-10}$
q_x	-0.0000102275	$\pm 16.2842 \cdot 10^{-6}$
q_y	0.0000096789	$\pm 5.3390 \cdot 10^{-6}$
q_z	-0.0000001724	$\pm 3.6459 \cdot 10^{-6}$
ω	$-4.2''$	$\pm 6.7''$
φ	$4.0''$	$\pm 2.2''$
κ	$-0.1''$	$\pm 1.5''$
T_x	0.000148 m	± 0.000293 m
T_y	0.000096 m	± 0.000360 m
T_z	-0.001275 m	± 0.000731 m
λ	+67.3 ppm	± 4.3 ppm

Table 5.20: Estimated transformation parameters and standard deviations of epochs 4 with respect to epoch 1

Point	$\Delta Easting$	$\Delta Northing$	$\Delta Height$	$\hat{\sigma}_{\Delta Easting}$	$\hat{\sigma}_{\Delta Northing}$	$\hat{\sigma}_{\Delta Height}$
1	0.6	0.4	-5.3	± 1.0	± 0.7	± 2.4
2	0.0	2.2	1.0	± 1.3	± 1.1	± 2.7
12	-0.3	0.3	5.5	± 1.1	± 1.0	± 4.7
13	0.5	-1.7	2.3	± 1.3	± 1.0	± 2.5
14	0.0	0.3	-2.5	± 0.6	± 0.7	± 1.9
15	-0.0	-0.1	-0.1	± 0.9	± 0.6	± 2.1
17	0.0	-0.4	-0.1	± 0.8	± 0.8	± 2.1

Table 5.21: Estimated deformations and standard deviations between epochs 1 and 2 in [mm]

in *Height* with several millimetres in magnitude. The same can be seen in the standard deviations. This is not surprising since the precision of the coordinates is worst in the vertical, especially in epoch 1.

In epoch 3 only point 1 was found to be unstable with respect to epoch 1. Point 1 exhibits movements mainly in vertical direction accompanied by smaller horizontal movements in a north-westerly direction. Notable are the larger movements of point 13, at the level of 2 mm to 3 mm in all three coordinate directions, although this point was identified as part of the largest similar point group between epochs 1 and 3.

In epoch 4, again, only point 1 shows a significant deformation with respect to epoch 1. The

Point	$\Delta Easting$	$\Delta Northing$	$\Delta Height$	$\hat{\sigma}_{\Delta Easting}$	$\hat{\sigma}_{\Delta Northing}$	$\hat{\sigma}_{\Delta Height}$
1	**−1.2**	**1.5**	**−6.5**	±1.1	±0.7	±2.3
2	1.6	0.9	2.0	±1.3	±1.1	±2.6
12	−0.3	0.6	6.6	±1.2	±1.0	±4.5
13	−3.3	−2.3	2.2	±1.3	±1.1	±2.3
14	−0.0	0.2	−1.4	±0.6	±0.7	±1.6
15	0.0	−0.1	−0.6	±0.9	±0.7	±2.0
17	0.1	−0.4	−1.7	±0.8	±0.8	±1.8

Table 5.22: Estimated deformations and standard deviations between epochs 1 and 3 in [mm]

movement occurs completely in vertical direction. Furthermore, an increase in the apparent movements of the remaining points is visible compared to the previous epochs, although none of these points were found to be unstable.

Point	$\Delta Easting$	$\Delta Northing$	$\Delta Height$	$\hat{\sigma}_{\Delta Easting}$	$\hat{\sigma}_{\Delta Northing}$	$\hat{\sigma}_{\Delta Height}$
1	**0.0**	**0.2**	**−9.2**	±1.1	±0.8	±2.3
2	2.4	3.0	−4.5	±1.3	±1.2	±2.6
12	0.5	0.2	6.5	±1.3	±1.1	±4.5
13	−1.9	−2.1	1.7	±1.3	±1.1	±2.3
14	−0.4	0.8	−2.3	±0.6	±0.8	±1.6
15	−0.2	−0.2	−0.3	±0.9	±0.7	±2.0
17	0.2	−0.9	−0.8	±0.8	±0.9	±1.8

Table 5.23: Estimated deformations and standard deviations between epochs 1 and 4 in [mm]

The estimated deformations of epoch 3 with respect to epoch 2 are shown in Table 5.24 below. Point 1 again exhibits a movement in north-westerly direction while point 2 shows a north-easterly trend. Point 13 moves due west. The apparent movements of the stable points are smaller now compared to previous epochs. Likewise, the standard deviations have improved slightly, mainly in vertical direction. This can be attributed to the increased network redundancy in epochs 2 to 4.

In epoch 4 point 1 continues its previous downward trend with only very little horizontal movements. Point 2 as well continues on its previous course in north-easterly direction, now

Point	$\Delta Easting$	$\Delta Northing$	$\Delta Height$	$\hat{\sigma}_{\Delta Easting}$	$\hat{\sigma}_{\Delta Northing}$	$\hat{\sigma}_{\Delta Height}$
1	**−1.7**	**1.2**	**−1.2**	±1.3	±0.8	±2.5
2	**1.6**	**1.3**	**1.0**	±0.8	±0.7	±2.2
12	0.0	0.3	1.1	±1.1	±0.8	±1.8
13	**−3.8**	**−0.7**	**−0.1**	±0.8	±0.7	±1.4
14	−0.1	−0.1	1.1	±0.6	±0.7	±1.7
15	0.0	0.0	−0.5	±1.0	±0.7	±2.0
17	0.1	0.0	−1.6	±0.9	±0.9	±1.9

Table 5.24: Estimated deformations and standard deviations between epochs 2 and 3 in [mm]

accompanied by a downward movement of over 5 mm in magnitude. Likewise, Point 13 shows the same trend as before moving in a mainly westerly direction. The apparent movements of the stable points are still very small in magnitude. The estimated standard deviations of all points are comparable to those of the epoch 2–3 comparison.

Point	$\Delta Easting$	$\Delta Northing$	$\Delta Height$	$\hat{\sigma}_{\Delta Easting}$	$\hat{\sigma}_{\Delta Northing}$	$\hat{\sigma}_{\Delta Height}$
1	**−0.6**	**−0.2**	**−4.0**	±1.3	±0.8	±2.5
2	**2.3**	**0.8**	**−5.5**	±0.8	±0.8	±2.2
12	0.8	−0.1	1.0	±1.1	±0.9	±1.8
13	**−2.3**	**−0.4**	**−0.6**	±0.8	±0.8	±1.5
14	−0.4	0.5	0.2	±0.6	±0.7	±1.7
15	−0.2	−0.1	−0.2	±1.0	±0.8	±2.1
17	0.2	−0.4	−0.6	±0.9	±0.9	±1.9

Table 5.25: Estimated deformations and standard deviations between epochs 2 and 4 in [mm]

Transformation between epochs 3 and 4

Epochs 3 and 4 cannot be compared in the datum defined by points 12, 14, 15 and 17, as points 14 and 17 were found to be unstable between epochs 3 and 4. For this reason, a separate transformation adjustment was carried out between epochs 3 and 4 with points 1, 12, 13, 15 as computational base. The statistical results are shown in Table 5.26. The a priori standard deviation was again chosen as $\sigma_0 = \pm 1$.

Number of points	4
Number of observations	24
Number of conditions	13
Number of unknowns	8
Redundancy	5
A posteriori standard deviation $\hat{\sigma}_0$	± 0.565520
Global test statistic T_χ	1.60
Lower boundary value $\chi^2_{S=0.025,\,r}$	0.83
Upper boundary value $\chi^2_{S=0.975,\,r}$	12.83
Test outcome	pass

Table 5.26: Summary of statistics for transformation adjustment of all epochs

The estimated transformation parameters between epoch 3 and epoch 4 and their standard deviations are listed in Table 5.27. As before, the parameters are very precisely determined

Parameter	Value	$\hat{\sigma}$
q_0	0.999999999823570	$\pm 0.6484 \cdot 10^{-10}$
q_x	0.0000062265	$\pm 3.8612 \cdot 10^{-6}$
q_y	-0.0000114750	$\pm 2.0422 \cdot 10^{-6}$
q_z	-0.0000135061	$\pm 1.7682 \cdot 10^{-6}$
ω	$2.6''$	$\pm 1.6''$
φ	$-4.7''$	$\pm 0.8''$
κ	$-5.6''$	$\pm 0.7''$
T_x	0.000319 m	± 0.000177 m
T_y	-0.001295 m	± 0.000123 m
T_z	-0.000195 m	± 0.000211 m
λ	-0.3 ppm	± 2.8 ppm

Table 5.27: Estimated transformation parameters and standard deviations of epochs 4 with respect to epoch 3

with standard deviations at about the $1''$-level for the rotations and at sub-millimetre level for the translations. The rotation parameters for the y- and z-rotations exceed their standard deviations by more than 2σ while the x-rotation is below that threshold. The y-translation exceeds its standard deviation by an order of magnitude. The x- and z-translations on the other hand, are within 2σ of their standard deviations. The scale factor is negligible.

The estimated deformations between epochs 3 and 4 and their standard deviations are shown in Table 5.28 below. The three unstable points are highlighted in bold. The deformations of

point 2, a downward movement accompanied by a mainly northerly horizontal component, agree with those of previous epochs. The two previously stable points 14 and 17 both show a trend mainly to the west, accompanied by smaller movements in *Northing* and *Height*. The four stable points all show apparent movements at the sub-millimetre level. A further improvement in the standard deviations in all three coordinate directions is apparent, compared to those derived with respect to epoch 2. This explains why now points 14 and 17 can be identified as unstable in epoch 4 with respect to epoch 3, when they previously were found to be part of the stable computational base.

Point	$\Delta Easting$	$\Delta Northing$	$\Delta Height$	$\hat{\sigma}_{\Delta Easting}$	$\hat{\sigma}_{\Delta Northing}$	$\hat{\sigma}_{\Delta Height}$
1	−0.1	−0.1	0.0	±0.4	±0.5	±0.7
2	**−0.3**	**3.4**	**−3.8**	±0.4	±0.6	±0.9
12	0.7	−0.4	−0.4	±0.9	±0.9	±1.1
13	−0.2	0.3	0.2	±0.4	±0.7	±0.8
14	**−3.6**	**0.5**	**0.7**	±0.4	±0.7	±0.8
15	−0.2	0.1	0.0	±0.5	±0.5	±0.7
17	**−5.4**	**−1.5**	**1.9**	±0.6	±0.8	±0.9

Table 5.28: Estimated deformations and standard deviations between epochs 3 and 4 in [mm]

To gain a better understanding of the deformation behaviour on Turtle Mountain, the deformations for all epochs are graphically presented below. Figure 5.9 shows a horizontal plot of the HPTN points together with their horizontal deformation vectors for Summer 2008 to Fall 2009, Fall 2009 to Fall 2010 and Fall 2010 to Fall 2011. Figure 5.10 depicts in a similar manner the elevations of the HPTN points with their vertical deformation vectors.

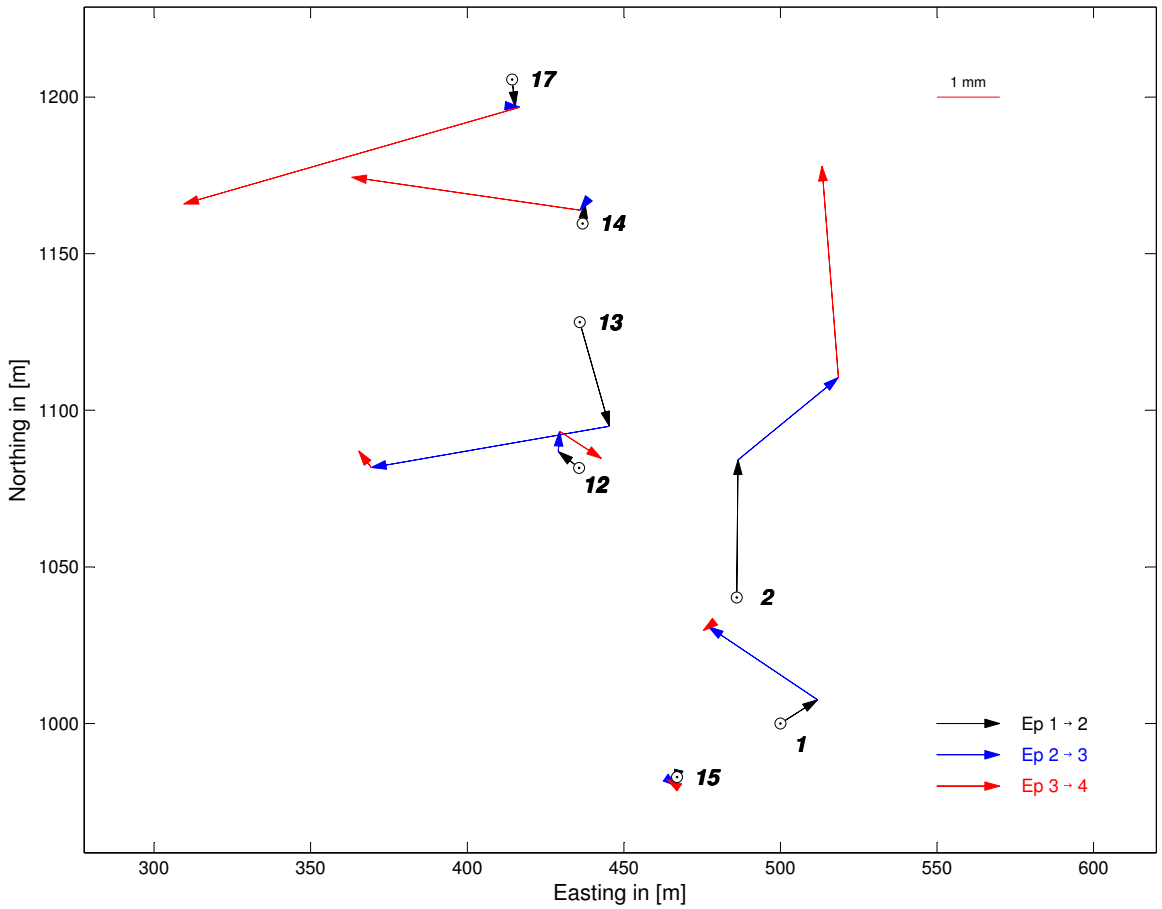

Figure 5.9: Horizontal deformations of HPTN points between Summer 2008 (epoch 1) and Fall 2011 (epoch 4)

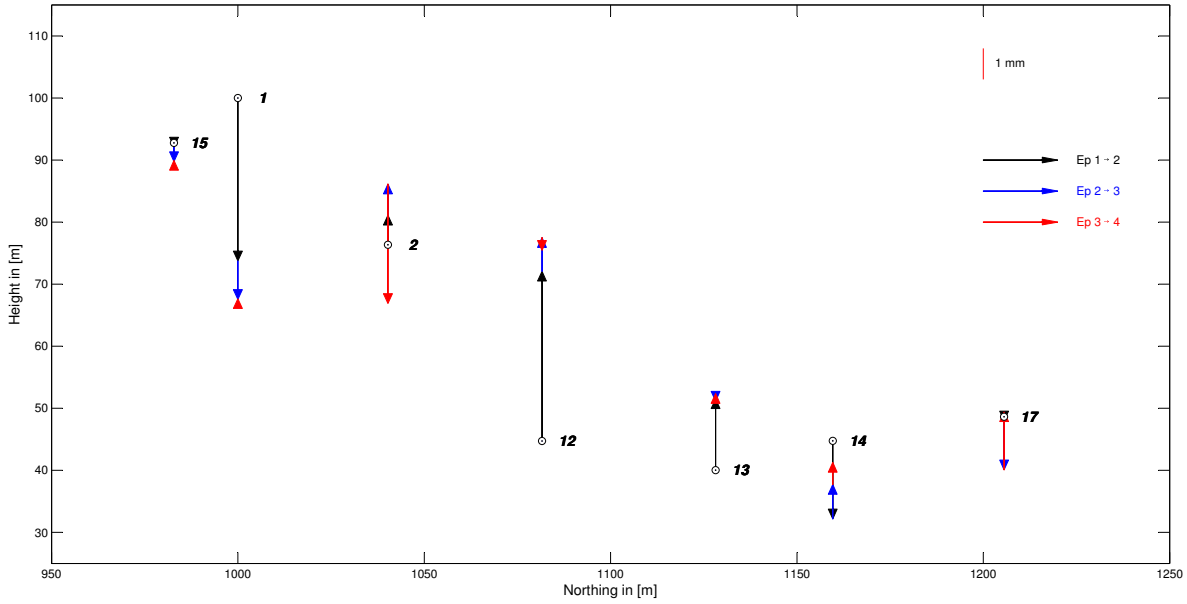

Figure 5.10: Vertical deformations of HPTN points between Summer 2008 (epoch 1) and Fall 2011 (epoch 4)

5.5 Discussion

The monitoring application presented here differs from the two simulated scenarios shown in Chapter 4 in several aspects. The network consists of considerably fewer points and has a poor geometry. All network points are located in the deformation zone, so that a stable reference frame does not exist. The high-precision terrestrial network on Turtle Mountain was observed in four epochs between Summer 2008 and Fall 2011. Since scale changes are expected between epochs, the global congruency tests and localization are carried out using scale- and datum-invariant observations, so that furthermore the geodetic datum of the epochs is of no concern. The test statistics for the global congruency tests are derived from angular differences between epochs. The global congruency test indicates deformations in all epochs with the exception of epoch 2.

The localization of the largest similar point group was performed using the MSS-method with distance ratios as well as the angle-based MSS-approach. Both approaches deliver the same results. When analyzing epochs with respect to Summer 2008 (epoch 1), only point 1 is found unstable in epochs 3 and 4. No movements were found in the second epoch, confirming the outcome of the global congruency test. The results with respect to Fall 2009 (epoch 2), in addition to point 2, points 2 and 13 show signs of movements, which were not discovered with respect to epoch 1. This leads to the conclusion that the coordinates in Summer 2008 (epoch 1) are not precise enough to pick up these movements. And indeed, a look at Table C.1 in Appendix C.1 confirms that the coordinates in epoch 1 are of lesser precision compared to those of the following epochs. This is due to the addition of a fifth instrument station and several observation lines starting in Fall 2009 (epoch 2).

Analyzing the Fall 2010 epoch (3) with respect to to Fall 2011 (epoch 4) indicates a change in the deformation behaviour. The movements of points 1 and 13 appear to have ceased, but now points 14 and 17 at the northern end of the Saddle start moving. Overall only

two points, namely points 12 and 15, were found to be stable throughout all four epochs. The only point experiencing deformations consistently throughout epochs 3 and 4 is point 2. Due to this change in point movements between the last two epochs, two different stable computational bases had to be chosen to determine the deformations, as no sufficiently large stable base exists for all four epochs.

No significant deformations were recovered in Fall 2009 (epoch 2). By Fall 2010 (epoch 3) movements can be observed in the southern and central parts of the Saddle. Point 1, just below South Peak, shows a down-slope movement into the Saddle. Point 2 is drifting towards the north-east. This indicates a widening of the southern part of the major fracture running through the Saddle by Fall 2010. Point 13, located in the central area of the Saddle, shows a due west movement, also indicating a widening of the same fracture. By Fall of 2011 movements in the southern and central parts of the Saddle have mostly ceased, except for point 2 which continues its trend towards the slide, now coupled with a significant downward movement. Further movements can now be observed at the northern end of the Saddle area, where both, points 14 and 17, exhibit a strong movement in westerly direction, away from the slide.

Two major problems exist in this monitoring network, which make it very difficult to obtain accurate and conclusive information about the deformation behaviour on Turtle Mountain. One is the small magnitude of the occurring movements, which makes it very difficult to distinguish between true deformations and apparent movements, despite the high level of precision of the observations. The second problem is the fact that all points are potentially subject to deformations, so that no stable reference frame exists. However, certain movement patterns become recognizable. For one, a down-slope movement of South Peak towards the centre of the Saddle is observable in conjunction with a widening of the major fracture in the southern part between Summer 2008 and Fall 2010. Furthermore, between Fall 2010 and Fall 2011 a westerly movement at the northern end of the Saddle is observable.

A comparison with results from previous analyses is difficult because the HPT network is limited to a small area of Turtle Mountain where few other sensors, or targets respectively, exist for the time period during which the network was actively observed. The only comparison that can be made is with two photogrammetric targets, p-4 and p-6, that are located in the Saddle near the top of the Frank Slide. For these targets 3D movements of 38 mm and 88 mm between 1982 and 2005 have been reported in Froese et al. (2009). Point p-4 moves east-south-east and point p-6 moves in a north-easterly direction. Both points exhibit deformations directed towards the slide which indicates a widening of the major fracture that runs through the Saddle. This behaviour was also observed from the HPT network. Therefore, a general agreement with movement patterns of the Saddle area from Froese et al. (2009) exists.

Chapter 6

CONCLUSIONS

The final chapter summarizes the findings from this thesis for each chapter and points out the contributions to the field of deformation monitoring that have been accomplished with this work.

6.1 Findings from this Thesis

Chapter 2 - Background

In Chapter 2 it has been shown that a variety of very different geodetic observation types can be used to recover geometrical movements of a structure. Thus, the need of a network analysis arises in order to combine the different heterogeneous observation types and produce a homogeneous set of coordinates that describe the state of the monitored object at each epoch. The effect of the datum definition on the adjusted coordinates and their standard deviations has been illustrated in a series of examples.

The basic mathematical model for the classical congruence analysis has been discussed and demonstrated on two examples. It becomes obvious that, if scale changes occur between epochs, both global and local tests fails. Examination of different strategies for the localization of deformed points leads to the conclusion that an approach based on a combinatorial search should be applied. Two such approaches, one based on distance differences between epochs, the other based on distance ratios, are investigated. While both reliably deliver correct results, the distance difference approach is not applicable when scale changes occur. The scale-ratios approach on the other hand uses only an error estimate for the unknown

scale factor, which can lead to a large number of candidates. Moreover, a full least-squares adjustment has to be computed to evaluate each of the candidates.

3D Helmert transformations are discussed as an alternative way to determine deformations. Two approaches based on a Gauss-Markov model utilize a minimal configuration of fictitious observations to separate the deterministic and stochastical information inherent in the singular cofactor matrices of the coordinates. The implicit transformation approach presents a very elegant solution in which the scale factor is the only transformation parameter that is estimated. A solution that directly uses the coordinates in both systems is offered by the non-linear Gauss-Helmert model. This approach allows to process the singular cofactor matrix of the coordinate vectors directly without any preprocessing. But due to the explicit formulation of the transformation, it is a highly non-linear problem that requires good initial approximations for the unknown parameters and can cause numerical stability issues.

Chapter 3 - Methodology

Based on the findings of Chapter 2, a combinatorial search method for the localization of the largest similar point group between two epochs based on angles rather than distances is derived. The angle-based approach combines the advantages of the two distance approaches discussed earlier. It is unaffected by scale changes and angular differences can be directly compared between epochs, which allows the elimination of impossible combinations before the search is conducted. Moreover, the angular differences between epochs can be used to derive a global congruency test statistic for each candidate, so that no additional least-squares adjustment is required to evaluate the candidates resulting from the search. Furthermore, the angular differences between epochs can as well be used to derive the test statistic for the initial global congruency test to identify epochs in which deformations are inherent. If scale changes are suspected, neither coordinate nor distance differences can be used in the global

congruency test.

To derive the deformations a transformation-based approach is introduced in the form of a non-linear Gauss-Helmert model. Although the transformation between the members of the largest similar point group between epochs is formulated explicitly, there is no need for the computation of initial approximations for the transformation parameters. Standard values can be used and will lead to convergence independent of the magnitude of the transformation. No assumptions that restrict the validity of the model, such as small-angle approximations, are made. This is possible because of the use of quaternions to describe the rotations instead of Euler-angles. This also results in a bi-linear, numerically more stable normal equation system. Another advantage of this approach is that it directly utilizes the adjusted coordinates of each epoch together with their fully-populated and singular cofactor matrix as input without requiring any preprocessing. It has been shown that this approach can easily be extended to allow for the transformation of multiple epochs into the system of a common base epoch simultaneously in one single adjustment. In combination with the angle-based MSS-method, this allows to locate and determine deformations independent of the reference frame and datum of the given epochs.

Chapter 4 - Simulations

The methodology for the localization and determination of deformations proposed in Chapter 3 is tested in a series of simulations and results are compared to the classical congruence analysis as well as the distance-based MSS-methods. In the localization step of Scenario A it is found that the angle-based MSS-approach produces the correct results in all cases, identical to the other two MSS-approaches based on distances. While the angle-based approach provides more candidates then the distance-difference approach, it is significantly more efficient than than the distance-ratios approach. The traditional single-point analysis produces incorrect results in two out of four comparisons. In Scenario B only the MSS-methods based

on distance-ratios and angles can be applied since a full seven-parameter transformation of the network has been introduced in epochs 2 to 4. Again, both approaches identify the correct candidates, but the computational effort for the distance-ratios based approach is a lot higher, so that the MSS-approach based on angles is the preferred method if scale changes between epochs are suspected.

In Scenario A the deformations were determined using a re-adjustment of the combined observations of the epochs under consideration as well as the transformation-based approach proposed in Chapter 3. In the re-adjustment, for the epochs where the stable computational base was correctly identified, also the deformations were accurately recovered. For all stable points only one set of coordinates is estimated so no deformations for these points result. As a consequence, the RMS error is lower than for the transformation-based approach, but the coordinates of the stable points change with each re-adjustment.

With the transformation-based approach the transformation parameters as well as the deformations could be accurately recovered in both scenarios. The RMS error of the deformations is higher because discrepancies result for all points due to the propagation of random observation errors. However, adjusted coordinates originally estimated for each epoch remain unchanged. In Scenario B it shows that this approach can successfully be applied between epochs with coordinates given in completely different systems.

Chapter 5 - Case Study

In Chapter 5 a real-world application very different from the computer-simulated scenarios was presented. The case of the Frank Slide / Turtle Mountain represents a small, high-precision monitoring network without a stable reference frame and with the goal of detecting long-term trends in the behaviour of the Saddle area. Highly-precise coordinates are obtained for all epochs, but the existing deformations are very small which makes it difficult to distinguish between apparent movements caused by random observation errors and real

deformations. Because scale changes are expected, the global congruency tests were derived from angular differences between epochs rather than coordinate- or distance differences. For the same reason only the MSS-approaches based on distance ratios and angles were applied for the localization of the largest similar point group. Both methods, again, deliver the same results. The deformations were determined using the transformation-based approach introduced in Chapter 3. The analysis reveals a changing movement pattern. A downslope movement of South Peak coupled with a widening of the southern part of the major fracture is recognizable between Fall 2009 and Fall 2010. While this movement ceases almost entirely by Fall 2011, a strong westerly shift, away from the Frank Slide, at the northern part of the Saddle can be observed.

6.2 Research Contributions

In this dissertation a generalized model for a deformation analysis has been derived that allows one to locate and determine deformations between multiple epochs of a monitoring network simultaneously and independent of the coordinate systems to which these epochs refer.

In the course of this work it has been shown that only a combinatorial search method can reliably yield the largest congruent / similar point group between two epochs of a network. As a combinatorial search of all possible point combinations is generally not feasible, the MSS-method proposed in Neitzel (2004) based on distance differences and distance ratios was closely examined and applied to simulated as well as real-world data. This led to the conclusion that a more efficient approach is required for the case that scale changes are to be expected between the epochs under consideration.

The key contribution of this thesis lies in the development and application of a *datum-*, and particularly, *scale-invariant* approach to the MSS-method based on *angular differences*

between epochs to reduce the number of possible combinations that have to be examined in order to locate the largest similar point group between epochs. The isolation of a scale change achieved with this approach, here demonstrated on the example of multiple epochs of a monitoring network, can also be applied to the integration of different data types that refer to different scale factors.

The angle-based MSS approach may be further improved by combination with a single-point analysis in form of a local test of either each individual point in the group or the group's centroid. This could potentially resolve the ambiguous solutions where multiple candidates pass the global congruency test. A (preliminary) transformation may have to be applied in order to ensure that the point groups in both systems refer to the same reference frame and datum, which is a prerequisite for the local test.

A further application of the angle-based MSS-method lies in the datum-independent identification of group movements. Points that exhibit a similar deformation behaviour can be categorized into groups whose average movements can then be determined to allow a better understanding of the deformation behaviour of the monitored structure. The angle-based MSS-method can be used to find not only the *largest* similar point group between two data sets but *all* similar point groups. This can simply be accomplished by first identifying the largest similar point group, eliminating the members of that group from the set of all points and continuing the search for further similar point groups.

Deformations are determined by applying a transformation-based approach to the largest similar point groups. The combination of an interconnected 3D Helmert transformation of multiple epochs of coordinates with a quaternion rotation in a non-linear Gauss-Markov model with singular cofactor matrix of the observations and its application in the derivation of deformations constitute another significant contribution of this work.

Bibliography

Abatzoglou, T.J. and J.M. Mendel (1991). "The constrained total least-squares technique and its applications to harmonic superresolution". In: *IEEE Transactions on Signal Processing* 39.5, pp. 1070–1087.

Acar, M, M.T. Özlüdemir, O. Akyilmaz, R.N. Çelik, and T. Ayan (2006). "Deformation analysis with Total Least Squares". In: *Natural Hazards and Earth System Sciences* 6.4, pp. 663–669.

Akyilmaz, O. (2007). "Total Least Squares Solution of Coordinate transformation". In: *Survey Review* 39.303, pp. 68–80.

Baarda, W. (1968). "A testing procedure for use in geodetic networks". In: *Publications on Geodesy* 2.5, p. 97.

Bond, J., A. Chrzanowski, and D. Kim (2008). "Bringing GPS into harsh environments for fully automated deformation monitoring". In: *GPS Solutions* 12.1, pp. 1–11.

Caspary, W. (1996). "Anmerkungen zum robusten Schätzen". In: *Allgemeine Vermessungs-Nachrichten* 103.7, pp. 287–289.

DeLoach, S.R. (1989). "Contiuous Deformation Monitoring with GPS". In: *Journal of Surveying Engineering* 115.1, pp. 93–110.

Denli, H. (2004). "Crustal Deformation Analysis in the Marmara Sea Region". In: *Journal of Surveying Engineering* 130.4, pp. 151–155.

Detchev, I., A. Habib, and M. El-Badry (May 2011a). "Case study of beam deformation monitoring using conventional close range photogrammetry". In: *ASPRS 2011 Annual Conference*. ASPRS. Milwaukee, Wisconsin, USA.

Detchev, I., A. Habib, and M. El-Badry (Aug. 2011b). "Estimation of vertical deflections in concrete beams through digital close range photogrammetry". In: *ISPRS 2011 Laser Scanning Workshop*. ISPRS. Calgary, Canada.

Detchev, I., A. Habib, and M. El-Badry (Aug. 2012). "Image-Based Deformation Monitoring of Statically and Dynamically Loaded Beams". In: *XXII ISPRS Congress*. ISPRS. Melbourne, Australia.

Dunnicliff, J. (1988). *Geotechnical Instrumentation For Monitoring Field Performance*. John Wiley and Sons.

Ebeling, A., J. Chow, and W.F. Teskey (Mar. 2011). "Deformation Analysis of Terrestrial Monitoring Observations on Turtle Mountain, Alberta". In: *Journal of Applied Geodesy* 5 (1), pp. 47–58.

Ebeling, A., R.S. Radovanovic, and W.F. Teskey (2009). "Deformation Analysis Using a Multi-Parameter Transformation". In: *Geomatica* 63.3, pp. 97–107.

Erol, S., B. Erol, and T. Ayan (July 2004). "A General Review of the Deformation Monitoring Techniques and a Case Study: Analyzing Deformations Using GPS/Levelling". In: *Proceedings of the* 20^{th} *ISPRS Congress*. Vol. XXXV, part B7. Istanbul, pp. 622–627.

Featherstone, W.E., M.C. Dentith, and J.F. Kirby (Jan. 1998). "Strategies for the Accurate Determination of Orthometric Heights from GPS". In: *Survey Review* 34.267, pp. 278–296.

Fraser, C.S. and L. Gründig (Feb. 1985). "The Analysis of Photogrammetric Deformation Measurements on Turtle Mountain". In: *Photogrammetric Engineering and Remote Sensing* 51.2, pp. 207–216.

Fraser, C.S. and B. Riedel (2000). "Monitoring the thermal deformations of steel beams via vision metrology". In: *ISPRS Journal of Photogrammetry & Remote Sensing* 55, pp. 268–276.

Froese, C.R. et al. (2009). "25 years of movement monitoring on South Peak, Turtle Mountain: understandig the hazard". In: *Canadian Geotechnical Journal* 46, pp. 256–269.

Gielsdorf, F., L. Gründig, and I. Milev (May 2008). "Deformation Analysis with 3D Laser Scanning". In: *Proceedings of the FIG/IAG Symposium "Measuring the Changes"*. Lisbon, p. 9.

Golub, Gene H. and Charles F. Van Loan (1980). "An Analysis of the Total Least Squares Problem". In: *SIAM Journal on Numerical Analysis* 17.6, pp. 883–893.

Gordon, S. and D. Lichti (2007). "Modeling Terrestrial Laser Scanner Data for Precise Structural Deformation Measurement". In: *Journal of Surveying Engineering* 133.2, pp. 72–80.

Gründig, L. and J. Bahndorf (Aug. 1984). "Accuracy and Reliability in Geodetic Networks – Program System OPTUN". In: *Journal of Surveying Engineering* 110.2, pp. 133–145.

Gründig, L., M. Neureither, and J. Bahndorf (Aug. 1985). "Detection and Localization of Geometrical Movements". In: *Journal of Surveying Engineering* 111.2, pp. 118–132.

Guler, G., H. Kilic, G. Hosbas, and K. Ozaydin (2006). "Evaluation of the Movements of the Dam Embankments by Means of Geodetic and Geotechnical Methods". In: *Journal of Surveying Engineering* 132.1, pp. 31–39.

Horn, Berthold K. P. (Apr. 1987). "Closed-form solution of absolute orientation using unit quaternions". In: *Journal of the Optical Society of America* 4.4, pp. 629–642.

Kim, D., R.B. Langley, J. Bond, and A. Chrzanowski (2003). "Local deformation monitoring using GPS in an open mine: initial study". In: *GPS Solutions* 7.3, pp. 176–185.

Kuang, Shanlong (1996). *Geodetic Network Analysis and Design: Concepts and Applications*. 3^{rd}. Berlin Heidelberg: Springer Verlag.

Kuipers, Jack B. (1996). *Quaternions and Rotation Sequences: A Primer with Applications to Orbits, Aerospace, and Virtual Reality*. 121 South Main Street, Chelsea Michigan 48118: Ann Arbor Press Inc.

Lenzmann, Lothar and Enno Lenzmann (2004). "Strenge Auswertung des nichtlinearen Gauss-Helmert-Modells". In: *Allgemeine Vermessungs-Nachrichten* 111.2, pp. 68–73.

Lichti, D.D., M.P. Stewart, M. Tsakiri, and A.J. Snow (2000). "Calibration and Testing of a Terrestrial Laser Scanner". In: *International Archives of Photogrammetry and Remote Sensing* , Vol. XXXIII(Part B5), pp. 485–492.

Lo, Daniel, Axel Ebeling, W.F. Teskey, and Robert Radovanovic (2013). "Turtle Mountain Deformation Monitoring 2008-2011". In: *Geomatica* 67.1, pp. 293–309.

Lovse, J.W., W.F. Teskey, G. Lachapelle, and M.E. Cannon (1995). "Dynamic Deformation Monitoring of Tall Structures Using GPS Technology". In: *Journal of Surveying Engineering* 121.1, pp. 35–40.

Mateus, P. (May 2008). "Testing: An Application For Motorized Tacheometers". In: *Proceedings of the FIG/IAG Symposium "Measuring the Changes"*. Ed. by FIG/IAG. Lisbon, p. 8.

McGlone, J.C., ed. (2004). *Manual of Photogrammetry*. 5^{th}. 5410 Grosvenor Lane, Suite 210, Bethesda, Maryland 20814, USA: American Society for Photogrammetry and Remote Sensing.

Misra, P. and P. Enge (2006). *Global Positioning System: Signals Measurements, and Performance*. 2^{nd}. P.O. Box 692, Lincoln, Massachusetts 01 773: Ganga-Jamuna Press.

Monserrat, O. and M. Crosetto (2008). "Deformation Measurement using terrestrial laser scanning data and least squares 3D surface matching". In: *ISPRS Journal of Photogrammetry & Remote Sensing* 63, pp. 142–154.

Mühlich, Matthias and Rudolf Mester (2004). "Unbiased Errors-In-Variables Estimation Using Generalized Eigensystem Analysis". In: *Statistical Methods in Video Processing*. Ed. by Dorin Comaniciu, Rudolf Mester, Kenichi Kanatani, and David Suter. Vol. 3247. Lecture Notes in Computer Science. Springer Verlag Berlin Heidelberg, pp. 38–49.

Neitzel, Frank (2004). "Identifizierung konsistenter Datengruppen am Beispiel der Kongruenzuntersuchung geodätischer Netze". PhD thesis. German Geodetic Commission, Series C, No. 565: Technical University of Berlin.

Neitzel, Frank (Dec. 2010). "Generalization of total least-squares on example of unweighted and weighted 2D similarity transformation". In: *Journal of Geodesy* 84.12, pp. 751–762.

Neitzel, Frank and Burkhard Schaffrin (2013a). "2-D coordinate transformation within a Gauss-Helmert Model with singular dispersion matrix when rank BQ < rank B". In: *Journal of Applied Geodesy*, p. 19. In press.

Neitzel, Frank and Burkhard Schaffrin (2013b). "On the Gauss-Helmert Model with a Singular Dispersion Matrix where BQ is of Lesser Row Rank than B". In: *Studia Geophysica et Geodaetica*, p. 15. In press.

Niemeier, Wolfgang (2002). *Ausgleichungsrechnung*. Berlin New York: Walter de Gruyter.

Pope, A.J. (1972). "Some pitfalls to be avaoided in the iterative adjustment of nonlinear problems". In: *Proceedings of the 38th Annual Meeting of the American Society of Photogrammetry*. Washington, D.C., pp. 449–477.

Radovanovic, R.S. (Oct. 2002). "Adjustment of Satellite-Based Ranging Observations for Precise Positioning and Deformation Monitoring". Dissertation. Calgary: Deptartment of Geomatics Engineering, University of Calgary.

Rao, C. Radhakrishna (1962). "A note on a generalized inverse of a matrix with applications to problems in mathematical statistics". In: *Journal of the Royal Statistical Society. Series B (Methodological)*, pp. 152–158.

Rüeger, J.M. (1990). *Electronic Distance Measurement*. 3rd. Berlin Heidelberg: Springer Verlag.

Schaffrin, Burkhard (2006). "A note on constrained total least-squares estimation". In: *Linear Algebra Applications* 417.1, pp. 245–258.

Schaffrin, B. and A. Wieser (2009). "Empirical Affine Reference Frame Transformations by Weighted Multivariate TLS Adjustment". In: *Geodetic Reference Frames*. Ed. by Hermann Drewes. Vol. 134. International Association of Geodesy Symposia. Springer Verlag Berlin Heidelberg, pp. 213–218.

Schut, G.H. (1959). "Construction of orthogonal matrices and their application in analytical photogrammetry". In: *Photogrammetria* 15, pp. 149–162.

Teskey, W.F. (May 1987). "Integrated Analysis of Geodetic, Geotechnical, and Physical Model Data to Describe the Actual Deformation Behaviour of Earthfill Dams Under Static Loading. (Integrierte Analyse geodätischer und geotechnischer Daten sowie physikalischer Modelldaten zur Beschreibung des Deformationsverhaltens grosser Erddämme unter statischer Belastung)". PhD thesis. Universität Stuttgart. Published by the German Geodetic Commision (DGK).

Teskey, W.F. (1989). *ENGO 519 - Survey Networks*. Lecture Notes. University of Calgary.

Teskey, W.F., Bijoy Paul, and J.W. Lovse (Oct. 2005). "New Instrumentation and Methodology for Deformation Monitoring". In: *Proceedings of the* 7^{th} *Conference on Optical 3-D Measurement Techniques*. Vienna, p. 9.

Teskey, W.F., Bijoy Paul, and J.W. Lovse (May 2006). "Application of a Multi-Parameter-Transformation for Deformation Monitoring of a Large Structure". In: *Proceedings of the* 12^{th} *International FIG Symposium on Deformation Measurements*. Baden, p. 9.

Thompson, E.H. (1959). "On exact linear solution of the problem of absolute orientation". In: *Photogrammetria* 15, pp. 163–179.

Tong, Xiaohua, Yanmin Jin, and Lingyun Li (Nov. 2011). "An Improved Weighted Total Least Squares Method with Applications in Linear Fitting and Coordinate Transformation". In: *Journal of Surveying Engineering* 137, pp. 120–128.

Uren, J. and W.F. Price (2006). *Surveying for Engineers*. 4^{th}. Hampshire New York: Palgrave MacMillan.

Van Huffel, Sabine (1991). "The Generalized Total Least Squares Problem: Formulation, algorithm and properties". In: *Numerical Linear Algebra, Digital Signal Processing and Parallel Algorithms*. Ed. by Gene H. Golub and P.V. Dooren. Series F, No. 70. NATO ASI. Berlin: Springer Verlag, pp. 651–660.

Van Huffel, Sabine and H.Y. Zha (1991). "The restricted total least-squares problem: Formulation, algorithm, and properties". In: *SIAM Journal on Matrix Analysis and Applications* 12.2, pp. 292–309.

Welsch, W., O. Heunecke, and H. Kuhlmann (2000b). *Handbuch Ingenieurgeodäsie. Auswertung geodätischer Überwachungsmessungen*. Ed. by M. Möser, G. Müller, H. Schlemmer, and H. Werner. Heidelberg: Herbert Wichmann Verlag.

Whitaker, C., M.A. Duffy, and A. Chrzanowski (2000). "Design of an Automated Dam Deformation Monitoring System: A Case Study". In: *Journal of Geospatial Engineering* 2.1, pp. 23–34.

Wolf, Paul R. and Charles D. Ghilani (1997). *Adjustment Computations: Statistics and Least Squares in Surveying and GIS*. 3^{rd}. New York: John Wiley & Sons, Inc.

Wolf, Paul R. and Charles D. Ghilani (2006). *Elementary Surveying: An Introduction to Geomatics*. 11^{th}. Upper Saddle River, New Jersey 07 458: Pearson Prentice Hall.

Appendix A

A.1 Error propagation for computation of angles from coordinates

For a network consisting of p points, $n = p \cdot \sum_{i=1}^{p-2} i$ angles can be derived. Three points contribute to each angle α as origin (at), starting point ($from$) and end point (to). The table below shows the order in which the n angles α_k are arranged.

k	at	$from$	to
1	1	2	3
2	1	2	4
⋮	⋮	⋮	⋮
i	2	1	3
$i+1$	2	1	4
⋮	⋮	⋮	⋮
n	p	$p-2$	$p-1$

Table A.1: Order of angles α_k

The angles are computed in two steps. First, the difference vectors $\vec{b}$ and $\vec{c}$ are computed from the coordinate vector $\vec{x}$ for all n angles according to (3.1). Concatenating the pairs of difference vectors $\vec{b}_i,\ \vec{c}_i$ for all angles in the order given in Table A.1, yields the overall difference vector $\vec{y}$:

$$\vec{y} = \begin{pmatrix} \vec{b}_1^T & \vec{c}_1^T & \vec{b}_2^T & \vec{c}_2^T & \cdots & \vec{b}_i^T & \vec{c}_i^T & \vec{b}_{i+1}^T & \vec{c}_{i+1}^T & \cdots & \vec{b}_n^T & \vec{c}_n^T \end{pmatrix}^T . \tag{A.1}$$

The functional relationship between the difference vectors in $\vec{y}$ and the coordinates $\vec{x}$ can then be described by

$$\vec{y} = \mathbf{F}_1^T \vec{x} \qquad \text{with } \mathbf{F}_1 = \frac{\partial \vec{y}}{\partial \vec{x}} . \tag{A.2}$$

The structure of $\mathbf{F}_1$ in accordance with Table A.1 is given by:

$$\underset{(3p\times 6n)}{\mathbf{F}_1} = \begin{array}{c} \\ \vec{x}_1 \\ \vec{x}_2 \\ \vec{x}_3 \\ \vec{x}_4 \\ \vdots \\ \vec{x}_{p-2} \\ \vec{x}_{p-1} \\ \vec{x}_p \end{array} \begin{array}{c} \begin{array}{cccccccccccc} \vec{b}_1^T & \vec{c}_1^T & \vec{b}_2^T & \vec{c}_2^T & \cdots & \vec{b}_i^T & \vec{c}_i^T & \vec{b}_{i+1}^T & \vec{c}_{i+1}^T & \cdots & \vec{b}_n^T & \vec{c}_n^T \end{array} \\ \left[\begin{array}{cccccccccccc} -\mathbf{I} & -\mathbf{I} & -\mathbf{I} & -\mathbf{I} & \cdots & \mathbf{I} & 0 & \mathbf{I} & 0 & \cdots & 0 & 0 \\ \mathbf{I} & 0 & \mathbf{I} & 0 & \cdots & -\mathbf{I} & -\mathbf{I} & -\mathbf{I} & -\mathbf{I} & \cdots & 0 & 0 \\ 0 & \mathbf{I} & 0 & 0 & \cdots & 0 & \mathbf{I} & 0 & 0 & \cdots & 0 & 0 \\ 0 & 0 & 0 & \mathbf{I} & \cdots & 0 & 0 & 0 & \mathbf{I} & \cdots & 0 & 0 \\ \vdots & \vdots & \vdots & \vdots & \ddots & \vdots & \vdots & \vdots & \vdots & \ddots & \vdots & \vdots \\ 0 & 0 & 0 & 0 & \cdots & 0 & 0 & 0 & 0 & \cdots & \mathbf{I} & 0 \\ 0 & 0 & 0 & 0 & \cdots & 0 & 0 & 0 & 0 & \cdots & 0 & \mathbf{I} \\ 0 & 0 & 0 & 0 & \cdots & 0 & 0 & 0 & 0 & \cdots & -\mathbf{I} & -\mathbf{I} \end{array}\right] \end{array} \tag{A.3}$$

where $\mathbf{I}$ denotes a (3×3) identity matrix.

In the second step the angles α_k are computed from the difference vectors in $\vec{y}$ according to (3.3). Combining all angles α_k in the vector $\vec{\alpha}$ in the order given in Table A.1, the functional relationship between the angles and difference vectors is described by

$$\vec{\alpha} = \mathbf{F}_2^T \vec{y} \qquad \text{with } \mathbf{F}_2 = \frac{\partial \vec{\alpha}}{\partial \vec{y}} \; . \tag{A.4}$$

The structure of $\mathbf{F}_2$, again in accordance with Table A.1, is given by equation (A.6) below.

Given the cofactor matrix $\mathbf{Q}_{xx}$ of the coordinate vector $\vec{x}$, the error propagation to obtain the cofactor matrix of the angles $\mathbf{Q}_{\alpha\alpha}$ can now be carried out as follows:

$$\underset{(n\times n)}{\mathbf{Q}_{\alpha\alpha}} = \underset{(n\times 3p)}{\mathbf{F}^T} \cdot \underset{(3p\times 3p)}{\mathbf{Q}_{xx}} \cdot \underset{(3p\times n)}{\mathbf{F}} \qquad \text{with } \underset{(3p\times n)}{\mathbf{F}} = \underset{(3p\times 6n)}{\mathbf{F}_1} \cdot \underset{(6n\times n)}{\mathbf{F}_2} \; . \tag{A.5}$$

$$\underset{(6n\times n)}{\mathbf{F}_2} = \begin{bmatrix} \partial\alpha_1/\partial\vec{b}_1 & 0 & \cdots & 0 & 0 & \cdots & 0 \\ \partial\alpha_1/\partial\vec{c}_1 & 0 & \cdots & 0 & 0 & \cdots & 0 \\ 0 & \partial\alpha_2/\partial\vec{b}_2 & \cdots & 0 & 0 & \cdots & 0 \\ 0 & \partial\alpha_2/\partial\vec{c}_2 & \cdots & 0 & 0 & \cdots & 0 \\ \vdots & \vdots & \ddots & \vdots & \vdots & \ddots & \vdots \\ 0 & 0 & \cdots & \partial\alpha_i/\partial\vec{b}_i & 0 & \cdots & 0 \\ 0 & 0 & \cdots & \partial\alpha_i/\partial\vec{c}_i & 0 & \cdots & 0 \\ 0 & 0 & \cdots & 0 & \partial\alpha_{i+1}/\partial\vec{b}_{i+1} & \cdots & 0 \\ 0 & 0 & \cdots & 0 & \partial\alpha_{i+1}/\partial\vec{c}_{i+1} & \cdots & 0 \\ \vdots & \vdots & \ddots & \vdots & \vdots & \ddots & \vdots \\ 0 & 0 & \cdots & 0 & 0 & \cdots & \partial\alpha_n/\partial\vec{b}_n \\ 0 & 0 & \cdots & 0 & 0 & \cdots & \partial\alpha_n/\partial\vec{c}_n \end{bmatrix} \tag{A.6}$$

The six partial derivatives of an arbitrary angle α with respect to the components of its two difference vectors $\vec{b} = (x_b \;\; y_b \;\; z_b)^T$ and $\vec{c} = (x_c \;\; y_c \;\; z_c)^T$, as contained in (A.6), are given by

$$\frac{\partial\alpha}{\partial x_b} = \frac{-x_c\left(y_b^2+z_b^2\right)+x_b\left(y_by_c+z_bz_c\right)}{s_b^3\cdot s_c\cdot\sqrt{1-\dfrac{\left(x_bx_c+y_by_c+z_bz_c\right)^2}{s_b^2\cdot s_c^2}}} \qquad \frac{\partial\alpha}{\partial x_c} = \frac{x_c\left(y_by_c+z_bz_c\right)-x_b\left(y_c^2+z_c^2\right)}{s_b\cdot s_c^3\cdot\sqrt{1-\dfrac{\left(x_bx_c+y_by_c+z_bz_c\right)^2}{s_b^2\cdot s_c^2}}}$$

$$\frac{\partial\alpha}{\partial y_b} = \frac{x_bx_cy_b-x_b^2y_c+z_b\left(-y_cz_b+y_bz_c\right)}{s_b^3\cdot s_c\cdot\sqrt{1-\dfrac{\left(x_bx_c+y_by_c+z_bz_c\right)^2}{s_b^2\cdot s_c^2}}} \qquad \frac{\partial\alpha}{\partial y_c} = \frac{-x_c^2y_b+x_bx_cy_c+z_c\left(y_cz_b-y_bz_c\right)}{s_b\cdot s_c^3\cdot\sqrt{1-\dfrac{\left(x_bx_c+y_by_c+z_bz_c\right)^2}{s_b^2\cdot s_c^2}}}$$

$$\frac{\partial\alpha}{\partial z_b} = \frac{\left(x_bx_c+y_by_c\right)z_b-\left(x_b^2+y_b^2\right)z_c}{s_b^3\cdot s_c\cdot\sqrt{1-\dfrac{\left(x_bx_c+y_by_c+z_bz_c\right)^2}{s_b^2\cdot s_c^2}}} \qquad \frac{\partial\alpha}{\partial z_c} = \frac{-\left(x_c^2+y_c^2\right)z_b+\left(x_bx_c+y_by_c\right)z_c}{s_b\cdot s_c^3\cdot\sqrt{1-\dfrac{\left(x_bx_c+y_by_c+z_bz_c\right)^2}{s_b^2\cdot s_c^2}}}$$

with

$$s_b = \sqrt{x_b^2+y_b^2+z_b^2} \quad \text{and} \quad s_c = \sqrt{x_c^2+y_c^2+z_c^2}\,.$$

A.2 Design and condition matrices for two-epoch comparison

The structure of the design matrix $\mathbf{A}$ is as follows:

$$\underset{(b\times u)}{\mathbf{A}} = \left[\begin{array}{cccccccc} \partial f_{x_1}/\partial q_0 & \partial f_{x_1}/\partial q_x & \partial f_{x_1}/\partial q_y & \partial f_{x_1}/\partial q_z & \partial f_{x_1}/\partial T_x & \partial f_{x_1}/\partial T_y & \partial f_{x_1}/\partial T_z & \partial f_{x_1}/\partial \lambda \\ \partial f_{y_1}/\partial q_0 & \partial f_{y_1}/\partial q_x & \partial f_{y_1}/\partial q_y & \partial f_{y_1}/\partial q_z & \partial f_{y_1}/\partial T_x & \partial f_{y_1}/\partial T_y & \partial f_{y_1}/\partial T_z & \partial f_{y_1}/\partial \lambda \\ \partial f_{z_1}/\partial q_0 & \partial f_{z_1}/\partial q_x & \partial f_{z_1}/\partial q_y & \partial f_{z_1}/\partial q_z & \partial f_{z_1}/\partial T_x & \partial f_{z_1}/\partial T_y & \partial f_{z_1}/\partial T_z & \partial f_{z_1}/\partial \lambda \\ \vdots & \vdots & \vdots & \vdots & \vdots & \vdots & \vdots & \vdots \\ \partial f_{x_p}/\partial q_0 & \partial f_{x_p}/\partial q_x & \partial f_{x_p}/\partial q_y & \partial f_{x_p}/\partial q_z & \partial f_{x_p}/\partial T_x & \partial f_{x_p}/\partial T_y & \partial f_{x_p}/\partial T_z & \partial f_{x_p}/\partial \lambda \\ \partial f_{y_p}/\partial q_0 & \partial f_{y_p}/\partial q_x & \partial f_{y_p}/\partial q_y & \partial f_{y_p}/\partial q_z & \partial f_{y_p}/\partial T_x & \partial f_{y_p}/\partial T_y & \partial f_{y_p}/\partial T_z & \partial f_{y_p}/\partial \lambda \\ \partial f_{z_p}/\partial q_0 & \partial f_{z_p}/\partial q_x & \partial f_{z_p}/\partial q_y & \partial f_{z_p}/\partial q_z & \partial f_{z_p}/\partial T_x & \partial f_{z_p}/\partial T_y & \partial f_{z_p}/\partial T_z & \partial f_{z_p}/\partial \lambda \\ \hline \partial g/\partial q_0 & \partial g/\partial q_x & \partial g/\partial q_y & \partial g/\partial q_z & \partial g/\partial T_x & \partial g/\partial T_y & \partial g/\partial T_z & \partial g/\partial \lambda \end{array}\right] \tag{A.7}$$

with the following partial derivatives:

$$\begin{array}{lll} \dfrac{\partial f_x}{\partial q_0} = T_x - x_i + \lambda \cdot x_j & \dfrac{\partial f_y}{\partial q_0} = T_y - y_i + \lambda \cdot y_j & \dfrac{\partial f_z}{\partial q_0} = T_z - z_i + \lambda \cdot z_j \\ \dfrac{\partial f_x}{\partial q_x} = 0 & \dfrac{\partial f_y}{\partial q_x} = T_z - z_i - \lambda \cdot z_j & \dfrac{\partial f_z}{\partial q_x} = -T_y + y_i + \lambda \cdot y_j \\ \dfrac{\partial f_x}{\partial q_y} = -T_z + z_i + \lambda \cdot z_j & \dfrac{\partial f_y}{\partial q_y} = 0 & \dfrac{\partial f_z}{\partial q_y} = T_x - x_i - \lambda \cdot x_j \\ \dfrac{\partial f_x}{\partial q_z} = T_y - y_i - \lambda \cdot y_j & \dfrac{\partial f_y}{\partial q_z} = -T_x + x_i + \lambda \cdot x_j & \dfrac{\partial f_z}{\partial q_z} = 0 \\ \dfrac{\partial f_x}{\partial T_x} = q_0 & \dfrac{\partial f_y}{\partial T_x} = -q_z & \dfrac{\partial f_z}{\partial T_x} = q_y \\ \dfrac{\partial f_x}{\partial T_y} = q_z & \dfrac{\partial f_y}{\partial T_y} = q_0 & \dfrac{\partial f_z}{\partial T_y} = -q_x \\ \dfrac{\partial f_x}{\partial T_z} = -q_y & \dfrac{\partial f_y}{\partial T_z} = q_x & \dfrac{\partial f_z}{\partial T_z} = q_0 \\ \dfrac{\partial f_x}{\partial \lambda} = q_0 x_j - q_z y_j + q_y z_j & \dfrac{\partial f_y}{\partial \lambda} = q_z x_j + q_0 y_j - q_x z_j & \dfrac{\partial f_z}{\partial \lambda} = -q_y x_j + q_x y_j + q_0 z_j \end{array} \tag{A.8}$$

$$\begin{array}{llll} \dfrac{\partial g}{\partial q_0} = 2q_0 & \dfrac{\partial g}{\partial q_x} = 2q_x & \dfrac{\partial g}{\partial q_y} = 2q_y & \dfrac{\partial g}{\partial q_z} = 2q_z \\ \dfrac{\partial g}{\partial T_x} = 0 & \dfrac{\partial g}{\partial T_y} = 0 & \dfrac{\partial g}{\partial T_z} = 0 & \dfrac{\partial g}{\partial \lambda} = 0 \end{array} \tag{A.9}$$

The structure of the condition matrix $\mathbf{B}$ is as follows:

$$\underset{(n\times b)}{\mathbf{B}^T} = \left[\begin{array}{ccccccc|c}
\partial f_{x_1}/\partial x_{1_i} & \partial f_{y_1}/\partial x_{1_i} & \partial f_{z_1}/\partial x_{1_i} & \cdots & 0 & 0 & 0 & 0 \\
\partial f_{x_1}/\partial y_{1_i} & \partial f_{y_1}/\partial y_{1_i} & \partial f_{z_1}/\partial y_{1_i} & \cdots & 0 & 0 & 0 & 0 \\
\partial f_{x_1}/\partial z_{1_i} & \partial f_{y_1}/\partial z_{1_i} & \partial f_{z_1}/\partial z_{1_i} & \cdots & 0 & 0 & 0 & 0 \\
\vdots & \vdots & \vdots & \ddots & \vdots & \vdots & \vdots & \vdots \\
0 & 0 & 0 & \cdots & \partial f_{x_p}/\partial x_{p_i} & \partial f_{y_p}/\partial x_{p_i} & \partial f_{z_p}/\partial x_{p_i} & 0 \\
0 & 0 & 0 & \cdots & \partial f_{x_p}/\partial y_{p_i} & \partial f_{y_p}/\partial y_{p_i} & \partial f_{z_p}/\partial y_{p_i} & 0 \\
0 & 0 & 0 & \cdots & \partial f_{x_p}/\partial z_{p_i} & \partial f_{y_p}/\partial z_{p_i} & \partial f_{z_p}/\partial z_{p_i} & 0 \\
\hline
\partial f_{x_1}/\partial x_{1_j} & \partial f_{y_1}/\partial x_{1_j} & \partial f_{z_1}/\partial x_{1_j} & \cdots & 0 & 0 & 0 & 0 \\
\partial f_{x_1}/\partial y_{1_j} & \partial f_{y_1}/\partial y_{1_j} & \partial f_{z_1}/\partial y_{1_j} & \cdots & 0 & 0 & 0 & 0 \\
\partial f_{x_1}/\partial z_{1_j} & \partial f_{y_1}/\partial z_{1_j} & \partial f_{z_1}/\partial z_{1_j} & \cdots & 0 & 0 & 0 & 0 \\
\vdots & \vdots & \vdots & \ddots & \vdots & \vdots & \vdots & \vdots \\
0 & 0 & 0 & \cdots & \partial f_{x_p}/\partial x_{p_j} & \partial f_{y_p}/\partial x_{p_j} & \partial f_{z_p}/\partial x_{p_j} & 0 \\
0 & 0 & 0 & \cdots & \partial f_{x_p}/\partial y_{p_j} & \partial f_{y_p}/\partial y_{p_j} & \partial f_{z_p}/\partial y_{p_j} & 0 \\
0 & 0 & 0 & \cdots & \partial f_{x_p}/\partial z_{p_j} & \partial f_{y_p}/\partial z_{p_j} & \partial f_{z_p}/\partial z_{p_j} & 0 \\
0 & 0 & 0 & \cdots & 0 & 0 & 0 & \partial g/\partial l_{\|\tilde{q}\|}
\end{array}\right] \tag{A.10}$$

with the following partial derivatives:

$$\begin{array}{lll}
\dfrac{\partial f_x}{\partial x_i} = -q_0 & \dfrac{\partial f_y}{\partial x_i} = q_z & \dfrac{\partial f_z}{\partial x_i} = -q_y \\
\dfrac{\partial f_x}{\partial y_i} = -q_z & \dfrac{\partial f_y}{\partial y_i} = -q_0 & \dfrac{\partial f_z}{\partial y_i} = q_x \\
\dfrac{\partial f_x}{\partial z_i} = q_y & \dfrac{\partial f_y}{\partial z_i} = -q_x & \dfrac{\partial f_z}{\partial z_i} = -q_0 \\
\dfrac{\partial f_x}{\partial x_j} = \lambda \cdot q_0 & \dfrac{\partial f_y}{\partial x_j} = \lambda \cdot q_z & \dfrac{\partial f_z}{\partial x_j} = -\lambda \cdot q_y \\
\dfrac{\partial f_x}{\partial y_j} = -\lambda \cdot q_z & \dfrac{\partial f_y}{\partial y_j} = \lambda \cdot q_0 & \dfrac{\partial f_z}{\partial y_j} = \lambda \cdot q_x \\
\dfrac{\partial f_x}{\partial z_j} = \lambda \cdot q_y & \dfrac{\partial f_y}{\partial z_j} = -\lambda \cdot q_x & \dfrac{\partial f_z}{\partial z_j} = \lambda \cdot q_0
\end{array} \tag{A.11}$$

$$\frac{\partial g}{\partial l_{\|\tilde{q}\|}} = -1 \tag{A.12}$$

A.3 Error propagation for derivation of deformations from coordinates and transformation parameters

For the coordinate vector $\vec{x}_j$ consisting of the coordinates of the p network points in the system of epoch j, the transformation into the system of epoch i can be accomplished according to (3.27), yielding the transformed coordinate vector $\vec{x}_j^{tr}$. Formally, this can be expressed by:

$$\vec{x}_j^{tr} = \mathbf{F}_1^T \vec{y} \qquad \text{with } \mathbf{F}_1 = \frac{\partial \vec{x}_j^{tr}}{\partial \vec{y}} \text{ and } \vec{y} = \begin{pmatrix} \vec{x}_j^T & \vec{x}_{TP}^T \end{pmatrix}^T \tag{A.13}$$

where $\vec{x}_{TP}$ is the vector of the adjusted transformation parameters. The functional matrix $\mathbf{F}_1$ has the following structure:

$$\underset{(3p+8)\times 3p}{\mathbf{F}_1} = \left[\begin{array}{ccccccc}
\partial x_{1_j}^{tr}/\partial x_{1_j} & \partial y_{1_j}^{tr}/\partial x_{1_j} & \partial z_{1_j}^{tr}/\partial x_{1_j} & \cdots & 0 & 0 & 0 \\
\partial x_{1_j}^{tr}/\partial y_{1_j} & \partial y_{1_j}^{tr}/\partial y_{1_j} & \partial z_{1_j}^{tr}/\partial y_{1_j} & \cdots & 0 & 0 & 0 \\
\partial x_{1_j}^{tr}/\partial z_{1_j} & \partial y_{1_j}^{tr}/\partial z_{1_j} & \partial z_{1_j}^{tr}/\partial z_{1_j} & \cdots & 0 & 0 & 0 \\
\vdots & \vdots & \vdots & \ddots & \vdots & \vdots & \vdots \\
0 & 0 & 0 & \cdots & \partial x_{p_j}^{tr}/\partial x_{p_j} & \partial y_{p_j}^{tr}/\partial x_{p_j} & \partial z_{p_j}^{tr}/\partial x_{p_j} \\
0 & 0 & 0 & \cdots & \partial x_{p_j}^{tr}/\partial y_{p_j} & \partial y_{p_j}^{tr}/\partial y_{p_j} & \partial z_{p_j}^{tr}/\partial y_{p_j} \\
0 & 0 & 0 & \cdots & \partial x_{p_j}^{tr}/\partial z_{p_j} & \partial y_{p_j}^{tr}/\partial z_{p_j} & \partial z_{p_j}^{tr}/\partial z_{p_j} \\
\hline
\partial x_{1_j}^{tr}/\partial q_0 & \partial y_{1_j}^{tr}/\partial q_0 & \partial z_{1_j}^{tr}/\partial q_0 & \cdots & \partial x_{p_j}^{tr}/\partial q_0 & \partial y_{p_j}^{tr}/\partial q_0 & \partial z_{p_j}^{tr}/\partial q_0 \\
\partial x_{1_j}^{tr}/\partial q_x & \partial y_{1_j}^{tr}/\partial q_x & \partial z_{1_j}^{tr}/\partial q_x & \cdots & \partial x_{p_j}^{tr}/\partial q_x & \partial y_{p_j}^{tr}/\partial q_x & \partial z_{p_j}^{tr}/\partial q_x \\
\partial x_{1_j}^{tr}/\partial q_y & \partial y_{1_j}^{tr}/\partial q_y & \partial z_{1_j}^{tr}/\partial q_y & \cdots & \partial x_{p_j}^{tr}/\partial q_y & \partial y_{p_j}^{tr}/\partial q_y & \partial z_{p_j}^{tr}/\partial q_y \\
\partial x_{1_j}^{tr}/\partial q_z & \partial y_{1_j}^{tr}/\partial q_z & \partial z_{1_j}^{tr}/\partial q_z & \cdots & \partial x_{p_j}^{tr}/\partial q_z & \partial y_{p_j}^{tr}/\partial q_z & \partial z_{p_j}^{tr}/\partial q_z \\
\partial x_{1_j}^{tr}/\partial T_x & \partial y_{1_j}^{tr}/\partial T_x & \partial z_{1_j}^{tr}/\partial T_x & \cdots & \partial x_{p_j}^{tr}/\partial T_x & \partial y_{p_j}^{tr}/\partial T_x & \partial z_{p_j}^{tr}/\partial T_x \\
\partial x_{1_j}^{tr}/\partial T_y & \partial y_{1_j}^{tr}/\partial T_y & \partial z_{1_j}^{tr}/\partial T_y & \cdots & \partial x_{p_j}^{tr}/\partial T_y & \partial y_{p_j}^{tr}/\partial T_y & \partial z_{p_j}^{tr}/\partial T_y \\
\partial x_{1_j}^{tr}/\partial T_z & \partial y_{1_j}^{tr}/\partial T_z & \partial z_{1_j}^{tr}/\partial T_z & \cdots & \partial x_{p_j}^{tr}/\partial T_z & \partial y_{p_j}^{tr}/\partial T_z & \partial z_{p_j}^{tr}/\partial T_z \\
\partial x_{1_j}^{tr}/\partial \lambda & \partial y_{1_j}^{tr}/\partial \lambda & \partial z_{1_j}^{tr}/\partial \lambda & \cdots & \partial x_{p_j}^{tr}/\partial \lambda & \partial y_{p_j}^{tr}/\partial \lambda & \partial z_{p_j}^{tr}/\partial \lambda
\end{array}\right] \tag{A.14}$$

with the partial derivatives:

$$\begin{array}{lll}
\frac{\partial x_j^{tr}}{\partial x_j} = \lambda - 2\lambda\left(q_y^2 + q_z^2\right) & \frac{\partial y_j^{tr}}{\partial x_j} = 2\lambda\left(q_x q_y - q_0 q_z\right) & \frac{\partial z_j^{tr}}{\partial x_j} = 2\lambda\left(q_x q_z - q_0 q_y\right) \\
\frac{\partial x_j^{tr}}{\partial y_j} = 2\lambda\left(q_x q_y - q_0 q_z\right) & \frac{\partial y_j^{tr}}{\partial y_j} = \lambda - 2\lambda\left(q_x^2 + q_z^2\right) & \frac{\partial z_j^{tr}}{\partial y_j} = 2\lambda\left(q_y q_z - q_0 q_x\right) \\
\frac{\partial x_j^{tr}}{\partial z_j} = 2\lambda\left(q_x q_z - q_0 q_y\right) & \frac{\partial y_j^{tr}}{\partial z_j} = 2\lambda\left(q_y q_z - q_0 q_x\right) & \frac{\partial z_j^{tr}}{\partial z_j} = \lambda - 2\lambda\left(q_x^2 + q_y^2\right)
\end{array} \tag{A.15}$$

$$\begin{array}{lll}
\frac{\partial x_j^{tr}}{\partial q_0} = 2\lambda\left(q_0 x_j - q_z y_j + q_y z_j\right) & \frac{\partial y_j^{tr}}{\partial q_0} = 2\lambda\left(q_z x_j + q_0 y_j - q_x z_j\right) & \frac{\partial z_j^{tr}}{\partial q_0} = 2\lambda\left(-q_y x_j + q_x y_j + q_0 z_j\right) \\
\frac{\partial x_j^{tr}}{\partial q_x} = 2\lambda\left(q_x x_j + q_y y_j + q_z z_j\right) & \frac{\partial y_j^{tr}}{\partial q_x} = 2\lambda\left(q_y x_j - q_x y_j - q_0 z_j\right) & \frac{\partial z_j^{tr}}{\partial q_x} = 2\lambda\left(q_z x_j + q_0 y_j - q_x z_j\right) \\
\frac{\partial x_j^{tr}}{\partial q_y} = 2\lambda\left(-q_y x_j + q_x y_j + q_0 z_j\right) & \frac{\partial y_j^{tr}}{\partial q_y} = 2\lambda\left(q_x x_j + q_y y_j + q_z z_j\right) & \frac{\partial z_j^{tr}}{\partial q_y} = 2\lambda\left(-q_0 x_j + q_z y_j - q_y z_j\right) \\
\frac{\partial x_j^{tr}}{\partial q_z} = 2\lambda\left(-q_z x_j - q_0 y_j + q_x z_j\right) & \frac{\partial y_j^{tr}}{\partial q_z} = 2\lambda\left(q_0 x_j - q_z y_j + q_y z_j\right) & \frac{\partial z_j^{tr}}{\partial q_z} = 2\lambda\left(q_x x_j + q_y y_j + q_z z_j\right) \\
\frac{\partial x_j^{tr}}{\partial T_x} = 1 & \frac{\partial y_j^{tr}}{\partial T_x} = 0 & \frac{\partial z_j^{tr}}{\partial T_x} = 0 \\
\frac{\partial x_j^{tr}}{\partial T_y} = 0 & \frac{\partial y_j^{tr}}{\partial T_y} = 1 & \frac{\partial z_j^{tr}}{\partial T_y} = 0 \\
\frac{\partial x_j^{tr}}{\partial T_z} = 0 & \frac{\partial y_j^{tr}}{\partial T_z} = 0 & \frac{\partial z_j^{tr}}{\partial T_z} = 1
\end{array} \tag{A.16}$$

$$\begin{aligned}
\frac{\partial x_j^{tr}}{\partial \lambda} &= q_y\left(-q_y x_j + q_x y_j + q_0 z_j\right) - q_z\left(q_z x_j + q_0 y_j - q_x z_j\right) + q_0\left(q_0 x_j - q_z y_j + q_y z_j\right) \\
&\quad -q_x\left(-q_x x_j - q_y y_j - q_z z_j\right) \\
\frac{\partial y_j^{tr}}{\partial \lambda} &= -q_x\left(-q_y x_j + q_x y_j + q_0 z_j\right) + q_0\left(q_z x_j + q_0 y_j - q_x z_j\right) + q_z\left(q_0 x_j - q_z y_j + q_y z_j\right) \\
&\quad -q_y\left(-q_x x_j - q_y y_j - q_z z_j\right) \\
\frac{\partial y_j^{tr}}{\partial \lambda} &= q_0\left(-q_y x_j + q_x y_j + q_0 z_j\right) + q_x\left(q_z x_j + q_0 y_j - q_x z_j\right) - q_y\left(q_0 x_j - q_z y_j + q_y z_j\right) \\
&\quad -q_z\left(-q_x x_j - q_y y_j - q_z z_j\right) \ .
\end{aligned} \tag{A.17}$$

Now the cofactor matrix of the transformed coordinates $\vec{x}_j^{tr}$ from epoch j to the system of epoch i can be determined from:

$$\underset{(3p\times 3p)}{\mathbf{Q}_{xx_j^{tr}}} = \underset{3p\times(3p+8)}{\mathbf{F}_1^T} \cdot \underset{(3p+8)\times(3p+8)}{\mathbf{Q}_{yy}} \cdot \underset{(3p+8)\times 3p}{\mathbf{F}_1} \quad \text{with} \quad \underset{(3p+8)\times(3p+8)}{\mathbf{Q}_{yy}} = \begin{bmatrix} \underset{(3p\times 3p)}{\mathbf{Q}_{xx_j}} & 0 \\ 0 & \underset{(8\times 8)}{\mathbf{Q}_{xx_{TP}}} \end{bmatrix} . \tag{A.18}$$

With the coordinates $\vec{x}_i$ of epoch i and the transformed coordinates $\vec{x}_j^{tr}$ of epoch j in the system of epoch i and their corresponding cofactor matrices $\mathbf{Q}_{xx_i}$ and $\mathbf{Q}_{xx_j^{tr}}$, the deformations $\vec{d}_{ij}$ can be derived according to (3.28). The cofactor matrix of the deformations $\mathbf{Q}_{dd_{ij}}$ is given by:

$$\underset{(3p\times 3p)}{\mathbf{Q}_{dd_{ij}}} = \underset{(3p\times 3p)}{\mathbf{Q}_{xx_i}} + \underset{(3p\times 3p)}{\mathbf{Q}_{xx_j^{tr}}} \quad . \tag{A.19}$$

A.4 Design and condition matrices for multiple-epoch comparison

In a multiple-epoch comparison of m epochs and $t = m - 1$ transformations from epoch $2 \ldots m$ to the base epoch 1, the design matrix $\mathbf{A}$ has the following structure:

$$\underset{(b\times u)}{\mathbf{A}} = \begin{bmatrix} \mathbf{A}_1 = \begin{bmatrix} \partial\vec{f}_1 \big/ \partial\vec{x}_{TP_1} \\ \partial g_1 / \partial\vec{x}_{TP_2} \end{bmatrix} & \cdots & 0 \\ \vdots & \ddots & \vdots \\ 0 & \cdots & \mathbf{A}_t = \begin{bmatrix} \partial\vec{f}_t \big/ \partial\vec{x}_{TP_t} \\ \partial g_t / \partial\vec{x}_{TP_t} \end{bmatrix} \end{bmatrix} \tag{A.20}$$

where each of the sub-matrices $\mathbf{A}_k$ with $k = 1 \ldots t$ and their partial derivatives are identical to the design matrix of a two-epoch comparison as shown in Appendix A.2.

In a multiple epoch comparison of m epochs and with $t = m-1$ transformations the condition matrix $\mathbf{B}$ has the following structure:

$$\underset{(n\times b)}{\mathbf{B}^T} = \begin{array}{c} \\ \vec{x}_1 \\ \vec{x}_2 \\ \vdots \\ \vec{x}_{k+1} \\ \vdots \\ \vec{x}_m \\ \hline l_{\|\tilde{q}\|_1} \\ \vdots \\ l_{\|\tilde{q}\|_k} \\ \vdots \\ l_{\|\tilde{q}\|_t} \end{array} \begin{array}{c} \begin{array}{cccccccc} \vec{f}_1 & g_1 & \cdots & \vec{f}_k & g_k & \cdots & \vec{f}_t & g_t \end{array} \\ \left[\begin{array}{cccccccc} \mathbf{B}_{1_1} & 0 & \cdots & \mathbf{B}_{1_k} & 0 & \cdots & \mathbf{B}_{1_t} & 0 \\ \mathbf{B}_1 & 0 & \cdots & 0 & 0 & \cdots & 0 & 0 \\ \vdots & \vdots & \ddots & \vdots & \vdots & \ddots & \vdots & \vdots \\ 0 & 0 & \cdots & \mathbf{B}_k & 0 & \cdots & 0 & 0 \\ \vdots & \vdots & \ddots & \vdots & \vdots & \ddots & \vdots & \vdots \\ 0 & 0 & \cdots & 0 & 0 & \cdots & \mathbf{B}_t & 0 \\ \hline 0 & -1 & \cdots & 0 & 0 & \cdots & 0 & 0 \\ \vdots & \vdots & \ddots & \vdots & \vdots & \ddots & \vdots & \vdots \\ 0 & 0 & \cdots & 0 & -1 & \cdots & 0 & 0 \\ \vdots & \vdots & \ddots & \vdots & \vdots & \ddots & \vdots & \vdots \\ 0 & 0 & \cdots & 0 & 0 & \cdots & 0 & -1 \end{array}\right] \end{array} . \tag{A.21}$$

The sub-matrices $\mathbf{B}_{1_k}$ for $k = 1 \ldots t$ contain the partial derivatives of the conditions $\vec{f}_k$ for the transformation of epoch $k+1$ to the base epoch 1 with respect to the coordinates of the target system (base epoch) 1:

$$\mathbf{B}_{1_k} = \frac{\partial \vec{f}_k}{\partial \vec{x}_1} = \begin{bmatrix} \partial f^k_{x_1}/\partial x_{1_1} & \partial f^k_{y_1}/\partial x_{1_1} & \partial f^k_{z_1}/\partial x_{1_1} & \cdots & 0 & 0 & 0 \\ \partial f^k_{x_1}/\partial y_{1_1} & \partial f^k_{y_1}/\partial y_{1_1} & \partial f^k_{z_1}/\partial y_{1_1} & \cdots & 0 & 0 & 0 \\ \partial f^k_{x_1}/\partial z_{1_1} & \partial f^k_{y_1}/\partial z_{1_1} & \partial f^k_{z_1}/\partial z_{1_1} & \cdots & 0 & 0 & 0 \\ \vdots & \vdots & \vdots & \ddots & \vdots & \vdots & \vdots \\ 0 & 0 & 0 & \cdots & \partial f^k_{x_p}\big/\partial x_{p_1} & \partial f^k_{y_p}\big/\partial x_{p_1} & \partial f^k_{z_p}\big/\partial x_{p_1} \\ 0 & 0 & 0 & \cdots & \partial f^k_{x_p}\big/\partial y_{p_1} & \partial f^k_{y_p}\big/\partial y_{p_1} & \partial f^k_{z_p}\big/\partial y_{p_1} \\ 0 & 0 & 0 & \cdots & \partial f^k_{x_p}\big/\partial z_{p_1} & \partial f^k_{y_p}\big/\partial z_{p_1} & \partial f^k_{z_p}\big/\partial z_{p_1} \end{bmatrix} \tag{A.22}$$

with the following partial derivatives:

$$\begin{array}{lll} \frac{\partial f^k_x}{\partial x_1} = -q_0 & \frac{\partial f^k_y}{\partial x_1} = q_z & \frac{\partial f^k_z}{\partial x_1} = -q_y \\ \frac{\partial f^k_x}{\partial y_1} = -q_z & \frac{\partial f^k_y}{\partial y_1} = -q_0 & \frac{\partial f^k_z}{\partial y_1} = q_x \\ \frac{\partial f^k_x}{\partial z_1} = q_y & \frac{\partial f^k_y}{\partial z_1} = -q_x & \frac{\partial f^k_z}{\partial z_1} = -q_0 \end{array} \tag{A.23}$$

The sub-matrices $\mathbf{B}_k$ for $k = 1 \ldots t$ contain the partial derivatives of the conditions $\vec{f}_k$ for the transformation of epoch $k+1$ to the base epoch 1 with respect to the coordinates of the source system (epoch $k+1$):

$$\mathbf{B}_k = \frac{\partial \vec{f}_k}{\partial \vec{x}_{k+1}}$$

$$\mathbf{B}_k = \begin{bmatrix} \partial f^k_{x_1}/\partial x_{1_{k+1}} & \partial f^k_{y_1}/\partial x_{1_{k+1}} & \partial f^k_{z_1}/\partial x_{1_{k+1}} & \cdots & 0 & 0 & 0 \\ \partial f^k_{x_1}/\partial y_{1_{k+1}} & \partial f^k_{y_1}/\partial y_{1_{k+1}} & \partial f^k_{z_1}/\partial y_{1_{k+1}} & \cdots & 0 & 0 & 0 \\ \partial f^k_{x_1}/\partial z_{1_{k+1}} & \partial f^k_{y_1}/\partial z_{1_{k+1}} & \partial f^k_{z_1}/\partial z_{1_{k+1}} & \cdots & 0 & 0 & 0 \\ \vdots & \vdots & \vdots & \ddots & \vdots & \vdots & \vdots \\ 0 & 0 & 0 & \cdots & \partial f^k_{x_p}\big/\partial x_{p_{k+1}} & \partial f^k_{y_p}\big/\partial x_{p_{k+1}} & \partial f^k_{z_p}\big/\partial x_{p_{k+1}} \\ 0 & 0 & 0 & \cdots & \partial f^k_{x_p}\big/\partial y_{p_{k+1}} & \partial f^k_{y_p}\big/\partial y_{p_{k+1}} & \partial f^k_{z_p}\big/\partial y_{p_{k+1}} \\ 0 & 0 & 0 & \cdots & \partial f^k_{x_p}\big/\partial z_{p_{k+1}} & \partial f^k_{y_p}\big/\partial z_{p_{k+1}} & \partial f^k_{z_p}\big/\partial z_{p_{k+1}} \end{bmatrix} \tag{A.24}$$

with the following partial derivatives:

$$\begin{array}{lll} \frac{\partial f^k_x}{\partial x_{k+1}} = \lambda \cdot q_0 & \frac{\partial f^k_y}{\partial x_{k+1}} = \lambda \cdot q_z & \frac{\partial f^k_z}{\partial x_{k+1}} = -\lambda \cdot q_y \\ \frac{\partial f^k_x}{\partial y_{k+1}} = -\lambda \cdot q_z & \frac{\partial f^k_y}{\partial y_{k+1}} = \lambda \cdot q_0 & \frac{\partial f^k_z}{\partial y_{k+1}} = \lambda \cdot q_x \\ \frac{\partial f^k_x}{\partial z_{k+1}} = \lambda \cdot q_y & \frac{\partial f^k_y}{\partial z_{k+1}} = -\lambda \cdot q_x & \frac{\partial f^k_z}{\partial z_{k+1}} = \lambda \cdot q_0 \end{array} \tag{A.25}$$

Appendix B

B.1 Scenario A: adjusted coordinates and standard deviations after network analysis for epochs 1 to 5

Point	x [m]	y [m]	z [m]	$\hat{\sigma}_x$ [mm]	$\hat{\sigma}_y$ [mm]	$\hat{\sigma}_z$ [mm]
101	10922.229	5081.200	97.135	±3.0	±2.6	±3.8
102	10836.930	5332.831	98.227	±1.6	±1.4	±1.7
103	10947.371	5568.027	101.060	±2.8	±2.8	±3.5
104	10873.497	5786.001	103.964	±3.0	±2.4	±3.2
105	10748.029	5481.271	96.702	±2.6	±2.3	±2.4
106	10687.767	5474.069	99.646	±2.6	±2.2	±2.3
107	10714.329	5544.369	105.578	±2.6	±2.2	±2.3
108	10739.428	5710.701	98.082	±1.6	±1.3	±1.7
109	10526.474	5804.631	101.347	±3.0	±2.6	±3.8
110	10575.931	5539.329	104.209	±1.5	±1.4	±1.6
111	10712.205	5171.499	100.819	±1.8	±1.3	±2.0
112	10526.469	5028.831	99.561	±3.0	±2.6	±4.3

Table B.1: Scenario A: adjusted coordinates and standard deviations of epoch 1

Point	x [m]	y [m]	z [m]	$\hat{\sigma}_x$ [mm]	$\hat{\sigma}_y$ [mm]	$\hat{\sigma}_z$ [mm]
101	10922.231	5081.205	97.129	±3.2	±2.8	±4.1
102	10836.929	5332.828	98.231	±1.7	±1.5	±1.8
103	10947.368	5568.029	101.057	±3.0	±3.0	±3.8
104	10873.499	5786.003	103.959	±3.2	±2.6	±3.5
105	10748.026	5481.267	96.698	±2.9	±2.5	±2.7
106	10687.769	5474.070	99.652	±2.9	±2.4	±2.5
107	10714.329	5544.367	105.578	±2.8	±2.3	±2.5
108	10739.431	5710.701	98.079	±1.8	±1.4	±1.8
109	10526.473	5804.631	101.356	±3.3	±2.8	±4.1
110	10575.934	5539.329	104.209	±1.6	±1.6	±1.8
111	10712.200	5171.501	100.821	±2.0	±1.4	±2.2
112	10526.469	5028.828	99.562	±3.3	±2.8	±4.7

Table B.2: Scenario A: adjusted coordinates and standard deviations of epoch 2

Point	x [m]	y [m]	z [m]	$\hat{\sigma}_x$ [mm]	$\hat{\sigma}_y$ [mm]	$\hat{\sigma}_z$ [mm]
101	10922.231	5081.204	97.133	±2.8	±2.4	±3.6
102	10836.912	5332.853	98.224	±1.5	±1.3	±1.6
103	10947.371	5568.025	101.066	±2.6	±2.6	±3.3
104	10873.497	5786.007	103.962	±2.8	±2.3	±3.1
105	10748.049	5481.253	96.696	±2.5	±2.2	±2.3
106	10687.767	5474.075	99.652	±2.5	±2.1	±2.2
107	10714.330	5544.369	105.582	±2.5	±2.0	±2.2
108	10739.439	5710.677	98.067	±1.5	±1.2	±1.6
109	10526.464	5804.633	101.348	±2.9	±2.4	±3.6
110	10575.931	5539.332	104.212	±1.4	±1.4	±1.5
111	10712.195	5171.503	100.825	±1.7	±1.2	±1.9
112	10526.474	5028.831	99.562	±2.9	±2.4	±4.1

Table B.3: Scenario A: adjusted coordinates and standard deviations of epoch 3

Point	x [m]	y [m]	z [m]	$\hat{\sigma}_x$ [mm]	$\hat{\sigma}_y$ [mm]	$\hat{\sigma}_z$ [mm]
101	10922.234	5081.207	97.140	±2.9	±2.5	±3.7
102	10836.900	5332.871	98.220	±1.6	±1.3	±1.6
103	10947.368	5568.044	101.069	±2.7	±2.7	±3.4
104	10873.484	5786.009	103.968	±2.9	±2.3	±3.2
105	10748.062	5481.249	96.690	±2.6	±2.2	±2.4
106	10687.783	5474.047	99.653	±2.6	±2.1	±2.3
107	10714.322	5544.374	105.588	±2.5	±2.1	±2.3
108	10739.454	5710.658	98.061	±1.6	±1.2	±1.7
109	10526.471	5804.612	101.344	±3.0	±2.5	±3.7
110	10575.924	5539.330	104.219	±1.5	±1.4	±1.6
111	10712.204	5171.503	100.828	±1.8	±1.3	±1.9
112	10526.454	5028.856	99.549	±3.0	±2.5	±4.2

Table B.4: Scenario A: adjusted coordinates and standard deviations of epoch 4

Point	x [m]	y [m]	z [m]	$\hat{\sigma}_x$ [mm]	$\hat{\sigma}_y$ [mm]	$\hat{\sigma}_z$ [mm]
101	10922.223	5081.219	97.149	±2.9	±2.5	±3.7
102	10836.963	5332.876	98.220	±1.6	±1.4	±1.7
103	10947.381	5568.054	101.063	±2.7	±2.7	±3.5
104	10873.480	5786.012	103.976	±2.9	±2.4	±3.2
105	10748.064	5481.244	96.691	±2.6	±2.3	±2.4
106	10687.796	5474.049	99.642	±2.6	±2.1	±2.3
107	10714.295	5544.355	105.589	±2.6	±2.1	±2.3
108	10739.465	5710.651	98.061	±1.6	±1.2	±1.7
109	10526.467	5804.597	101.350	±3.0	±2.5	±3.7
110	10575.900	5539.318	104.214	±1.5	±1.4	±1.6
111	10712.193	5171.510	100.839	±1.8	±1.3	±2.0
112	10526.433	5028.874	99.536	±3.0	±2.5	±4.2

Table B.5: Scenario A: adjusted coordinates and standard deviations of epoch 5

B.2 Scenario A: Candidates for largest congruent point group from MSS-method using distance ratios and statistical evaluation

Epoch 4

Candidate	$\hat{\sigma}_0$	Redundancy	T_{χ^2}	Test outcome
101, 103, 104, 106, 109, 111	±2.795876	11	85.99	fail
101, 103, 104, 106, 109, 112	±3.273539	11	117.88	fail
101, 103, 104, 107, 109, 110	±1.925376	11	40.78	fail
101, 103, 104, 107, 109, 111	±1.889759	11	39.28	fail
101, 103, 104, 107, 109, 112	±2.423599	11	64.61	fail
101, 103, 104, 107, 110, 112	±1.934068	11	41.15	fail
101, 103, 104, 107, 111, 112	±2.093582	11	48.21	fail
101, 103, 104, 109, 110, 111	±2.021863	11	44.97	fail
101, 103, 104, 109, 110, 112	±2.651976	11	77.36	fail
101, 103, 104, 109, 111, 112	±2.587089	11	73.62	fail
101, 103, 104, 110, 111, 112	±2.173533	11	51.97	fail
101, 103, 107, 109, 110, 111	±2.017840	11	44.79	fail
101, 103, 107, 109, 110, 112	±2.580725	11	73.26	fail
101, 103, 107, 109, 111, 112	±2.577236	11	73.06	fail
101, 103, 107, 110, 111, 112	±2.100029	11	48.51	fail
101, 103, 109, 110, 111, 112	±2.727938	11	81.86	fail
101, 104, 107, 109, 110, 111	±1.834313	11	37.01	fail
101, 104, 107, 109, 110, 112	±2.480814	11	67.70	fail
101, 104, 107, 109, 111, 112	±2.478369	11	67.57	fail
101, 104, 107, 110, 111, 112	±2.048025	11	46.14	fail
101, 104, 108, 110, 111, 112	±7.677094	11	648.32	fail
101, 104, 109, 110, 111, 112	±2.611387	11	75.01	fail
101, 107, 109, 110, 111, 112	±2.467928	11	67.00	fail
103, 104, 106, 109, 111, 112	±3.356262	11	123.91	fail
103, 104, 107, 109, 110, 111	±1.972311	11	42.79	fail
103, 104, 107, 109, 110, 112	±2.427648	11	64.83	fail
103, 104, 107, 109, 111, 112	±2.562934	11	72.25	fail
103, 104, 107, 110, 111, 112	±2.130690	11	49.94	fail
103, 104, 109, 110, 111, 112	±2.717767	11	81.25	fail
103, 107, 109, 110, 111, 112	±2.638031	11	76.55	fail
104, 107, 109, 110, 111, 112	±2.505584	11	69.06	fail

Table B.6: Scenario A: candidates of six points and statistical test for epoch 4

Epoch 5

Candidate	$\hat{\sigma}_0$	Redundancy	T_{χ^2}	Test outcome
101, 102, 104, 109	±6.537849	5	213.72	fail
101, 102, 107, 110	±9.145285	5	418.18	fail
101, 103, 104, 109	±3.991700	5	79.67	fail
101, 103, 104, 111	±2.916361	5	42.53	fail
101, 103, 104, 112	±3.624380	5	65.68	fail
101, 103, 109, 111	±5.123925	5	131.27	fail
101, 103, 111, 112	±4.674301	5	109.25	fail
101, 104, 106, 109	±4.564026	5	104.15	fail
101, 104, 106, 111	±5.661140	5	160.24	fail
101, 104, 109, 111	±3.781701	5	71.51	fail
101, 104, 110, 111	±3.466943	5	60.10	fail
101, 104, 111, 112	±4.402490	5	96.91	fail
101, 106, 109, 111	±4.539636	5	103.04	fail
101, 107, 109, 110	±3.464338	5	60.01	fail
101, 107, 109, 111	±2.422434	5	29.34	fail
101, 107, 110, 111	±2.212606	5	24.48	fail
101, 109, 110, 111	±3.599707	5	64.79	fail
102, 103, 104, 109	±1.958538	5	19.18	fail
103, 104, 105, 106	±2.356033	5	27.75	fail
103, 104, 105, 109	±2.789195	5	38.90	fail
103, 104, 105, 112	±7.451246	5	277.61	fail
103, 104, 106, 109	±1.743114	5	15.19	fail
103, 104, 106, 112	±6.705478	5	224.82	fail
103, 104, 109, 111	±5.374912	5	144.45	fail
103, 104, 109, 112	±5.982987	5	178.98	fail
103, 104, 111, 112	±5.017315	5	125.87	fail
103, 105, 106, 109	±2.851010	5	40.64	fail
103, 106, 109, 112	±7.029241	5	247.05	fail

Table B.7: Scenario A: candidates of four points and statistical test for epoch 5

Candidate	$\hat{\sigma}_0$	Redundancy	T_{χ^2}	Test outcome
104, 105, 106, 109	±2.324588	5	27.02	fail
104, 106, 108, 111	±10.096690	5	509.72	fail
104, 106, 108, 112	±10.390932	5	539.86	fail
104, 106, 109, 111	±5.991099	5	179.47	fail
104, 106, 109, 112	±6.591458	5	217.24	fail
104, 106, 111, 112	±6.029988	5	181.80	fail
104, 108, 111, 112	±10.357596	5	536.40	fail
104, 109, 111, 112	±5.515072	5	152.08	fail
105, 108, 111, 112	±3.657526	5	66.89	fail
106, 107, 108, 112	±5.894474	5	173.72	fail
106, 108, 111, 112	±3.043597	5	46.32	fail
106, 109, 111, 112	±5.755020	5	165.60	fail
107, 109, 110, 111	±2.995121	5	44.85	fail
107, 109, 110, 112	±1.613215	5	13.01	fail
107, 109, 111, 112	±4.095904	5	83.88	fail
107, 110, 111, 112	±4.652050	5	108.21	fail
109, 110, 111, 112	±4.517620	5	102.04	fail

Scenario A: candidates of four points and statistical test for epoch 5 [continued]

Candidate	$\hat{\sigma}_0$	Redundancy	T_{χ^2}	Test outcome
101, 102, 104	±8.748508	2	153.07	fail
101, 102, 107	±13.620816	2	371.05	fail
101, 102, 109	±9.871276	2	194.88	fail
101, 102, 110	±12.263941	2	300.81	fail
101, 102, 112	±3.787959	2	28.70	fail
101, 103, 104	±3.666498	2	26.89	fail
101, 103, 109	±5.863621	2	68.76	fail
101, 103, 111	±2.833258	2	16.05	fail
101, 103, 112	±1.792092	2	6.42	fail
101, 104, 106	±6.867610	2	94.33	fail
101, 104, 108	±14.233649	2	405.19	fail
101, 104, 109	±4.557114	2	41.53	fail
101, 104, 110	±4.427026	2	39.20	fail
101, 104, 112	±3.995233	2	31.92	fail
101, 105, 108	±1.326597	2	3.52	pass
101, 106, 108	±1.197400	2	2.87	pass
101, 106, 109	±5.033671	2	50.68	fail
101, 106, 111	±5.167616	2	53.41	fail
101, 107, 108	±11.952548	2	285.73	fail
101, 107, 109	±3.163548	2	20.02	fail
101, 107, 110	±2.254367	2	10.16	fail

Table B.8: Scenario A: candidates of three points and statistical test for epoch 5

Candidate	$\hat{\sigma}_0$	Redundancy	T_{χ^2}	Test outcome
101, 107, 111	±2.626132	2	13.79	fail
101, 109, 110	±5.394422	2	58.20	fail
101, 109, 111	±2.553401	2	13.04	fail
101, 110, 111	±1.785842	2	6.38	fail
101, 111, 112	±4.521669	2	40.89	fail
102, 103, 104	±1.884607	2	7.10	fail
102, 103, 109	±3.027306	2	18.33	fail
102, 104, 109	±1.639191	2	5.37	pass
102, 106, 108	±7.510231	2	112.81	fail
102, 107, 109	±6.802490	2	92.55	fail
102, 107, 110	±7.710768	2	118.91	fail
103, 104, 105	±2.740523	2	15.02	fail
103, 104, 106	±1.196560	2	2.86	pass
103, 104, 109	±1.135231	2	2.58	pass
103, 104, 111	±4.239632	2	35.95	fail
103, 104, 112	±4.995687	2	49.91	fail
103, 105, 106	±3.403912	2	23.17	fail
103, 105, 109	±4.282837	2	36.69	fail
103, 105, 112	±10.257379	2	210.43	fail
103, 106, 109	±2.211954	2	9.79	fail
103, 106, 112	±9.640977	2	185.90	fail
103, 109, 111	±8.003352	2	128.11	fail
103, 109, 112	±9.160103	2	167.81	fail
103, 111, 112	±4.779765	2	45.69	fail
104, 105, 106	±2.821021	2	15.92	fail
104, 105, 109	±3.043551	2	18.53	fail
104, 105, 112	±10.342479	2	213.93	fail
104, 106, 108	±12.333960	2	304.25	fail
104, 106, 109	±1.640300	2	5.38	pass
104, 106, 111	±8.136498	2	132.41	fail
104, 106, 112	±9.471857	2	179.43	fail
104, 108, 111	±15.773915	2	497.63	fail
104, 108, 112	±16.317570	2	532.53	fail
104, 109, 111	±5.718845	2	65.41	fail
104, 109, 112	±7.182237	2	103.17	fail
104, 110, 111	±5.200990	2	54.10	fail
104, 111, 112	±5.017629	2	50.35	fail

Scenario A: candidates of three points and statistical test for epoch 5 [continued]

Candidate	$\hat{\sigma}_0$	Redundancy	T_{χ^2}	Test outcome
105, 106, 109	±2.119067	2	8.98	fail
105, 108, 111	±3.572505	2	25.53	fail
105, 108, 112	±4.525534	2	40.96	fail
105, 111, 112	±3.204609	2	20.54	fail
106, 107, 108	±7.482205	2	111.97	fail
106, 107, 112	±1.349942	2	3.64	pass
106, 108, 111	±1.594532	2	5.09	pass
106, 108, 112	±3.189289	2	20.34	fail
106, 109, 111	±6.563425	2	86.16	fail
106, 109, 112	±7.938848	2	126.05	fail
106, 111, 112	±3.470238	2	24.09	fail
107, 108, 111	±11.177592	2	249.88	fail
107, 108, 112	±7.149830	2	102.24	fail
107, 109, 110	±1.848122	2	6.83	fail
107, 109, 111	±2.349115	2	11.04	fail
107, 109, 112	±1.355051	2	3.67	pass
107, 110, 111	±2.258779	2	10.20	fail
107, 110, 112	±1.687271	2	5.69	pass
107, 111, 112	±5.810416	2	67.52	fail
108, 111, 112	±3.874961	2	30.03	fail
109, 110, 111	±4.547237	2	41.35	fail
109, 110, 112	±1.174018	2	2.76	pass
109, 111, 112	±5.097455	2	51.97	fail
110, 111, 112	±6.439910	2	82.94	fail

Scenario A: candidates of three points and statistical test for epoch 5 [continued]

B.3 Scenario A: Candidates for largest congruent point group from MSS-method using angles and statistical evaluation

Candidate	T_G	Test outcome
101, 103, 112	3.21	fail
101, 105, 106	3.16	fail
101, 105, 108	1.76	pass
101, 106, 108	0.80	pass
101, 107, 111	6.90	fail
101, 109, 111	6.56	fail
101, 110, 111	3.19	fail
102, 103, 104	3.55	fail
102, 104, 109	2.69	pass
102, 105, 107	75.45	fail
102, 105, 109	86.40	fail
103, 104, 106	1.43	pass
103, 104, 109	1.02	pass
104, 106, 109	2.69	pass
104, 107, 110	5.50	fail
104, 107, 112	41.13	fail
105, 106, 108	2.77	pass
105, 106, 109	4.49	fail
105, 106, 111	2.52	pass
105, 106, 112	1.78	pass
105, 111, 112	10.27	fail
106, 107, 112	1.82	pass
106, 108, 111	2.54	pass
107, 109, 110	3.42	fail
107, 109, 112	1.13	pass
107, 110, 112	2.85	pass
109, 110, 112	1.38	pass

Table B.9: Scenario A: candidates and test statistics for epoch 5

B.4 Scenario A: Adjusted coordinates and standard deviations from combined re-adjustment of observations

Point	x [m]	y [m]	z [m]	$\hat{\sigma}_x$ [mm]	$\hat{\sigma}_y$ [mm]	$\hat{\sigma}_z$ [mm]
101	10922.230	5081.203	97.132	±2.2	±1.9	±2.8
102	10836.930	5332.830	98.229	±1.2	±1.0	±1.2
103	10947.370	5568.028	101.059	±2.0	±2.0	±2.6
104	10873.498	5786.002	103.961	±2.2	±1.8	±2.4
105	10748.028	5481.269	96.700	±1.9	±1.7	±1.8
106	10687.768	5474.069	99.649	±1.9	±1.6	±1.7
107	10714.329	5544.368	105.578	±1.9	±1.6	±1.7
108	10739.429	5710.701	98.080	±1.2	±0.9	±1.2
109	10526.474	5804.631	101.351	±2.2	±1.9	±2.8
110	10575.932	5539.329	104.209	±1.1	±1.0	±1.2
111	10712.202	5171.500	100.820	±1.3	±0.9	±1.4
112	10526.469	5028.830	99.561	±2.2	±1.9	±3.1

Table B.10: Scenario A: adjusted coordinates and standard deviations for epoch 2

Point	x [m]	y [m]	z [m]	$\hat{\sigma}_x$ [mm]	$\hat{\sigma}_y$ [mm]	$\hat{\sigma}_z$ [mm]
101	10922.230	5081.201	97.133	±2.0	±1.7	±2.5
102	10836.931	5332.832	98.227	±1.8	±1.5	±1.9
103	10947.372	5568.025	101.062	±1.9	±1.8	±2.3
104	10873.498	5786.003	103.962	±2.0	±1.6	±2.2
105	10748.030	5481.272	96.702	±2.8	±2.4	±2.6
106	10687.767	5474.071	99.648	±1.8	±1.5	±1.6
107	10714.330	5544.369	105.579	±1.8	±1.4	±1.6
108	10739.428	5710.702	98.082	±1.8	±1.4	±1.7
109	10526.470	5804.632	101.346	±2.0	±1.7	±2.5
110	10575.931	5539.330	104.209	±1.0	±1.0	±1.1
111	10712.206	5171.500	100.819	±2.2	±1.4	±2.1
112	10526.472	5028.831	99.560	±1.9	±1.7	±2.8
302	10836.912	5332.850	98.221	±1.8	±1.5	±1.9
305	10748.050	5481.250	96.693	±2.8	±2.4	±2.6
308	10739.440	5710.674	98.065	±1.8	±1.4	±1.7
311	10712.194	5171.500	100.823	±2.2	±1.4	±2.1

Table B.11: Scenario A: adjusted coordinates and standard deviations for epoch 3

Point	x [m]	y [m]	z [m]	$\hat{\sigma}_x$ [mm]	$\hat{\sigma}_y$ [mm]	$\hat{\sigma}_z$ [mm]
101	10922.228	5081.198	97.133	±1.4	±1.7	±2.4
102	10836.929	5332.831	98.227	±1.8	±1.6	±1.9
103	10947.373	5568.031	101.060	±1.8	±1.8	±2.3
104	10873.498	5786.001	103.962	±1.7	±1.6	±2.1
105	10748.028	5481.272	96.702	±2.8	±2.5	±2.7
106	10687.766	5474.070	99.646	±2.8	±2.3	±2.4
107	10714.329	5544.370	105.578	±1.7	±1.4	±1.6
108	10739.428	5710.702	98.081	±2.0	±1.4	±1.8
109	10526.475	5804.633	101.347	±3.9	±3.0	±4.0
110	10575.931	5539.330	104.209	±1.1	±1.0	±1.2
111	10712.202	5171.499	100.819	±1.3	±0.9	±1.4
112	10526.467	5028.833	99.561	±4.1	±3.0	±4.5
402	10836.901	5332.864	98.211	±1.8	±1.6	±1.9
405	10748.068	5481.244	96.681	±2.8	±2.5	±2.7
406	10687.788	5474.045	99.644	±2.8	±2.3	±2.4
408	10739.465	5710.654	98.053	±2.0	±1.4	±1.8
409	10526.485	5804.613	101.335	±3.9	±3.0	±4.0
412	10526.447	5028.857	99.539	±4.1	±3.0	±4.5

Table B.12: Scenario A: adjusted coordinates and standard deviations for epoch 4

Point	x [m]	y [m]	z [m]	$\hat{\sigma}_x$ [mm]	$\hat{\sigma}_y$ [mm]	$\hat{\sigma}_z$ [mm]
101	10922.236	5081.205	97.136	±7.6	±5.4	±4.4
102	10836.934	5332.835	98.228	±3.6	±3.6	±2.3
103	10947.372	5568.033	101.061	±3.2	±5.6	±4.0
104	10873.495	5786.006	103.965	±5.0	±4.6	±3.7
105	10748.031	5481.275	96.703	±3.1	±3.2	±2.8
106	10687.768	5474.072	99.647	±3.1	±2.6	±2.5
107	10714.328	5544.370	105.581	±1.0	±0.0	±0.9
108	10739.426	5710.704	98.083	±3.2	±2.4	±2.1
109	10526.472	5804.632	101.348	±5.2	±3.2	±4.2
110	10575.932	5539.330	104.209	±1.0	±0.0	±0.9
111	10712.211	5171.502	100.820	±5.8	±2.2	±2.7
112	10526.477	5028.832	99.562	±8.3	±3.2	±4.9
501	10922.253	5081.231	97.143	±7.6	±5.4	±4.4
502	10836.994	5332.888	98.214	±3.6	±3.6	±2.3
503	10947.413	5568.066	101.057	±3.2	±5.6	±4.0
504	10873.513	5786.024	103.969	±5.0	±4.6	±3.7
505	10748.095	5481.256	96.685	±3.1	±3.2	±2.8
506	10687.827	5474.061	99.637	±3.1	±2.6	±2.5
508	10739.497	5710.663	98.055	±3.2	±2.4	±2.1
509	10526.500	5804.610	101.344	±5.2	±3.2	±4.2
511	10712.223	5171.523	100.833	±5.8	±2.2	±2.7
512	10526.463	5028.887	99.530	±8.3	±3.2	±4.9

Table B.13: Scenario A: adjusted coordinates and standard deviations for epoch 5

B.5 Scenario B: Adjusted coordinates and standard deviations after network analysis for epochs 1 to 5

Point	x [m]	y [m]	z [m]	$\hat{\sigma}_x$ [mm]	$\hat{\sigma}_y$ [mm]	$\hat{\sigma}_z$ [mm]
101	10922.207	5081.244	97.128	±3.5	±3.2	±3.8
102	10836.918	5332.844	98.229	±1.8	±1.8	±1.7
103	10947.342	5568.012	101.062	±3.5	±3.4	±3.6
104	10873.484	5785.962	101.961	±3.6	±3.0	±3.3
105	10748.028	5481.264	99.699	±3.0	±2.9	±2.5
106	10687.775	5474.069	99.649	±3.1	±2.7	±2.3
107	10714.330	5544.363	102.582	±2.9	±2.6	±2.3
108	10739.427	5710.672	98.078	±1.9	±1.6	±1.7
109	10526.497	5804.585	101.357	±3.6	±3.2	±3.8
110	10575.951	5539.320	102.209	±1.8	±1.8	±1.6
111	10712.202	5171.539	100.819	±2.1	±1.7	±2.0
112	10526.499	5028.887	99.558	±3.6	±3.3	±4.3

Table B.14: Scenario B: adjusted coordinates and standard deviations of epoch 1

Point	x [m]	y [m]	z [m]	$\hat{\sigma}_x$ [mm]	$\hat{\sigma}_y$ [mm]	$\hat{\sigma}_z$ [mm]
101	-1713147.042	-3774007.522	4834108.569	±3.3	±4.4	±5.9
102	-1713101.527	-3774263.209	4834164.711	±1.9	±2.2	±2.7
103	-1712926.078	-3774441.862	4834095.252	±3.8	±3.7	±5.4
104	-1712886.680	-3774663.356	4834143.845	±4.4	±3.1	±5.4
105	-1713100.938	-3774425.958	4834223.469	±2.6	±3.5	±4.1
106	-1713145.718	-3774438.375	4834262.505	±2.5	±3.6	±4.0
107	-1713096.521	-3774493.244	4834247.517	±2.8	±2.6	±3.9
108	-1713013.032	-3774638.013	4834227.811	±2.1	±1.9	±2.7
109	-1713119.913	-3774789.678	4834368.376	±3.4	±4.4	±5.9
110	-1713194.768	-3774532.305	4834336.971	±1.9	±2.0	±2.6
111	-1713253.146	-3774154.853	4834247.559	±2.2	±2.1	±3.2
112	-1713441.602	-3774083.712	4834367.014	±4.4	±3.7	±6.7

Table B.15: Scenario B: adjusted coordinates and standard deviations of epoch 2

Point	x [m]	y [m]	z [m]	$\hat{\sigma}_x$ [mm]	$\hat{\sigma}_y$ [mm]	$\hat{\sigma}_z$ [mm]
101	-1713147.038	-3774007.521	4834108.577	±3.3	±4.4	±6.0
102	-1713101.532	-3774263.235	4834164.711	±1.9	±2.2	±2.7
103	-1712926.089	-3774441.871	4834095.257	±3.8	±3.8	±5.4
104	-1712886.679	-3774663.351	4834143.832	±4.4	±3.2	±5.4
105	-1713100.935	-3774425.932	4834223.452	±2.6	±3.6	±4.2
106	-1713145.721	-3774438.372	4834262.503	±2.5	±3.7	±4.1
107	-1713096.517	-3774493.236	4834247.511	±2.9	±2.6	±4.0
108	-1713013.043	-3774637.990	4834227.788	±2.1	±2.0	±2.8
109	-1713119.912	-3774789.686	4834368.381	±3.5	±4.4	±6.0
110	-1713194.762	-3774532.304	4834336.967	±1.9	±2.1	±2.6
111	-1713253.145	-3774154.853	4834247.558	±2.2	±2.1	±3.2
112	-1713441.598	-3774083.723	4834367.027	±4.5	±3.7	±6.8

Table B.16: Scenario B: adjusted coordinates and standard deviations of epoch 3

Point	x [m]	y [m]	z [m]	$\hat{\sigma}_x$ [mm]	$\hat{\sigma}_y$ [mm]	$\hat{\sigma}_z$ [mm]
101	-1713147.036	-3774007.525	4834108.564	±3.2	±4.2	±5.8
102	-1713101.545	-3774263.252	4834164.713	±1.9	±2.1	±2.6
103	-1712926.083	-3774441.872	4834095.259	±3.7	±3.6	±5.2
104	-1712886.683	-3774663.354	4834143.832	±4.2	±3.0	±5.2
105	-1713100.927	-3774425.923	4834223.431	±2.5	±3.4	±4.0
106	-1713145.719	-3774438.346	4834262.485	±2.4	±3.5	±3.9
107	-1713096.514	-3774493.240	4834247.509	±2.8	±2.5	±3.8
108	-1713013.045	-3774637.963	4834227.766	±2.0	±1.9	±2.6
109	-1713119.924	-3774789.662	4834368.371	±3.3	±4.2	±5.8
110	-1713194.760	-3774532.303	4834336.971	±1.8	±2.0	±2.5
111	-1713253.144	-3774154.853	4834247.558	±2.2	±2.0	±3.1
112	-1713441.624	-3774083.755	4834367.032	±4.3	±3.6	±6.5

Table B.17: Scenario B: adjusted coordinates and standard deviations of epoch 4

Point	x [m]	y [m]	z [m]	$\hat{\sigma}_x$ [mm]	$\hat{\sigma}_y$ [mm]	$\hat{\sigma}_z$ [mm]
101	-1713147.041	-3774007.527	4834108.561	±3.3	±4.4	±6.0
102	-1713101.554	-3774263.265	4834164.722	±1.9	±2.2	±2.7
103	-1712926.071	-3774441.890	4834095.228	±3.8	±3.8	±5.4
104	-1712886.678	-3774663.360	4834143.835	±4.4	±3.1	±5.4
105	-1713100.926	-3774425.902	4834223.423	±2.6	±3.5	±4.1
106	-1713145.719	-3774438.339	4834262.466	±2.5	±3.6	±4.0
107	-1713096.546	-3774493.227	4834247.506	±2.8	±2.6	±4.0
108	-1713013.044	-3774637.951	4834227.743	±2.1	±1.9	±2.8
109	-1713119.927	-3774789.633	4834368.364	±3.4	±4.4	±6.0
110	-1713194.787	-3774532.291	4834336.969	±1.9	±2.0	±2.6
111	-1713253.143	-3774154.851	4834247.558	±2.2	±2.1	±3.2
112	-1713441.648	-3774083.779	4834367.006	±4.5	±3.7	±6.7

Table B.18: Scenario B: adjusted coordinates and standard deviations of epoch 5

B.6 Scenario B: Candidates for largest congruent point group from MSS-method using distance ratios and statistical evaluation

Epoch 4

Candidate	$\hat{\sigma}_0$	Redundancy	T_χ	Test outcome
101, 103, 104, 106, 109, 111	±1.708940	11	32.13	fail
101, 103, 104, 106, 109, 112	±2.620323	11	75.53	fail
101, 103, 104, 107, 109, 110	±1.557207	11	26.67	fail
101, 103, 104, 107, 109, 111	±1.428295	11	22.44	fail
101, 103, 104, 107, 109, 112	±2.116667	11	49.28	fail
101, 103, 104, 107, 110, 112	±2.115251	11	49.22	fail
101, 103, 104, 107, 111, 112	±2.312691	11	58.83	fail
101, 103, 104, 109, 110, 111	±1.561536	11	26.82	fail
101, 103, 104, 109, 110, 112	±2.333914	11	59.92	fail
101, 103, 104, 109, 111, 112	±2.328141	11	59.62	fail
101, 103, 104, 110, 111, 112	±2.355923	11	61.05	fail
101, 103, 107, 109, 110, 111	±1.740370	11	33.32	fail
101, 103, 107, 109, 110, 112	±2.463407	11	66.75	fail
101, 103, 107, 109, 111, 112	±2.380963	11	62.36	fail
101, 103, 107, 110, 111, 112	±2.342326	11	60.35	fail
101, 103, 109, 110, 111, 112	±2.632363	11	76.22	fail
101, 104, 107, 109, 110, 111	±1.667433	11	30.58	fail
101, 104, 107, 109, 110, 112	±2.410419	11	63.91	fail
101, 104, 107, 109, 111, 112	±2.303939	11	58.39	fail
101, 104, 107, 110, 111, 112	±2.393513	11	63.02	fail
101, 104, 109, 110, 111, 112	±2.615803	11	75.27	fail
101, 107, 109, 110, 111, 112	±2.633537	11	76.29	fail
102, 103, 104, 109, 110, 112	±3.668955	11	148.07	fail
103, 104, 106, 109, 111, 112	±2.728366	11	81.88	fail
103, 104, 107, 109, 110, 111	±1.716117	11	32.40	fail
103, 104, 107, 109, 110, 112	±2.275642	11	56.96	fail
103, 104, 107, 109, 111, 112	±2.361948	11	61.37	fail
103, 104, 107, 110, 111, 112	±2.358554	11	61.19	fail
103, 104, 109, 110, 111, 112	±2.621946	11	75.62	fail
103, 107, 109, 110, 111, 112	±2.669703	11	78.40	fail
104, 107, 109, 110, 111, 112	±2.607840	11	74.81	fail

Table B.19: Scenario B: candidates of six points and statistical test for epoch 4

Epoch 5

Candidate	$\hat{\sigma}_0$	Redundancy	T_χ	Test outcome
101, 103, 104, 106	±4.094482	5	83.82	fail
101, 103, 104, 109	±3.843804	5	73.87	fail
101, 103, 104, 111	±2.667292	5	35.57	fail
101, 103, 106, 109	±4.271428	5	91.23	fail
101, 103, 109, 111	±4.357430	5	94.94	fail
101, 103, 110, 111	±3.517961	5	61.88	fail
101, 103, 111, 112	±5.434011	5	147.64	fail
101, 104, 106, 108	±9.014754	5	406.33	fail
101, 104, 106, 109	±3.205931	5	51.39	fail
101, 104, 106, 111	±3.562890	5	63.47	fail
101, 104, 107, 110	±2.814900	5	39.62	fail
101, 104, 107, 111	±2.765655	5	38.24	fail
101, 104, 108, 111	±9.795991	5	479.81	fail
101, 104, 109, 110	±3.173768	5	50.36	fail
101, 104, 109, 111	±2.665296	5	35.52	fail
101, 104, 110, 111	±1.641897	5	13.48	fail
101, 104, 111, 112	±5.128177	5	131.49	fail
101, 105, 108, 111	±3.405762	5	58.00	fail
101, 106, 107, 108	±5.087478	5	129.41	fail
101, 106, 108, 111	±2.654852	5	35.24	fail
101, 106, 109, 111	±2.528894	5	31.98	fail
101, 107, 108, 111	±5.263101	5	138.50	fail
101, 107, 109, 110	±2.963354	5	43.91	fail
101, 107, 109, 111	±1.598172	5	12.77	fail
101, 107, 110, 111	±2.252421	5	25.37	fail
101, 109, 110, 111	±2.478685	5	30.72	fail
102, 103, 104, 112	±5.199785	5	135.19	fail
102, 103, 111, 112	±10.381986	5	538.93	fail
102, 104, 111, 112	±10.144118	5	514.52	fail

Table B.20: Scenario B: candidates of four points and statistical test for epoch 5

Candidate	$\hat{\sigma}_0$	Redundancy	T_χ	Test outcome
103, 104, 105, 109	±3.007018	5	45.21	fail
103, 104, 105, 112	±6.731617	5	226.57	fail
103, 104, 106, 109	±2.296140	5	26.36	fail
103, 104, 106, 112	±5.754963	5	165.60	fail
103, 104, 109, 111	±4.503668	5	101.42	fail
103, 104, 109, 112	±5.405712	5	146.11	fail
103, 104, 111, 112	±5.693417	5	162.07	fail
103, 105, 109, 112	±7.287213	5	265.52	fail
103, 106, 109, 112	±6.417968	5	205.95	fail
104, 105, 109, 111	±5.292176	5	140.04	fail
104, 105, 109, 112	±6.644291	5	220.73	fail
104, 105, 111, 112	±6.036243	5	182.18	fail
104, 106, 108, 111	±9.669506	5	467.50	fail
104, 106, 108, 112	±10.462443	5	547.31	fail
104, 106, 109, 111	±3.968003	5	78.73	fail
104, 106, 109, 112	±5.358530	5	143.57	fail
104, 106, 111, 112	±5.366112	5	143.98	fail
104, 107, 110, 111	±3.018982	5	45.57	fail
104, 108, 111, 112	±10.426134	5	543.52	fail
104, 109, 110, 111	±3.188368	5	50.83	fail
104, 109, 110, 112	±4.571194	5	104.48	fail
104, 109, 111, 112	±5.785011	5	167.33	fail
104, 110, 111, 112	±5.918210	5	175.13	fail
105, 108, 111, 112	±3.273066	5	53.56	fail
105, 109, 111, 112	±5.755058	5	165.60	fail
106, 107, 108, 111	±4.537959	5	102.97	fail
106, 107, 108, 112	±3.723641	5	69.33	fail
106, 108, 111, 112	±3.042563	5	46.29	fail
106, 109, 111, 112	±4.740790	5	112.38	fail
107, 108, 111, 112	±5.056851	5	127.86	fail
107, 109, 110, 111	±2.772306	5	38.43	fail
107, 109, 110, 112	±2.340996	5	27.40	fail
107, 109, 111, 112	±4.935281	5	121.79	fail
107, 110, 111, 112	±5.950665	5	177.05	fail
109, 110, 111, 112	±4.574161	5	104.61	fail

Scenario B: candidates of four points and statistical test for epoch 5 [continued]

Candidate	$\hat{\sigma}_0$	Redundancy	T_χ	Test outcome
101, 102, 103	±8.118225	2	131.81	fail
101, 103, 104	±3.601313	2	25.94	fail
101, 103, 106	±6.297582	2	79.32	fail
101, 103, 109	±5.869761	2	68.91	fail
101, 103, 110	±4.947843	2	48.96	fail
101, 103, 111	±2.191526	2	9.61	fail
101, 103, 112	±1.717855	2	5.90	pass
101, 104, 106	±4.618660	2	42.66	fail
101, 104, 107	±3.544904	2	25.13	fail
101, 104, 108	±13.853936	2	383.86	fail
101, 104, 109	±3.690087	2	27.23	fail
101, 104, 110	±2.156652	2	9.30	fail
101, 104, 111	±0.649365	2	0.84	pass
101, 104, 112	±3.766557	2	28.37	fail
101, 105, 108	±1.129678	2	2.55	pass
101, 105, 111	±4.907770	2	48.17	fail
101, 106, 107	±3.929568	2	30.88	fail
101, 106, 108	±2.002797	2	8.02	fail
101, 106, 109	±2.532029	2	12.82	fail
101, 106, 111	±3.266815	2	21.34	fail
101, 107, 108	±8.036070	2	129.16	fail
101, 107, 109	±1.576305	2	4.97	pass
101, 107, 110	±3.374556	2	22.78	fail
101, 107, 111	±1.430071	2	4.09	pass
101, 108, 111	±4.169672	2	34.77	fail
101, 109, 110	±3.855200	2	29.73	fail
101, 109, 111	±1.493244	2	4.46	pass
101, 110, 111	±0.687337	2	0.94	pass
101, 111, 112	±5.266154	2	55.46	fail
102, 103, 104	±5.775571	2	66.71	fail
102, 103, 111	±11.777903	2	277.44	fail
102, 103, 112	±6.692837	2	89.59	fail
102, 104, 109	±5.741758	2	65.94	fail
102, 104, 111	±11.980447	2	287.06	fail
102, 104, 112	±4.964532	2	49.29	fail
102, 109, 110	±4.573586	2	41.84	fail
102, 111, 112	±12.306651	2	302.91	fail
103, 104, 105	±2.915492	2	17.00	fail
103, 104, 106	±2.336125	2	10.91	fail
103, 104, 109	±0.739836	2	1.09	pass
103, 104, 111	±3.885346	2	30.19	fail

Table B.21: Scenario B: candidates of three points and statistical test for epoch 5

Candidate	$\hat{\sigma}_0$	Redundancy	T_χ	Test outcome
103, 104, 112	±4.410165	2	38.90	fail
103, 105, 109	±4.618281	2	42.66	fail
103, 105, 112	±9.649335	2	186.22	fail
103, 106, 109	±3.597513	2	25.88	fail
103, 106, 112	±8.790116	2	154.53	fail
103, 107, 110	±4.786216	2	45.82	fail
103, 109, 111	±6.900744	2	95.24	fail
103, 109, 112	±8.482845	2	143.92	fail
103, 110, 111	±5.379992	2	57.89	fail
103, 111, 112	±5.810704	2	67.53	fail
104, 105, 109	±3.099901	2	19.22	fail
104, 105, 111	±7.686860	2	118.18	fail
104, 105, 112	±9.124567	2	166.52	fail
104, 106, 108	±12.491877	2	312.09	fail
104, 106, 109	±2.284500	2	10.44	fail
104, 106, 111	±5.249893	2	55.12	fail
104, 106, 112	±7.457707	2	111.23	fail
104, 107, 110	±2.642133	2	13.96	fail
104, 107, 111	±3.950984	2	31.22	fail
104, 108, 111	±15.286720	2	467.37	fail
104, 108, 112	±16.297026	2	531.19	fail
104, 109, 110	±5.002554	2	50.05	fail
104, 109, 111	±4.146090	2	34.38	fail
104, 109, 112	±5.714553	2	65.31	fail
104, 110, 111	±2.434049	2	11.85	fail
104, 110, 112	±5.680898	2	64.55	fail
104, 111, 112	±6.002588	2	72.06	fail
105, 106, 110	±1.828006	2	6.68	fail
105, 108, 111	±3.124300	2	19.52	fail
105, 108, 112	±4.637669	2	43.02	fail
105, 109, 111	±6.290570	2	79.14	fail
105, 109, 112	±8.047415	2	129.52	fail
105, 111, 112	±2.514275	2	12.64	fail
106, 107, 108	±5.527029	2	61.10	fail
106, 107, 111	±4.227110	2	35.74	fail
106, 107, 112	±2.706019	2	14.65	fail
106, 108, 111	±0.697183	2	0.97	pass
106, 108, 112	±1.708316	2	5.84	pass
106, 109, 111	±3.559845	2	25.34	fail
106, 109, 112	±5.685244	2	64.64	fail
106, 111, 112	±3.652909	2	26.69	fail

Scenario B: candidates of three points and statistical test for epoch 5 [continued]

Candidate	$\hat{\sigma}_0$	Redundancy	T_χ	Test outcome
107, 108, 111	±7.104928	2	100.96	fail
107, 108, 112	±5.033745	2	50.68	fail
107, 109, 110	±2.407674	2	11.59	fail
107, 109, 111	±0.951328	2	1.81	pass
107, 109, 112	±1.631059	2	5.32	pass
107, 110, 111	±3.398431	2	23.10	fail
107, 110, 112	±2.527212	2	12.77	fail
107, 111, 112	±5.876108	2	69.06	fail
108, 111, 112	±4.010775	2	32.17	fail
109, 110, 111	±3.580341	2	25.64	fail
109, 110, 112	±0.850427	2	1.45	pass
109, 111, 112	±5.874974	2	69.03	fail
110, 111, 112	±6.869511	2	94.38	fail

Scenario B: candidates of three points and statistical test for epoch 5 [continued]

B.7 Scenario B: Candidates for largest congruent point group from MSS-method using angles and statistical evaluation

Candidate	T_G	Test outcome
101, 103, 111	4.50	fail
101, 103, 112	2.87	pass
101, 104, 107	12.13	fail
101, 104, 110	4.48	fail
101, 105, 108	1.26	pass
101, 106, 108	3.97	fail
101, 106, 109	6.38	fail
101, 107, 109	2.42	pass
101, 107, 111	2.01	pass
101, 109, 111	2.19	pass
101, 110, 111	0.36	pass
102, 107, 109	29.01	fail
103, 104, 109	1.18	pass
104, 106, 109	5.00	fail
104, 107, 111	15.10	fail
104, 110, 111	5.72	fail
105, 106, 109	4.29	fail
105, 106, 110	3.24	fail
105, 106, 112	7.14	fail
105, 111, 112	6.17	fail
106, 108, 111	2.08	pass
106, 108, 112	2.88	pass
107, 109, 110	5.70	fail
107, 109, 111	0.89	pass
107, 109, 112	2.59	pass
109, 110, 112	1.20	pass

Table B.22: Scenario B: candidates and test statistics for epoch 5

Appendix C

C.1 Turtle Mountain: adjusted coordinates and standard deviations of HPTN points after network analysis for epochs 1 to 4

Point	*Easting* [m]	*Northing* [m]	*Height* [m]	$\hat{\sigma}_{Easting}$ [mm]	$\hat{\sigma}_{Northing}$ [mm]	$\hat{\sigma}_{Height}$ [mm]
1	500.001	999.993	100.001	±0.5	±0.4	±1.5
2	486.013	1040.261	76.354	±1.2	±1.0	±2.2
12	435.709	1081.598	44.729	±0.9	±0.8	±4.4
13	435.949	1128.172	40.023	±1.2	±0.9	±2.2
14	436.843	1159.604	44.741	±0.5	±0.5	±1.3
15	466.980	982.861	92.753	±0.6	±0.4	±1.4
17	414.325	1205.584	48.629	±0.5	±0.5	±1.4

Table C.1: Adjusted HPTN coordinates and standard deviations in Summer 2008 (epoch 1)

Point	*Easting* [m]	*Northing* [m]	*Height* [m]	$\hat{\sigma}_{Easting}$ [mm]	$\hat{\sigma}_{Northing}$ [mm]	$\hat{\sigma}_{Height}$ [mm]
1	500.003	999.992	99.993	±0.2	±0.2	±0.7
2	486.013	1040.262	76.353	±0.2	±0.3	±0.9
12	435.707	1081.598	44.735	±0.4	±0.4	±1.3
13	435.948	1128.171	40.027	±0.2	±0.3	±0.9
14	436.843	1159.604	44.740	±0.2	±0.3	±1.2
15	466.980	982.860	92.751	±0.2	±0.2	±0.7
17	414.326	1205.585	48.632	±0.2	±0.3	±1.0

Table C.2: Adjusted HPTN coordinates and standard deviations in Fall 2009 (epoch 2)

Point	$Easting$ [m]	$Northing$ [m]	$Height$ [m]	$\hat{\sigma}_{Easting}$ [mm]	$\hat{\sigma}_{Northing}$ [mm]	$\hat{\sigma}_{Height}$ [mm]
1	499.998	999.999	99.989	±0.3	±0.3	±0.4
2	486.013	1040.264	76.353	±0.3	±0.4	±0.6
12	435.709	1081.599	44.737	±0.6	±0.6	±0.8
13	435.947	1128.168	40.028	±0.3	±0.4	±0.5
14	436.845	1159.600	44.743	±0.2	±0.4	±0.4
15	466.979	982.867	92.748	±0.3	±0.3	±0.4
17	414.330	1205.577	48.632	±0.3	±0.4	±0.5

Table C.3: Adjusted HPTN coordinates and standard deviations in Fall 2010 (epoch 3)

Point	$Easting$ [m]	$Northing$ [m]	$Height$ [m]	$\hat{\sigma}_{Easting}$ [mm]	$\hat{\sigma}_{Northing}$ [mm]	$\hat{\sigma}_{Height}$ [mm]
1	499.997	999.998	99.990	±0.3	±0.3	±0.4
2	486.013	1040.267	76.350	±0.3	±0.5	±0.7
12	435.711	1081.599	44.737	±0.6	±0.7	±0.8
13	435.949	1128.168	40.028	±0.3	±0.5	±0.6
14	436.844	1159.600	44.743	±0.2	±0.4	±0.5
15	466.978	982.867	92.750	±0.4	±0.3	±0.5
17	414.328	1205.575	48.632	±0.3	±0.5	±0.5

Table C.4: Adjusted HPTN coordinates and standard deviations in Fall 2011 (epoch 4)

C.2 Turtle Mountain: candidates for similar point groups from MSS-method based on distance ratios

Candidate	$\hat{\sigma}_0$	Redundancy	T_χ	Test outcome
1, 12, 13, 14, 15, 17,	±3.70757790	11	151.21	fail
2, 12, 13, 14, 15, 17,	±3.01817633	11	100.20	fail
1, 12, 13, 14, 15,	±4.31998870	8	149.30	fail
1, 12, 13, 14, 17,	±3.15713198	8	79.74	fail
1, 12, 13, 15, 17,	±3.28432589	8	86.29	fail
1, 12, 14, 15, 17,	±2.00972007	8	32.31	fail
1, 13, 14, 15, 17,	±4.15059794	8	137.82	fail
2, 12, 13, 14, 15,	±3.18311543	8	81.06	fail
2, 12, 13, 14, 17,	±3.10860325	8	77.31	fail
2, 12, 13, 15, 17,	±2.63885411	8	55.71	fail
2, 12, 14, 15, 17,	±1.48418403	8	17.62	fail
2, 13, 14, 15, 17,	±3.35389068	8	89.99	fail
12, 13, 14, 15, 17,	±3.04393873	8	74.12	fail
1, 12, 13, 14,	±3.35832533	5	56.39	fail
1, 12, 13, 15,	±1.79033346	5	16.03	fail
1, 12, 13, 17,	±2.36057956	5	27.86	fail
1, 12, 14, 15,	±2.18445330	5	23.86	fail
1, 12, 14, 17,	±0.97836648	5	4.79	pass
1, 12, 15, 17,	±2.42522287	5	29.41	fail
1, 13, 14, 15,	±5.22000141	5	136.24	fail
1, 13, 14, 17,	±3.35518004	5	56.29	fail
1, 13, 15, 17,	±3.73531161	5	69.76	fail
1, 14, 15, 17,	±2.36487435	5	27.96	fail
2, 12, 13, 14,	±3.35127857	5	56.16	fail
2, 12, 13, 15,	±2.96634041	5	44.00	fail
2, 12, 13, 17,	±2.55308923	5	32.59	fail
2, 12, 14, 15,	±1.69310918	5	14.33	fail
2, 12, 14, 17,	±1.11952796	5	6.27	pass
2, 12, 15, 17,	±1.75065164	5	15.32	fail
2, 13, 14, 15,	±3.56136592	5	63.42	fail

Table C.5: Statistical evaluation of candidates for largest similar point group between epochs 2 and 3

Candidate	$\hat{\sigma}_0$	Redundancy	T_χ	Test outcome
2, 13, 14, 17,	±3.35347656	5	56.23	fail
2, 13, 15, 17,	±2.93162327	5	42.97	fail
2, 14, 15, 17,	±1.78747571	5	15.98	fail
12, 13, 14, 15,	±2.97307878	5	44.20	fail
12, 13, 14, 17,	±3.26903430	5	53.43	fail
12, 13, 15, 17,	±2.31908232	5	26.89	fail
13, 14, 15, 17,	±3.29323215	5	54.23	fail

Statistical evaluation of candidates for largest similar point group between epochs 2 and 3 [continued]

Candidate	$\hat{\sigma}_0$	Redundancy	T_χ	Test outcome
1, 2, 12, 13, 14, 15,	±3.20486173	11	112.98	fail
1, 2, 12, 13, 14, 17,	±3.03285573	11	101.18	fail
1, 2, 12, 13, 15, 17,	±3.04622871	11	102.07	fail
1, 2, 12, 14, 15, 17,	±2.56852615	11	72.57	fail
1, 2, 13, 14, 15, 17,	±3.17350532	11	110.78	fail
1, 12, 13, 14, 15, 17,	±1.85128539	11	37.70	fail
2, 12, 13, 14, 15, 17,	±2.27616214	11	56.99	fail
1, 2, 12, 13, 14,	±3.52379590	8	99.34	fail
1, 2, 12, 13, 15,	±3.41773932	8	93.45	fail
1, 2, 12, 13, 17,	±3.35379235	8	89.98	fail
1, 2, 12, 14, 15,	±2.97864573	8	70.98	fail
1, 2, 12, 14, 17,	±2.59561275	8	53.90	fail
1, 2, 12, 15, 17,	±2.81989328	8	63.61	fail
1, 2, 13, 14, 15,	±3.67607013	8	108.11	fail
1, 2, 13, 14, 17,	±3.49449906	8	97.69	fail
1, 2, 13, 15, 17,	±3.49232042	8	97.57	fail
1, 2, 14, 15, 17,	±2.96790492	8	70.47	fail
1, 12, 13, 14, 15,	±2.07898625	8	34.58	fail
1, 12, 13, 14, 17,	±1.90748004	8	29.11	fail
1, 12, 13, 15, 17,	±1.74045162	8	24.23	fail
1, 12, 14, 15, 17,	±1.40904752	8	15.88	fail
1, 13, 14, 15, 17,	±1.78767724	8	25.57	fail
2, 12, 13, 14, 15,	±2.43699299	8	47.51	fail
2, 12, 13, 14, 17,	±1.67180736	8	22.36	fail
2, 12, 13, 15, 17,	±2.38695973	8	45.58	fail
2, 12, 14, 15, 17,	±2.15012930	8	36.98	fail
2, 13, 14, 15, 17,	±2.47749060	8	49.10	fail
12, 13, 14, 15, 17,	±1.87709754	8	28.19	fail

Table C.6: Statistical evaluation of candidates for largest similar point group between epochs 2 and 4

Candidate	$\hat{\sigma}_0$	Redundancy	T_χ	Test outcome
1, 2, 12, 13,	±3.62681160	5	65.77	fail
1, 2, 12, 14,	±2.98794287	5	44.64	fail
1, 2, 12, 15,	±3.25327496	5	52.92	fail
1, 2, 12, 17,	±2.88331549	5	41.57	fail
1, 2, 13, 14,	±4.35054492	5	94.64	fail
1, 2, 13, 15,	±4.19723341	5	88.08	fail
1, 2, 13, 17,	±4.14587722	5	85.94	fail
1, 2, 14, 15,	±3.69439126	5	68.24	fail
1, 2, 14, 17,	±2.95336143	5	43.61	fail
1, 2, 15, 17,	±3.45840191	5	59.80	fail
1, 12, 13, 14,	±2.13897767	5	22.88	fail
1, 12, 13, 15,	±1.91683378	5	18.37	fail
1, 12, 13, 17,	±1.80907496	5	16.36	fail
1, 12, 14, 15,	±1.67771763	5	14.07	fail
1, 12, 14, 17,	±1.17240757	5	6.87	pass
1, 12, 15, 17,	±1.63147662	5	13.31	fail
1, 13, 14, 15,	±1.98616934	5	19.72	fail
1, 13, 14, 17,	±1.83405980	5	16.82	fail
1, 13, 15, 17,	±1.30167265	5	8.47	pass
1, 14, 15, 17,	±1.48642214	5	11.05	pass
2, 12, 13, 14,	±1.82870027	5	16.72	fail
2, 12, 13, 15,	±2.94313512	5	43.31	fail
2, 12, 13, 17,	±1.42516685	5	10.16	pass
2, 12, 14, 15,	±2.60727593	5	33.99	fail
2, 12, 14, 17,	±1.06593491	5	5.68	pass
2, 12, 15, 17,	±2.51040965	5	31.51	fail
2, 13, 14, 15,	±2.57159565	5	33.07	fail
2, 13, 14, 17,	±1.73145009	5	14.99	fail
2, 13, 15, 17,	±2.65742479	5	35.31	fail
2, 14, 15, 17,	±2.65402974	5	35.22	fail
12, 13, 14, 15,	±2.06037820	5	21.23	fail
12, 13, 14, 17,	±1.78670561	5	15.96	fail
12, 13, 15, 17,	±1.77799488	5	15.81	fail
13, 14, 15, 17,	±1.83876104	5	16.91	fail

Statistical evaluation of candidates for largest similar point group between epochs 2 and 4 [continued]

Candidate	$\hat{\sigma}_0$	Redundancy	T_χ	Test outcome
1, 12, 13, 14, 15, 17,	±2.19151457	11	52.83	fail
1, 12, 13, 14, 15,	±2.46413727	8	48.58	fail
1, 12, 13, 14, 17,	±1.51563797	8	18.38	fail
1, 12, 13, 15, 17,	±1.94285597	8	30.20	fail
1, 12, 14, 15, 17,	±1.58352816	8	20.06	fail
1, 13, 14, 15, 17,	±2.55406730	8	52.19	fail
2, 12, 13, 14, 17,	±1.77735245	8	25.27	fail
12, 13, 14, 15, 17,	±1.55629790	8	19.38	fail
1, 12, 13, 14,	±1.68104631	5	14.13	fail
1, 12, 13, 17,	±0.85404243	5	3.65	pass
1, 12, 14, 15,	±1.56385338	5	12.23	fail
1, 12, 14, 17,	±0.95937816	5	4.60	pass
1, 12, 15, 17,	±1.71196917	5	14.65	fail
1, 13, 14, 15,	±3.08096739	5	47.46	fail
1, 13, 14, 17,	±1.66889526	5	13.93	fail
1, 13, 15, 17,	±2.42840539	5	29.49	fail
1, 14, 15, 17,	±1.68648657	5	14.22	fail
2, 12, 13, 14,	±2.13269054	5	22.74	fail
2, 12, 13, 17,	±1.68355815	5	14.17	fail
2, 12, 14, 17,	±1.09150480	5	5.96	pass
2, 13, 14, 17,	±1.72545911	5	14.89	fail
2, 14, 15, 17,	±2.43489756	5	29.64	fail
12, 13, 14, 15,	±1.04593884	5	5.47	pass
12, 13, 14, 17,	±1.76375176	5	15.55	fail
12, 13, 15, 17,	±0.78497415	5	3.08	pass
12, 14, 15, 17,	±1.21366683	5	7.36	pass
13, 14, 15, 17,	±1.94393809	5	18.89	fail

Table C.7: Statistical evaluation of candidates for largest similar point group between epochs 3 and 4

C.3 Turtle Mountain: candidates for similar point groups from MSS-method based on angles

Candidate	T_G	Test outcome
1, 2, 13, 17	21.63	fail
1, 2, 14, 17	8.06	fail
1, 12, 13, 14	11.22	fail
1, 12, 13, 17	5.52	fail
1, 12, 14, 17	0.96	pass
2, 12, 14, 17	1.25	pass
12, 13, 14, 15	8.78	fail
12, 13, 15, 17	5.34	fail

Table C.8: Statistical evaluation of candidates for largest similar point group between epochs 2 and 3

Candidate	T_G	Test outcome
1, 2, 14, 17	2.32	fail
1, 12, 13, 14	4.44	fail
1, 12, 13, 17	3.18	fail
1, 12, 14, 17	1.38	pass
1, 13, 14, 15	3.84	fail
1, 13, 15, 17	1.65	pass
1, 14, 15, 17	2.22	pass
2, 12, 13, 14	3.26	fail
2, 12, 13, 17	1.97	pass
2, 12, 14, 17	1.15	pass
12, 13, 14, 15	4.12	fail
12, 13, 15, 17	3.06	fail

Table C.9: Statistical evaluation of candidates for largest similar point group between epochs 2 and 4

Candidate	T_G	Test outcome
1, 12, 13, 14, 15	6.06	fail
1, 12, 13, 15, 17	3.76	fail
1, 12, 14, 15, 17	2.49	fail
1, 12, 13, 14	2.81	fail
1, 12, 13, 17	0.72	pass
1, 12, 14, 15	2.43	fail
1, 12, 14, 17	0.91	pass
1, 12, 15, 17	2.92	fail
1, 13, 14, 15	9.47	fail
1, 13, 15, 17	5.87	fail
1, 14, 15, 17	2.83	fail
2, 12, 13, 14	4.52	fail
2, 12, 13, 15	5.01	fail
2, 12, 13, 17	2.81	fail
2, 12, 14, 17	1.18	pass
12, 13, 14, 15	1.09	pass
12, 13, 15, 17	0.61	pass
12, 14, 15, 17	1.46	pass

Table C.10: Statistical evaluation of candidates for largest similar point group between epochs 3 and 4